uOttawa

L'Université canadienne
Canada's university

FACULTÉ DES ÉTUDES SUPÉRIEURES ET POSTOCTORALES

uOttawa

L'Université canadienne
Canada's university

FACULTY OF GRADUATE AND POSDOCTORAL STUDIES

Terris Yakimovich

AUTEUR DE LA THÈSE / AUTHOR OF THESIS

M.A.Sc. (Mechanical Engineering)

GRADE / DEGREE

Department of Mechanical Engineering

FACULTÉ, ÉCOLE, DÉPARTEMENT / FACULTY, SCHOOL, DEPARTMENT

Design and Evaluation of a Dynamic Knee-Ankle-Foot Orthosis

TITRE DE LA THÈSE / TITLE OF THESIS

J. Kofman

DIRECTEUR (DIRECTRICE) DE LA THÈSE / THESIS SUPERVISOR

E. Lemaire

CO-DIRECTEUR (CO-DIRECTRICE) DE LA THÈSE / THESIS CO-SUPERVISOR

EXAMINATEURS (EXAMINATRICES) DE LA THÈSE / THESIS EXAMINERS

M. Munro

D. Russell

Gary W. Slater

LE DOYEN DE LA FACULTÉ DES ÉTUDES SUPÉRIEURES ET POSTDOCTORALES /
DEAN OF THE FACULTY OF GRADUATE AND POSTDOCORAL STUDIES

DESIGN AND EVALUATION OF A DYNAMIC KNEE-ANKLE-FOOT ORTHOSIS

Terris Yakimovich

A thesis submitted to the Faculty of Graduate and Postdoctoral Studies in partial fulfillment of the requirements for the degree of

MASTER OF APPLIED SCIENCE

in Mechanical Engineering

Ottawa-Carleton Institute for Mechanical and Aerospace Engineering
University of Ottawa
Ottawa, Canada

May 2005

Your file Votre référence
ISBN: 0-494-11461-4
Our file Notre référence
ISBN: 0-494-11461-4

ABSTRACT

Conventional knee-ankle-foot orthoses (KAFOs) or leg braces lock the knee in full extension and therefore do not permit a natural gait pattern. A new electro-mechanical dynamic knee-ankle-foot orthosis (DKAFO) that incorporates a new dynamic knee joint (DKJ) was designed to provide a more natural gait for people with knee extensor muscle weakness. The DKAFO inhibits knee flexion while allowing knee extension during weight bearing. During swing or other non-weight bearing activities, the DKAFO allows free knee motion. A prototype knee joint was mechanically tested to determine the moment at failure, loading behaviour, and device safety. Quantitative kinematic gait analysis of three able-bodied subjects and three KAFO users showed that walking with the DKAFO had a minimal effect on normal gait. The DKAFO offered increased knee motion in swing and a reduction in gait abnormalities for some subjects with disabilities. Future efforts will be made to modify the design to increase the factor of safety, and reduce DKJ dimensions.

To my wife,
for putting so much into this thesis and carrying me when I needed the help,

my father,
my engineering mentor, inspiration and life-long teacher of science,

my mother,
for her constant encouragement, love and first teaching me how to count.

ACKNOWLEDGEMENTS

I owe a sincere thank you to the many people who have both directly and indirectly made this work possible. Thank you to my two supervisors Dr. Jonathan Kofman from Department of Mechanical Engineering, University of Ottawa, and Department of Systems Design Engineering, University of Waterloo and Dr. Edward Lemaire from the Rehabilitation Centre, Ottawa Hospital and Faculty of Medicine, University of Ottawa, for their guidance, encouragement, and help throughout this research project.

The orthotists at the Rehabilitation Centre donated an appreciable amount of time to this project, constructing the orthoses and offering their clinical expertise throughout the development and clinical testing stages. A sincere thank you to Rajiv Kalsi, Mark Russell, Carla Serwotka, Hanna Abel-Armstrong, and David Nielen. I am indebted to Shawn 'Sherlock MacGyver' Millar, Joao Elias Tomas and Louis Goudreax for their outstanding work on the control system and the Rehabilitation Centre's Engineering Services for their constant support. A special thank you to Shawn for his help and support in capturing and processing the gait analysis data.

Many thanks to Dr. Mike Munro, Dr. Robert Harrison and Cagri Ayranci for offering their time, expertise and helpful suggestions in the development and testing stages of the orthotic device. Thank you to Brent Cotter, Michael Burns, James MacDermid, Paul Deegan and Herve Beaudoin who did such a fine job machining the prototype knee joints and offered many helpful suggestions and answered all of my questions concerning manufacturing.

Thank you to my fellow colleagues Siddharth Verma, Jeff Wu, Jeff Bottomley and Peirong Jia for their advice and moral and technical support. Thank you also to my brothers and sisters for their constant moral support and always making me laugh.

I gratefully acknowledge the support of the University of Ottawa's Inter-Faculty Collaborative Research Award for providing financial assistance for this project.

TABLE OF CONTENTS

List of Figures

List of Tables

Nomenclature

The following symbols are used frequently in this thesis. Symbols used in only one or two paragraphs are defined in the text when they are introduced and are not included in this section.

Latin Symbols

Symbol	Unit	Description
A	-	Axis of disc rotation
B	-	Location where the belt leaves the disc at a tangent
C	-	Location where the belt leaves the hammer at a tangent
D	-	Mid-point of θ on the leading edge of the hammer radius R_2
E	-	Location where the upper hammer radius R_2 becomes tangent with the straight leading edge of the hammer
G	-	Location of the mid-point of the clamp length on the hammer
L	m	Perpendicular distance between the knee-joint axis and the vertical compressive force W applied in DKJ mechanical testing
P	-	Axis of hammer rotation
S	-	Location of the lower bound of the clamp site on the hammer
U	-	Location of the upper bound of the clamp site on the hammer
W	N	Compressive force applied by the testing machine on the DKJ

Greek Symbols

Symbol	Unit	Description
β	deg	Negligible-resistance knee flexion angle
γ	deg	Angle between the vertical axis and the tangent at point D
δ	m	Distance traveled by point C as the hammer rotates by angle Ψ
θ	deg	Belt-hammer contact angle
λ	deg	DKJ flexion angle measured in mechanical testing
μ	-	Coefficient of friction of the belt with the hammer
ϕ	deg	Angle between the vertical axis and the tangent at point C
Ψ	deg	Hammer rotation angle between the open and closed hammer position
Ω	deg	Angle between the length of the clamped hammer and the vertical axis

Subscripts

Symbol	Unit	Description
F_B	N	Force applied to the anvil by the bumper
F_C	N	Clamping force at point G
F_D	N	Force applied by the belt on hammer at point D
F_{Dx}	N	Force applied by the belt on hammer at point D (x-component)
F_{Dy}	N	Force applied by the belt on hammer at point D (y-component)
F_{fx}	N	Belt friction force on the hammer (x-component)
F_{fy}	N	Belt friction force on the hammer (y-component)
F_G	N	Friction force between the belt and the hammer/anvil at the clamp site
F_s	N	Hammer recoil spring force
H_1	m	Vertical distance between point F_{Dx} and the hammer axis of rotation
H_2	m	Vertical distance from force F_C to the hammer axis of rotation
H_3	m	Horizontal distance from point F_{Dy} to the hammer axis of rotation
H_4	m	Half of the width of the hammer
H_5	m	Width of the hammer
H_6	m	Vertical distance from the top of the anvil to hammer axis of rotation
H_7	m	Vertical distance from the anvil bottom to hammer axis of rotation
H_8	m	Distance from point C on the hammer to hammer axis of rotation
M_B	Nm	Moment created by the bumper on the anvil
M_E	Nm	Extension moment about the orthotic knee joint axis
M_F	Nm	Flexion moment about the orthotic knee joint axis
M_{H1}	Nm	Moment imposed on the hammer by the belt reaction force F_{Dx}
M_{H2}	Nm	Moment imposed on the hammer by hammer recoil spring force F_s
M_{H3}	Nm	Moment imposed on the hammer by belt tension in swing
M_{Kmax}	Nm	Predicted peak knee moment applied to a single DKJ
R_1	m	Distance from the disc center to the midline of the outer belt
R_2	m	Radius of curvature of the upper hammer
T_{BC}	N	Tension in belt section BC
T_{BCx}	N	Tension in belt section BC (x-component)

Symbol	Unit	Description
T_{BCy}	N	Tension in belt section *BC* (*y*-component)
T_{EF}	N	Tension in belt section *EF*
T_{EFx}	N	Tension in belt section *EF* (*x*-component)
T_{EFy}	N	Tension in belt section *EF* (*y*-component)
μ_{req}	-	Required belt-hammer coefficient of friction

Glossary

Acronym	Description
AFO	Ankle-foot orthosis
ASTM	American Society of Testing and Materials
DAQ	Data acquisition board
DKAFO	Dynamic knee-ankle-foot orthosis
DKJ	Dynamic knee joint
EAP	Electroactive polymer
ERF	Electro-rheological fluid
FSR	Force sensing resistor
GAMA	Gait and motion analysis
IB-II	Intelligent Brace-II
KAFO	Knee-ankle-foot orthosis
LED	Light emitting diode
MRF	Magneto-rheological fluid
MSA	Memory shape alloy
NASA	National Aeronautics and Space Administration
PMOSFET	Power MOSFET transistor
PTFE	Polytetrafluoroethylene
QFD	Quality function deployment
SCO	Signal correction board
SCKAFO	Stance control knee-ankle-foot orthosis

Chapter 1. Introduction

Approximately 866,000 Americans use a brace on a lower extremity [1]. The number of Canadian cases is estimated to be proportionally similar, typically 10 times fewer than the United States. People inflicted with isolated quadriceps or thigh muscle weakness or partial or total paralysis of the quadriceps, often lack the muscle strength to walk safely without collapsing under their own weight and falling. Usually these people are prescribed a standard knee-ankle-foot orthosis (KAFO), (Figure 1.1). A KAFO is a full leg brace that locks the knee in *constant* full extension and prevents the leg from collapsing while weight bearing.

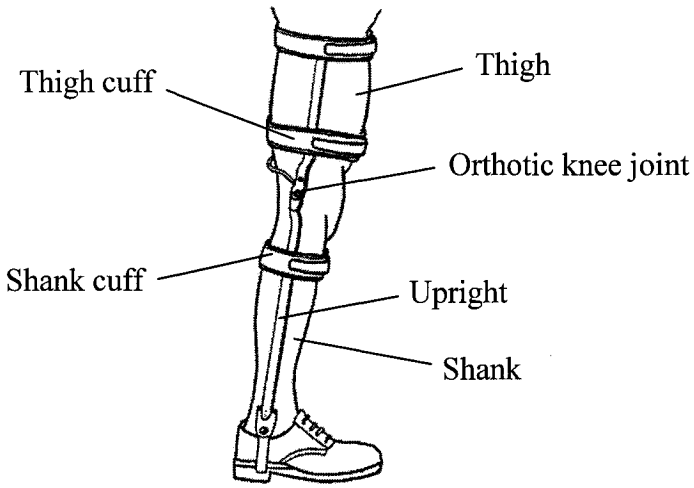

Figure 1.1 - A conventional KAFO (adapted from [2]).

The major problem with the standard KAFO is that the user cannot flex their knee while swinging their leg forward during walking. This period of the gait cycle, when the leg is swinging forward and the foot is off the ground, is referred to as the *swing* phase of gait. Without knee flexion, the KAFO user is required to bring their leg forward around the side of their body, adopt an increased lateral sway of the upper body, or lift their hip during the swing phase in order to bring their leg forward for initial heel contact. These gait abnormalities can lead to problems in the soft tissues and joints of the hip and back, causing pain and loss of motion [3]. As well, walking with an immobilized knee requires more energy than normal gait and often leads to user fatigue during ambulation [4]. The standard KAFO rarely meets the user's cosmetic needs as they are forced to walk in a

very unnatural manner. A standard KAFO also limits where a user can walk. Without the ability to flex the knee, stairs and inclined surfaces are difficult to navigate; even walking onto a curb is met with difficulty.

Recently, the orthotics market has seen the emergence of a new type of KAFO that allows the wearer to flex their knee while swinging the leg forward, and still provide knee stability by locking the knee in full extension during weight bearing. These new functional KAFOs have been labelled Stance Control Knee-Ankle-Foot Orthoses (SCKAFOs). Four different SCKAFOs have been released to the commercial market in the past three years. Unfortunately, these designs either provide no support while walking stairs or inclines, will not support stumbling, or are too heavy and bulky for many clients.

This thesis describes research undertaken to design, build and test an original dynamic orthotic knee joint and incorporate it in an electromechanical KAFO system to fully address the functional and cosmetic needs of potential users. Functionally, the ideal joint will allow unimpeded knee motion when the leg is in swing phase and inhibit knee flexion when the leg is bearing weight. The newly designed orthosis must allow the knee to extend in stance so that the user can climb stairs, walk on uneven ground, and recover from a stumble. The orthosis must also be lightweight and have an unobtrusive form if the user is to find the brace cosmetically appealing and practical for everyday use.

The scope of this research involves the complete design and development of an orthotic knee joint and integration of the joint in an electromechanical KAFO, through to mechanical and clinical evaluation. The project began with researching the problem and defining the design specifications for the ideal orthotic knee joint. The conceptual design phase involved researching potential technologies and generating numerous conceptual designs. The most promising design was developed further. Static and dynamic stress calculations were utilized to drive the dimensions of the joint design. Materials were selected and three identical prototype joints were manufactured. One prototype joint was mounted in a material testing machine and subjected to static loading to determine the joint's strength, loading behaviour, maximum holding moment and endurance. The

remaining two prototype joints were integrated into a KAFO and tested for clinical performance. A clinical test was performed employing able-bodied subjects and KAFO users, to gauge the effectiveness of the new joint design.

Following this introduction, Chapter 2 will continue by reviewing human gait, the function of conventional KAFOs, KAFO limitations, attempts to design a better KAFO, the effectiveness of current SCKAFOs and potential technologies relevant to the development of a superior orthosis. A statement of the rationale for this research and research objectives will follow in Chapter 3 along with the entire design process from the conceptual design stage to the prototype stage. The procedure and results of mechanical testing will be presented in Chapter 4 followed by the procedure and results of clinical testing in Chapter 5. This thesis will finish with a discussion of the mechanical and clinical test results and recommendations for further research and development in Chapter 6, followed by research conclusions in Chapter 7.

Chapter 2. Literature Review

The following literature review provides a foundation of knowledge for understanding the limitations of current commercial SCKAFOs and the challenges associated with developing an effective solution. This section will briefly examine relevant elements of human gait, the function of conventional KAFOs, their limitations, attempts to design a better KAFO, the effectiveness of current SCKAFOs and review potential technologies which may be employed to generate a superior dynamic orthotic knee joint.

2.1 Review of the Knee in Walking

In order to define the design requirements for an ideal SCKAFO, an examination of the function of the knee in fundamental activities such as level walking and stair walking is required.

2.1.1 Components of the Gait Cycle

Gait is comprised of a complex sequence of body movements repeated consecutively in a cycle. To facilitate analysis, the human gait cycle can be broken down into functional components: *phases, tasks* and *sub-phases* [5].

2.1.1.1 Phases

The human gait cycle is composed of two distinct phases – stance and swing [5]. The period of time during which the foot is on the ground is termed *stance. Swing* involves the period from when the foot leaves the ground, travels to the front of the body, and finally contacts the ground again (Figure 2.1). The lower limb is in stance for approximately 60% of the gait cycle at normal cadence. During the first 10% and last 10% of stance, both feet are in contact with the ground in a state designated *double support.* For 40% of the gait cycle, the stance limb is the sole support in a state designated *single support.* Swing lasts 40% of the gait cycle – equal to the duration of single support, occurring simultaneously on the contralateral (opposite) limb. For KAFO users, stance phase may be longer than 60% due to instability related to the person's disability.

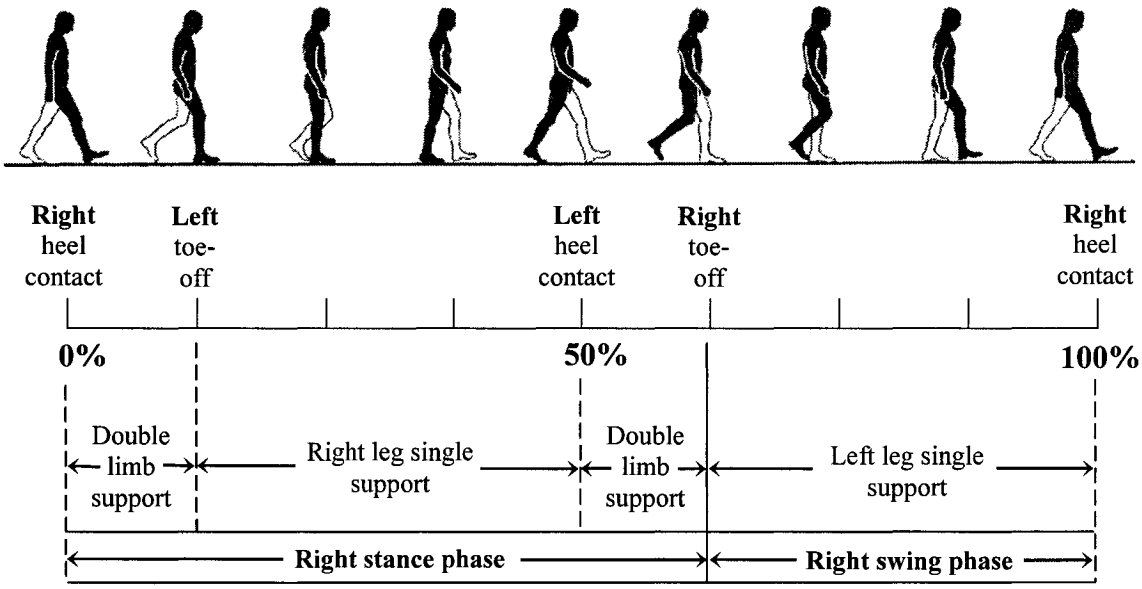

Figure 2.1 - The gait cycle showing subdivision into stance and swing phases and functional tasks (adapted from [6]).

2.1.1.2 Tasks

The stance and swing phases can be further decomposed into three functional *tasks*. Stance involves the tasks of both *weight acceptance* and *single limb support* [5]. Weight acceptance serves three main functions – absorbing the shock of initial floor contact, providing initial limb stability, and preserving forward progression. The main function of single limb support is to support the weight of the body while maintaining forward progression and controlling the body's centre of gravity. The sole task of swing is *limb advancement*. Limb advancement involves preparing the limb for swing, lifting the limb to ensure that the foot clears the ground, advancing the limb and preparing the limb for initial floor contact [5].

2.1.1.3 Sub-phases

The gait cycle consists of eight *sub-phases*, each with a functional goal defined by limb position landmarks in the gait cycle. Table 2.1 lists the eight sub-phases of gait, their respective time interval within the gait cycle, the definitive landmarks of the sub-phase and their principle function [5].

Table 2.1– Sub-phases of the gait cycle.

Sub-Phase	Time Interval (% of Gait Cycle)	Definitive Landmarks	Principle Function
Initial Contact	0-2%	-Begins when the stance foot touches the ground	-Provide stable weight bearing
Limb Loading	2-10%	-Begins with heel-strike of the stance foot	- Shock absorption - Weight bearing stability - Preservation of progression
Mid-stance	10-30%	-Begins when stance foot is flat -Contralateral foot is lifted for swing	- Stable weight bearing - Progression over the stance foot
Terminal Stance	30-50%	-Begins with heel-rise of the stance foot	-Stable weight bearing -Further stride
Pre-Swing	50-60%	-Begins with heel-strike of contralateral limb	-Preparation for swing
Initial Swing	60-73%	-Begins with toe-off of the stance foot	-Foot clearance for limb advance -Limb advancement
Mid-swing	73-87%	-Begins when swing foot is opposite contralateral foot	-Foot clearance for limb advance -Limb advancement
Terminal Swing	87-100%	-Begins when swing tibia is vertical -Ends when foot strikes the floor	-Finish step length -Stance preparation

2.1.2 Function of the Leg in Gait

In normal gait, the leg performs four fundamental goals [5]:

1. Generate a propulsive force;
2. Provide upright stance stability through a continually changing posture;
3. Shock absorption during initial loading of the limb;
4. Conserve energy by minimizing the muscular effort of gait.

The knee plays a direct role in all four goals and is the main instrument in establishing stance stability and shock absorption.

2.1.3 Function of the Knee in Gait

The knee plays a fundamental role in the stability and mobility of the lower limb throughout the gait cycle. The knee joins the thigh and shank sections of the leg together. A small amount of knee rotation results in a large amount foot translation. Throughout the gait cycle, the knee is either flexing or extending, with both movements holding equal functional significance.

2.1.3.1 Knee Kinematics in Gait

The most important knee motions are in the body's sagittal or side plane of the body. Figure 2.2 shows sagittal knee joint angle, knee movement and muscle activation throughout the gait cycle.

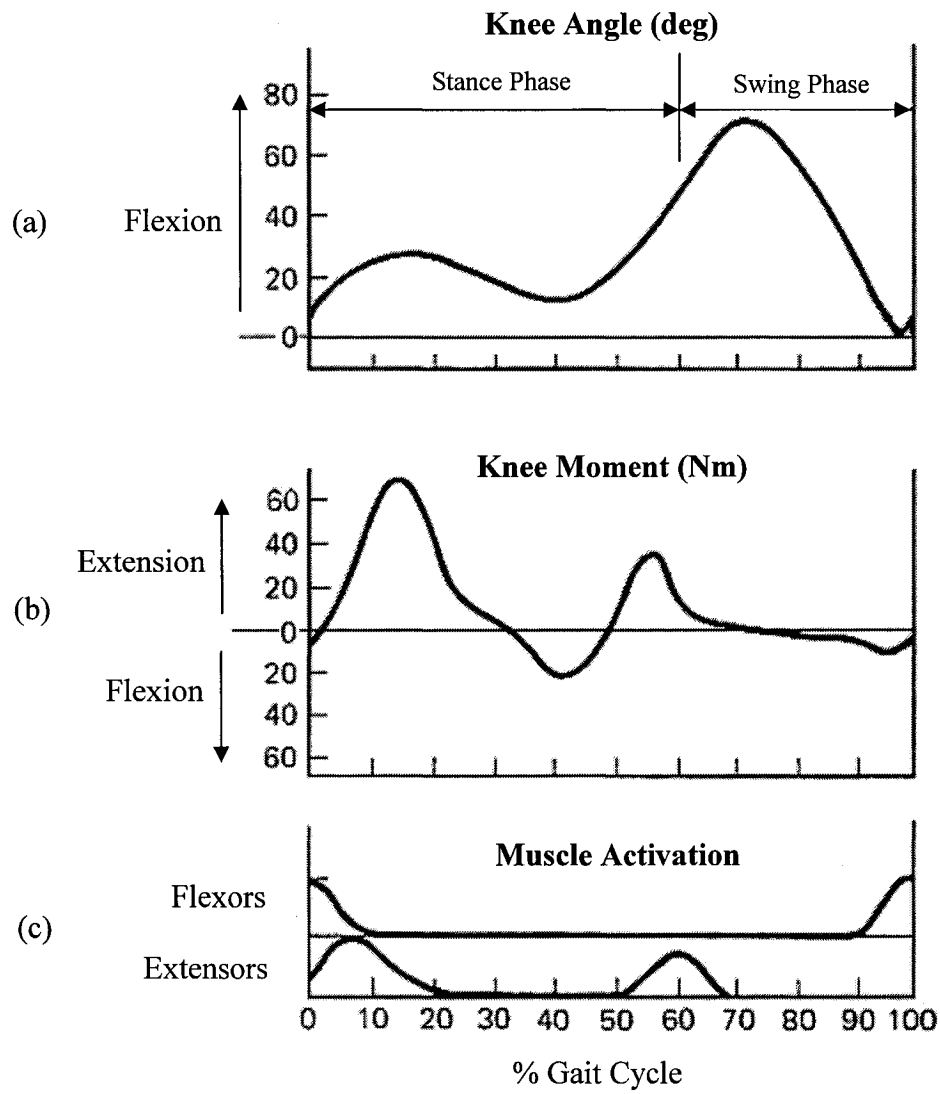

Figure 2.2 - Normal knee joint kinematics and kinetics: (a) joint angle; (b) joint moment; (c) knee extensor and flexor muscle activity (adapted from [8]).

The knee flexes and extends twice in a normal gait cycle – once in stance and once in swing. The knee first flexes during initial limb loading to absorb forces during weight acceptance, reaching a peak of approximately 20° flexion. Throughout mid-stance, the knee extends to near full extension. Nearing the end of terminal stance, the

knee prepares for swing and begins to flex again. Knee flexion is rapid once double limb support is achieved, flexing to 40° by toe off. Flexion peaks at approximately 70° in initial swing. In the later half of mid swing the knee begins to extend, reaching approximately 3° flexion just before the end of terminal swing. The knee finally falls into 5° of flexion before heel contact [5]. Knee angular velocity peaks at 350°/second during both flexion and extension in swing.

Knee movement also occurs in the transverse and frontal planes. The knee experiences up to 13° range of rotation in the transverse plane, rotating internally throughout swing and externally throughout stance. In the coronal plane, the knee rotates toward the midline, or abducts up to 8° in limb loading, returning to its neutral position during swing [5].

2.1.3.2 Function of the Knee in Flexion

As described earlier, the knee flexes twice throughout the normal gait cycle - once, during rapid loading of the lower limb and again in the early stages of swing. Knee flexion during limb loading is a shock absorbing mechanism to smooth the downward acceleration of the body's mass and alleviate high normal forces on the knee. In mid-stance, as the body passes over the weight-bearing leg, the knee remains slightly flexed from initial loading to reduce elevation of the body's center of mass as the body passes over the leg. Minimizing the vertical displacement of the body's center of mass during walking leads to a more efficient gait pattern that requires less energy expenditure.

Knee flexion in swing is greater than in stance so that the foot can clear the floor while swinging forward. In normal gait, the pelvis pitches in the frontal plane, dropping slightly downward on the side of the non-weight-bearing limb. This reduces the body's center of mass elevation as the body passes over the weight-bearing leg. Due to this pelvic drop in mid stance, the swinging leg becomes too long to clear the floor in mid swing. The knee therefore flexes to allow foot clearance [6].

2.1.3.3 Function of the Knee in Stance

The location, magnitude and direction of the ground reaction force on the foot, directs the magnitude and direction of the external moment acting on the knee. An external flexion moment on the knee sets the knee in a state of instability. The magnitude and direction of the ground reaction force changes continuously throughout the gait cycle as depicted in Figure 2.3.

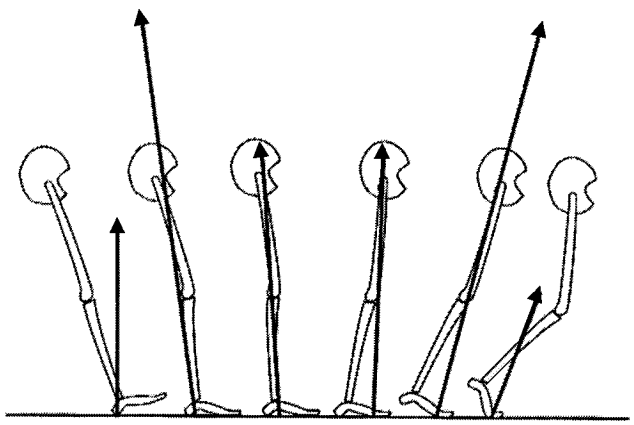

Figure 2.3 - Ground-reaction force vectors during gait. The arrows describe the magnitude and direction of the instantaneous ground reaction force vectors from initial contact to pre-swing. The magnitude of the ground reaction force is proportional to the length of the vector line (adapted from [5]).

When the ground reaction force vector is posterior to (behind) the knee-joint axis (Figure 2.4a), the knee is subjected to an external flexing moment that can flex the knee, placing it in a state of instability. When the ground reaction force vector is anterior to (in front of) the knee joint axis (Figure 2.4b), an external extension moment will act on the knee. In this case, the knee is in a stable state. The ground reaction force moves behind the knee joint axis into a state of instability twice throughout the gait cycle (Figure 2.3). A peak external flexion moment of 0.615 Nm/kg (mean plus one standard deviation) is reached during limb loading [7]. An opposing knee extension moment is therefore needed to prevent the knee from flexing during these periods of instability.

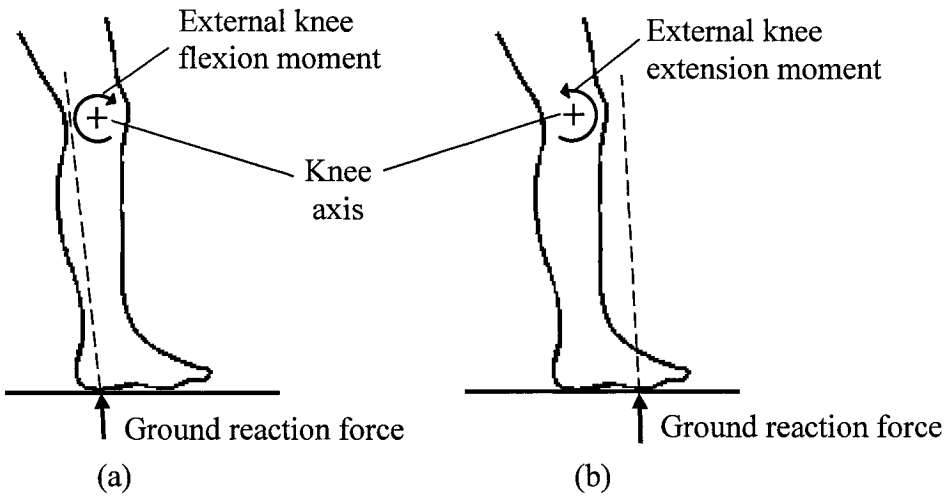

Figure 2.4– Stabilizing and destabilizing effect of the ground reaction force: (a) the ground reaction force positioned posterior to the knee axis creates a destabilizing external flexion moment on the knee; (b) the ground reaction force positioned anterior to the knee axis creates a stabilizing external extension moment on the knee (adapted from [8]).

2.1.3.4 The Knee Extensors

The knee extensors (quadriceps muscles) generate the internal knee extension moment necessary to prevent knee flexion during knee instability (Figure 2.5).

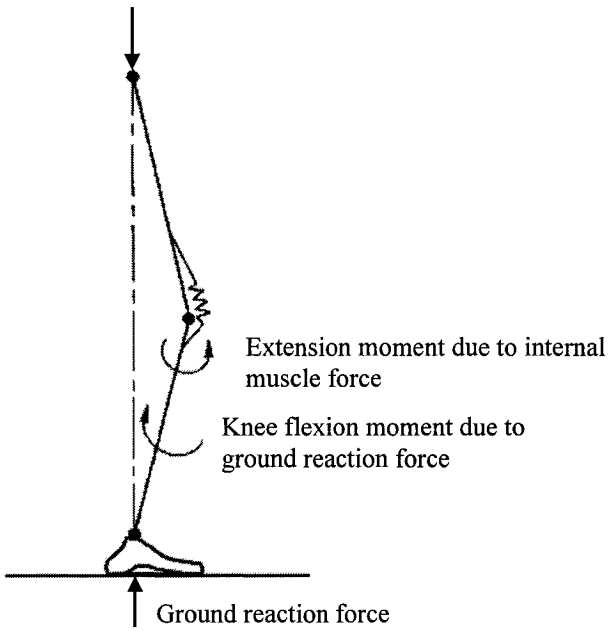

Figure 2.5 - The knee extensors, represented by the spring, generate an internal extension moment to counteract the external flexion moment created by the destabilizing ground reaction force (adapted from [8]).

Stance stability in limb loading is the chief role of the knee extensors in normal gait. The knee extensors act as shock absorbers, working eccentrically (exerting effort while extending) to resist knee flexion. The knee extensor muscles therefore absorb rapid loading of the limb. Following initial limb loading, the knee enters a stable state. Only at the end of terminal stance does the knee return to a state of instability. By this point, the opposite foot has made contact with the floor and accepts the transfer of body weight, reinforcing knee stability with double leg support. The knee extensor muscles are momentarily active at two other points in the gait cycle to prevent excessive flexion of the knee in pre-swing and to move the shank into complete knee extension in terminal swing.

The knee extensors are most often used to absorb load and eccentrically reduce knee flexion while the knee is flexing. In fact, the knee extensors have little to no role in extending the knee except for a brief push in terminal stance. Knee extension, shown in Figure 2.2a by a negative slope in the angle curve between 20%-40% and 75%-95% of the gait cycle, does not correspond with effort from the knee extensors, which occurs from 0%-20% and 50%-70% of the gait cycle, shown in Figure 2.2c. Other mechanisms such as gravity, inertia, and peripheral muscle effort, work to achieve extension of the knee in normal gait [5].

2.1.4 Kinematics and Kinetics of the Knee in Stair Walking

The kinematic and kinetic patterns of stair walking can be divided into similar phases of gait as those of level walking [9]. In stair walking, however, the range of knee angle and external moments are much greater [10]. The knee retains the same functional roles as in level walking; however, higher external knee moments place greater demand on the knee extensors. Riener et al. [9] reported mean external knee flexion moments (+1 standard deviation) reaching 1.2 Nm/kg in stair ascent and 1.5 Nm/kg in stair descent. Using only three subjects Marovich et al. [11] recorded mean external knee flexion moments (+1 standard deviation) peaking as high as 1.7 Nm/kg. External moments imposed on the knee are therefore 2 to 3 times larger than moments experienced in level walking. Maintaining the ability to walk stairs with relative ease and reliability is an

important quality of life issue [12]. Unfortunately, due to the large external knee flexion moments generated in stair walking, the activity can become unsafe or impossible for those inflicted with knee-extensor weakness [8].

2.2 Knee-Ankle-Foot Orthoses

2.2.1 Application of a Knee-Ankle-Foot Orthosis

Persons inflicted with weakness or absence of the quadriceps, lose the ability to confidently resist knee flexion while walking. If the knee extensors are too weak to resist knee flexion, the knee will collapse under a minimal external knee-flexion moment. Knee extensor weakness can result from spinal cord damage due to trauma, congenital abnormalities, aging or diseases such as polio, post-polio, muscular dystrophy or multiple sclerosis. Weak knee extensors foster insecure gait that is sensitive to external flexion moments that may cause the knee to collapse [8]. Total absence of knee-extensor muscle activity renders normal walking impossible [8]. In some cases, compensatory hip extension will allow the person to walk, however in an abnormal manner.

Individuals inflicted with weak or absent knee extensors can maintain constant knee stability in stance by influencing the ground reaction force to constantly remain anterior to the knee axis. A common method is to flex the trunk forward, thereby placing the body's center of mass constantly anterior to the knee joint axis and forcing the knee into a constant state of stability. Persons of light stature, inflicted with moderate unilateral quadriceps weakness, can sometimes use a Floor Reaction Ankle-Foot Orthosis (AFO) to inhibit instability of the knee [8] (Figure 2.6). This device keeps the ground reaction force in front of the knee axis through most of stance by inhibiting dorsiflexion of the foot. Dorsiflexion refers to foot rotation about the ankle pointing the toes upward or toward the body, while plantar flexion of the foot refers to foot rotation about the ankle pointing the toes downward or away from the body. Eccentric free-knee joint KAFOs position the orthotic knee joint axis posterior to the natural knee joint axis. The orthosis allows knee flexion at all times and the orthotic knee joint axis remains posterior to the ground reaction force through stance, ensuring a state of constant knee stability. However, this orthosis is applicable for a limited population as described above.

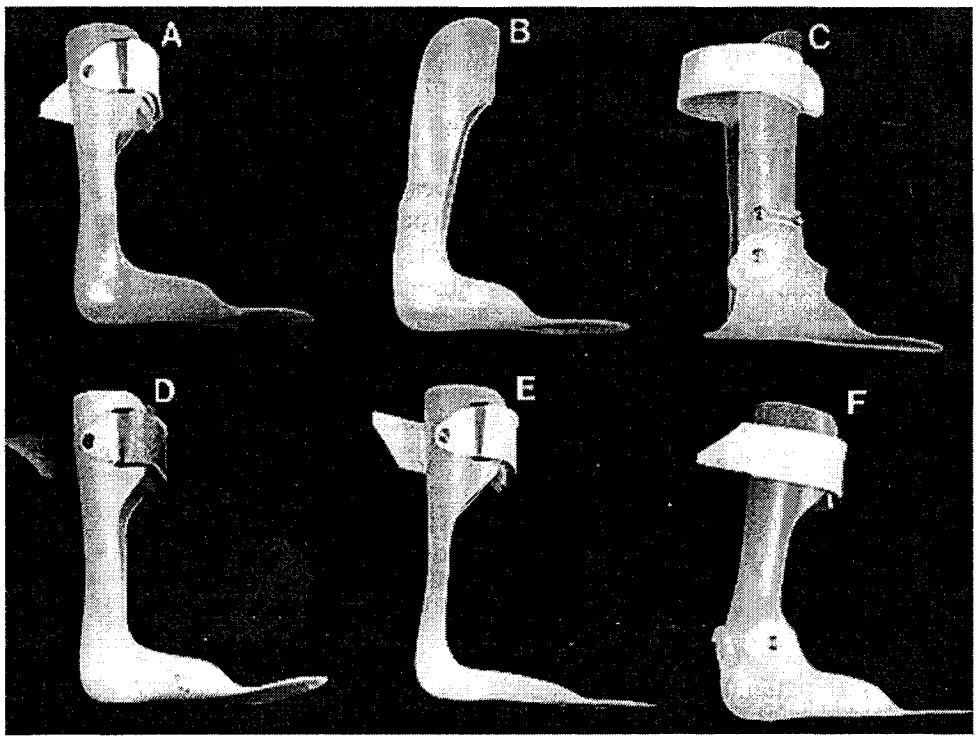

Figure 2.6 - Thermoplastic AFOs: (a) solid ankle; (b) floor-reaction; (c) articulated floor-reaction; (d) thermoplastic elastomer; (e) dorsiflexion-assist; (f) articulated [13].

Another method of maintaining knee stability involves applying an external extension moment to the knee to counter external flexion moments during periods of instability. Some individuals create a constant knee stabilizing moment in stance by using their hand to push back on the anterior (front) surface of their thigh. While effective, this method consumes excessive energy and can result in an unnatural gait pattern [8]. A device is usually required to inhibit or resist knee instability in stance.

Mild to severe cases of quadriceps weakness or absence usually require the application of a full leg brace to prevent the knee from collapsing. The most effective way to create a knee extension moment with a brace is to apply three reaction forces to the leg as shown in Figure 2.7. Reaction force Q_1 is ideally located posterior to the thigh, as proximal or close to the pelvis as possible and acting in the forward direction. Reaction force Q_2 is ideally located on the anterior side of the leg, as close to the knee joint axis as possible and acting in the backward direction. Reaction force Q_3 is ideally located posterior to the shank, as distal or far from the pelvis as possible and acting in the

forward direction [8]. These forces are achieved using knee-ankle-foot orthoses (KAFOs).

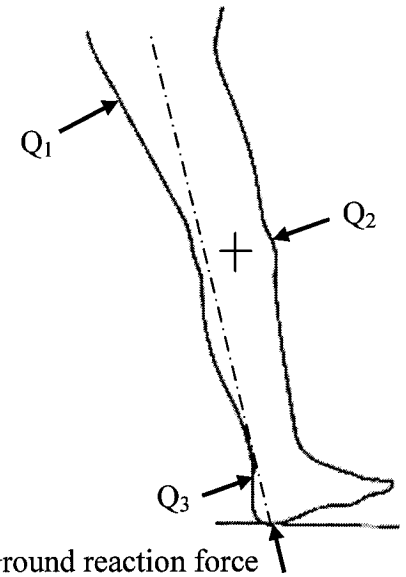

Figure 2.7 – Ideal reaction force positions to prevent knee flexion with a knee-ankle-foot orthosis (adapted from [8]).

2.2.2 Conventional Knee-Ankle-Foot Orthoses

A KAFO is often prescribed to obtain a stabilizing extension moment about the knee. A KAFO is a long-leg brace that locks the knee in full extension, counteracting any destabilizing forces in gait. Conventional KAFOs use metal sidebars, referred to as *uprights*, held to the lateral and medial sides of the thigh and shank by transverse leather cuffs or molded thermoplastic sections (Figure 2.8). Orthotic knee joints connect the orthosis thigh and shank segments. The joints lock the knee in fixed extension, offering minimal knee movement during ambulation. The orthotic knee joints can be manually unlocked to allow free knee movement for sitting.

Technicians typically use metal sidebars of aluminium or stainless steel, depending on the strength and weight requirements of the client. Depending on the client's condition, the KAFO may require control over the foot and ankle for effective function. If the KAFO does rely on concurrent ankle and foot control, or if the client has impaired ankle or foot function, an orthotic ankle or thermoplastic AFO (Figure 2.8a) may be used to control the ankle or foot [8].

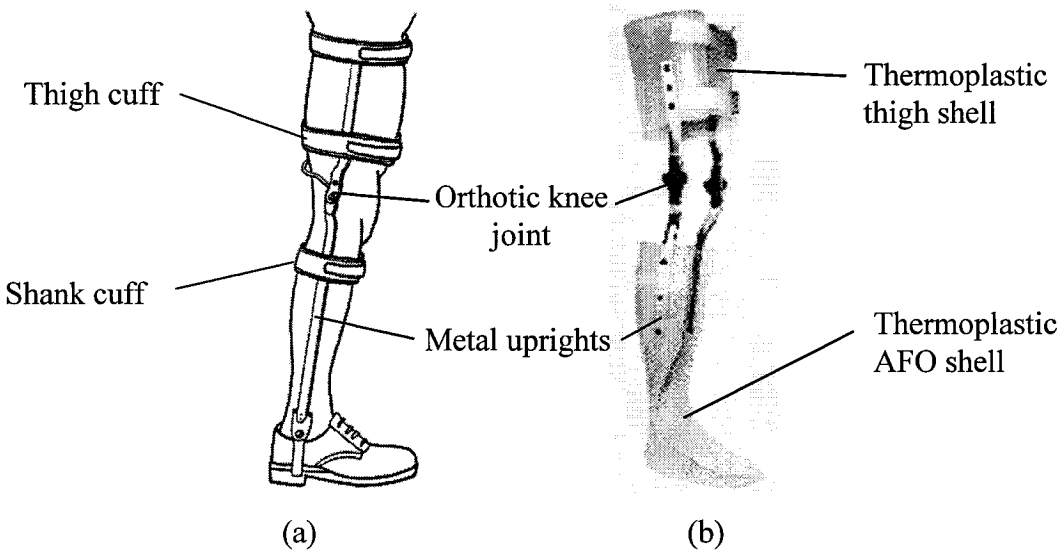

Figure 2.8 - Conventional KAFOs: (a) padded leather cuff design (adapted from [2]); (b) molded thermoplastic design (adapted from [14]).

When the knee is subjected to an external flexion moment, the rigid uprights and locked orthotic knee joints resist knee flexion by delivering an extension moment to the knee via the leather cuffs or thermoplastic sections. The locked orthotic knee joints are subject to substantial moments when resisting knee flexion. Body weight support is nearly completely transmitted through the natural legs with the KAFO accepting a negligible amount of load along the longitudinal axis of the uprights. KAFOs are therefore designed to primarily resist bending moments about the knee joint axis.

2.2.3 Disadvantages of Conventional Knee-Ankle-Foot Orthoses

The main disadvantage of the conventional KAFO is constant knee extension. Without the ability to flex the knee in gait, initial loading of the limb is more abrupt, disrupting the smooth progression of the body's center of mass. More importantly, due to downward pitching of the pelvis in swing, the leg becomes too long to clear the floor. To compensate for this situation, KAFO users must adopt abnormal gait patterns. Users often raise their pelvis on the side of the swinging leg to allow the leg to clear the floor. Other accommodative methods include swinging the leg forward around the side of the body, planter flexing the ankle of the opposite foot, or assuming an exaggerated lateral trunk sway [8]. These abnormal gait patterns can lead to soft tissue and joint dysfunction of the

hip and lower back, causing pain and loss of motion [3]. As well, walking with a fixed knee decreases gait efficiency by 24% [4] and using a conventional KAFO increases vertical displacement of the body's center of mass by up to 65% [15]. The associated increased muscular effort leads to higher energy expenditure [16] and early fatigue for the client during ambulation [4]. Surveys have shown that the increased energy demand from using a KAFO is one of the major reasons that KAFO rejection rates can range from 60% to nearly 100% [16].

Other quality of life issues associated with the conventional KAFO are the cosmetic implications of an unnatural gait and the inconvenience of reduced mobility. Without the ability to flex the knee, stairs and inclined surfaces are often insurmountable and even walking onto a curb poses a challenge. Walking with a fully extended knee also presents a potential threat should the client stumble, since the leg cannot flex to control the direction of the fall [17].

While standard KAFOs do foster a somewhat secure gait, the associated health and quality of life issues demand a better solution. A superior KAFO design is required - one that resists knee flexion during periods of unstable stance and allows uninhibited knee flexion in swing.

2.3 Functional Knee-Ankle-Foot Orthosis Designs

There have been several attempts to design a KAFO that provides knee support in stance and free knee motion in swing. These functional KAFOs are often referred to as Stance Control Knee-Ankle-Foot Orthoses (SCKAFOs). All designs are intended to benefit users with weak leg extensors, but require sufficient strength of the hip muscles to preserve forward progression in walking.

2.3.1 Gait Study Indications for Stance Control Knee-Ankle-Foot Orthoses

Based on discussions with clinical orthotists, an appreciable portion of the population using fixed-knee leg braces have sufficient hip strength to benefit from a KAFO that provides knee support in stance and free knee motion in swing. This includes

patients inflicted with multiple sclerosis, muscular dystrophy, polio, post-polio, incomplete spinal injury, unilateral leg paralysis/paresis, trauma, congenital defects, and isolated quadriceps weakness or absence.

A limited number of studies have suggested that lower limb braces that allow uninhibited knee motion in swing, promote improved gait kinematics and greater gait efficiency than conventional KAFOs. McMillan et al. [3] analyzed the gait patterns and heart rates of three subjects with lower limb weakness walking with a SCKAFO built by Horton Technology Inc. The subjects participated in a series of gait analysis, obstacle course and treadmill trials. The study reported faster walking speeds, longer strides, less compensatory movements, increased mobility and more symmetrical gait patterns than walking with a fixed-knee KAFO.

Lehmann et al. [18] investigated the effects of a SCKAFO on the oxygen consumption of two able bodied subjects and two patients with spinal-cord lesions. Significant energy savings were reported for able-bodied subjects for ambulation rates at or above 73 m/min (normal walking speed). Both disabled subjects showed little improvement in energy expenditure, since they did not have sufficient muscle strength to adequately flex their knee in swing or sufficient hip flexor strength to reach normal walking speeds.

Kaufman et al. [16] studied the effect of their wrap-spring SCKAFO on the gait and energy cost of a single poliomyelitis victim. An examination of the subject's gait patterns and oxygen consumption revealed an improvement in knee motion and metabolic energy requirements when wearing a SCKAFO compared to a conventional KAFO.

Although each of the studies dealt with four test subjects or less, all indicated an improvement in mobility walking with a brace that allowed uninhibited knee motion in swing over walking with a fixed-knee KAFO.

2.3.2 Previous Attempts at Designing a Stance Control KAFO

Numerous attempts have been made over the past century to design a practical SCKAFO. Records of early designs exist mainly in patents and journal articles. Until 2002, no single design was developed that could deliver the function and compact structure required of a practical SCKAFO. Since January 2002, four SCKAFOs have been released on the market [19]; however, all four designs suffer from inherent limitations. To design an improved SCKAFO that addresses the limitations of commercial SCKAFOs, a thorough investigation of existing SCKAFO designs and past design attempts was carried out.

2.3.2.1 Impingement Lock

Harris [20] developed a dynamic knee orthosis that unlocked when the wearer achieved a pre-selected dorsiflexion angle of the ankle, followed by a pre-selected plantar flexion angle of the ankle. The automatic locking knee joint used impingement to lock the knee by incorporating a complex linkage system of levers and springs. The design was highly impractical, because it required the patient to make specific ankle movements during the gait cycle to engage the knee lock. People with fused, deformed or spastic ankles cannot use a brace that relies on ankle motions to engage and disengage the locking mechanism. Dynamic knee joints that rely on impingement are often prone to jamming and require large disengagement forces to unlock the knee if any external knee moment is present [21]. This orthosis would not be suitable for standing or stumbling as achieving the required ankle angle would be difficult.

2.3.2.2 Roller-Clutch

Harrison et al. [22] developed a prototype SCKAFO knee joint based on a roller-clutch design (Figure 2.9). As is common to most roller-clutches, the rollers are contained in a cage to promote simultaneous wedging of all the rollers. The knee joint design connected a control arm to the roller cage. Actuation of the control arm would position the cage to hold the rollers at the wide end of their respective wedge-shaped chambers. The rollers would therefore be prevented from contacting both the inner and outer race of the clutch, thus inhibiting them from locking up. Pivoting the cage back to its original

position, via the control arm, would return the rollers to their intended duty of providing unidirectional rotation of the concentric races. The roller-clutch joint could provide uninhibited movement during swing and unidirectional motion during stance. Unfortunately, the joint had an excessively thick profile, and the rollers were prone to jamming into the wedges and therefore required an impractically high disengagement force that tended to deform the cage.

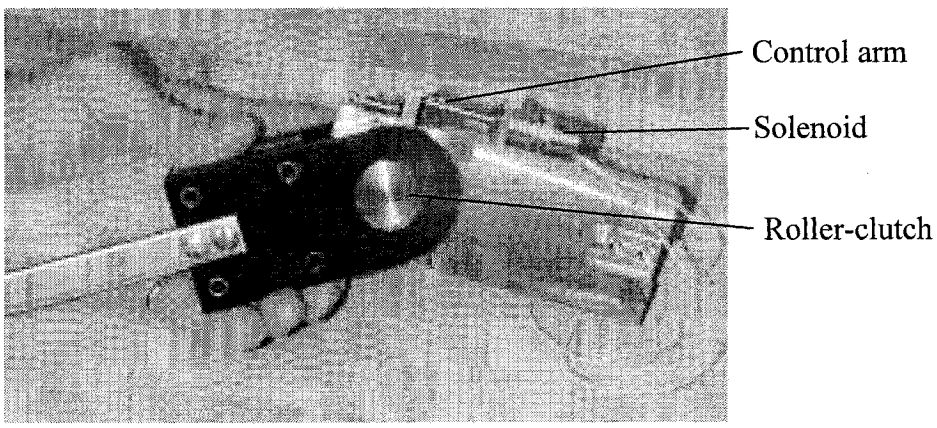

Figure 2.9 - The Rehabilitation Centre's Roller-clutch Knee-Joint prototype [22].

2.3.2.3 Wedge-Joint

As a second effort, Harrison et al. [22] developed a wedge-joint model (Figure 2.10). The wedge-joint model used a solenoid-actuated wedge that lodged itself into the rear space of a polycentric knee joint during stance, thus allowing extension while preventing flexion. During swing, the solenoid would retract the wedge from the joint space and allow free extension and flexion. An excessive amount of force was needed to retract the wedge from the joint space. The wedge also experienced substantial plastic deformation due to the high, localized loads endured while preventing flexion.

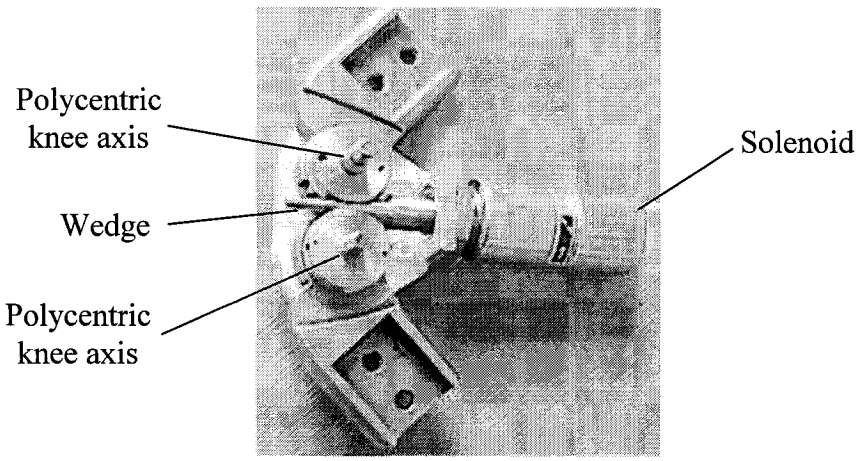

Figure 2.10 - The Rehabilitation Centre's Wedge Knee-Joint prototype [22].

2.3.2.4 Lever-Lock Joint

As a third design, Harrison et al. [22] developed and tested a lever-lock knee joint design (Figure 2.11). The lever-lock design consisted of a ring attached to the lower portion of the orthosis that rotated freely through a hole made in an actuation bar, connected to the upper portion of the orthosis. While the hole remained perpendicular to the ring's tangent, the joint allowed rotation in both directions.

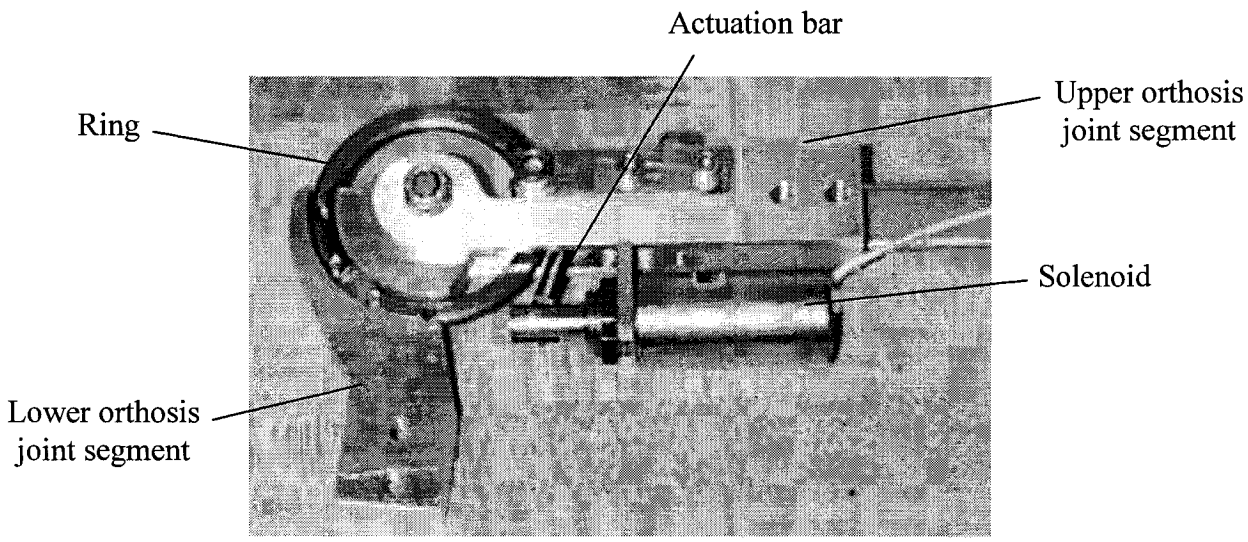

Figure 2.11 - The Rehabilitation Centre's Lever-Lock Knee-Joint prototype [22].

When the solenoid pivoted the actuation bar, the hole in the bar would sit at an angle to the ring and the ring would jam to prevent flexion. Along with being potentially

expensive to manufacture, the joint sliding action was too rough and the ring was subject to scoring under medium loads.

2.3.2.5 Hydraulic Foot Switch

A hydraulic-based, automatic locking knee device was designed by the University of Toledo [23]. The joint system consisted of a hydraulic fluid-filled bulb positioned below the heel, attached to a hydraulic line running to the knee and attached to a piston that engaged and disengaged the knee locking mechanism. At heel strike, the bulb was compressed and the displaced hydraulic fluid would extend the piston to engage the lock. At heel off, the bulb relaxed and the piston would fall downward to disengage the lock. The mechanism required full knee extension to lock. This requirement did not provide security for climbing stairs or walking on uneven ground.

2.3.2.6 Thrust Brake

Weddendorf [24] of the National Aeronautics and Space Administration (NASA) designed a friction-based, automatic-locking, orthotic knee device (Figure 2.12). At the knee joint, two bevelled, serrated brake plates were fixed to the lower portion of the orthosis. The plates were positioned against either side of a bevelled shoe, fixed to the upper portion of the orthosis. The lower portion of the orthotic joint could move up and down relative to the upper portion at the knee joint. A spring at the knee joint kept the serrated brake plates and the bevelled shoe vertically separated. Loading the knee joint at heel strike thrust the lower portion of the orthosis toward the upper portion, pushing the serrated brake plates into the bevelled shoe. This action jammed the shoe between the sandwiching plates. Releasing the body weight at heel-off allowed the spring to separate the brake plates from the sandwiched shoe. Disadvantages of this design included the inability of the knee joint to allow extension during stance, potential jamming issues, and wear of the bevelled shoe and brake plates from repeated use.

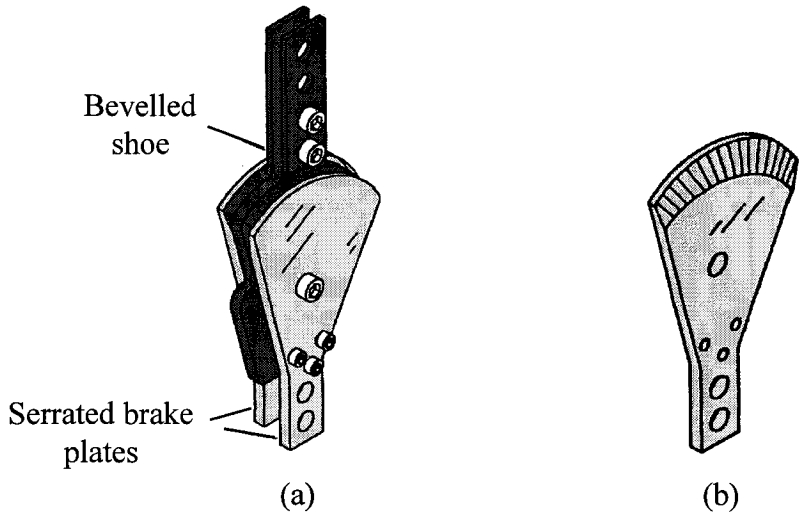

Figure 2.12 – NASA's thrust brake knee joint that consisted of (a) a beveled shoe and two sandwiching serrated brake plates; (b) an isolated view of a serrated brake plates (adapted from [24]).

2.3.2.7 Intelligent Brace II

Researchers at the International University for Women in Osaka, Japan developed a dynamic knee joint that incorporated a band brake to inhibit knee flexion [25] (Figure 2.13). The Intelligent Brace II (IB-II) had a rotary encoder to detect knee angle and a heel contact switch that activated the band brake in stance. An onboard microcomputer calculated the optimal braking force to be imparted to the knee via a stepping motor.

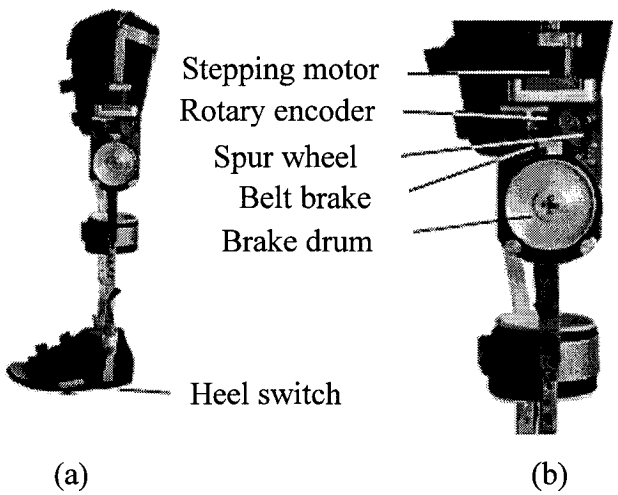

Figure 2.13 – The Intelligent Brace II shown in (a) full view; (b) close-up view of knee joint (adapted from [25]).

Weighing 3.7 kg (8.2 lbs), the IB-II was too heavy for practical application. Discussions with certified orthotists suggest that a practical SCKAFO must weigh less than 2.3 kg (5 lbs.).

2.3.2.8 Cone Brake

Myers [26] of NASA developed an orthotic knee joint that used a cone brake to resist excessive knee flexion in stance. Unfortunately, the mating surfaces of the brake experienced excessive wear with repeated actuation [27]. Another major limitation of the joint was its inability to allow knee extension in stance mode.

2.3.2.9 Conical Roller-Clutch

Myers [27, 28] of NASA developed a releasable conical roller-clutch knee joint with tapered, conical races (Figure 2.14). The conical clutch geometry allowed the joint to disengage by pulling the inner race axially away from the outer race. Separation of the concentric races eliminated the possibility of roller jamming between the races. Forcing the races together in the axial direction allowed the mechanism to function as a conventional roller-clutch. A cam positioned between the races and connected to a heel-strike mechanism beneath the foot controlled the relative position of the inner race.

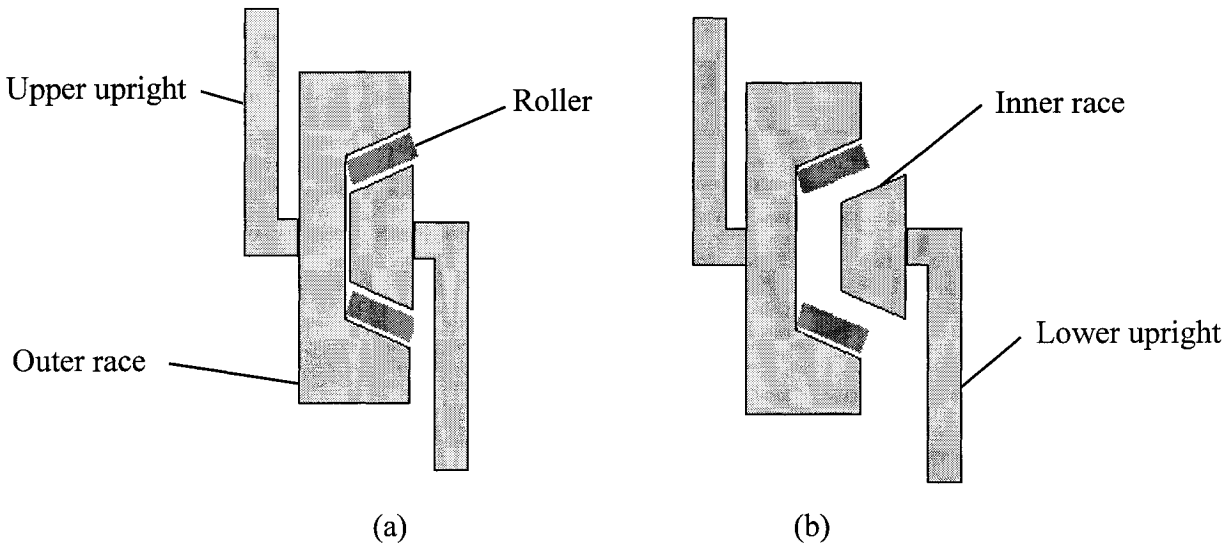

Figure 2.14 – A drawing of the conical roller-clutch cross-section showing its function. (a) When the conical inner race is brought into contact with the rollers, the joint functions as a conventional roller-clutch; (b) a pushrod-driven cam pushes the conical inner race out of contact with the rollers to allow free knee rotation in both directions.

Horton Technologies Inc. investigated the feasibility of the design and found that the relatively poor manufacturability of the joint rendered the design impractical for commercial development.

2.3.2.10 Elastic Knee Joint

Kofman et al. [29] used an elastic cord to allow resisted knee flexion in stance and uninhibited knee movement beyond 25° of knee flexion. The pre-stressed elastic cord was attached across the knee joint, anchored on the upper and lower sections of the KAFO. The eccentric knee joint was positioned posterior to the line of force of the elastic-tightened cable (Figure 2.15a). Knee joint eccentricity provided a greater knee extension moment due to the increased distance between the knee joint axis and the cable's line tension. Knee flexion was resisted by an extension moment created by the tension in the elastic-tightened cable.

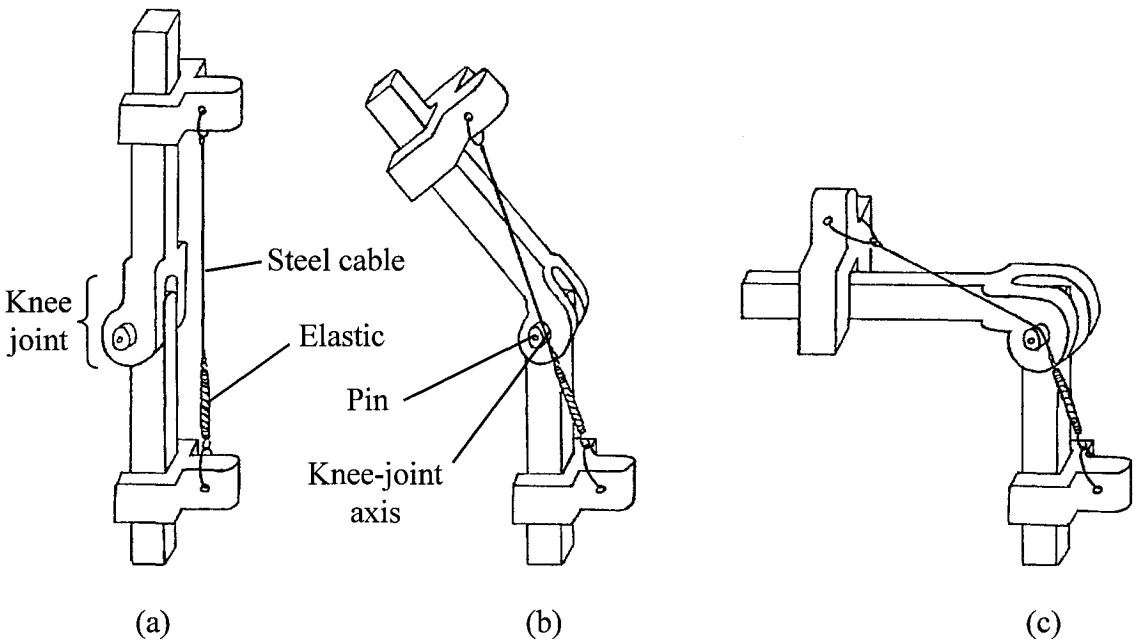

Figure 2.15 – The spring-loaded knee joint mechanism with (a) the joint in full extension, (b) the knee joint at 25° knee flexion (moment=0), and (c) the knee joint beyond 25° knee flexion (moment=0) [29].

When the knee was brought to 25° flexion (Figure 2.15b), the distance between the line of force of the cable and the knee-joint axis was zero, resulting in an external knee moment of zero. Further flexion of the brace beyond 25° caused the steel cable to

wrap around a pin protruding from the knee axis (Figure 2.15c). The pin held the cable's line of force at the knee axis, maintaining a zero external extension moment. This functionality also allowed for uninhibited knee flexion while sitting.

In theory, loading the braced limb would not cause the knee to flex beyond 25° in stance because the elastic cord would provide a stabilizing extension moment throughout stance. The elastic cable design was able to provide some knee flexion in early stance, as observed in able-bodied gait [29]. In terminal stance the knee would flex beyond 25° in preparation for swing. The external extension moment would disappear beyond 25° knee flexion allowing uninhibited movement of the knee in swing.

Since the design required a straight line of action for the cable and the spring, large spacers were required to anchor the orthosis uprights to the AFO component (i.e., the orthosis uprights could not follow the curvature of the limb). This made the device bulky medial-laterally. The brace was designed for children. Designing the brace to accommodate the higher knee moments generated by adults would have required even bulkier spring attachments.

2.3.3 Ongoing Design Projects

2.3.3.1 Wrap-spring Clutch

San Diego State University developed a SCKAFO that integrated a conventional unidirectional clutch into the joint [16, 21]. The orthosis was electro-mechanically actuated using pressure sensors beneath the heel and forefoot to detect heel strike and heel rise. An onboard microprocessor was used to interpret signals from the pressure sensors and control a solenoid that engaged and disengaged a wrap-spring clutch built onto the knee joint.

The wrap-spring clutch (Figure 2.16) used a close-wound helical spring to transmit torque across a pair of mating concentric clutch hubs. When the knee attempted to flex, the spring tightened over both concentric hubs, thus preventing knee flexion by stopping relative motion between the two hubs. Knee extension caused the spring to

unwind and allow relative motion of the two hubs. To selectively disengage the clutch in swing, the spring was loosened by pulling back on one end of the spring, called the control tang, via a solenoid.

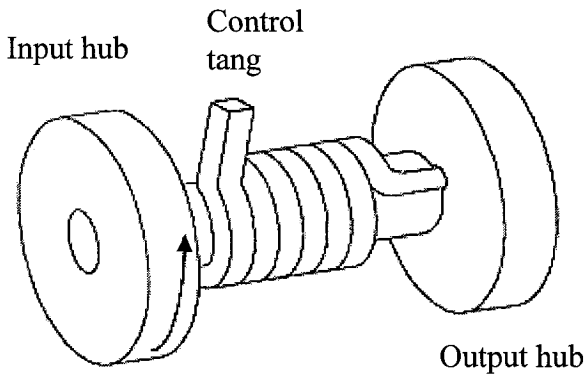

Figure 2.16 – An isolated view of the wrap-spring clutch (adapted from [21]).

Clinical testing was in progress to determine the effectiveness of the electromechanical orthosis compared to conventional KAFOs. The excessive profile of the device and significant bulk, however, may limit the orthosis' practicality.

2.3.4 Commercial Stance Control Knee-Ankle-Foot Orthoses

Four commercial SCKAFOs have been released on the market, each one incorporating a very different locking mechanism.

2.3.4.1 Otto Bock Free Walk/Becker UTX

Manufactured by two different companies under two different names, the Free Walk and UTX share the same ratchet/pawl design [30] (Figure 2.17). A compression-spring-loaded pawl locked the knee automatically when the knee achieved full extension prior to heel strike (Figure 2.17a). A 10° ankle dorsiflexion angle caused a control cable, connected to the pawl, to be pulled down and disengage the lock. Simultaneous hyperextension of the knee with the 10° dorsiflexion was required to eliminate any flexion moment about the knee and free the pawl from friction for disengagement (Figure 2.17b).

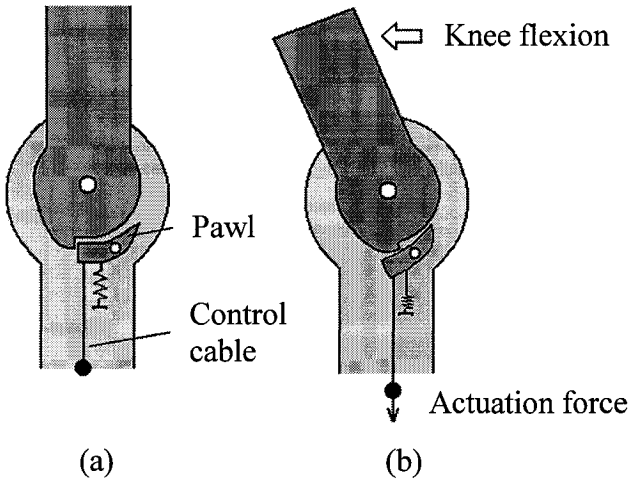

Figure 2.17 – The Otto Bock Free Walk Stance Control System/Becker UTX. (a) A spring-loaded pawl locks the knee from flexion when full knee extension is attained. (b) Dorsiflexion of the foot at the end of stance pulls on a control cable connected to the pawl to disengage the lock for swing.

The main disadvantage of this design was that full knee extension was required to engage the knee flexion lock before weight bearing. Therefore, the brace provided no support if the knee was in a state of flexion when the leg was loaded, a common event in walking stairs, inclines, uneven ground, or in stumbling and relaxed standing. This SCKAFO did not practically serve many potential SCKAFO clients that may be too weak to fully extend their leg while walking. Since the disengagement mechanism required 10° dorsiflexion, the device cannot be used for patients with fused, deformed and spastic feet. The Free Walk/UTX is the lightest and most cosmetically attractive of all commercial SCKAFOs, however, the delicate tubular steel structure was unappealing to clients who felt they needed more support [49].

2.3.4.2 Horton's Stance Control Orthosis

Horton Technology Inc. produced Horton's Stance Control Orthosis (Figure 2.18). The locking mechanism was modeled after a standard unidirectional clutch design and involved an eccentric cam that jammed into a friction ring attached to the upper knee joint (Figure 2.19a). A thermoplastic stirrup shell was positioned just below the thermoplastic AFO shell. The thermoplastic stirrup travelled along the length of the brace and was attached to a pushrod that was attached to the eccentric cam.

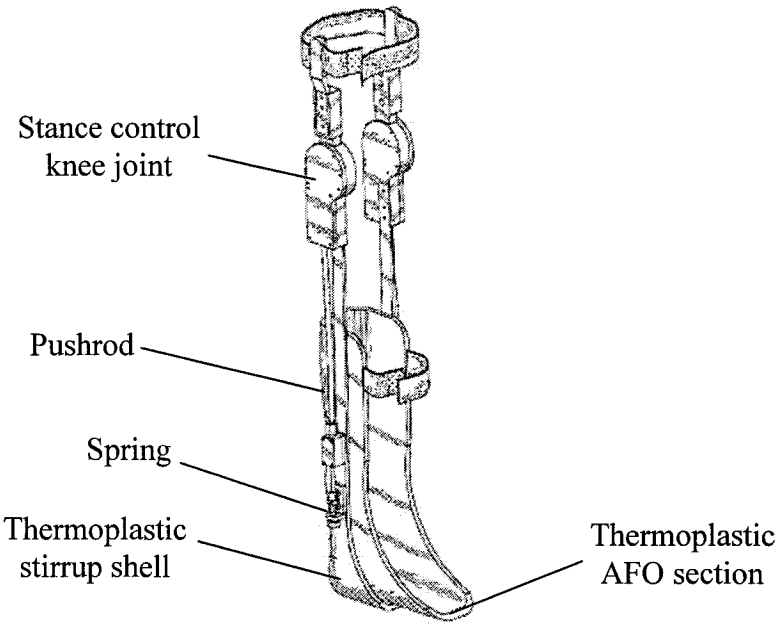

Figure 2.18 – Horton's Stance Control Orthosis (adapted from [32]).

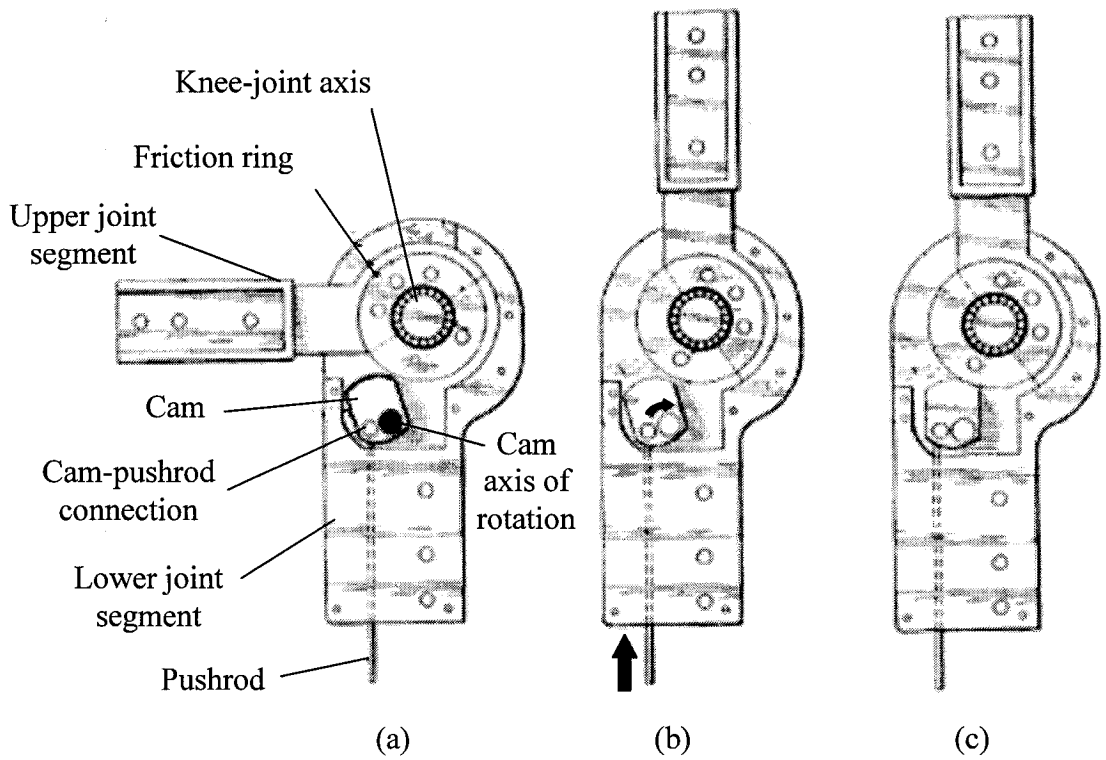

Figure 2.19 – A cross-sectional view of the Horton Stance Control locking mechanism. (a) The unlocked joint in 90° knee flexion. (b) Foot pressure drives the pushrod upward and positions the cam to resist any knee flexion. (c) The cam jams into the friction ring with knee flexion, but is pushed clear in knee extension (adapted from [32]).

Heel contact pushes the stirrup upward to engage the pushrod and drive the cam into the upper joint head (Figure 2.19b). The surface of both the steel cam and steel friction ring were textured with micro-grooves. These grooves eliminated slipping between the friction ring and the cam. When the cam was engaged (Figure 2.19c), knee flexion caused the friction ring to pull the cam into itself, thereby locking the joint. Knee extension pushed the cam away from the friction ring, allowing uninhibited knee extension. Once heel contact ceased, a spring pushed the pushrod down, the cam disengaged, and the knee was allowed to move freely. A hyperextension moment about the knee was required to eliminate any impinging force on the cam and allow the joint to disengage freely. The Horton Stance Control locking mechanism could also be outfitted on a KAFO with a free moving ankle. In this case, the pushrod was attached to the heel. Whenever the foot planterflexed (pointing toes downward), the cam was pushed upward to engage.

The orthosis as a whole was somewhat bulky [33] and the joints themselves were relatively large and heavy by KAFO standards, weighing 365 grams with a medio-lateral profile of 2.3 cm. While Horton's Stance Control Orthosis does have the ability to lock at any knee angle, the major downfall lies in the weight and bulk of the orthosis, which will not be tolerated by many users.

Both mechanical actuation methods for the Horton Stance Control Orthosis have their shortcomings. Objects can become lodged between the foot and the stirrup, such as clothing, a sock or debris from walking outdoors. The bulky thermoplastic foot shell may prevent the user from donning a shoe because the shoe may severely affect the performance of the stirrup mechanism and the free ankle option cannot be used for clients with fused, deformed or spastic feet. Due to inherently high local stresses, the cam is subject to wearing, leading to sloppy engagement of the knee lock; however, this problem can be serviced.

2.3.4.2.1 The Smart Knee

In response to the limitations of the mechanical actuation methods of the Stance Control Orthosis, Horton Technology Inc. had planned to release the Smart Knee - an electromechanical orthosis that used the same locking mechanism as Horton's Stance Control Orthosis but replaced the stirrup and pushrod with pressure sensors below the foot and solenoids to actuate the lock [34]. The Smart Knee was to be released in 2003, but weight and cost issues prevented its commercial release. The addition of solenoids to an already bulky orthosis design resulted in an excessively heavy orthosis. As well, the integration of an electronic control system moved the orthosis out of the practical price range to compete on the market. A SCKAFO joint that is relatively easy and inexpensive to manufacture could afford to integrate an electronic control system into its design and still be sold at a practical price.

2.3.4.3 The Fillauer Swing Phase Lock Orthosis

Basko Healthcare has developed a gravity actuated knee joint locking mechanism for its Swing Phase Lock orthosis distributed by Fillauer. As shown in Figure 2.20, a weighted pawl falls in and out of locking position, depending on the user's hip angle.

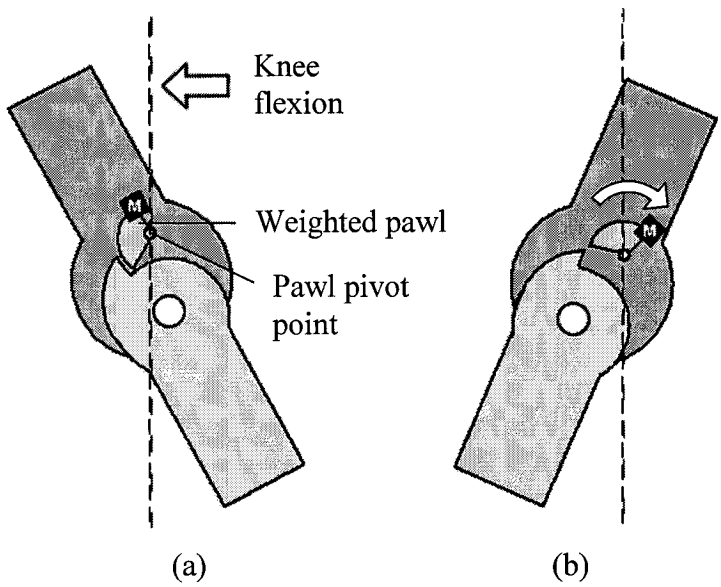

Figure 2.20 – A simplified illustration of the gravity activated Stance Phase Lock. (a) When the thigh is anterior to the user's body and the knee is fully extended, the weighted pawl falls into the locked position; (b) with the thigh posterior to the user's body and a knee hyperextension moment, the pawl falls out of engagement.

When the hip was flexed with the thigh anterior to the body, as in terminal swing, the weighted pawl fell into the locked position to prevent knee flexion (Figure 2.20a). The knee must be fully extended for the pawl to fall into this locked position. When the hip swung behind the body, prior to swing, the weighted pawl fell out of engagement and the knee was allowed to flex freely (Figure 2.20b). A hyperextension knee moment was required to eliminate impinging forces on the pawl and allow the pawl to fall out of engagement freely. The hip angle required to engage and disengage the pawl was manually set on the joint head by an orthotist. Only one Swing Phase Lock was mounted on the KAFO. The second orthotic knee joint, mounted on the medial side of the KAFO, was a simple mechanism that used friction and a spring to regulate knee flexion in the swing phase [35].

As the locking mechanism was position dependent, this approach was not effective for climbing stairs or walking on uneven ground. The joint only locked with full knee extension. This requirement limited where the patient can walk and provided no support if the patient stumbled in mid-step.

2.3.4.4 Becker Orthopedic 9001 E-Knee

Becker's 9001 E-Knee used a magnetically activated one-way dog clutch (Figure 2.21). The joint integrated two ratchet plates that were spring biased apart. One of the ratchet plates was positioned within an electro-magnetic coil. When pressure sensors below the foot detected foot contact, the electro-magnetic coil was energized and the ratchet plates were forced together. When engaged, the ratchet plates allowed relative angular motion in only one direction. In stance, knee flexion was resisted while knee extension was still allowed. Ratchet devices suffer from two inherent disadvantages, noise and a limited number of locking positions. Like a household ratchet tool, the 9001 E-Knee generates a clicking sound when rotated under engagement. The joint will therefore generate an unnatural ratchet sound whenever the user extends their knee in stance. This is a serious limitation for the 9001 E-Knee. Cosmetics are equally as important as function to KAFO users. If an orthosis looks or sounds unnatural, it will draw unwanted attention to the user and the orthosis may simply not be used.

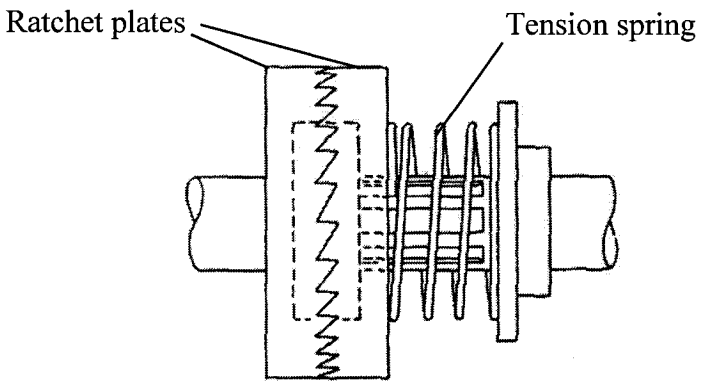

Figure 2.21 – An illustration of a one-way dog clutch. The 9001 E-Knee integrates a dog clutch into its design where the ratchet plates are spring loaded to separate. A surrounding electromagnetic coil works against the spring to engage the plates in stance (adapted from [36]).

Unlike most friction-based clutches, a ratchet device only has a finite number of locked positions. The 9001 E-Knee houses 60 ratchet teeth, thereby allowing up to 6° of free-fall knee flexion before the joint settles into the locked position. Users that require the confidence of a rapid engaging knee lock may not tolerate this lack of support.

The 9001 E-Knee's biggest drawback is its size, weight and cost. Measuring approximately 24 mm thick, the 9001 E-Knee has a significant profile that can be obtrusive and adversely affect the cosmetic appeal of the orthosis. The electromagnetic coil contributes to make the 9001 E-Knee the heaviest of all SCKAFO joints on the market. The excessive weight of the joint places an unnecessary burden on the user that would likely increase energy expenditure during ambulation and lead to premature exhaustion. The 9001 E-Knee is the most expensive of all SCKAFO joints, costing nearly double the price of other commercial SCKAFO joints.

2.4 Review of Relevant Technologies

The main functions of an ideal dynamic knee joint for KAFO users with knee extensor weakness would be to allow free knee extension while resisting flexion in stance and permit free knee rotation in swing. The following is a review of mechanisms that provide similar function and technologies that may inspire the development of a device with the desired function.

2.4.1 Stance Control Technologies in Lower Limb Prosthetics

There are considerable differences in the design constraints of prosthetic and orthotic knee joint mechanisms [17]. Prostheses replace an absent body part while KAFOs support an existing body part. Lower limb prostheses have the convenience of housing heavier mechanisms because the absent mass and volume of an amputated leg can be exploited. KAFOs add weight and bulk to an existing limb and have to resist knee moments similar to those experienced by lower limb prostheses. Mass and size are therefore critical in the design of orthotic devices. Stance-swing control functions, also critical in prostheses, have been available in lower-limb prostheses for decades. Three different mechanisms have been employed to achieve stance-swing control: friction-brakes, linear hydraulic cylinders and a rotary hydraulic cylinder.

2.4.1.1 Friction-Brake

The *friction-brake* stance control prosthesis is the simplest form of prosthetic knee brake. The design uses a spring-loaded external drum brake integrated into a single axis knee joint. In stance, body weight forces the brake shoe against the drum to lock the knee. While mechanically simple, the friction-brake knee carries with it several disadvantages. The frictional nature of the brake leads to wearing of the brake surfaces, requiring regular servicing. The brake is also unable to support full body weight in extreme knee flexion [37]. Since the loaded knee is locked throughout weight bearing, inefficient gait results from the lack of knee flexion in pre-swing [17]. This braking mechanism cannot be applied to a KAFO since the brake requires a substantial amount of force to lock effectively. On lower limb prostheses, engagement of the friction brake requires the entire body weight of the user to be transmitted through the knee joint during stance. Most KAFOs support little of the user's body weight through the uprights and knee joint; therefore, no substantial force is available to engage the brake.

2.4.1.2 Linear Hydraulic Cylinders

Linear hydraulic and pneumatic cylinders have been used in transfemoral prosthetics for over four decades. The cylinder is mounted posterior to the knee joint and connected to the thigh section and tibial section of the prosthesis (Figure 2.22). This

mounting configuration transforms moment resistance at the knee into linear resistance in the cylinders. Hydraulic and pneumatic knee cylinders are complex mechanisms, incorporating two pistons. Both types of cylinders provide stiff resistance to flexion during stance. For some products, hyperextension of the knee for approximately 0.1 seconds during terminal stance triggers the cylinder to allow uninhibited knee motion in swing.

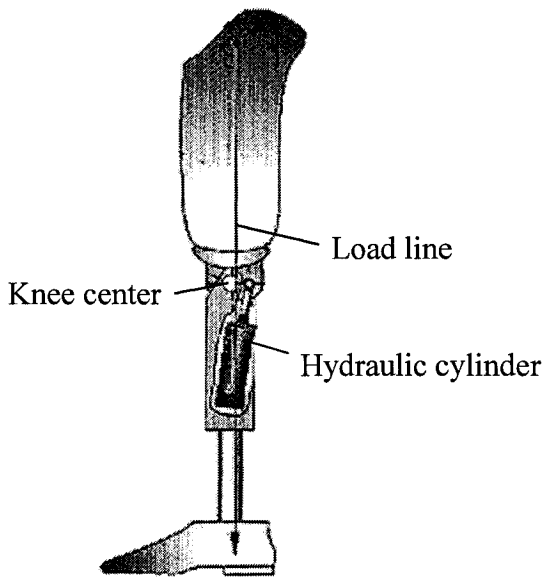

Figure 2.22 – A typical transfemoral prosthesis integrating a linear hydraulic cylinder.

The computer-controlled transfemoral prosthesis is the newest class of prosthetic knee technology to reach the market. An on-board microprocessor controls knee stiffness by controlling the flow rate of the hydraulic fluid within the system's hydraulic cylinder. Current designs control fluid flow via servo-valves or, in the case of designs using magneto-rheological fluid, by applying a magnetic field to the fluid. On-board sensors read the user's level of activity and adjust the stiffness of the hydraulic cylinder accordingly to obtain optimal knee kinematic performance and stance control.

The major drawback of fluid filled devices is that they are relatively heavy and expensive [37]. Hydraulic prosthetic devices also tend to leak, requiring more frequent maintenance [38]. Pneumatic devices are less prone to leakage problems. A major disadvantage in both hydraulic and pneumatic prosthetic technologies is that they are too

big to install directly onto a KAFO. A typical cylinder measures approximately 3.5 cm in diameter and 15 cm in length. Installing such a relatively large cylinder on a KAFO would result in an excessively heavy and bulky brace.

2.4.1.3 Rotary Hydraulic Piston

The 3R80 Modular Single-Axis Knee Joint with rotary hydraulic stance and swing control is a relatively new design developed by Otto Bock. Unlike linear cylinder designs, the 3R80 is weight bearing activated and does not have the disadvantage of relying on knee extension to switch between stance and swing modes [40].

The central component of the joint is the piston vane. The piston vane is fixed to the proximal or upper segment of the knee joint while the hydraulic chamber is fixed to the distal or lower joint segment. The rotary axis of the piston vane is the same as the rotary axis of the knee joint. The piston vane divides the hydraulic chamber into two sections – the extension chamber and the flexion chamber (Figure 2.23). The chambers are connected to each other via two channels – an extension channel and a flexion channel. Each channel contains a one-way valve. When the knee flexes, the piston vane sweeps counter-clockwise and the hydraulic fluid in turn moves counter-clockwise through the flexion channel, blocked from the extension channel by a one-way valve.

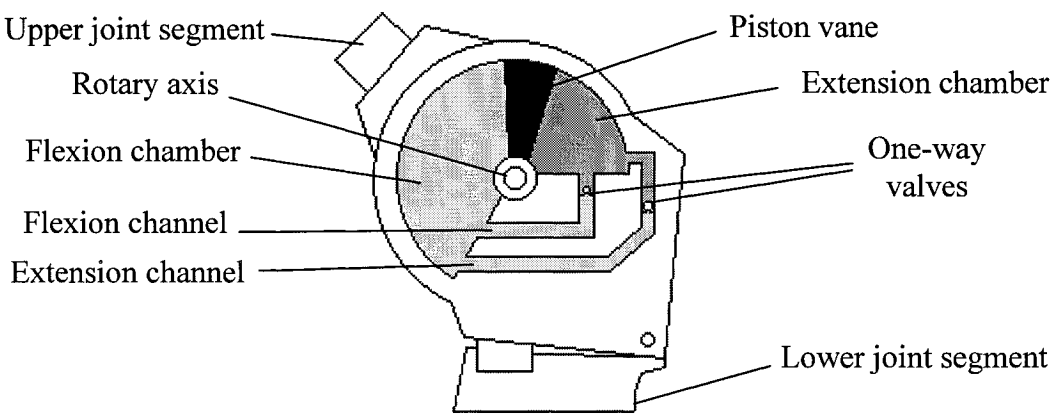

Figure 2.23 – The 3R80 rotary hydraulic knee contains a piston vane, which divides the hydraulic chamber into two sections (adapted from [40]).

The opposite occurs when the knee extends. Weight bearing on the prosthetic limb triggers valves in the flexion channel to close, forcing the joint to inhibit knee flexion. As with linear hydraulic cylinders, the major shortfall of a rotary hydraulic device is its size, weight and cost.

2.4.2 Smart Materials

2.4.2.1 Electro-Rheological Fluid

Electro-rheological fluid (ERF) is a material with flow properties that vary under the influence of an electric field. ERFs are generally composed of a dispersion of conductive solid particles within a dielectric carrier fluid [41]. In the absence of an electric field, the dispersed solid particles move freely in the carrier fluid, exhibiting Newtonian fluid behaviour. When an electric field is applied to the ERF, the solid particles become polarized and form long chains running in the direction of the electric field. This organization of the solid particles significantly changes the viscous and rheological properties of the fluid to that of a near solid. ERFs can reach maximum stiffness in less than 10 ms and revert from near solid form, back to liquid within 1 ms [41]. Electro-rheologic devices exploit the dynamic flow characteristics of the fluid – particularly its dynamic shearing properties. ERFs are typically applied to low-torque clutches, vibration dampers, hydraulic valves, shock absorbers and engine mount designs.

Electro-rheological fluid systems are quiet, have a very quick reaction time, possess high yield strength, and have high controllability. Unfortunately, the high voltage required to control the fluid creates a serious safety issue, particularly if the technology is integrated into a device that will be in contact with the human body [41].

2.4.2.2 Magneto-Rheological Fluid

Magneto-rheological fluids (MRFs) are very similar to ERFs in composition, function, and application. MRFs are activated in the presence of a magnetic field and can attain yield strengths up to 20 times greater than ERFs. However, as MRF mechanisms require a strong electro-magnet, MRF devices are much larger and heavier than ERF devices and too heavy and bulky to find practical application on a SCKAFO.

Biedermann Motech currently markets a transfemoral prosthesis integrating a linear hydraulic cylinder using MRF. The cylinder employs sensors and an onboard microprocessor to optimize knee-extension resistance in swing. However, the device is too large for orthotic applications.

2.4.2.3 Memory Shape Alloys

Memory shape alloys (MSAs) have found limited use in commercial products for approximately 30 years. A MSA that has experienced plastic deformation has the ability to revert back to its pre-deformed shape when subjected to a specific heating condition. When a MSA is plastically deformed in its martensitic phase, it exhibits significant considerable change in macroscopic form but still maintains order at the crystalline level. Heating the deformed martensite above the phase-transition temperature will transform the MSA to austenite and realign the crystal structure to its original form. MSAs are often heated with an electrical current.

MSAs are an attractive option in biomedical applications due to their very high force-to-weight ratio. Some MSA actuators can lift up to 78,000 times their own weight [41]. MSA actuators are also very simple and compact relative to conventional actuators. Unfortunately, MSAs have a relatively slow cycle time, as the alloy requires time to heat and cool. Recovery of the original alloy shape lies in the order of 1 second [41]. Since an entire gait cycle is often completed in less than 1 second the slow recovery rate of MSAs render the technology impractical for integration into a SCKAFO design.

2.4.2.4 Electroactive Polymers

Electroactive polymers (EAPs), sometimes referred to as artificial muscles or soft actuators are still in the early stages of development. There are two types of EAP: *ionic EAPs* and *electronic EAPs*. Ionic EAPs have the advantage of functioning on relatively low voltages; however they rely on the diffusion of charged ions and must be constantly submerged in liquid. The actuator and surrounding liquid can be sealed within a flexible coating, though this can lead to a bulky actuator. Electronic EAPs function in the presence of an electric field and do not require a surrounding fluid to work.

Unfortunately, electronic EAPs require voltages that can be a safety issue if the device is in contact with the human body (in the order of 1-5 kilovolts,). With a density equal to water, weight can also be an issue.

Actuators built with current electronic EAPs can produce up to 30 N force and strokes as high as 2 cm. Such low actuation forces are too small to resist knee flexion on a SCKAFO. While current EAPs are not robust enough to be incorporated into a SCKAFO design, future developments may see EAPs revolutionizing the field of orthotics.

2.4.3 Relevant Mechanisms

2.4.3.1 Brakes

Brakes use friction to control speed by converting mechanical energy to heat. While solid materials are often used for braking surfaces, a liquid can be used to control the speed of a device by viscous force. Viscous brakes are mainly used on high-speed/low-torque devices. Standard braking systems include band brakes, external/internal drum brakes, disc brakes, cone brakes, magnetic particle brakes, hysteresis brakes, and eddy-current brakes [42].

All friction brakes prevent movement in opposite directions [43]. If integrated into a dynamic knee KAFO, a brake would prevent both flexion and extension when engaged. To practically integrate a conventional brake mechanism into a functional orthotic knee joint, a separate engagement mechanism or control system would be necessary to control braking during stance by engaging to resist knee flexion and disengaging to allow knee extension. Issues that may challenge the practicality of integrating conventional brakes into a functional orthotic knee joint include heat dissipation, size, weight and wearing of the friction material.

2.4.3.2 Clutches

Clutches are primarily used to transmit torque between two concentric shafts. Many different physical principles are employed by clutches to transmit torque including,

mechanical interlocking, friction, wedging, magnetic fields, and moving fluids [44]. Most clutches are impractical for orthotic applications due to their low-torque capabilities or the substantial forces required to engage and disengage the clutch. The category of clutch most relevant for integration into a functional orthotic knee joint is the overrunning clutch. Overrunning clutches are a specific type of clutch designed to inherently allow unidirectional rotation. Conventional overrunning clutches include roller-clutches, sprag clutches, wrap-spring clutches, one-way dog clutches and band clutches.

2.4.3.2.1 Roller-Clutch

Roller-clutches resemble a radial cylindrical roller bearing, with either the inner or the outer race outfitted with tapered chambers wherein the rollers reside. As shown in Figure 2.24, rotation of the inner race or *driver* in the clockwise direction will cause the rollers to roll up the inclined wall of the chamber and wedge between both races and lock the races together. Rotating the inner race counter-clockwise frees the rollers from their wedged position, allowing free relative rotation between both races. Springs are often used to bias the rollers toward the wide ends of the tapered chamber. Efforts have been made, with little success, to integrate a roller-clutch into a functional orthotic knee joint device. Size and seizing issues plagued the roller-clutch knee joint design developed by Harrison et al. [22] and extremely poor manufacturability prevented the conical roller-clutch joint design, developed by Myers [27], from further development.

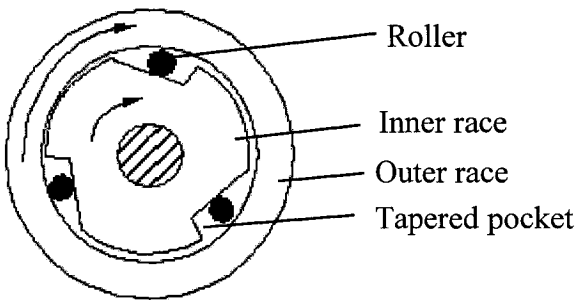

Figure 2.24 – An open view of a conventional roller-clutch.

2.4.3.2.2 Sprag Clutch

Sprag clutches closely resemble radial cylindrical roller bearings with the conventional rollers replaced by a plurality of eccentric rocking elements called *sprags*.

As shown in Figure 2.25, counter-clockwise rotation of the inner race will cause the cam-like sprag to rock into a position where the sprag is too large to fit between inner and outer races. The sprag jams between the concentric races, preventing relative motion between the inner and outer races. Rotating the inner race in the clockwise direction positions the sprag such that it is too short to make contact between the two races. Relative motion between the two races is therefore uninhibited. The high tolerances and difficult machining associated with manufacturing a custom sprag clutch makes integration into a KAFO an expensive, and therefore unattractive, option.

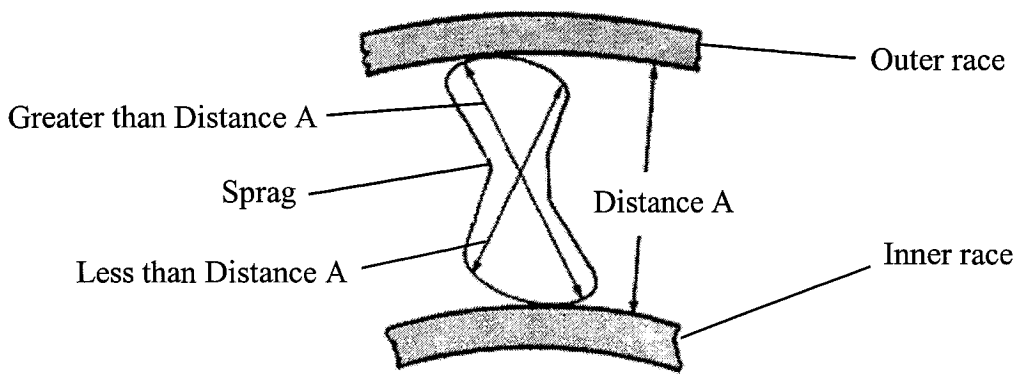

Figure 2.25 - A close up view of a single sprag in a sprag clutch (adapted from [45]).

2.4.3.2.3 Spring-Wound Clutch

Spring-wound clutches are composed of a helical spring wound around two concentric shafts (Figure 2.16). The spring is anchored to a driving shaft. Relative rotation of the driving shaft in one direction works to wind the helical spring, tightening its grip on the driven shaft. Relative rotation in the other direction serves to unwind the spring and loosen its grip on the driven shaft. Irby et al. [21] integrated a spring-wound clutch into their dynamic knee KAFO design; however, dimensional optimization of the clutch still produced a bulky orthosis.

2.4.3.2.4 One-Way Dog Clutch

As shown in Figure 2.21, a one-way dog clutch is comprised of two parallel plates with toothed faces. The toothed faces are forced to mate via a spring or other mechanism. Due to the inclined shape of the teeth, relative rotation of the plates is allowed in one

direction, but prevented in the other direction. A shortcoming of the clutch is that it produces a clicking sound as the plates rotate over each other. As well, the finite number of teeth limits the number of locking positions. Becker Orthopaedic has integrated a one-way dog clutch into their 9001 E-Knee. The device has proven to be noisy, heavy and allows up to 6° of knee flexion before the knee joint reaches the locked position. This could provide a long unsupported period of knee flexion during stance.

2.4.3.2.5 Band Clutch

A band clutch is essentially a flattened spring-wound clutch. A spiral spring or band wraps around a central shaft and is anchored to the inner wall of a concentric outer ring. Turning the outer ring in one direction causes the spiral spring or band to tighten its grip on the central shaft and inhibit further rotational motion between the ring and the shaft. Rotating the outer ring in the opposite direction loosens the grip of the spiral spring or band on the shaft, allowing unimpeded relative rotation of the ring over the shaft. Unfortunately, the band clutch design cannot be modified to selectively allow free motion in either direction – an essential requirement of a practical SCKAFO.

2.4.3.2.6 3-D Sprag Technology

Vranish [46] of NASA invented a roller/sprag geometry to reduce the high local stresses in sprag and roller-clutches. Conventional sprags and rollers achieved a line contact between the inner and outer races of a clutch, as shown in Figure 2.26. The 3-D sprag concept integrates grooves in the inner and outer races and rounds the corners of the roller or sprag to attain four single-point contacts between the roller or sprag and the races, as shown in Figure 2.27. This distribution of the localized loads can reduce stresses to approximately half the value experienced in conventional roller and sprag clutches [46]. Less material mass is therefore required to achieve a given holding torque. As a result, small, lightweight 3-D roller or sprag clutches can resist the same torque as conventional clutches twice their strength.

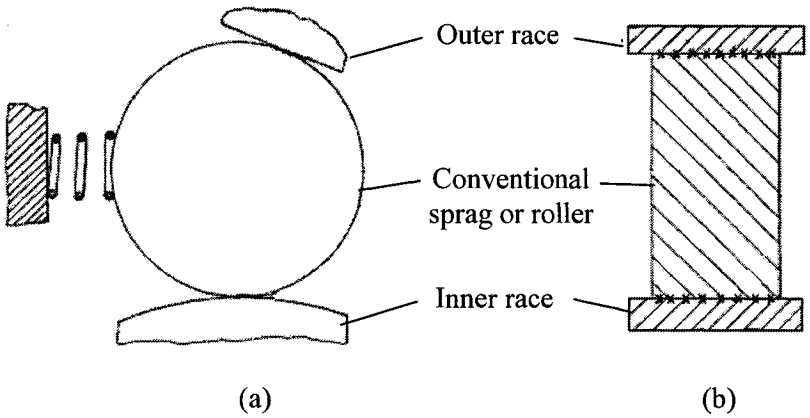

Figure 2.26 - (a) A side view of a roller in a conventional roller-clutch; (b) a front view of the roller reveals a line contact between the roller and the inner and outer races (adapted from [46]).

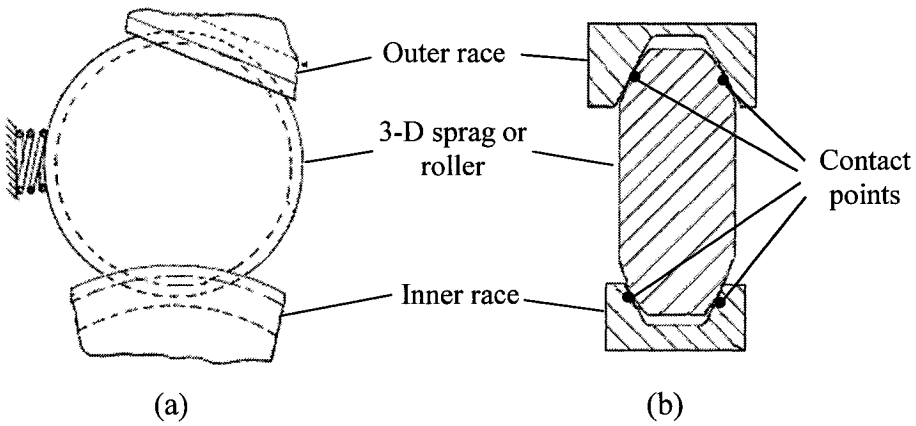

Figure 2.27 – (a) A side view of a roller in a roller-clutch with 3-D sprag geometry; (b) a front view of the modified roller and races reveals four point contacts between the roller and the races (adapted from [46]).

The complex geometry of the sprags and the races require high precision machining and the cost of manufacturing may be too great to integrate 3-D sprag technology into an orthotic knee joint design.

2.4.3.3 Ratchets

Ratchets are one of the most common types of unidirectional rotation mechanisms. As shown in Figure 2.28, simple ratchets are comprised of a toothed *ratchet wheel*, and a pawl. The pawl is often forced to contact the ratchet wheel via a spring or gravity. The pawl allows the ratchet wheel to rotate in one direction, but impedes wheel rotation in the opposite direction.

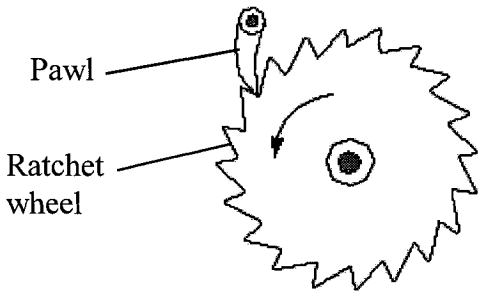

Figure 2.28 – A simple ratchet mechanism.

The pawl can create excessive noise as it travels over the teeth of the ratchet wheel. Stress is localized at the pawl-wheel pins and the ratchet-pawl point of contact. Ratchets offer a limited number of locking positions, therefore an orthotic knee joint integrating a ratchet mechanism would allow several degrees of free-fall knee flexion before locking. Many users would find such performance unacceptable.

2.4.3.4 Miscellaneous One-Way Mechanisms

The coaster brake is a conventional type of bicycle brake that allows the rider to pedal forward but engages a brake when the rider pedals backwards. The mechanism is essentially a combination of an overrunning clutch and an internal drum brake. The axial profile of the mechanism is too long to be packaged in a compact manner on a practical orthotic knee joint. The brake pads of the device are also subject to considerable wear.

The unidirectional device used in common window blinds was investigated. This device incorporates a ratchet mechanism. Ratchets are noisy and only allow a limited number of locking positions. Therefore window blind locking devices are unsuitable for integration into an effective functional orthotic knee joint.

2.4.3.5 Selectably-Engagable One Way Mechanisms

An extensive search for *selectably-engagable one way mechanisms* in the United States Patent Office database uncovered a number of devices intended for use in fishing reels, transmissions, brakes, sports equipment, gas turbine engines and other miscellaneous applications. Common inherent limitations eliminated most designs from

further consideration. The reviewed designs were either too bulky [47-49], possessed an excessive axial profile [50-52], integrated a ratchet-based mechanism offering a limited number of locking positions [53-57], were overly complex [49, 50, 52, 57-59], or incorporated clutch mechanisms that have already been applied to SCKAFOs with limited success [60-62].

One design, that warranted further investigation, was the conical cable lock [63]. Conical cable locks are commonly used as a tensioning mechanism on clotheslines. The concept functions much like a roller-clutch that works in a linear fashion. As shown in Figure 2.29a, a cable passes through a conical chamber aligned with the primary axis of the chamber. A plurality of ball bearings resides between the cable and the tapered inner wall of the conical chamber. A spring biased plunger influences the ball bearings toward the narrow end of the conical chamber. If the cable is pulled through the narrow end of the chamber, the friction between the cable and the ball bearings causes the bearings to roll into the narrow end of the chamber. The ball bearings apply an increasing amount of pressure on the cable as they move further down the tapered walls of the chamber, eventually locking the cable from further travel. Pulling the cable through the wide end of the conical chamber causes the ball bearings to roll up to the wide end of the chamber. The ball bearings are no longer wedged into the cable and so the cable is allowed to travel through the cable lock unimpeded.

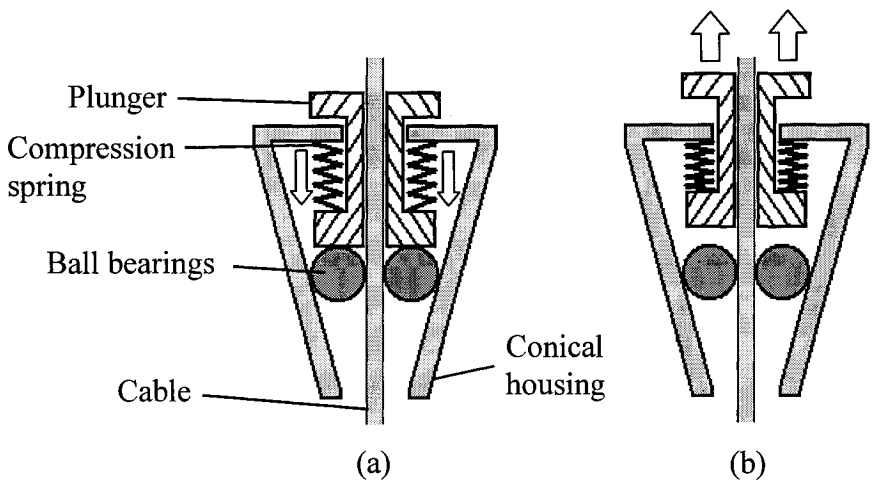

Figure 2.29 – A cross sectional view of a typical conical cable clutch; (a) the spring-loaded plunger forces the ball bearings toward the narrow end of the conical housing, (b) lifting the plunger relieves the force on the ball bearings.

Lifting the spring-loaded plunger away from the ball bearings, as shown in Figure 2.29b, eliminates the force that pushes the ball bearing down the tapered sides of the conical chamber. In this state, the ball bearings will not be forced to roll down the tapered walls of the chamber as the cable is pulled toward the narrow end of the lock. No wedging will therefore occur between the cable, the tapered walls and the ball bearings. The cable is thus free to travel through the cable lock in both directions as long as the plunger is prevented from forcing the balls toward the narrow end of the chamber. The conical cable lock delivers the selectably-engagable one-way locking behaviour required of an effective functional orthotic knee joint design. The device also provides an infinite number of locking positions, requires a relatively low force to disengage the lock, is a relatively simple mechanism, possesses a relatively low profile, and is relatively compact. Unfortunately, substantial local stresses can develop on the limited number of contact points between the rollers, the cable and the housing, leading to plastic deformation of the components.

2.4.3.6 Elastic Materials

As demonstrated by Kofman et al. [37] and Allard et al. [64], elastic materials can be integrated into a functional orthotic knee joint design. Elastic materials are noiseless, lightweight, commercially available, durable and inexpensive [65]. Another benefit of elastic materials is that they will not inhibit useful limb motion, such as the smooth shock-absorbing function of knee flexion at limb loading. To counter the high external knee flexion moments experienced in stance, a relatively strong and stiff material is required. Challenges in implementing elastic materials into a functional orthotic knee joint include hysteresis, sufficient strength, and controlling the backlash of loaded elastic components.

2.4.3.7 Seatbelts

A review of common seatbelt devices [66] currently in use in cars and alternative seatbelt designs housed in the United States Patent Office database uncovered a number of novel devices. Most relevant mechanisms allowed either an excessive amount of travel before locking [67, 68], presented an inherently excessive profile width [69], were

extremely complex and bulky [70], possessed a limited number of locking positions [66, 71, 72], or required excessive disengagement force to unlock the device [73, 74].

One seatbelt braking mechanism offered many of the functional and structural requisites of a practical functional orthotic knee joint. This specific class of mechanism employed tension in the seatbelt to clamp down on the belt itself and prevent further belt motion [69, 75-79]. Most of the mechanisms employed a central deflecting lever element that pivoted about a pin to clamp the belt with one end of the lever when the opposite end was forced to rotate due to belt tension. This type of mechanism provided noiseless unidirectional motion, an infinite number of locking positions, quick response, and can be modified to offer a discreet thickness profile. A mechanism could be added that disables the clamping component to allow free belt travel in both directions irrespective of belt tension. This seatbelt braking mechanism eventually inspired the functional orthotic knee joint design that is the focus of this thesis.

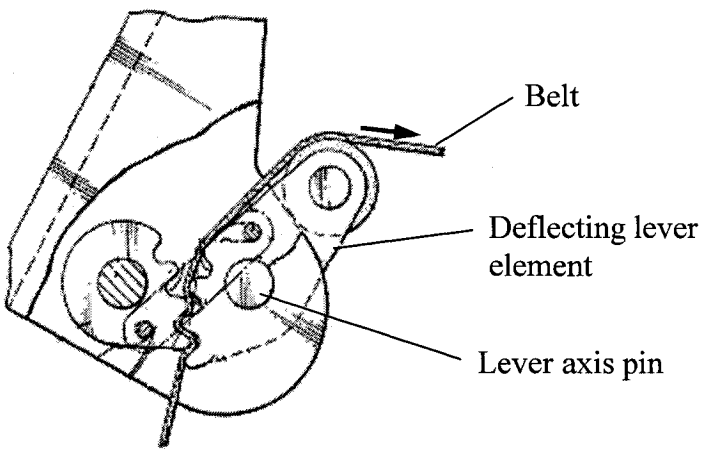

Figure 2.30 – Drawing of a seatbelt braking mechanism that inspired the design of the orthotic knee joint that is the focus of this thesis (adapted from [75]).

Chapter 3. Design and Development of a New Dynamic KAFO

3.1 Rationale

A limited number of studies indicated that SCKAFOs promoted a more symmetric gait, improved gait kinematics, provided greater mobility, and required less compensatory movement [3] and less energy expenditure during gait [80] than conventional locked knee KAFOs. Biomechanical evaluation studies remain to be completed on commercial SCKAFOs. A considerable portion of the population that use conventional KAFOs have sufficient lower limb muscle strength to benefit from a functional KAFO, including the elderly, and clients inflicted with multiple sclerosis, muscular dystrophy, polio, post-polio, incomplete spinal injury, unilateral leg paralysis or paresis, trauma, congenital defects or isolated quadriceps weakness or absence.

As summarized in Table 3.1, four different SCKAFO designs are currently available on the market. However, all four designs fall short of providing the user with a completely stable and practical orthosis.

Table 3.1 – Summary of commercial SCKAFO designs.

Model	Advantages	Disadvantages	Cost (CDN$)
Otto Bock Free Walk/ Becker UTX	Lightweight	Locks only in full knee extension	$2500 (SCKAFO)
Horton Technology's Stance Control KAFO	Good functionality	Bulky	$2200 (joints)
Fillauer's Swing Phase Lock	Lightweight, autonomous	Locks only in full knee extension	$2200 (joints)
Becker's 9001 E-Knee	Good functionality	Bulky, heavy, noisy, expensive	$4200 (joints, control system & uprights)

Current SCKAFOs either require the knee to be fully extended to engage the knee joint lock (no stumbling support or flexed-knee standing), or are too heavy and bulky for many potential clients (energy exhaustive, intimidating, obstructive, and awkward). Clients using these orthoses are thereby limited in where they can safely walk.

A major disadvantage of all commercial SCKAFOs is their cost. SCKAFOs are a relatively new product in the orthotics industry and most insurance plans do not recognize the technology or reimburse clients for it. A pair of conventional KAFO joints cost between $150-$300 CDN. The cost of a pair of commercial SCKAFO joints begins at $2200. The Becker 9001 E-Knee joint and control system costs nearly $4200 CDN. When the cost of material and labour to integrate the joints into a KAFO are added, the total cost of a SCKAFO is too expensive for many potential clients to afford.

A review of relevant technologies and devices has uncovered a mechanism, previously applied to seatbelt locking devices that may be integrated into a KAFO to produce a less expensive, lighter, more compact and functionally superior orthosis to current SCKAFOs. Creating a functional KAFO that addresses the limitations of current commercial designs will undoubtedly expand the potential user population of functional KAFOs, reduce the chance of device rejection, and give many clients inflicted with lower limb weakness an improved level of mobility, security, confidence, independence and health.

3.2 Objectives

The goals of this research were to design, develop, mechanically test and clinically test a new functional KAFO that addresses the limitations of current SCKAFOs for the population of KAFO users that possess unilateral knee extensor weakness or absence but still maintain some hip strength. The project objectives are to:

1. Design a new functional orthotic knee joint that addresses the price, performance, weight and size limitations of commercial SCKAFO joints. The joint must allow free knee rotation in swing, providing sufficient resistance to knee flexion while still permitting knee extension in stance, and offer a lower weight, thickness and price than current commercial SCKAFO joints.
2. Manufacture a prototype functional orthotic knee joint to be used as a proof of concept for function, resistance to failure, and clinical performance.

3. Evaluate the static strength and performance of the design by performing mechanical testing on the prototype, and refine the design as necessary for clinical testing.
4. Clinically test the performance of a KAFO prototype that incorporates the new functional orthotic knee joint and evaluate the clinical effectiveness of the design compared to conventional locked-knee KAFOs.

3.3 Design Criteria

3.3.1 Data Collection and Organization

A review of orthotic device and gait literature [5-8, 9, 12, 16], scientific papers [16, 22], and an informal survey of rehabilitation professionals and orthotists was performed to determine the functional and structural requirements of an ideal SCKAFO for brace users with unilateral knee extensor weakness. A chart known as a Quality Function Deployment (QFD) [81] was constructed to organize the design criteria data (Tables 3.2-3.3). The chart prioritizes the design requirements as perceived by the SCKAFO user, the orthotist, the marketer, and the manufacturer. The quantitative performance values and structural dimensions, together referred to as engineering parameters [81], of the four existing commercial SCKAFO's were compared along the bottom of Table 3.2 and were used to help set target values for the new SCKAFO design. Along the right side of Table 3.2, each commercial design was graded by the investigator on its ability to satisfy the design requirements of an ideal SCKAFO. The relationship between the design requirements and engineering parameters was represented by letter grades a, b, c in Table 3.3, determined by the investigator. The QFD highlights the weaknesses of each individual commercial design as well as the limitations common to all commercial designs. Following a thorough analysis of the QFD data, a set of target specifications was generated for the ideal SCKAFO.

Table 3.2 – Quality Function Deployment chart for the design of a SCKAFO. The party section ranks the design requirements. The existing SCKAFO section grades existing commercial designs (0-4 scale).

*** Essential feature**
† Performance feature
‡ Excitement feature

0-Design doesn't meet the requirement at all
1-Design meets the requirement slightly
2-Design meets the requirement somewhat
3-Design meets the requirement mostly
4-Design fulfills the requirement completely

Design Requirements	Party				Existing SCKAFOs			
	Client (user)	Orthotist	Marketing	Manufacturer	*Horton – Stance Control Orthosis*	*Otto Bock – Free Stance*	*Becker – 9001 E-Knee*	*Fillauer – Swing Phase Lock*
Functional Performance								
Resists excessive flexion in stance	1*				4	3	4	3
Allows extension in stance	12†				4	1	4	0
Allows limited flexion in stance	20‡				0	1	0	0
Resists flexion at any knee angle in stance	11†		10†		4	0	2	0
Allows free knee movement in swing	3*		1*		4	4	4	4
Quick reaction time	7*				3	3	3	3
Low noise	6*				3	2	1	3
Light weight	4*		3*		1	3	1	2
Unobtrusive form	8*	7*	12†		1	3	2	2
Will support ligament instability	22‡		16†		3	1	3	3
Human Factors								
Easy to don/doff	15†		11†		3	3	3	3
Manual override (automatic, free, locked)	10†		6*		3	1	1	3
No unnatural trigger movements required	9†		5*		3	2	3	3
Attractive (sleek, not bulky)	5*	6*	2*		1	3	1	2
Servicing								
Significant time between servicing	16†	4*	14†		1	3		2
Easy to adjust trim settings	19‡	3*			3	3	2	3
Easy to service/replace parts		5*	15†		3	1	1	3
Inexpensive replacement parts/servicing	17‡	9†			2	3	2	2
Sold as joint		1*	4*	2*	3	1	3	4
Ease of integration into a KAFO		2*			2		3	4
Electro-mechanical								
Sufficient use between charging	13†		13†				3	
Knee defaults to flexion restriction in failure	2*						4	
Miscellaneous								
Easy to machine				1*	2	2	1	2
New technology	21‡		8*		0	0	3	0
Self/contained autonomous device	18‡		9*		2	2	2	4
Competitive price	14†	8†	7*		1	2	1	2

Table 3.3 – Quality Function Deployment between SCKAFO design parameters and requirements.

a – Weak relationship
b – Medium relationship
c – Strong relationship

Design Requirements	Engineering Parameters: Flexion resistance (Nm)	Number of parts (#)	Joint thickness (mm)	Joint width (mm)	Joint length (mm)	KAFO weight (kg)	Power consumption (days/charge)	Reaction time (ms)	Combined weight of knee joints (kg)	Max. client weight (kg)	Lifetime (year)	Heat generation (°C)	Mean time between servicing (months)	Sale price (CDN$)
Functional Performance														
Resists excessive flexion in stance	b		b	b	b	b	c		b	c	a		b	a
Resists flexion at any knee angle in stance										c	a		a	
Free knee movement in swing		a				a			a					b
Quick reaction time														
Low noise												a		
Light weight	c	c	a	b	b	c			c	c				
Unobtrusive form	b		c	a	b					b				
Will support ligament instability						a			a	a				
Human Factors														
Easy to don/doff			a	a	a									
No unnatural trigger movements required														
Attractive (sleek, not bulky)	a	a	c	c	c	b			b	b				
Servicing														
Significant time between servicing	a									a	a		c	
Inexpensive replacement parts/servicing														
Sold as joint	a													b
Ease of integration into a KAFO			a	a	b									
Electro-Mechanical														
Sufficient use between charging	b						c			c		b		
Knee defaults to flexion restriction in failure	b	a												
Miscellaneous														
Easy to machine										b				
Self/contained autonomous device							b							
Competitive price		a								a				c
Values Measured or Obtained from Manufacturers														
Horton –Stance Control Orthosis		13+	23	60	165				0.73	90	3		4	2500
Otto Bock – Free Stance		13	10			0.9				120		0	12	2500
Becker – 9001 E-Knee			23				1		0.78	100				4000
Fillauer – Swing Phase Lock		16	14	60	123							0	6	2200
Target specifications	425	<20	15	50	120	<2.3	1	6	0.70	90	>3	<30	6	<2200

3.3.2 Design Criteria for an Ideal Dynamic KAFO

3.3.2.1 Functional Requirements

A truly effective SCKAFO will allow the user to walk on even ground, uneven ground, inclines, declines, and up and down stairs. While stair walking may be impossible for people with severe knee extensor weakness, a SCKAFO could be a useful safeguard for moderately weak individuals, such as the elderly, who have sufficient muscle strength to walk stairs but run a risk of stumbling or losing knee stability. To allow the user to perform the aforementioned activities while still providing security, the orthosis must allow knee extension while prohibiting excessive knee flexion during the stance phase of locomotion. During swing, the orthosis must allow both uninhibited knee flexion and extension. The SCKAFO must not restrict the fundamental functions of the knee in gait.

The mechanism employed to prevent excessive knee flexion should engage at any knee angle and react within a few milliseconds to provide immediate knee support in case the user stumbles. Knee flexion resistance need not be rigid, but must be stiff enough to provide stability if the patient loses balance. Since knee flexion does occur in stance during limb loading and pre-swing (Section 2.1.1.4), an ideal SCKAFO may allow some controlled knee flexion during stance.

The weight limit of the user must be sufficient to remain competitive with existing commercial SCKAFOs. The Horton Stance Control Orthosis and Becker's Model 9001 E-Knee can accommodate a maximum user weight of 90 kg and 100 kg respectively. The other commercial SCKAFOs are not considered as they will not support a partially flexed knee and are therefore not designed to support considerable loads. A user weight limit of 90 kg was chosen as an initial design goal.

3.3.2.2 Structural Requirements

Cosmetics are an extremely important issue for KAFO users. If an orthosis looks unnatural, sounds unnatural, or requires the user to move in an unnatural manner, the orthosis will often not be used no matter how well it functions. The ideal orthosis should

be discreet in size, unnoticeable under clothing, and generate little to no noise. A major reason among clients for abandoning the use of long leg braces is that the assist device is too bulky and unpleasant for frequent use [82]. Potential SCKAFO users are already taxed by a physical weakness and will not wear a heavy orthosis that demands an excessive amount of energy to walk. Orthoses add mass to the existing leg, and therefore increase limb inertia that may lead to abnormal gait patterns [84]. The ideal SCKAFO must therefore be as lightweight as possible weighing no more than 2.3 kg (5 lbs).

Ideally, the knee joints of the SCKAFO must also have a thin medial-lateral profile. An excessive profile can cause the outer lateral knee joint to collide with stationary objects and the inner medial joint to rub against the opposite knee. If the user is wearing a brace on both legs, the inner medial knee joints could collide during walking. Current SCKAFO joints offering adequate functionality measure 23 mm thick, 60 mm wide and 123-165 mm long. The target dimensions of a more practical SCKAFO knee joint are 15 mm of thickness, 50 mm of width and 120 mm of length. While compact size is important, the design must also be sufficiently strong to withstand the high moments experienced during common activities such as fast walking, stair ascent and stair descent. The peak external knee flexion moment experienced in stair ascent by a 90 kg individual is 154 Nm [11]. In order to increase product appeal for orthotists, the dynamic knee joint will preferably be a component of a modular KAFO system.

3.3.2.3 Control Requirements

A mechanical control system is preferred over an electro-mechanical one for simplicity reasons. The SCKAFO joint should ideally require no unnatural locomotor movements, such as plantarflexing or dorsiflexing the foot at irregular moments in the gait cycle or hyper-extending the knee to disengage the lock for swing or trigger the locking mechanism.

A mechanical control system can offer the potential benefit of relatively low-cost, lightweight components. Mechanical control system options include the use of a control cable, pushrod or hydraulic actuated pin to activate the knee joint mechanism, driven by

foot pressure or ankle angle. Although an electro-mechanical control system is often comprised of relatively heavy and costly components such as batteries and electro-mechanical actuators it can be much more versatile than a mechanical control system, delivering a greater level of control functionality and reliability through a range of user activities. Electro-mechanical control systems may include switches or pressure sensors positioned on the foot sole of the orthosis and direct-current micro-motors or solenoids as actuators installed in the knee-joint mechanism. If an electro-mechanical design is adopted, the power supply should provide at least one day of use per charge. Batteries, electronics and other peripheral components may be self-contained on the orthosis or clipped to the user's clothing. For safety reasons, the joint must default to the knee support mode in the case of control system failure. This could lead to a user stumbling, but is preferred over the user collapsing if the SCKAFO were to default to the free-knee mode. The SCKAFO will preferably require servicing no earlier than every six months.

3.3.2.4 Summary of Design Criteria

Table 3.4 summarizes the key design criteria for an ideal SCKAFO.

Table 3.4 – Design criteria for an ideal SCKAFO.

Item	Criteria
Motion in stance	Allow extension, inhibit flexion
Motion in swing	Free motion
Reaction time	~ 6 milliseconds
Maximum weight (entire orthosis)	2.3 kg (5 lbs)
Noise	Preferably none
Maximum frontal profile (per joint)	15 mm
Maximum width	50 mm
Maximum length	120 mm
Power consumption	Minimum 1 day use between charges
Range of motion	110°
Maximum client weight	90 kg
Maximum applied knee flexion moment: 90 kg person, stair ascent (+1 standard deviation)	154 Nm
Static loading safety factor	>3
Dynamic loading safety factor	>2-3
Mean time between servicing	6 months
Maximum sale price (entire system)	< CDN $2200

3.4 Conceptual Designs

A review of relevant technologies and existing mechanisms was carried out as summarized in Section 2.4. Several methods were used to generate ideas and device concepts. Functional Diagrams [81] were created to help define the energy requirements of each desired SCKAFO function. The required device functions were listed and matched with existing mechanisms that could satisfy each function. Events in the gait cycle were considered for their potential to trigger or power the device. Over 40 conceptual designs were generated which included clutch and brake mechanisms, hydraulic, magnetic, ERF and MRF devices and mechanical and electro-mechanical control systems. Three of the most promising designs were developed further and are discussed in Sections 3.4.1 to 3.4.3.

3.4.1 Roller-Clutch Design

A roller-clutch knee joint, similar to the design developed by Harrison, et al. [22] (Section 2.3.2.2) was explored. Their design used a plastic roller cage that deformed when actuated by a pushrod. Deformation of the cage inhibited clutch performance. Harrison et al. concluded that a standard roller clutch was too bulky to be incorporated into a practical brace.

The proposed roller clutch design incorporated a steel roller cage that would not deform under moderate loading. Integrating 3-D sprag geometry (Section 2.4.3.2.6) into the rollers and races was also proposed to reduce the size of the roller clutch by 50%. Unfortunately, incorporating 3-D sprag geometry would be insufficient in bringing the clutch down to a reasonable size. The prospective cost of manufacturing was also considered a significant design limitation.

3.4.2 Cam-and-Follower Design

Another conceptual design to warrant further investigation combined a cam and follower with a linear-clutch mechanism (Appendix A, Figure A.1). The clutch mechanism was very similar in design to the conical cable lock device described in Section 2.4.3.5. Due to the high-predicted stresses, wedge shaped blocks were substituted

for the rollers to increase the contact area between the jamming element and the housing and follower.

In stance, knee flexion would rotate the offset circular cam, which would displace the follower upward. Friction between the follower and the wedge blocks would force the blocks into the tapered chamber, causing them to jam against the follower and the tapered chamber wall. With the follower jammed, the cam and knee were immobilized from further rotation. Knee extension would relieve the force on the follower. Compression springs would force the follower downward, freeing the wedge blocks. The compression springs would also force the follower roller to remain in constant contact with the cam. At the onset of swing, a mechanical actuation force delivered by a solenoid, pushrod or hydraulic piston, would push down on the plunger. This downward displacement of the plunger would move the wedge blocks out of contact with the housing and the follower. The potential for jamming would therefore be eliminated and the knee would be free to flex and extend.

Typical knee moments would create very high stresses in the device. Stress analysis of the device determined that the contact stress between the cam and follower and the buckling stress in the follower would vastly exceed critical values. Designing the device with a sufficient safety factor would have resulted in an unreasonably large joint with excessive thickness.

3.4.3 Belt Clamp Design

The final conceptual orthotic knee-joint design was inspired by the deflecting lever arm, seatbelt retractor locking mechanisms described in Section 2.4.3.7. The joint (Figure A.2) was comprised of two segments that connect and pivot relative to each other about a pin. A flexible belt was spooled on, and anchored to, the first joint segment and passed through a clamping mechanism on the second joint segment. The opposite end of the belt was attached to the second joint segment by a recoil spring. In this thesis, this device is referred to as the dynamic knee joint (DKJ). The DKJ showed promise in

satisfying all of the predefined design requirements and therefore warranted further development.

3.5 Dynamic Knee Joint Design and Development

The dynamic knee joint (DKJ) was designed as an individual component of a modular DKAFO system (Figure 3.1a). Like most conventional orthotic joints, the DKJ has been designed to be installed into a custom orthosis by a certified orthotist. A single dynamic knee-ankle-foot orthosis (DKAFO) houses two DKJs, one in each of the medial and lateral uprights of the brace. The DKJs are connected remotely to three peripheral control system components installed elsewhere on the orthosis. These components include the foot pressure sensors, the dedicated logic circuit, and the power source. Force Sensing Resistors (FSRs) were used to detect foot pressure and were adhered to the sole of the AFO shell (Figure 3.1b).

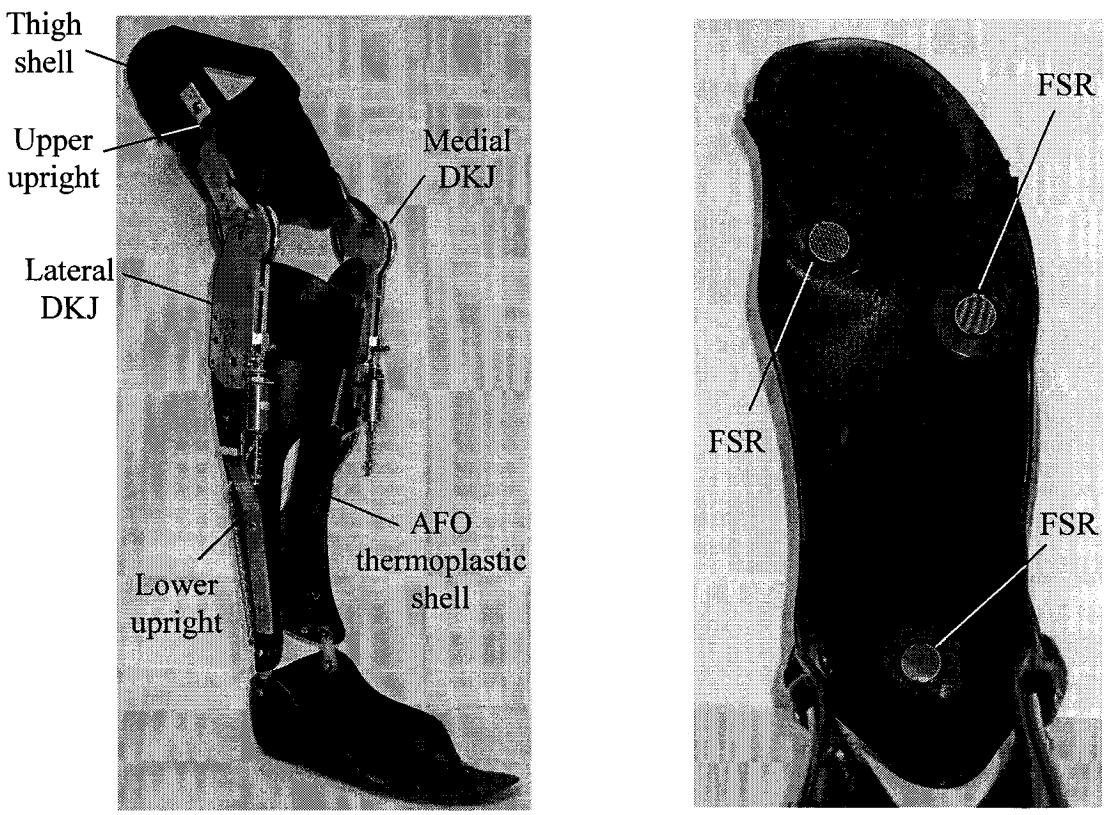

Figure 3.1 – (a) A photograph of two DKJs integrated into a modular DKAFO system. The dedicated logic circuit and power source have been omitted; (b) a photograph showing the force sensing resistors (FSRs) adhered to the sole of the AFO shell.

The DKJ itself is comprised of two rigid joint segments that pivot about the disc pin (Figure 3.2). Two brackets attach the upper joint segment to the upper upright of the DKAFO. The lower upright of the DKAFO is attached to the lower joint segment. A belt is spooled onto the upper segment of the joint with the end of the belt passing through an open clamp device integrated into the lower joint section. DKJ flexion causes the disc to spool the belt and pull the belt in the lower joint segment upward. The onset of belt tension causes the hammer to clamp the belt against the anvil in the lower joint segment. With the end of the belt clamped by the hammer, the upper joint segment is prevented from pulling the belt and is therefore inhibited from flexing. Knee extension by an external moment relieves tension in the belt and causes the clamping hammer to release its hold on the belt. The belt recoil spring collects the slack generated in the belt and the knee extension movement is unimpeded. In swing, a solenoid fixed to the joint disables the clamp device, to allow free movement of the belt and the joint, and thus permit knee flexion. The complete function of the DKJ is described with more detail in Section 3.5.2.

3.5.1 Dynamic Knee Joint Structure

The DKJ structure evolved considerably from the preliminary design stage. Figure A.2 in Appendix A includes drawings of earlier embodiments of the device. Figure 3.3 illustrates three isolated views of the prototype DKJ used in mechanical and clinical testing. All of the joint components are shown in Figure 3.2, where the lateral side-plate has been omitted to provide a clear view of the internal components. An exploded view and associated Bill of Materials of the device are included in Appendix B. The current DKJ measures 207.7 mm in length, 58.8 mm in width, and 16.4 mm in thickness (Figure 3.3).

All major DKJ components were machined from aluminium plate and rigidly connected by press fit stainless steel pins. The disc, hammer and anvil (Figure 3.2) pivot freely on their respective pins. The lateral side-plate (Figure 3.3c) maintains a sliding fit with its respective mating pins, thereby providing easy side-plate removal to allow access to the central joint components during orthotic servicing. The disc pin, hammer spring shoulder pin, and lower shoulder pin have shoulders to limit travel of the lateral side-

plate along the pins. The lateral ends of these pins house threaded UNC 4-40 holes. Face screws and washers were installed in the threaded holes to fix the lateral side-plate against the shoulders of the pins.

The belt is anchored to the disc by three clamping machine screws. The belt wraps around the disc, passes over the hammer, between the anvil and the hammer, and connects to a belt recoil spring that maintains tension in the belt at all times. The opposite end of the recoil spring is anchored to the lower upright by a bracket. A gap between the anvil and the hammer is just wide enough to allow the belt to travel between both components without resistance. The solenoid is employed to selectively deactivate the clamping mechanism and is connected to a bracket that is adhered to the lower upright. The solenoid is remotely connected to a control system comprised of pressure sensors adhered to the sole of the AFO section, and an integrated circuit and power source. The control system is more thoroughly described in Section 3.5.7.

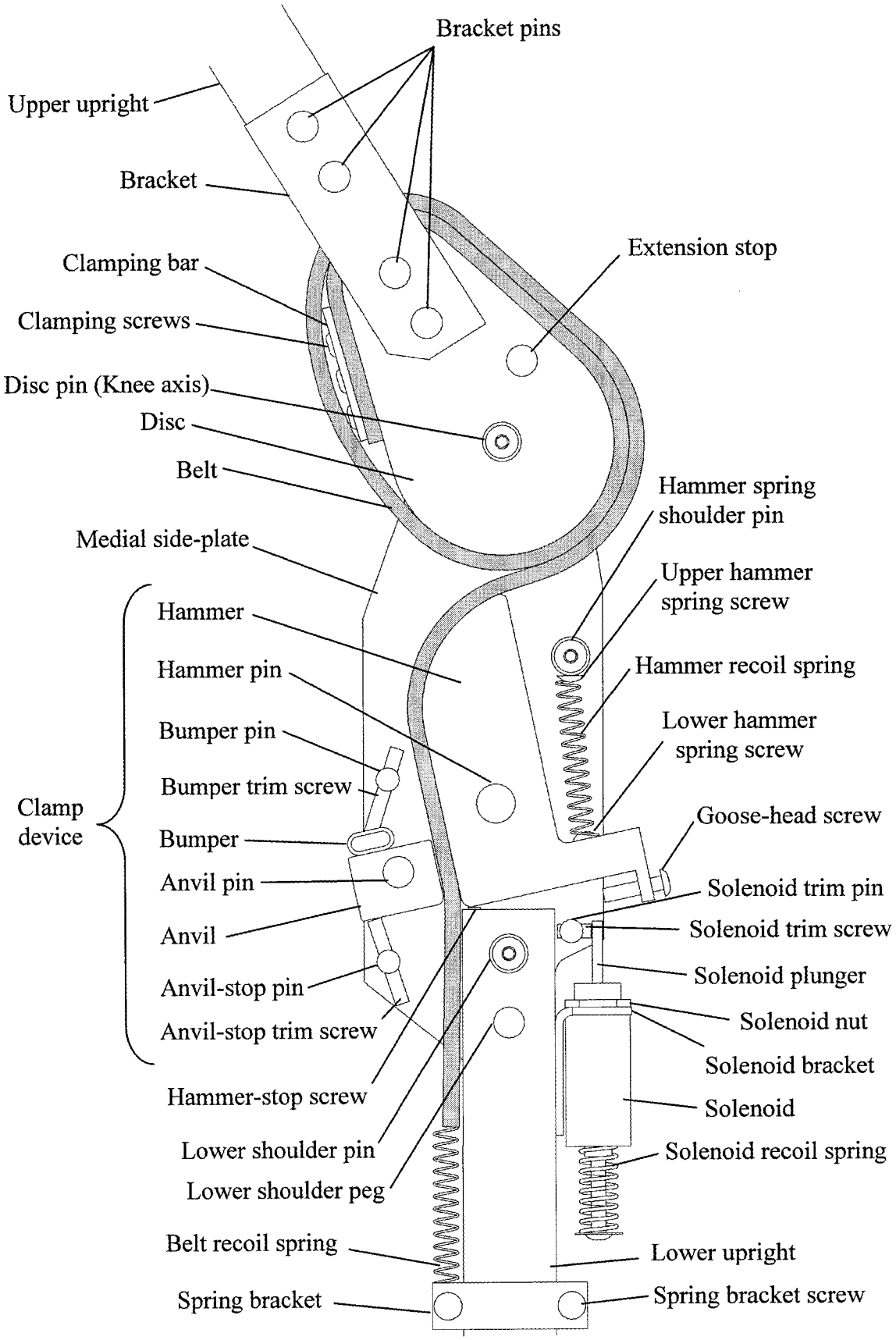

Figure 3.2 - An isolated view showing the main components of the DKJ without the lateral side-plate.

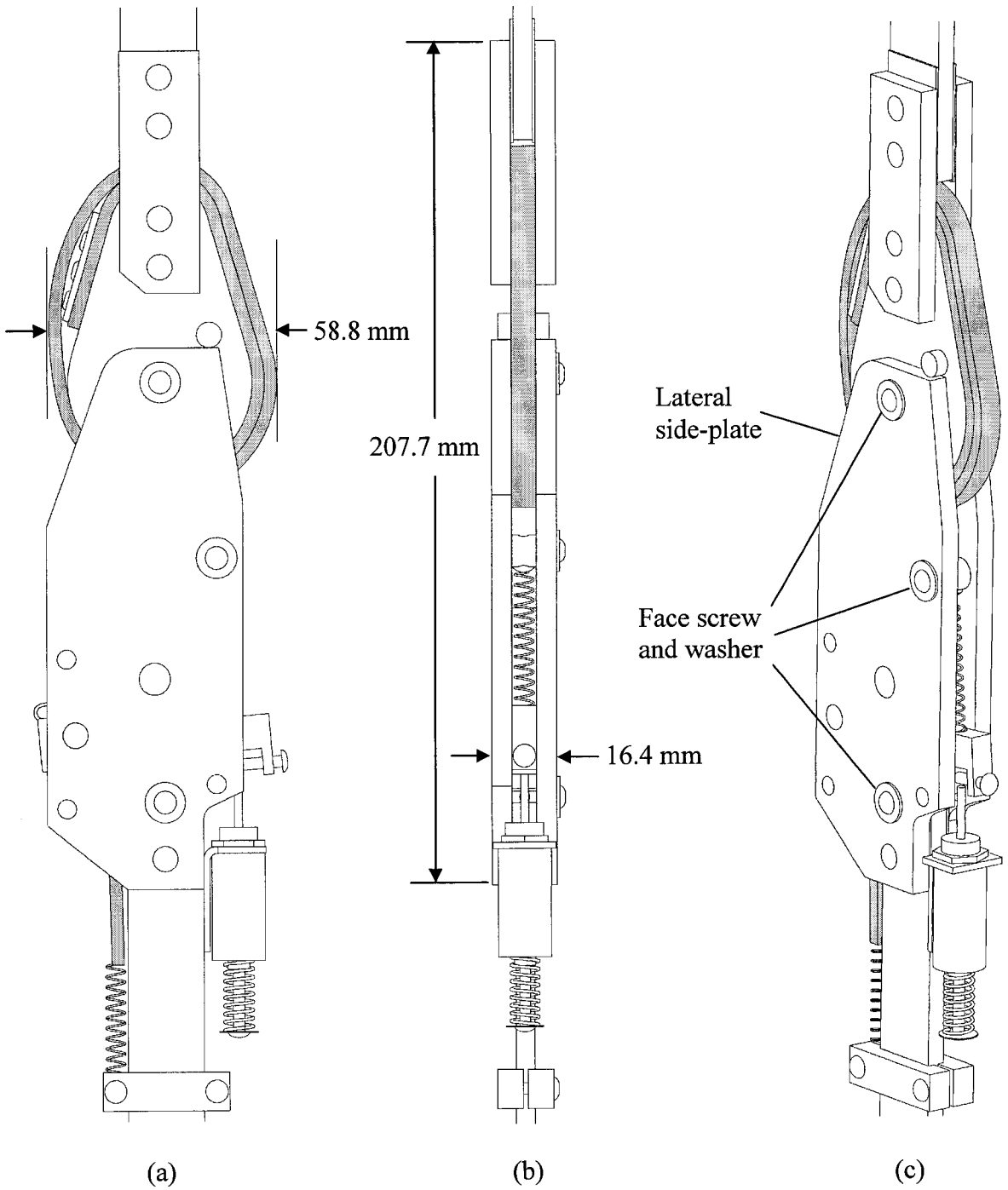

Figure 3.3 – Isolated view of DKJ: (a) side lateral view, (b) front view, (c) three-quarters profile view.

3.5.2 Dynamic Knee Joint Function

The dynamic knee joint was designed to inhibit knee flexion while allowing knee extension in the stance phase of gait and to allow free knee flexion and extension in the swing phase of gait. This section describes how the dynamic knee joint is expected to function during proper operation.

3.5.2.1 Stance Mode

At the onset of stance, pressure sensors located on the orthosis footpiece detect that the limb is weight bearing. An onboard dedicated logic circuit monitors the pressure sensors and the solenoid remains inactive, in the downward position (Figure 3.4). The hammer is therefore allowed to rotate clockwise about its axis pin (Figure 3.4). Initial loading of the braced leg would create a flexion moment on the knee and therefore a flexion moment M_F on the orthotic joint. Flexion moment M_F would cause the upper section of the orthosis to rotate counter-clockwise about the knee axis pin as shown in Figure 3.4. A counter-clockwise disc rotation would create tension in the belt that would impart a normal force F_D on the upper curved end of the hammer. The normal force imparted by the belt generates a clockwise moment M_{H1} on the hammer that would overcome the relatively small opposing counter-clockwise moment M_{H2} imposed on the hammer by

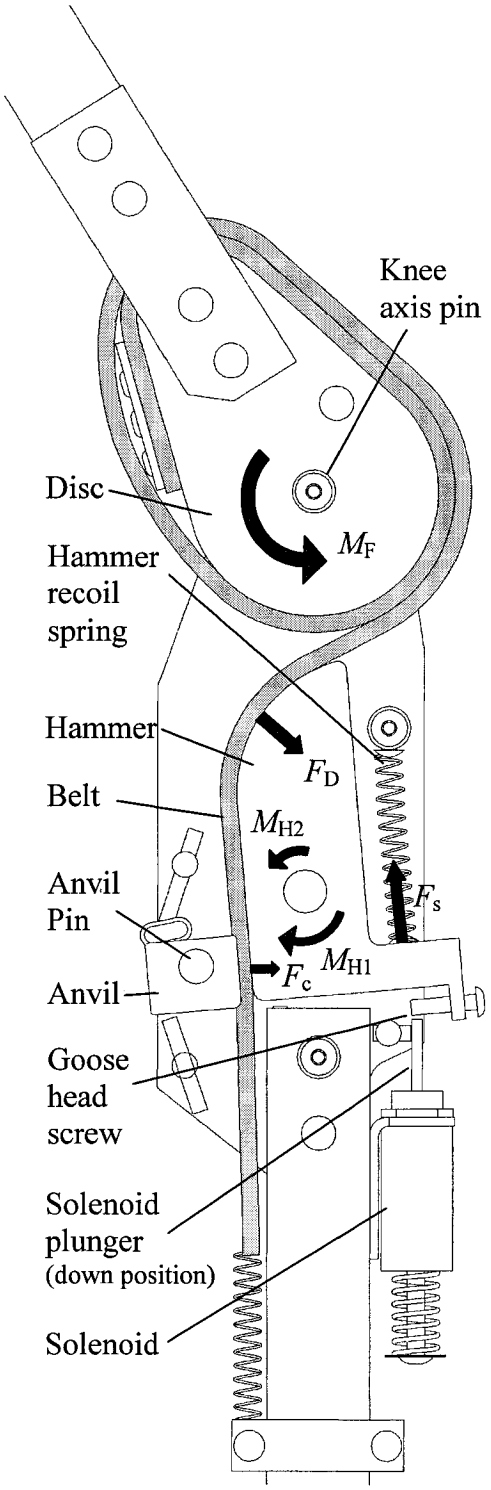

Figure 3.4 - Non-free-body diagram of the forces and moments in the DKJ during knee flexion in stance. The solenoid is deactivated.

the hammer recoil spring force F_s. Therefore, the hammer rotates clockwise to clamp the belt against the anvil with force F_c. The anvil pivots about the anvil pin to maintain a parallel clamping surface with the hammer. With the belt clamped between the hammer and the anvil, the belt is not permitted to travel and the upper section of the joint is prevented from rotating counter-clockwise into further flexion. The knee joint, and therefore the user's knee, is prevented from flexing.

The clamping force F_c (Figure 3.4) imparted by the hammer on the belt is directly proportional to the tension in the belt, which in turn is directly proportional to the moment M_F applied to the upper section on the orthotic joint. This is explained mathematically in Section 3.5.3. The result would be a proportional increase in clamping force F_c with an increase in the knee flexion moment M_F. The belt would therefore not slip between the anvil and the hammer as the flexion moment about the knee is increased further.

For the knee to achieve extension motion, a sufficient extension moment M_E about the knee axis on the upper joint section must be present to minimize the tension in the belt (Figure 3.5). A minimal amount of belt tension reduces the force F_D (Figure 3.4)

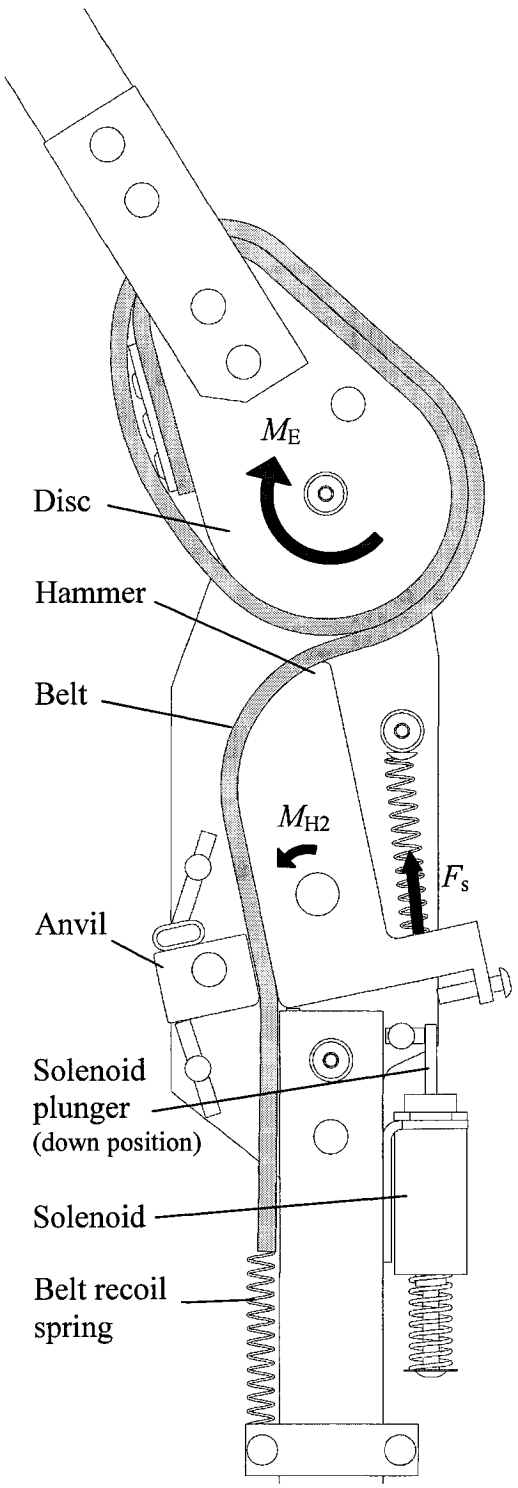

Figure 3.5 - Non-free-body diagram of the forces and moments in the DKJ during knee extension in stance. The solenoid is deactivated.

imposed on the upper end of the hammer ($M_{H1} \approx 0$). The counter-clockwise moment M_{H2} created by the hammer recoil spring force F_s dominates and causes the hammer to rotate counter-clockwise (Figure 3.5). The hammer ceases to clamp onto the belt ($F_c = 0$) and opens a gap to allow the belt to pass freely between the hammer and anvil. The orthotic joint would therefore be able to extend freely. The belt recoil spring collects the slack in the belt and keeps it taught throughout knee extension.

A belt with sufficiently low tensile modulus of elasticity is expected to allow some joint flexion even when the belt is clamped to resist excessive knee flexion. A belt with lower tensile modulus of elasticity would elongate more under tension and provide more knee flexion under loading (M_F) than one of higher elastic modulus. As illustrated in Section 2.1.1.6, a limited amount of controlled knee flexion is desirable for the wearer as it alleviates initial weight-bearing forces in the anatomical knee joint and helps smooth the path of the body's center of gravity. Too much knee flexion in limb loading, however, may not provide adequate knee support and control for the user. Since belt stiffness would not be adjustable, the DKJ would offer a different amount of knee flexion for users of different strength and body weight. A belt with sufficient

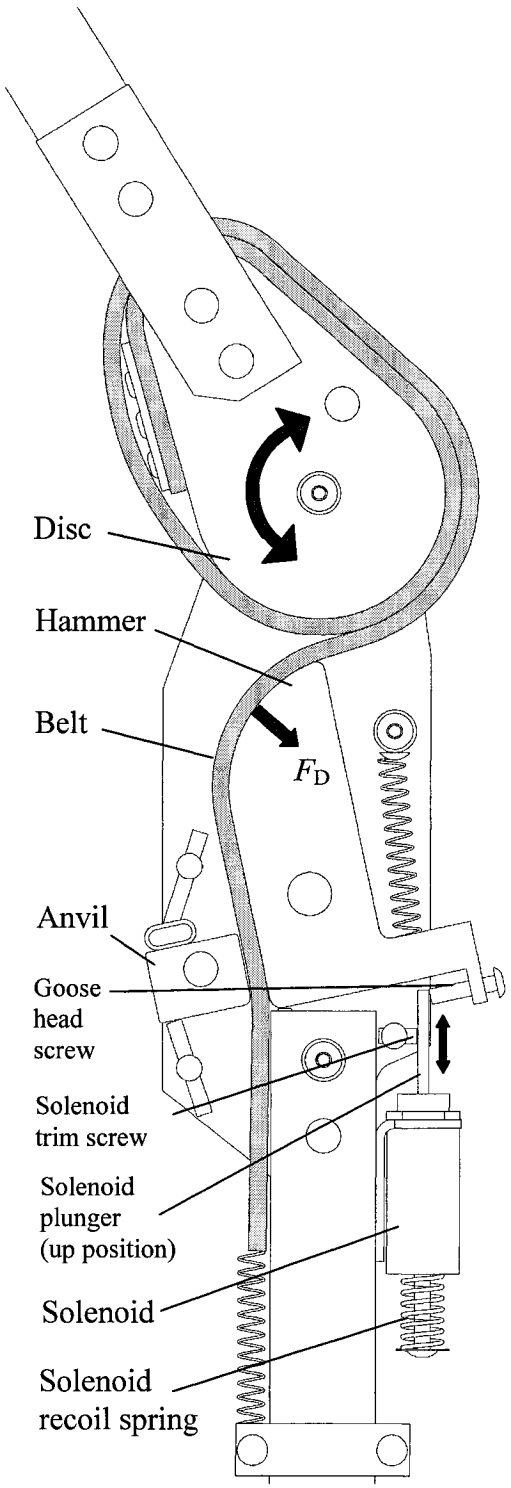

Figure 3.6 - Non-free-body diagram of the forces and moments generated in the DKJ during knee flexion and extension in swing. The solenoid is active.

stiffness to support all potential users would be used in a final commercial design.

3.5.2.2 Swing Mode

At the onset of the swing phase of gait, the pressure sensors positioned on the foot-sole of the orthosis detect a low level of force acting on the bottom surface of the foot and the dedicated logic circuit activates the solenoid. With low tension in the belt, and therefore a relatively low force F_D and thus low moment on the hammer, the solenoid plunger thrusts upward between the solenoid trim screw and the goose-head screw (Figure 3.6) and blocks the hammer from pivoting clockwise. The hammer is disabled from clamping the belt, thereby allowing the joint to flex and extend freely until the solenoid plunger disengages. When foot sole pressure is detected, the solenoid is deactivated and the solenoid recoil spring pulls the solenoid plunger out of the path of the goose-head screw. The hammer then pivots freely again, as required for the next heel strike and stance phase.

3.5.3 Theoretical Performance

During the preliminary design stage, an investigation of the DKJ's theoretical kinematic and kinetic performance was necessary. Static analyses of the kinematic and kinetic behaviour of the device during normal use of the DKJ as well as stress analysis were needed to determine the required dimensions, friction coefficients and materials of the DKJ components. The analytical procedure involved determining the forces imparted on the hammer by the belt, calculating the resulting clamping force between the hammer and the anvil, and calculating the minimal belt-hammer friction coefficient required to prevent belt slip under the respective clamping force. Subsequently, anticipated peak stresses were calculated for each component to optimize the dimensions and materials used for each component.

3.5.3.1 Tension in Belt Section BC

The maximum knee moment plus one standard deviation experienced in stair ascent by a 90 kg individual (154 Nm [11]) was used when designing the knee joint. Considering that the KAFO has two dynamic knee joints, the peak moment experienced by one joint was:

$$M_{K\,\max} = \frac{154Nm}{2}. \tag{3.1}$$

The tension in belt section BC (Figure 3.7), T_{BC} was determined from the moment about the knee joint axis, A, divided by the radius R_1 to the center of the belt:

$$T_{BC} = \frac{M_{K\,\max}}{R_1}. \tag{3.2}$$

T_{BC} was the greatest force experienced by the belt along its entire length. The belt was sized according to the value of T_{BC} at maximum knee loading.

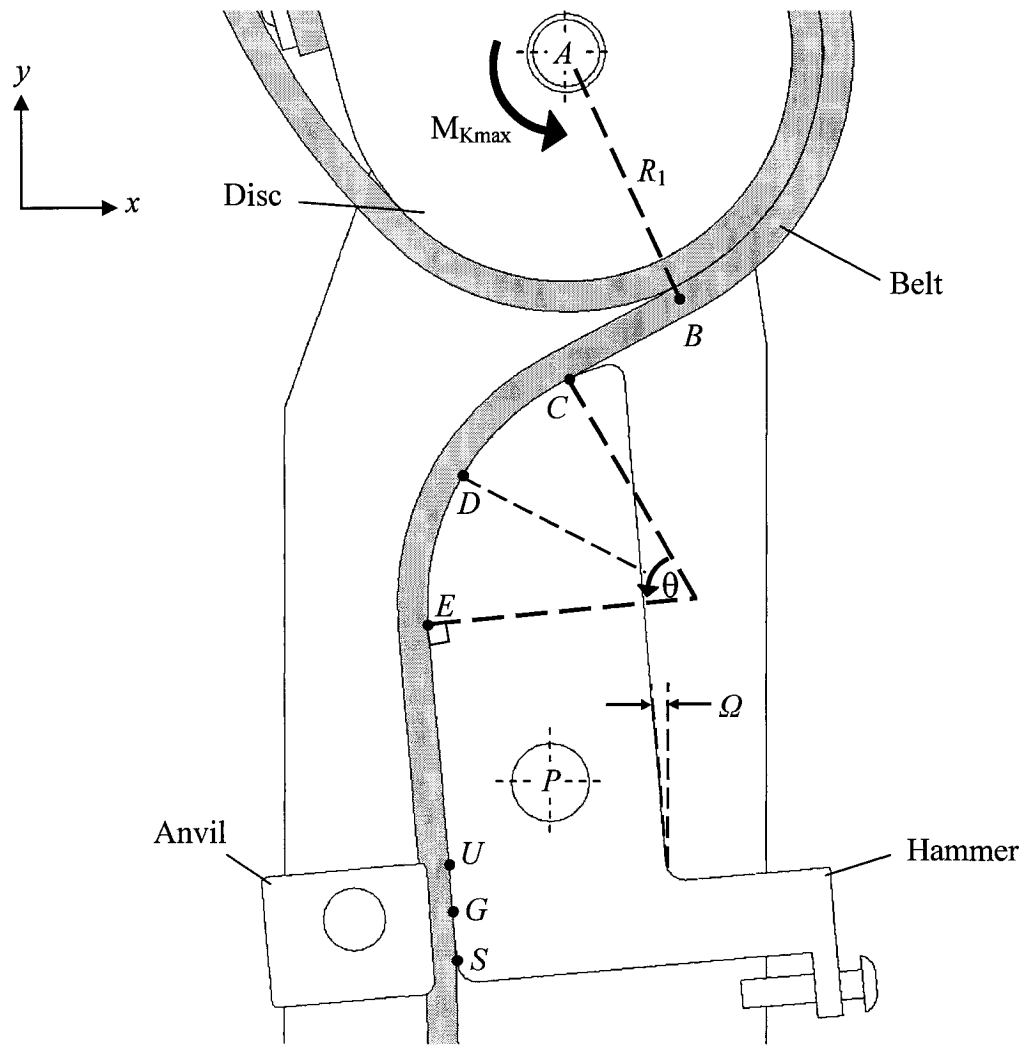

Figure 3.7 – Enlarged drawing of the dynamic knee joint showing relevant landmarks and dimensions.

3.5.3.2 Tension in Belt Section EF

Tension in belt section EF (Figure 3.7), T_{EF} was substantially lower than T_{BC} due to friction between the belt and the hammer. The reduction in tension of a flexible member wrapped around a curved, stationary object [84], T_{EF} was calculated by:

$$T_{EF} = \frac{T_{BC}}{e^{\mu\theta}}, \tag{3.3}$$

where μ is the coefficient of friction between the belt and the hammer and θ is the angle of wrap of the belt around the curved surface of the hammer.

3.5.3.3 Forces Applied to the Belt above the Clamp

A free-body diagram of the belt was used to calculate the reaction force F_D applied by the hammer on the belt (Figure 3.8). A simplified analysis was carried out as follows:

The x and y components of belt tension T_{BC} were calculated. Referring to Figure 3.8:

$$T_{BCx} = T_{BC}(\sin\phi), \tag{3.4}$$

$$T_{BCy} = T_{BC}(\cos\phi), \tag{3.5}$$

where ϕ is the angle between the y-axis and the tangent of the belt at point C on the hammer. Next, the x and y components of belt tension T_{EF} were calculated. Referring to Figure 3.8:

$$T_{EFx} = 0, \tag{3.6}$$

$$T_{EFy} = T_{EF}. \tag{3.7}$$

The tangential frictional force exerted by the hammer onto the belt F_f was found by calculating the difference between the upper belt tension T_{BC} and the lower belt tension T_{EF}. Referring to Figure 3.8:

$$F_f = T_{BC} - T_{EF} . \tag{3.8}$$

For simplicity, the frictional force F_f was assumed to act at the midpoint of belt wrap around the hammer, point D. The x and y components of the frictional force F_f were calculated at point D. Referring to Figure 3.8:

$$F_{fx} = F_f(\sin\gamma) , \tag{3.9}$$

$$F_{fy} = F_f(\sin\gamma) , \tag{3.10}$$

where γ is the angle between the y-axis and the tangent of the belt on the hammer at point D.

A simplified analysis to determine a single reaction force F_D acting at D from the hammer on the belt was carried out. The x and y components of F_D were calculated by applying equations of equilibrium including the other three forces acting on the belt T_{BC}, T_{EF}, and F_f. Referring to Figure 3.8:

$$\overset{+}{\rightarrow}\sum Fx = 0 \text{ on belt;} \quad T_{BCx} + T_{EFx} - F_{fx} - F_{Dx} = 0 , \tag{3.11}$$

$$F_{Dx} = T_{BCx} + T_{EFx} - F_{fx} ,$$

$$+\uparrow \sum Fy = 0 \text{ on belt;} \quad T_{BCy} - T_{EFy} - F_{fy} + F_{Dy} = 0 , \tag{3.12}$$

$$F_{Dy} = -T_{BCy} + T_{EFy} + F_{fy} .$$

The magnitude of the reaction force F_D was determined by:

$$F_D = \sqrt{F_{Dx}^2 + F_{Dy}^2} . \tag{3.13}$$

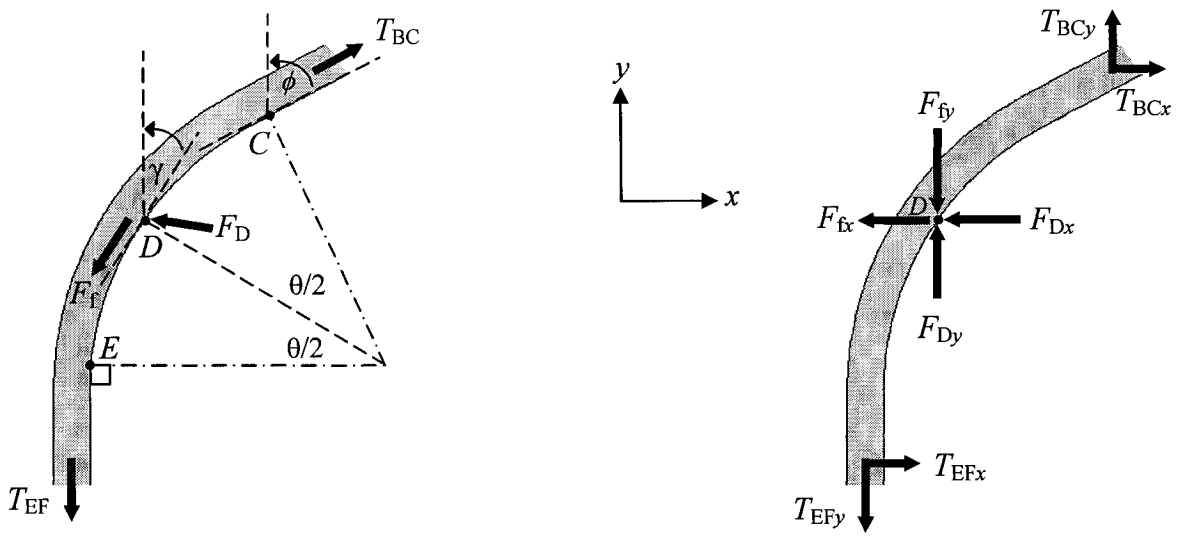

Figure 3.8 – A simplified free-body diagram of the segment of the belt that wraps over the upper hammer showing (a) the forces acting on the belt and (b) the force components.

3.5.3.4 Friction Forces Applied to the Belt in the Clamp

Figure 3.9 is a free-body diagram of the belt segment under tension T_{EF}, located in the closed clamp between points U and S in Figure 3.7. The relatively low belt recoil spring force was considered negligible. The total friction force generated by the hammer and the anvil must equal belt tension T_{EF} to prevent any belt travel through the clamp.

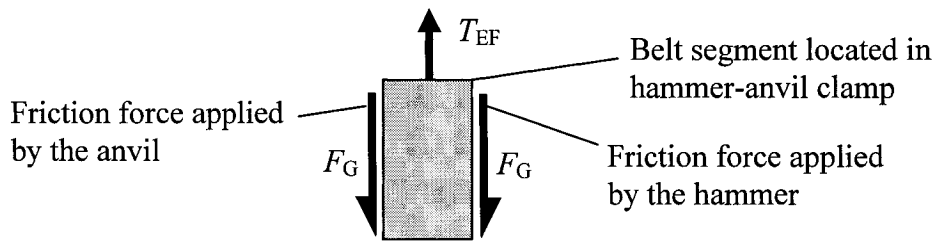

Figure 3.9 - A free-body diagram of the belt segment, under tension T_{EF}, in the closed clamp with associated friction forces applied by the hammer and the anvil. The relatively low belt recoil spring force was considered negligible and therefore not shown.

The friction force applied by the hammer and anvil within the clamp will be equal since the clamping surface of the anvil and hammer are of the same material. The friction force F_G (Figure 3.9) is therefore equal to:

$$F_G = \frac{T_{EF}}{2}. \tag{3.14}$$

3.5.3.5 Clamping Force Imparted by Hammer

The hammer clamping force F_C was determined by a summation of moments on the hammer about the hammer pin at point P (Figure 3.10). The hammer clamping force was assumed to act at point G, the midpoint of contact between the hammer and the anvil. Referring to Figure 3.10:

$$\oplus \sum M_P = 0 \text{ about } P; \qquad -(F_{Dx} H_1) + (F_C H_2) + (F_{Dy} H_3) - (F_G H_4) = 0,$$

$$F_C = \frac{(F_{Dx} H_1) - (F_{Dy} H_3) + (F_G H_4)}{H_2}. \tag{3.15}$$

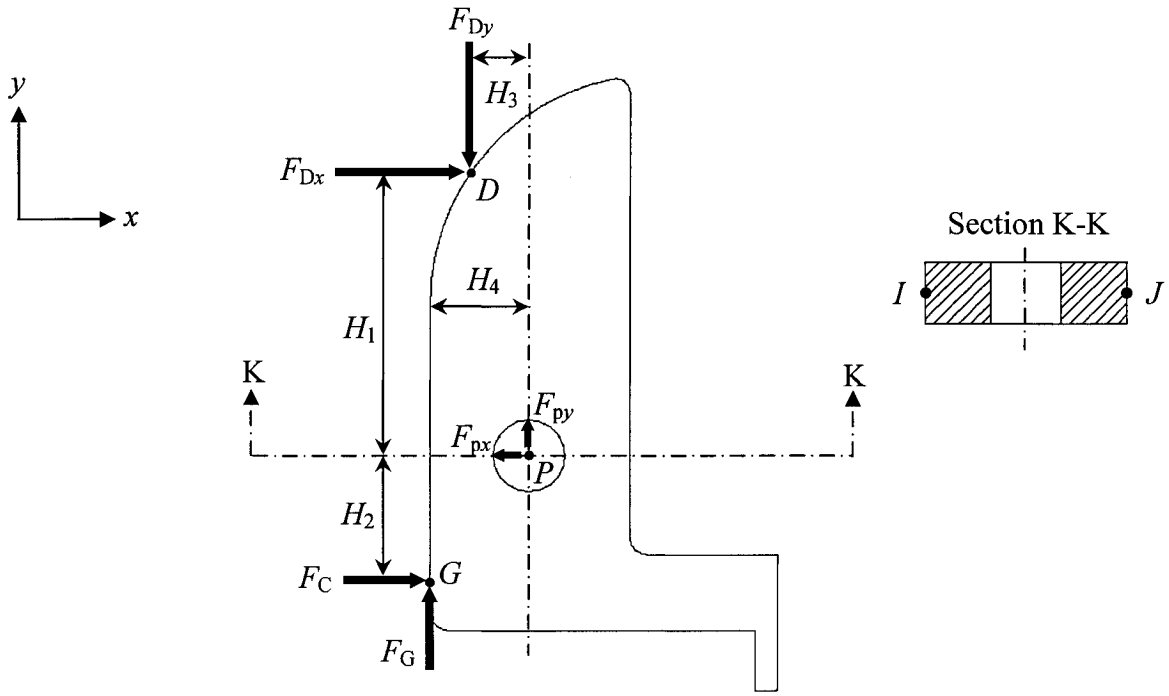

Figure 3.10 – A free-body diagram of the hammer used to determine the hammer clamping force by a summation of moments about the hammer pin at point P.

3.5.3.6 Required Belt Coefficient of Friction

The coefficient of friction between the belt and the hammer and anvil must be sufficient to prevent the belt from slipping in the clamp. The friction force generated at the clamp site is a product of the clamping force F_C between the hammer and the anvil and the coefficient of friction μ, between the belt and the hammer and anvil. The coefficient of friction must be sufficient to generate a friction force equal to F_G

(Section 3.5.3.4) under clamping force F_C (Section 3.5.3.5). Applying the standard friction equation [84], the required coefficient of friction μ_{req}, was:

$$F_G = F_C \mu_{req},$$

$$\mu_{req} = \frac{F_G}{F_C}. \tag{3.16}$$

Table 3.5 summarizes the important peak forces and required coefficient of friction predicted for a 90 kg user in stair ascent. A complete table of values for the aforementioned variables is presented in Appendix C.

Table 3.5 – Predicted peak forces and moments during stair ascent of a 90 kg user and required belt-hammer friction coefficient.

Symbol	Description	Value
M_{Kmax}	Maximum knee moment	77 Nm
T_{BC}	Belt tension between points *B* and *C* (Figure 3.7)	2800N
T_{EF}	Belt tension between points *E* and *U* (Figure 3.7)	1000 N
F_{Dx}	Belt force imposed on hammer, *x*-component (Figure 3.10)	1600 N
F_{Dy}	Belt force imposed on hammer, *y*-component (Figure 3.10)	1520 N
F_C	Clamping Force	3700 N
μ_{req}	Required belt-hammer friction coefficient	0.19

3.5.4 Structural Analysis

In order to size the components and select the optimal materials for the DKJ, an analysis of the peak static and dynamic stresses expected under normal use was performed. This section reviews the methods that were used to analyze the stresses in the most highly loaded components of the DKJ device. The calculated peak stress values are given in Appendix C.

3.5.4.1 Static Strength Analysis

3.5.4.1.1 Pin Stresses

The shear, bearing, bending and tearout stresses were calculated for all pins under peak loading conditions, using the following equations [84]:

$$\tau_s = \frac{F_p}{2A_p}, \tag{3.17}$$

$$\sigma_b = \frac{F_p}{t\, d_p}, \tag{3.18}$$

$$\sigma_d = \frac{M_p\left(\frac{d_p}{2}\right)}{I_p}, \tag{3.19}$$

$$\tau_t = \frac{F_p}{A_t}, \tag{3.20}$$

where τ_s is the shear stress, σ_b is the bearing stress, σ_d is the bending stress, τ_t is the tearout stress, F_p is the transverse load applied to the pin, A_p is the cross-sectional area of pin, t is the thickness of bearing component, d_p is the pin diameter, M_p is the moment applied to the pin, I_p is the second moment of inertia of the pin and A_t is the tearout area of the component loading the pin.

To determine the bending moment M_p acting on the pins, the loading condition for all pins was modeled as a double cantilever supported beam with uniform, distributed loading.

3.5.4.1.2 Bending Stresses

The bending stresses under peak loading were calculated for the hammer, brackets, uprights and side-plates using the standard beam bending equation [84]:

$$\sigma_d = \frac{My}{I_b}, \tag{3.21}$$

where M is the bending moment, y is the distance from neutral axis to edge of component and, I_b is the second moment of inertia of the component.

Simplifications were made in modeling some of the part geometries in order to facilitate calculation.

3.5.4.1.3 Bearing Stresses

The peak bearing stress imparted by the belt to the hammer was calculated for the leading edge of the hammer between points C and E (Figure 3.7). The bearing stress experienced on the clamping site of both the hammer and the anvil between points U and S (Figure 3.7) was also calculated.

3.5.4.1.4 Hammer Stress

As illustrated in Figure 3.10, the hammer is subjected to large bending forces F_{Dx}, F_C and F_{px}. Forces F_{Dy}, F_{py} and F_G create an additional compressive stress on the hammer. The greatest stress in the hammer is approximately located at point J (Figure 3.10) and was calculated by summing the compressive stress developed in bending with the compressive stress developed in axial loading [84]. The maximum tensile stress was experienced at point I (Figure 3.10). Though the maximum tensile stress was considerably lower than the maximum compressive stress, the maximum tensile stress was more relevant for analyzing the fatigue strength of the hammer because fatigue failure is a tensile phenomenon [84]. Point I is therefore most susceptible to fatigue failure.

3.5.4.2 Dynamic Strength Analysis

Dynamic strength analysis was performed on all components subject to substantial tensile stresses. The stresses were calculated for loading levels expected for a 90 kg user in normal cadence. This was a reasonable assumption since the brace will be subjected to loads generated in normal cadence the majority of the time. The Goodman line equation was used to calculate the infinite-life safety factor (n_∞) of the stressed part:

$$\frac{\sigma_a}{S_E} + \frac{\sigma_m}{S_{UT}} = \frac{1}{n_\infty}, \tag{3.22}$$

where σ_a is the alternating-stress amplitude, σ_m is the mean stress, S_{UT} is the ultimate tensile strength, S_e is the modified fatigue strength or endurance limit and n_∞ is the infinite-life safety factor.

The cycle life (N) of the highest stressed components was calculated [84] by:

$$N = \left(\frac{\sigma_R}{a}\right)^{\frac{1}{b}}, \tag{3.23}$$

where,

$$\sigma_R = \frac{\sigma_a S_{UT}}{(S_{UT} - \sigma_m)}, \tag{3.24}$$

$$\sigma_a = K_f \sigma_{nom}, \tag{3.25}$$

$$K_f = [1 + q(K_t - 1)], \tag{3.26}$$

a and b are constants determined from the S-N stress-cycle curve based on standard reference fatigue tests and using S_e and S_{UT} [85], σ_R is the equivalent reversed stress for combined alternating and mean stresses, K_f is the fatigue-stress concentration factor, σ_{nom} is the nominal stress, q is the notch sensitivity based on the notch radius and the ultimate strength of the chosen material and K_t is the geometric stress-concentration factor [86].

A summary of the calculated infinite-life safety factors is given in Table 3.6. The calculated cycle life of the highest stressed components can be found in Table C.7 in Appendix C.

Table 3.6 - Infinite-life safety factors of critically stressed components (90 kg user in normal cadence).

Description	Infinite Life Safety Factor, n_∞
Hammer tensile stress in bending	2.3
Side-plate bending	2.6
Bracket bending	2.8
Upright bending	1.6
Lower bracket pin bending stress (highest pin stress)	3.9

The minimum dynamic stress safety factor planned for the DKJ was 2 to 3. The calculated infinite-life safety factor values for the highest stressed components in the DKJ

were satisfactory with the exception of the upright, which had an infinite-life safety factor of 1.6. As discussed in Section 6.4.1.8, the upright may be made from stronger materials or reinforced in order to attain a greater factor of safety if necessary. The dynamic strength equations provide only a crude estimate of the cycle life of a part or device [84]. Despite the calculated results of the DKJ dynamic strength analysis, physical cyclic testing of the DKJ installed in a pair of uprights is required to obtain a more accurate estimate of the cycle life of the DKJ.

3.5.5 Part Functions

This section reviews the structural and functional details of each major component in the DKJ. The functional role of each component is defined and any issues affecting the structure or performance of the component are covered.

3.5.5.1 Disc

The *disc* connects the belt with the upper portion of the dynamic knee joint (Figure 3.2). Three UNC 4-40 screws and a flat *clamping bar* are used to anchor the belt to the disc. The clamping bar helps distribute the clamping force of the screws. The belt wraps completely around the disc at least once and then partially again to reduce the tension in the belt by exploiting friction (Equation 3.3). Friction alleviates the otherwise high shear force applied to the clamping screws by the belt. The belt may be wrapped around the disc more or less than one complete revolution, depending on the friction characteristics of the belt and the maximum anticipated belt tension.

The disc is used to spool the belt. The radius, R_1 (Figure 3.7) of the disc was determined as a trade-off between minimizing the stresses in the DKJ and minimizing the size of the DKJ. A higher disc radius R_1 permits a lower belt tension T_{BC}, which leads to lower stresses in the belt, hammer, anvil, side-plates and pins. Lower part stresses result in an increased cycle life of the individual components and the DKJ as a whole. A lower disc radius R_1, permits a lower dynamic knee joint size and weight but incurs higher stresses. The disc radius R_1 was designed as large as possible to reduce the belt tension and peak stresses throughout the device, yet still maintain a relatively compact size.

The disc was connected to the upper upright via two brackets and four press fit pins. The current embodiment of this connecting method may prove too bulky for future commercial designs and more discreet methods of connecting the disc to the upper strut may be employed such as using only one bracket, welding the disc and upper upright together, or machining the disc and upper upright as one piece.

3.5.5.2 Knee Flexion/Extension Stops

The brackets and the extension stop pin limit disc rotation. The extension stop pin was press fit through a hole in the disc (Figure 3.2), and limited the joint to a 0° knee hyper-extension angle by butting against the top edge of the side-plates. The chamfered bottom rear corner of both brackets acted as flexion stops by butting against the posterior edge of the side-plates and limiting the joint to a 110° flexion angle. Thin rubber bumpers can be adhered to the butting surfaces of the side-plates to reduce impact and noise. Bumpers of appropriate thickness can be fixed to the butting surfaces to reduce the range of motion of the joint.

3.5.5.3 Belt

The belt is the central component of the DKJ. The ideal belt must offer a static coefficient of friction with aluminium greater than $\mu_{req.}$ To achieve a safety factor of three for a 90 kg brace user in stair ascent, the belt must be capable of withstanding tensions of 8400 N. The belt must be durable enough to resist wear at the clamping site for at least three months of regular use, approximately quarter a million loading cycles. As the knee normally flexes to absorb the impact of initial limb loading in walking (Section 2.1.1.6), a minimal amount of belt elongation under loading is desirable, as it will allow some DKJ flexion. A belt material offering 2% elongation in loading will produce approximately 8° of DKJ flexion. Excessive DKJ flexion during limb loading will not provide sufficient support to the user. Belt elongation should therefore generate no more than 8° of joint flexion under the greatest loading condition. Since the stiffness of the belt is not adjustable, users of lesser weight will experience less knee flexion during limb loading.

In testing, two belts were installed in parallel in the DKJ to halve the belt stress; however, this method proved ineffective. Friction between the two belts interfered with the recoil spring's ability to eliminate belt slack. As a result, an excessive amount of slack built up in one of the belts, which lead to asymmetric loading between the belts.

Section 3.5.6.4 details the required physical and mechanical properties of the belt and material selection. Section 4.1 discusses strength testing performed on the obtained belt materials.

3.5.5.4 Hammer

The hammer pivots about the hammer pin and is constantly biased to rotate in the counter-clockwise direction (as shown in Figure 3.4) due to the hammer recoil spring.

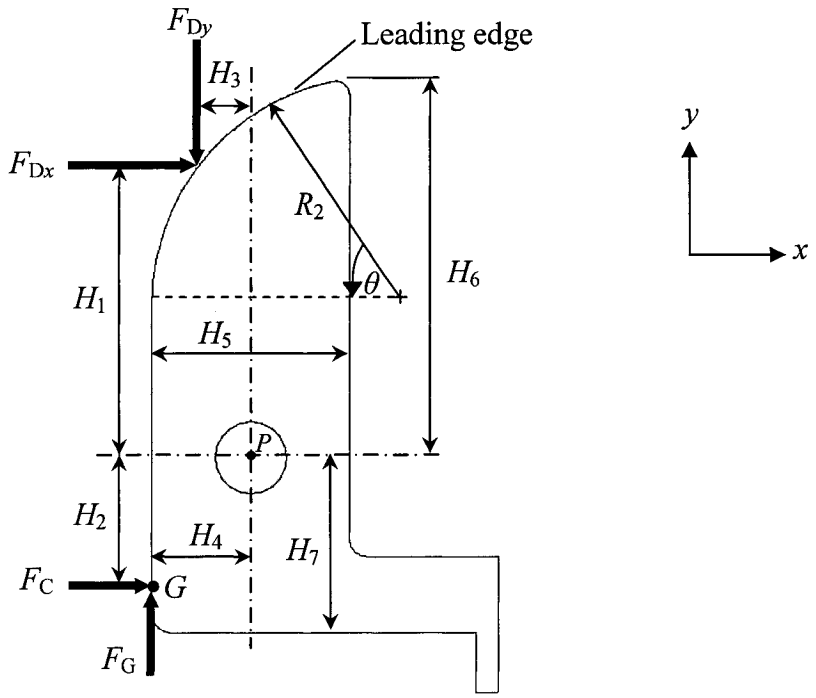

Figure 3.11 – Important hammer dimensions.

The hammer exploits the principle of levers, employing forces F_{Dx} and F_G imparted by the friction of the belt to deliver a sufficient clamping force F_C to the lower belt

(Figure 3.11). The length of the hammer was determined by the magnitude of the force F_{Dx} delivered by the belt and the magnitude of clamping force F_C required to prevent belt slip. A high friction belt will impart a larger force F_{Dx} and require a lower clamping force F_C than a belt of lesser friction. The length of the hammer can be shortened if a relatively high friction belt is used. The width of the hammer H_5 was influenced by the substantial bending and tearout stresses experienced in stance.

The bottom leading edge corner of the hammer was rounded to prevent damage to the belt during clamping between the hammer and the anvil. The upper leading edge of the hammer had a relatively large radius R_2 for the belt to wind around because a sufficiently small radius can adversely affect the cycle life of the belt. The upper radius was tangent to the leading edge of the hammer.

The hammer was positioned as close to the disc as possible to reduce joint size and maximize belt contact θ with the hammer (Figure 3.7). The proximity of the hammer and the disc was limited by the thickness of the belt, which in the clamped state must leave the hammer at a tangent to the hammer radius R_2. Setting the hammer excessively close to the disc would cause the belt to leave the hammer at an angle steeper than the tangent to hammer radius R_2, causing the belt to exceed its minimum pulley diameter. This scenario can compromise the cycle life of the belt. As the hammer pivots into the open position, the top apex of the hammer approaches the disc. The top apex of the hammer was therefore rounded to eliminate any belt pinching between the hammer and the disc.

A major design goal with the hammer was to deliver a maximum clamping force with a minimum hammer length H_6 (Figure 3.11). As described in Equation 3.15, the magnitude of the hammer clamping force F_C is a function of the sum of the external moments acting on the hammer. The greatest moments acting on the hammer are created by the x-y-components of the belt-hammer reaction force F_D. The moment created by the x-component of the belt-hammer reaction force F_{Dx}, acts at a distance H_1 from the hammer axis of rotation and contributes substantially to the clockwise moment acting on

the hammer and therefore adds to the clamping force F_C. The moment created by the y-component of the belt-hammer reaction force F_{Dy}, acts at a distance H_3 from the hammer axis of rotation and diminishes the clockwise moment acting on the hammer and therefore reduces the clamping force F_C imparted by the hammer. To achieve a sufficient clamping force F_C, the moment created by force F_{Dx} should be maximized and the moment created by force F_{Dy} should be minimized. Increasing dimension H_1 (Figure 3.11) will increase the moment contributing to clamping force F_C but will lead to a longer hammer and therefore a longer, bulkier DKJ. Decreasing hammer dimension H_4 (Figure 3.11) will decrease dimension H_3 and the associated moment that diminishes the clamping force F_C but will compromise the tearout failure safety factor of the hammer against the hammer pin.

An effective means of maximizing the clamping force F_C and minimizing the length of the hammer is to maximize the hammer-belt contact angle θ (Figure 3.12). As described in Equations 3.4 and 3.10 and Figure 3.8, increasing the hammer-belt contact angle θ, increases the x-component of the belt-hammer reaction force F_{Dx}, which contributes to the magnitude of the clamping force F_C (Equation 3.15). Figure 3.12b shows that a greater hammer-belt contact angle θ'', positions the belt-hammer reaction force F_D, higher up on the leading edge of the hammer than the loading condition in Figure 3.12a. The loading condition with the greater hammer-belt contact angle θ'' in Figure 3.12b also presents a greater vertical distance H_1'', between the reaction force F_D, and the hammer axis of rotation and a smaller horizontal distance H_3, between the reaction force F_D and the hammer axis of rotation. An increase in H_1 and a decrease in H_3 both contribute to an increase in clamping force F_C (Equation 3.15). The overall result of an increased hammer-belt contact angle θ is a greater clamping force under the same belt tension T_{BC}, belt friction μ, and hammer dimensions. The hammer-belt contact angle θ is maximized by positioning the fully clamped hammer at an angle Ω with respect to the vertical (Figure 3.7).

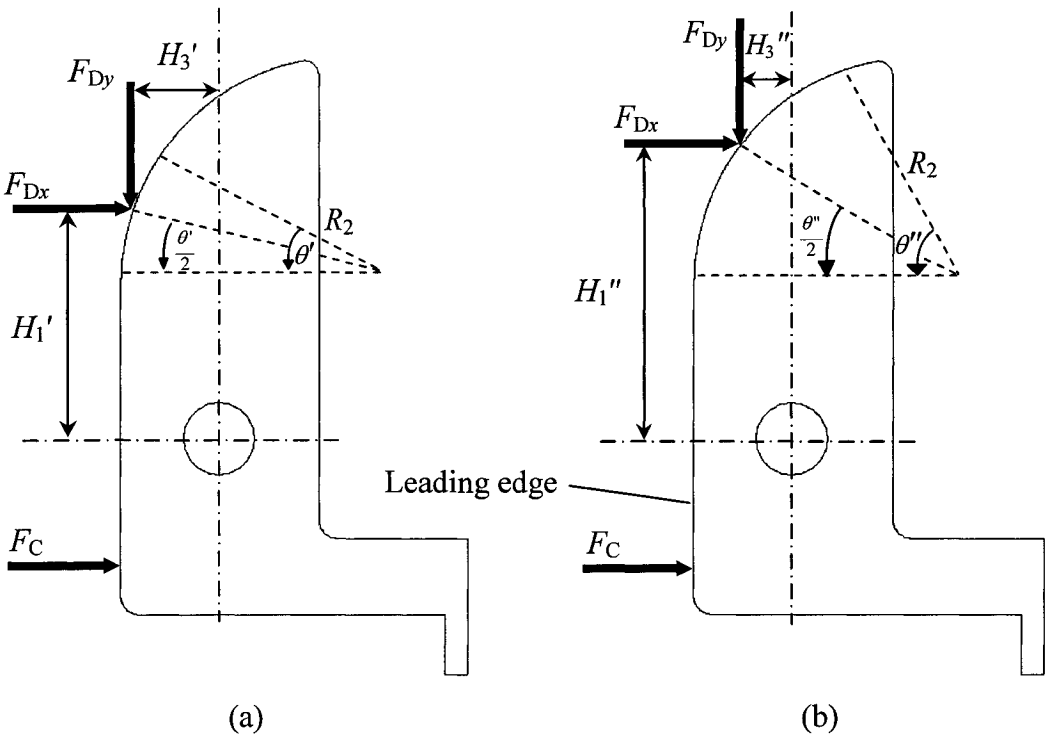

Figure 3.12 – An isolated view of the hammer with belt-reaction and clamping forces; (a) The center of pressure of the components of the belt-reaction force F_D with a relatively small hammer-belt contact angle θ' presents a relatively short distance H_1' and a relatively long distance H_3' when compared to (b) the location of the components of the belt-reaction force F_D with a relatively large hammer-belt contact angle θ'' which presents a relatively long distance H_1'' and a relatively short distance H_3''.

An inherent limitation of the DKJ is that it allows an initial amount of negligible-resistance knee flexion β (not shown), prior to full engagement of the clamping mechanism. As shown in Figure 3.13, point C on the hammer travels a distance δ as the hammer rotates by an angle Ψ, from the open position to the fully clamped position. Assuming no slip occurs between the belt and the hammer, the belt will travel the same distance as the hammer. As the belt displaces by arc δ, the disc and therefore the knee are allowed to rotate into flexion by an angle β (not shown).

KAFO users want immediate knee support when needed. Most users will not tolerate an excessive amount of negligible-resistance knee flexion. To minimize the amount of negligible-resistance knee flexion β, the magnitude of the belt displacement arc δ, must be minimized. The displacement arc δ can be reduced by decreasing the upper

length of the hammer H_8 (Figure 3.13) or by decreasing the required hammer rotation angle Ψ. As mentioned earlier, an adequate upper hammer length is important to develop an adequate clamping force F_C, therefore reducing the upper hammer length H_8 is unfavourable. Minimization of the required hammer rotation angle Ψ is the most effective means of reducing negligible-resistance knee flexion β. A belt with a high compressive elastic modulus will deform less under clamping and require the hammer to pivot less to achieve complete clamping. Section 3.5.5.5 describes how the anvil bumper mechanism reduces the required hammer rotation angle Ψ. A hammer stop screw was positioned below the lower leading edge corner of the hammer (Figure 3.13) to limit hammer rotation in the open (counter-clockwise) direction. The hammer stop screw can be positioned to trim the position of the open hammer and eliminate any excess in the anvil-hammer gap that would unnecessarily increase the required hammer rotation angle Ψ.

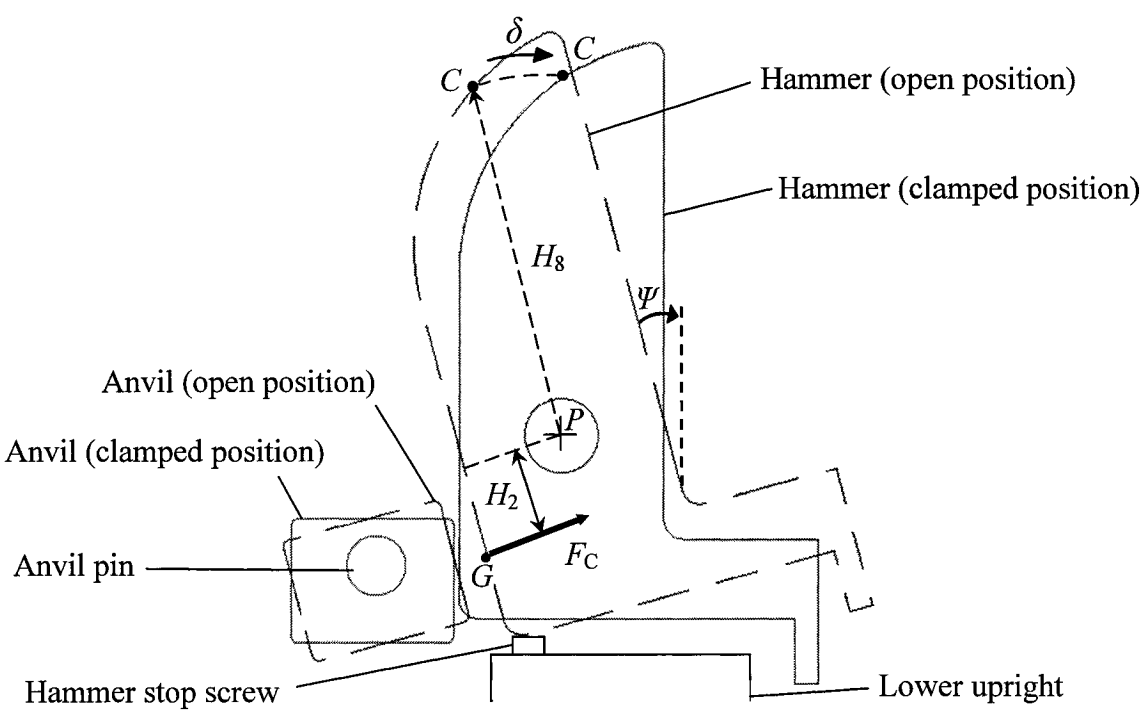

Figure 3.13 – An isolated view of the anvil and hammer in opened and closed states. The hammer rotates by a required hammer rotation angle Ψ between the fully open position (dashed line) and the fully closed position (solid line); arc distance δ indicates the magnitude of the belt displacement.

Hammer length H_2 (Figure 3.13) is the vertical distance between the center-point of clamping G, and the point of rotation P, of the hammer. As illustrated by Equation 3.15, a smaller dimension H_2, results in a greater clamping force, F_C (Figure 3.13). A larger dimension H_2, results in a smaller required hammer rotation angle Ψ since the further point G is from the axis of rotation, the greater its distance of travel is for any given hammer rotation angle and the less the hammer is required to rotate to achieve an adequate gap distance between the anvil and the hammer. Length H_2 is a compromise between two contradicting constraints. Length H_2, must be short enough to provide an adequate clamping force F_C (Equation 3.15), however, length H_2 must be maximized to decrease the required hammer rotation angle Ψ (Figure 3.13).

3.5.5.5 Anvil

The *anvil* (Figure 3.13), functions as the second component of the clamping mechanism. The anvil pivots freely about the *anvil pin*, to ensure a uniform force distribution on the belt during clamping, regardless of belt thickness irregularities. The corners of the anvil were rounded to reduce belt damage during clamping. The bottom of the anvil was located higher than the bottom of the hammer when both components were in the fully open position (Figure 3.13), to allow the hammer to align the anvil after initial contact of the two components. The range of motion of the anvil was limited by the *anvil-stop trim screw* and the *bumper* (Figure 3.2).

As explained in the previous section (Section 3.5.5.4), the required hammer rotation angle Ψ must be minimized in order to reduce the magnitude of negligible-resistance knee flexion β in stance. An anvil bumper mechanism (Figure 3.2) was integrated into the DKJ to reduce the required hammer rotation angle Ψ. The rubber elastic bumper applies a force F_B (Figure 3.14) to the top of the anvil creating a counter clockwise moment M_B on the anvil. Moment M_B positions the clamping surface of the anvil to remain parallel with the hammer's leading edge at all times. For a fixed hammer rotation angle Ψ (Figure 3.14b), a greater hammer-anvil gap d_1 is achievable if the anvil remains parallel with the hammer in the open position than if the anvil remained fixed, in which case the maximum attainable hammer-anvil gap d_2 would be smaller. An optimal

anvil-hammer gap can be achieved with minimal required hammer rotation angle Ψ if the anvil remains parallel with the leading edge of the hammer in the open position.

The *bumper trim screw* and *anvil-stop trim screw* were used to limit the anvil's range of motion (Figure 3.2). These trim screws allow the anvil to maintain alignment with the hammer over a range of required hammer rotation angles Ψ. The required hammer rotation angle Ψ can be adjusted by the position of the hammer stop screw. The ability to achieve a range of potential hammer rotation angles Ψ and therefore a range of hammer-anvil gap dimensions d_1 (Figure 3.16a), was useful in the prototyping stage since belts of different thickness were tested in the DKJ.

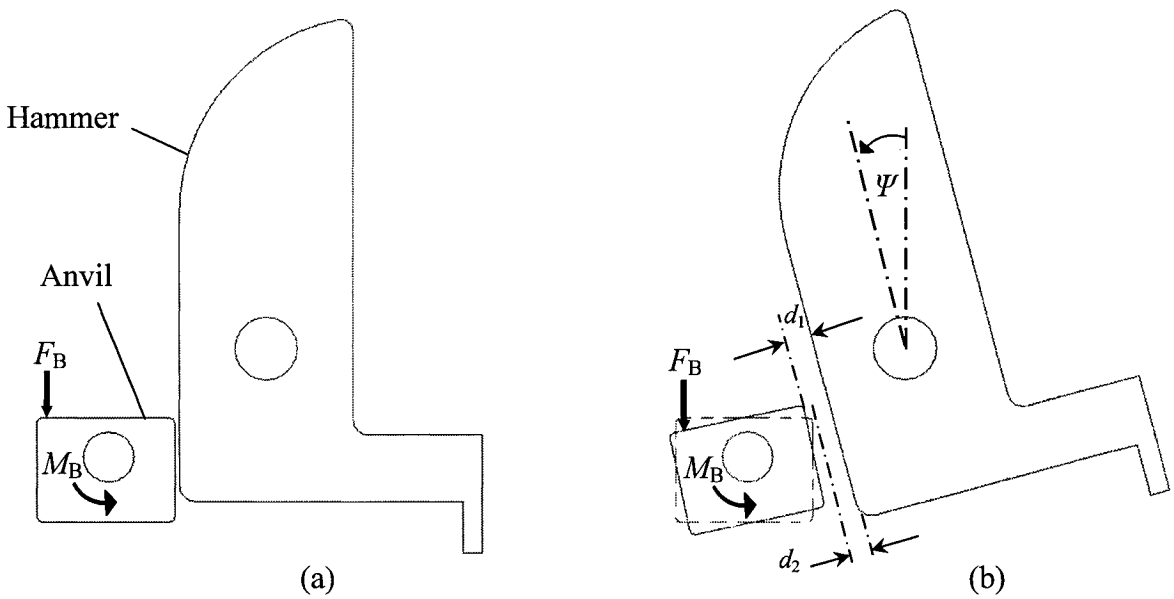

Figure 3.14 – An isolated view of the hammer and anvil. (a) The anvil and hammer in the fully clamped position; (b) the hammer and anvil in the fully open position where the gap between the hammer and anvil is greater for a given hammer rotation Ψ if the anvil remains parallel with the hammer (solid anvil), achieving gap d_1, than if the position of the anvil remains fixed (dashed anvil), achieving gap d_2.

3.5.5.6 Side-plates

The side-plates are the largest components of the DKJ. Minimization of the side-plate dimensions is important in achieving a minimal weight and size for the entire DKJ (Section 3.5.8). The bending, bearing and tearout stresses subjected by the loaded pins in stance influenced the designed side-plate dimensions. The side-plates also contain the belt and inner components of the DKJ.

3.5.5.7 Belt Recoil Spring

The belt recoil spring keeps the belt taught at all times and thus removes any slack that may develop in the belt. The recoil spring is a helical extension spring. On the prototype DKJ built for mechanical testing, the recoil spring was anchored to the lower upright by means of a bracket (Figure 3.2). An different fastening method was used on the DKAFO (Figure 3.15a).

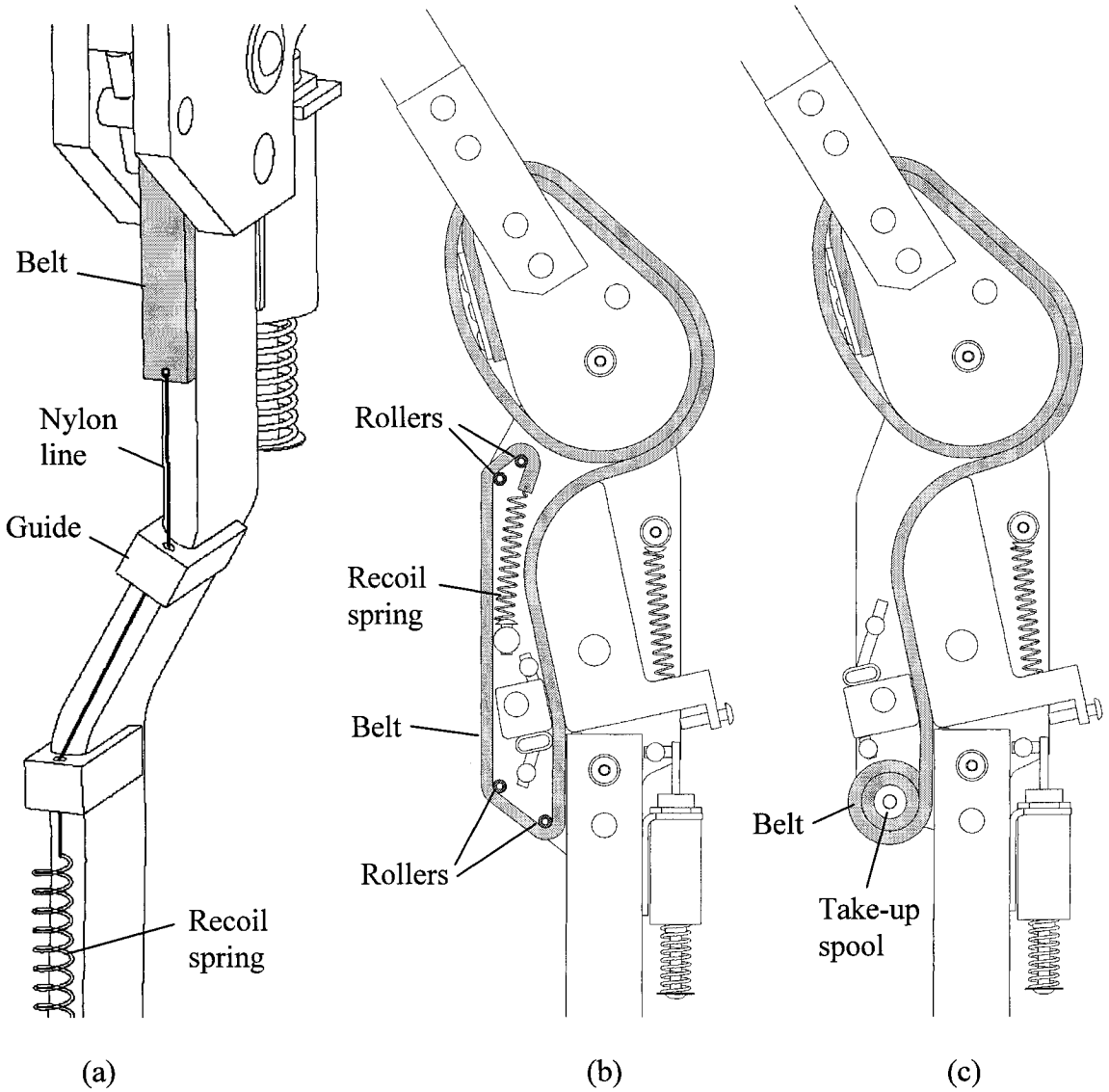

Figure 3.15 – Three alternative embodiments of the belt recoil spring mechanism: (a) the current clinical embodiment uses a nylon line and guides to direct the tensile spring force to the belt; (b) a more discreet future, alternative embodiment employs a series of rollers to contain the belt and recoil spring within the confines of the side-plates; (c) another discreet future, alternative embodiment employs a spring-driven take-up spool to provide a compact means of storing the belt and belt recoil mechanism.

On the DKAFO, the orthotic uprights were bent to conform to the wearer's leg; therefore, a different method of integrating the belt recoil spring was used in the clinical application of the DKJ than in the prototype application of the DKJ. The recoil spring installed on the DKAFO was bolted to the outer side of the thermoplastic AFO section above the ankle joint. The other end of the recoil spring was connected to the belt by a durable nylon line. The nylon line was aligned with the belt by guides located on the lower upright beneath the belt (Figure 3.15a).

The current clinical application of the recoil spring system (Figure 3.15a) was overtly bulky and prone to catching on foreign objects. A discreet alternative embodiment of the design will house the belt and recoil spring system within the side-plates. Future alternative embodiments may consider guiding the belt and recoil spring with a series of rollers to occupy space above the clamping element (Figure 3.15b). Another embodiment may attach the belt to a spring-driven take-up spool located underneath the anvil (Figure 3.15c). The take-up spool will function to remove slack in the belt and store the belt in a compact manner. Either of these designs will require a belt with considerable flexibility.

3.5.5.8 Uprights

The DKJ currently houses 3/16″ thick, 3/4″ wide, ¼ Temper 304-2B stainless steel uprights, supplied by Becker Orthopedic (Troy, MI 48083-4576; part #1001-A6S-7, 101-A6S-8). These are the strongest KAFO uprights available on the market.

3.5.5.9 Solenoid

Each DKJ houses an electro-magnetic push-type 9-volt solenoid (Saia Burgess Inc., Vandalia, OH 45377-0427; part #195205-127) measuring 48 mm in length and 19 mm in diameter. When the solenoid is activated, the goose-head screw butts against the solenoid plunger and prevents hammer rotation (clockwise) toward the anvil (Figure 3.16a). When the solenoid is deactivated, the solenoid plunger is biased downward in the lower position (Figure 3.4) and the goose-head screw and hammer are free to pivot toward the anvil and engage the belt. A solenoid trim screw minimizes

transverse deflection of the plunger from the goose-head screw when the hammer is forced to rotate clockwise, as shown in Figure 3.16a. The solenoid trim screw and goose-head screw can be adjusted to accommodate a variety of solenoid sizes.

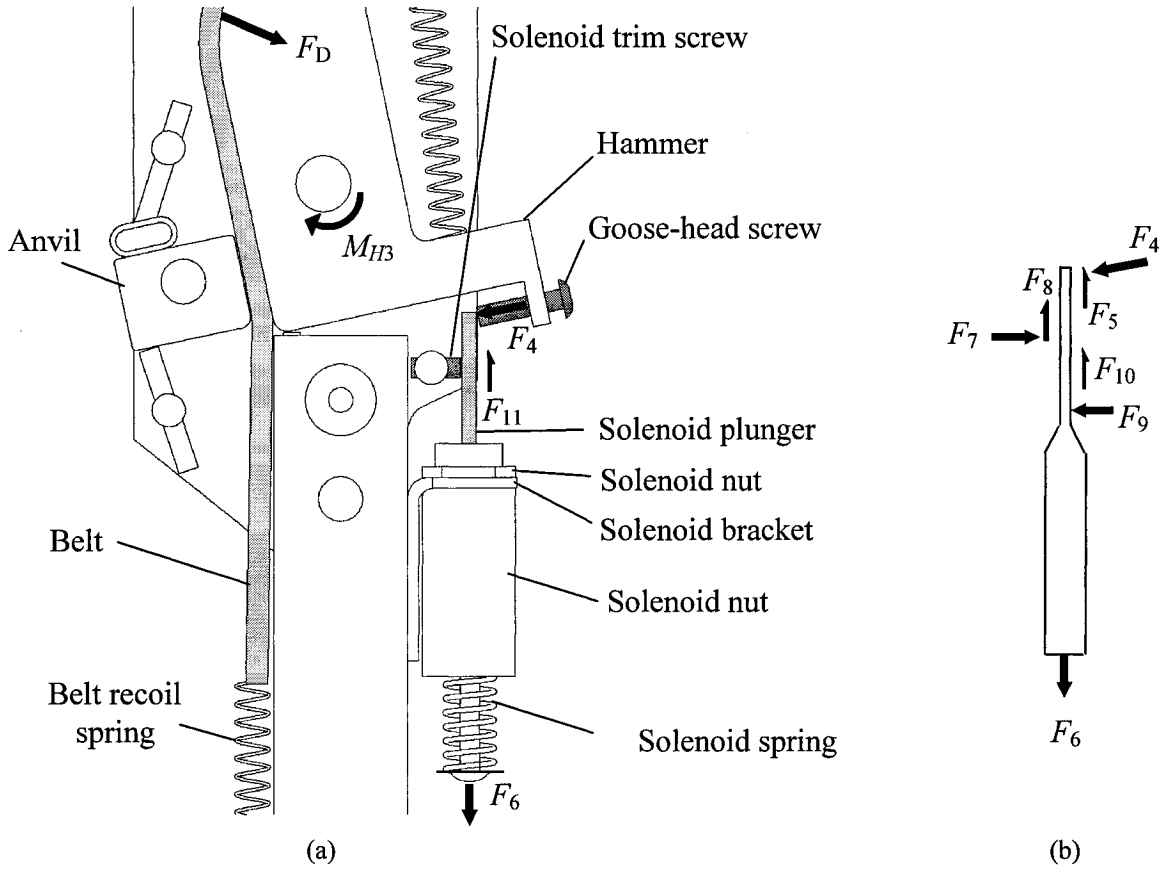

Figure 3.16 – (a) A cropped view of the solenoid and associated DKJ components shows the solenoid plunger in the raised position, engaging the goose-head screw; (b) a free-body diagram of the solenoid plunger with forces applied under engagement of the goose-head screw.

The solenoid head is threaded and held to the solenoid bracket with a nut. The solenoid bracket was adhered to the lower upright with high strength epoxy. Future embodiments of the DKJ may have the solenoid bracket spot-welded to the medial side-plate so that the lower upright can be changed without having to detach and reinstall the solenoid bracket.

A relatively low amount of belt tension is constantly maintained by the belt recoil spring. During knee flexion in swing, the belt tension will impart a small normal force F_D

(Figure 3.16a) on the hammer, and create a relatively weak clockwise hammer moment (M_{H3}). The moment M_{H3} will result in an applied force F_4 between the goose-head screw and the solenoid plunger. The application of force F_4 on the solenoid plunger creates reaction force F_7, applied by the solenoid trim screw on the solenoid plunger, and reaction force F_9, applied by the inner solenoid housing on the solenoid plunger (Figure 3.16b). Together, forces F_4, F_7 and F_9, create friction forces F_5, F_8 and F_{10} respectively (Figure 3.16b). Friction forces F_5, F_8 and F_{10} sum to create a combined friction force F_{11} (Figure 3.16a). The solenoid spring force F_6 must be sufficiently high to overcome the combined solenoid plunger friction force F_{11}, which is at a maximum when the knee moves into flexion in swing.

The solenoid plunger must disengage the hammer and move into the lowered position at the end of swing so that the DKJ can provide knee support in stance (Figure 3.4). Overcoming the combined solenoid plunger friction force F_{11} with a larger solenoid recoil spring requires a heavier solenoid with a greater length and diameter to overcome the spring force. Integration of a stronger solenoid into the DKJ design can add considerable weight and bulk to the entire joint and increase the electrical power demands of the control system. Diminishing F_{11} by reducing the coefficient of friction of the solenoid plunger and associated contact surfaces is therefore the most effective way of increasing solenoid reliability. The coefficient of friction between the solenoid plunger, the goose-head screw, the solenoid trim screw and the inner solenoid housing may be reduced if a low-friction material is adhered to their contact surfaces or a dry lubricant is applied.

In an alternative embodiment of the DKJ, a purely mechanical system may substitute the solenoid and solenoid plunger with a blocking pin that is spring biased upward. The blocking pin would passively block the hammer from engaging the belt during the swing phase of gait. A control cable, pushrod or hydraulic mechanism, triggered by pressure developed beneath the foot during the stance phase of gait may be utilized to pull the blocking pin downward and allow the hammer to engage the belt. This action would permit resistance to knee flexion.

3.5.5.10 Pins

Pin diameters were influenced by the magnitude of the pin bearing, bending, and shear stresses. The pin dimensions directly affected the dimensions of most DKJ components that housed the pins since these components had to offer a sufficient safety factor for tearout stresses.

3.5.6 Material Selection

The choice of machined component materials was influenced by several factors including density, strength, availability, friction coefficient, ease of machining, cost, and corrosion resistance.

3.5.6.1 Plate Material

The majority of sizable DKJ components must be made of a low-density material to minimize the overall DKJ mass. The disc, side-plates, hammer, anvil and brackets were manufactured from 7075-T651 aluminium plate. This aluminium alloy was chosen for its high strength, low density, availability, low cost and ease of machining.

3.5.6.2 Pin Material

The pins account for a small fraction of the overall DKJ volume, therefore, these components could be made from a high-density metal. The pins were machined from 17-4 PH precipitation hardened stainless steel due to its high strength, and availability.

3.5.6.3 Bushings

Bushings were installed to avoid galling of the pivoting aluminium disc and hammer components on their respective stainless steel pins. Bearing stress in the hammer component was calculated to reach 111.5 MPa for a 90 kg user in stair ascent. The load carrying capacities of conventional high strength bronze alloy bushings were rated at 31 MPa [87]. Following an extensive search of dry lubricants and composite bearings, a sufficiently strong metal-polymer plain bearing manufactured by GGB (GGB North America, Thorofare, NJ 08086; Part # 0806DU) was found.

GGB's DU™ bearing has a stainless steel backing bonded to a porous bronze sinter layer. The bronze sinter layer is impregnated and overlaid with a polytetrafluoroethylene (PTFE) bearing lining. The stainless steel backing provides the bearing strength and the sintered bronze-tin layer creates the strong mechanical bond between the low friction PTFE lining and the stainless steel backing. While the dynamic load capacity of the bearing is rated at 140 MPa, the yield strength of the bearing material is 310 MPa. Any unforeseen increase in the calculated bearing stress will lead to an increase in wear of the bearing liner. This failure mode is not considered catastrophic and therefore a lower safety factor for the bearings was considered acceptable.

3.5.6.4 Belt Material

The ideal belt would be 5 mm in width, flexible enough to wrap around the 25 mm hammer radius, highly resistant to wear under compressive stresses reaching 60 MPa at the clamp site, and would provide a coefficient of friction of at least 0.19 with aluminium, have sufficient fatigue strength, and be capable of withstanding very high tensile loads. Table 3.7 shows the predicted peak DKJ moment and DKJ belt tension plus one standard deviation for subjects of various body weights in slow cadence, normal cadence, fast cadence and stair ascent. A 90 kg person walking at normal cadence with a KAFO integrating the DKJs would potentially produce a peak belt tension of approximately 1700 N. The ideal belt must be capable of withstanding a tensile load of (2800 N x 3) = 8400 N in order to achieve a safety factor of 3 for a 90 kg user in stair ascent.

There is no limitation on the thickness of the belt as long as the belt is not overly stiff. A belt material with excessive stiffness will not effectively wrap around the upper hammer radius R_2 (Figure 3.11) and will not achieve the maximum potential hammer-belt contact angle θ. As described in Section 3.5.5.4, a decreased hammer-belt contact angle θ, leads to a substantial decrease in the clamping performance of the DKJ. As discussed in Section 3.5.5.7, future embodiments of the DKJ may store the lower portion of the belt between the side-plates of the device with a spring-driven spool or a series of rollers to

guide the belt. Both of these potential designs will require a belt with sufficient flexibility to wrap around the low radius spool or rollers.

Table 3.7 - Predicted peak DKJ moments and belt tensions, plus one standard deviation, for users of various body weights in four activities.

Body Weight		Activity							
		Slow Cadence*		Normal Cadence*		Fast Cadence*		Stair Ascent†	
lbs	kg	Knee Moment	Belt Tension	Knee Moment	Belt Tension	Knee Moment	Belt Tension	Knee Moment	Belt Tension
		Nm/joint	N/joint	Nm/joint	N/joint	Nm/joint	N/joint	Nm/joint	N/joint
88	40	15	549	21	756	33	1215	34	1244
99	45	17	618	23	851	38	1366	38	1399
110	50	19	686	26	945	42	1518	43	1555
121	55	21	755	29	1040	46	1670	47	1710
132	60	23	824	31	1135	50	1822	51	1865
143	65	25	892	34	1229	54	1974	56	2021
154	70	26	961	36	1324	58	2125	60	2176
165	75	28	1030	39	1418	63	2277	64	2332
176	80	30	1098	42	1513	67	2429	68	2487
187	85	32	1167	44	1607	71	2581	73	2643
198	90	34	1235	47	1702	75	2733	77	2798
209	95	36	1304	49	1796	79	2885	81	2954
220	100	38	1373	52	1891	84	3036	86	3109
231	105	40	1441	55	1985	88	3188	90	3265
243	110	42	1510	57	2080	92	3340	94	3420
254	115	43	1579	60	2175	96	3492	98	3575

* Calculated from normalized knee moment values referenced by Winter [7].
† Calculated from normalized knee moment values referenced by Marovich [11].

An extensive search of potential belt materials was performed (Appendix D). Coated belts, composed of polyurethane or neoprene and reinforced with a flexible high-strength synthetic fiber carcass, offered the best physical and mechanical properties of all the materials investigated. No belt was found with sufficient tensile strength to provide a safety factor of one or greater based on loading in stair ascent for a 90 kg person. The strongest belt materials found were the NE 18 GAV10535 manufactured by Brecoflex Co. and the T-155 MegaFlat belt manufactured by Megadyne. Table 3.8 summarizes the key characteristics of each belt.

As illustrated in Table 3.8, neither belt offered sufficient strength for a commercially practical product. However, both belts were rated strong enough to safely

test the practicality and performance of the DKJ in a controlled clinical test environment. As part of this research, tensile strength testing was performed on both belt materials. Details are given in Section 4.1.1. The median breaking loads of the 5 mm wide NE 18 GAV10535 and T-155 belts were found to be 1646 N and 1812 N, respectively. Megadyne's T-155 MegaFlat belt was the strongest and therefore a more suitable belt for the DKJ.

Table 3.8 – Properties of the NE 18 GAV10535 and T-155 MegaFlat belts.

Belt Name	Belt Material	Carcass Material	Rated Breaking Load (N/5 mm belt width)	Safety Factor Normal Cadence*	Safety Factor Stair Ascent**
NE 18 GAV10535	Neoprene	Kevlar®	2400	1.4	0.86
T-155 MegaFlat	Neoprene	Polyester	2000	1.2	0.71

*Based on a peak belt tensile load of 1700 N for a 90 kg user (+1 standard deviation) in normal cadence.
**Considering a peak belt tensile load of 2800 N for a 90 kg user (+1 standard deviation) in stair ascent.

3.5.7 Control System

The sole duty of the control system is to activate the solenoid when the leg is in swing and deactivate the solenoid when the leg is load bearing in stance. The commercial embodiment of the control system would consist of foot pressure sensors, a compact dedicated logic circuit, and a battery. The foot pressure sensors will be located between the foot and the footplate of the AFO section of the brace (Figure 3.1b). The battery and logic circuit will be fixed to the proximal-lateral area of the thigh section of the brace or clipped to the user's belt or clothing. Each component will be discreetly connected to the DKJs via cables positioned along the uprights of the brace. A preliminary control system was designed for the purpose of testing the performance of the DKJ and optimizing the control logic of the system in testing. Detailed design, construction and programming of the control system were not a focus of this research and were therefore developed by staff of the Rehabilitation Engineering Service at the Rehabilitation Centre, Ottawa.

To achieve versatility in initial functional and clinical testing of the DKAFO, a Pentium II, 400 MHz, 256 MB RAM desktop computer was used with electronic logic software to substitute the dedicated logic circuit, and an external power source was used to replace the battery in the preliminary control system. The system control logic was

simulated with LabVIEW 7.0 software and was interfaced with the pressure sensors and solenoids via a National Instruments Data Acquisition Board (DAQ). Force sensing resistors (FSRs) were used to detect pressures beneath the foot and a power MOSFET (PMOSFET) transistor acted as a gate to allocate power from the power source to the solenoid. A National Instruments Signal Connection Board (SCB), (model #SCB-100, configuration AT-MIO-64E-3), was used to connect the FSRs and the solenoids to the DAQ.

As illustrated in Figure 3.17, the adjustable power source provided 9 volts of power to the FSRs. In the absence of foot pressure, the FSRs provided an infinite resistance and no FSR voltage signal was returned to the computer. At the onset of stance, pressure on any of the FSRs caused that FSR to provide a finite resistance while a low voltage FSR signal was returned to the computer through the DAQ from any of the three FSRs that was not loaded.

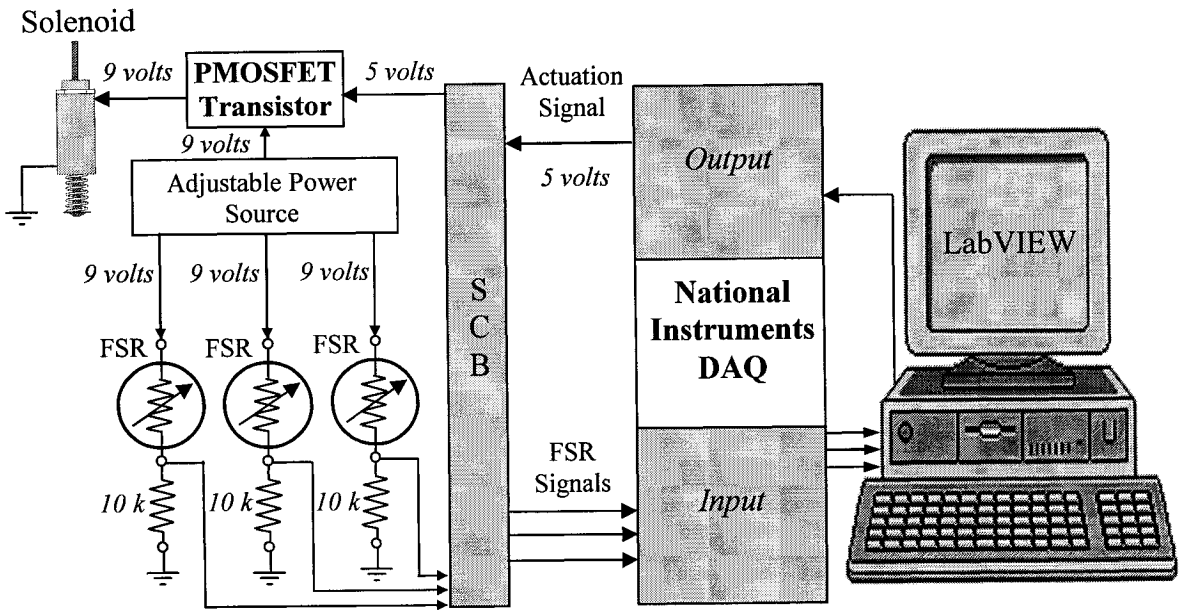

Figure 3.17 – A simple system schematic of the preliminary DKJ control system for testing.

The shoe of the braced foot had a tendency to create a constant level of low pressure on the foot-sole and the FSRs. Within the LabVIEW control program, an adjustable signal threshold was implemented for each FSR signal to set a new baseline for each signal. This allowed the program to distinguish foot pressure due to limb loading

from constant foot pressure created by the user's shoe. The input voltage threshold was adjusted in the control program for each individual FSR to alter the minimum FSR signal that would cause the solenoid to be activated.

The LabVIEW program instructed the computer to send a 5 volt output actuation signal to activate the solenoid *only* when sub-threshold foot pressure was indicated by all three FSR signals. The actuation signal was transmitted to a PMOSFET transistor through the DAQ. Upon receiving the 5 volt actuation signal from the computer, the PMOSFET transistor opened power to the solenoid. The result was activation of the solenoid in the absence of foot pressure on all of the FSRs and deactivation of the solenoid in the presence of above-threshold foot pressure on any one of the three FSRs.

3.5.8 Dynamic Knee Joint Weight

In clinical testing, two prototype DKJs were installed onto six custom KAFOs referred to as dynamic KAFOs (DKAFOs). The largest of the DKAFOs weighed 2.265 kg (4.99 lbs) including the solenoids and foot sensors. The individual weights of the major components of the DKAFO and the DKJ are represented in Figures 3.18 and 3.19 respectively. The hardware category includes nuts, bolts, washers and springs.

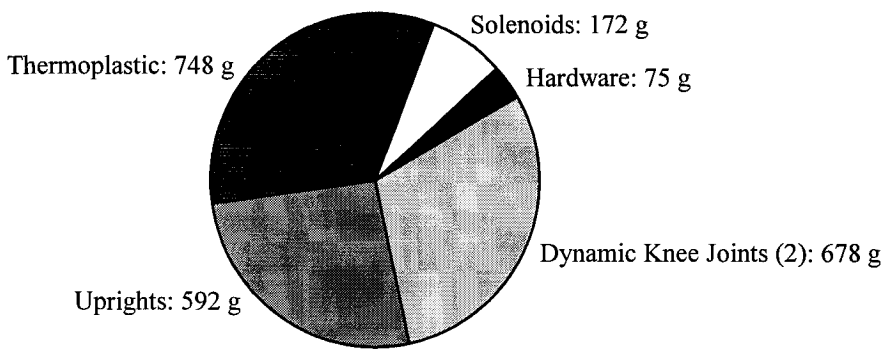

Figure 3.18 - Individual weights of the major components of the DKAFO.

The measured weight did not include the battery or dedicated control circuit planned for inclusion in future embodiments of the DKAFO. The DKJ assembly and

individual DKJ components were weighed separately. The DKJ weighed 339 grams excluding the solenoid, which weighed 86 grams.

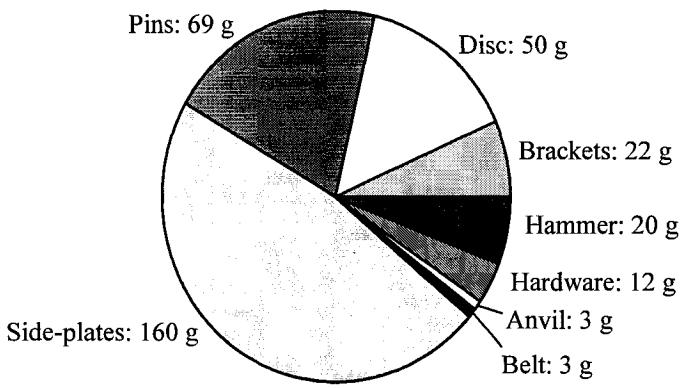

Figure 3.19 - Individual weights of the major components of the DKJ.

3.5.9 Projected Unit Cost

The projected cost of producing a pair of DKJs was calculated using quotes from machine shops and component suppliers based on a production run of 100 DKJ units. The predicted cost of a pair of DKJs was $570. The calculated DKJ cost does not include the dedicated control circuit, battery, sensors or labour to assemble the joint. Approximately 1 hour of unskilled labour would be required to assemble one DKJ unit. Figure 3.20 summarizes the individual costs of the components of the DKJ.

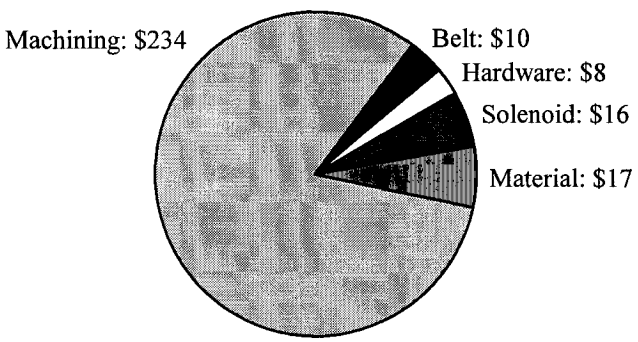

Figure 3.20 – The individual costs of the major components of a single DKJ unit. The total predicted cost of a single DKJ unit is $285.

The cost of springs, screws, washers and bushings are combined in the *Hardware* category. The costs of the plate and rod materials to be machined are covered in the *Material* category. The cost of machining includes the cost to manufacture all of the machined components.

3.5.10 Failure Mode Analysis

A failure mode analysis was performed on the DKJ device (Appendix E). Results of the analysis highlight the importance of belt reliability for user safety. The most severe failure modes included belt failure, failure of the solenoid to effectively engage or disengage the hammer, or extreme belt wear leading to insufficient clamping and belt slip. Results of the analysis highlight a number of issues that should be considered during development and testing of the device:

- The chosen belt material must have a high enough tensile strength and safety factor (discussed above in Section 3.5.6.4) to ensure that the belt does not fail in tension during use.
- The belt material must deliver consistent, reliable performance and withstand typical wear between servicing to prevent belt slip at the clamp site. Slip may result in an insufficient DKJ holding moment and therefore an excessive knee flexion during limb loading.
- The control logic must be highly reliable to ensure that the solenoid is activated and deactivated at appropriate times. The control logic may be designed to recognize and distinguish between limb loading events such as stair climbing, walking and stumbling by reading the timing, magnitude and order of the foot pressure signals.
- A sufficient safety factor must be used in the design of the hammer spring and belt recoil spring and their associated connections to ensure a minimal chance of failure.

3.5.11 Design Refinements

Initial testing of the DKJ prototype prompted a series of minor design refinements. The initial prototype did not integrate bushings on the disc or hammer. Early

mechanical testing was suspended due to severe galling between the stainless steel knee axis pin and the aluminium disc. High performance composite bushings (Section 3.5.6.3) were installed to prevent future wear of the disc and hammer bearing surfaces.

Plastic deformation of the solenoid plunger tip was detected during initial DKJ testing. As illustrated in Figure 3.16a, the solenoid plunger blocks clockwise rotation of the hammer in swing. In blocking clockwise hammer rotation, transverse force F_4 (Figure 3.16b), applied by the goose-head screw to the tip of the solenoid plunger, creates a large local bending stress on the plunger tip. A custom aluminium collar was machined to reinforce the plunger tip. In further mechanical testing, the belt was found slipping medial-laterally off the side of the disc when knee flexion moments were greater than 30 Nm. New side-plates were machined with an extension to cover the lower front quadrant of the disc and belt (Figure 3.21). The modification proved very successful in preventing the belt from slipping off the disc.

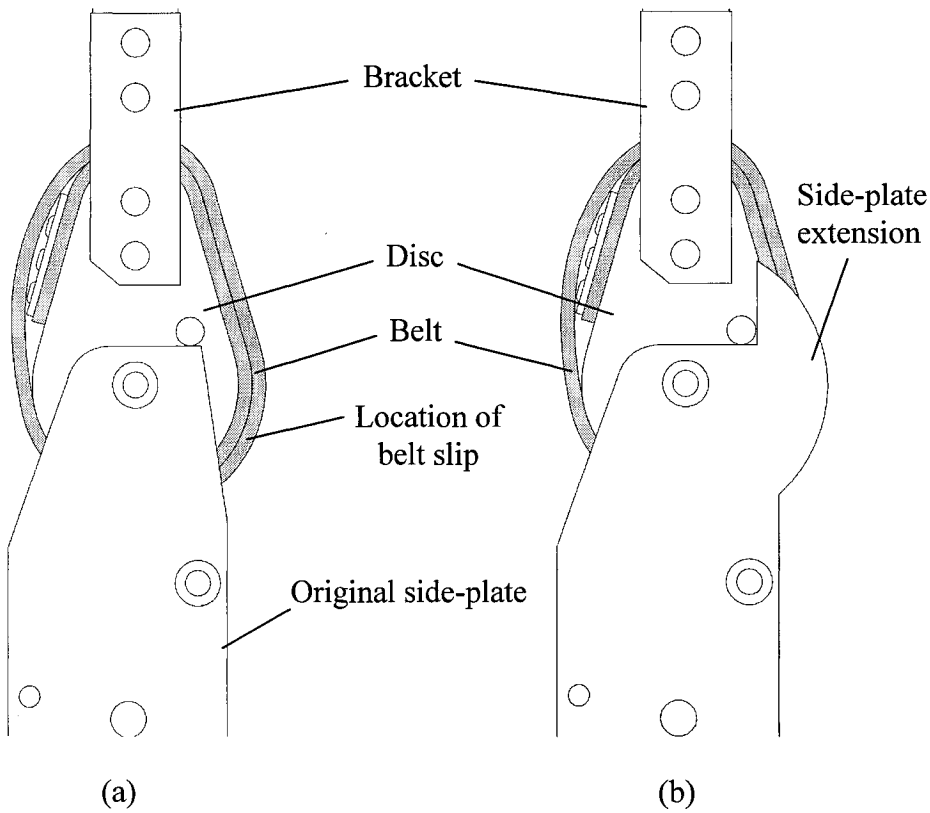

Figure 3.21 – Side-plate modification; (a) initial side-plate design; (b) modified side-plate design.

The disc was designed to accommodate the 3.1 mm thick NE 18 GAV10535 belt, which possessed the greatest published break strength of all belt materials on the market. Belt breaking load testing (Section 4.1.1) later proved the 1.6 mm thick T-155 MegaFlat belt to be considerably stronger than the NE 18 GAV10535 belt. Due to the discrepancy in belt thickness, installation of the T-155 MegaFlat belt directly onto the disc achieved an insufficient distance R_1 between the knee axis and the centre of the outer belt (Figure 3.7). A smaller distance R_1 between the belt and the knee axis would lead to an inversely proportional increase in belt tension throughout the DKJ. To achieve the desired distance R_1 with the T-155 MegaFlat belt, a short piece of NE 18 GAV10535 belt was inserted between the disc and the belt to act as a spacer.

Chapter 4. Mechanical Testing

This chapter reviews mechanical testing performed on the belt material and on the entire DKJ.

4.1 Belt Testing

Two tests were performed on the belt materials to determine the empirical breaking loads and the static coefficients of friction.

4.1.1 Belt Breaking Load Test

4.1.1.1 Purpose

As discussed in Section 3.5.6.4, an extensive materials search uncovered two belt materials that were claimed to possess adequate tensile strength for safe use in the DKJ for clinical testing. To determine which of the two belts was stronger and more suitable for the DKJ, a tension test was performed to verify the rated breaking load of the NE 18 GAV10535 belt by Brecoflex and the T-155 MegaFlat belt by Megadyne.

4.1.1.2 Test Procedure

The NE 18 GAV10535 and T-155 belts are manufactured as endless belts. The test method employed by both Brecoflex and Megadyne to determine the breaking load of their belt material involves slipping the endless belt over two parallel shafts and forcing the shafts apart.

The breaking load test procedure followed in this research conformed to the ASTM standard test method for rubber flat belting – designation ASTM-D378, entitled: *Standard Test Methods for Rubber (Elastomeric) Belting, Flat Type* [88]. The dimensions of the test specimens could not comply with ASTM standard. ASTM protocol requires a specimen of at least 150 mm plus twice the clamp length in length and 50 mm in width. The NE 18 GAV10535 and T-155 belt specimens obtained measured 200 mm in length and less than 8 mm in width. The DKJ requires a 5 mm wide belt. The test specimens were therefore hand-trimmed to 5 mm of width using a razor and a steel straight edge. In

this manner, the results of the tensile test were expected to most accurately represent the breaking load of the belts installed in the DKJ for mechanical and clinical testing. The hand-cut belts were used only in the breaking load test to help choose the most suitable belt material. The belts used in mechanical and clinical testing of the DKJ were factory-cut by the manufacturer.

4.1.1.3 Apparatus

A 4482 Instron Material Testing Machine was used to test the specimens in tension. The machine was controlled via a computer terminal using Instron 9 Series software. Clamps with transverse serrated grip surfaces were used to connect the specimen to the mounts of the testing machine. An uninterrupted tensile load was applied to each specimen at a separation rate of 100 mm/min.

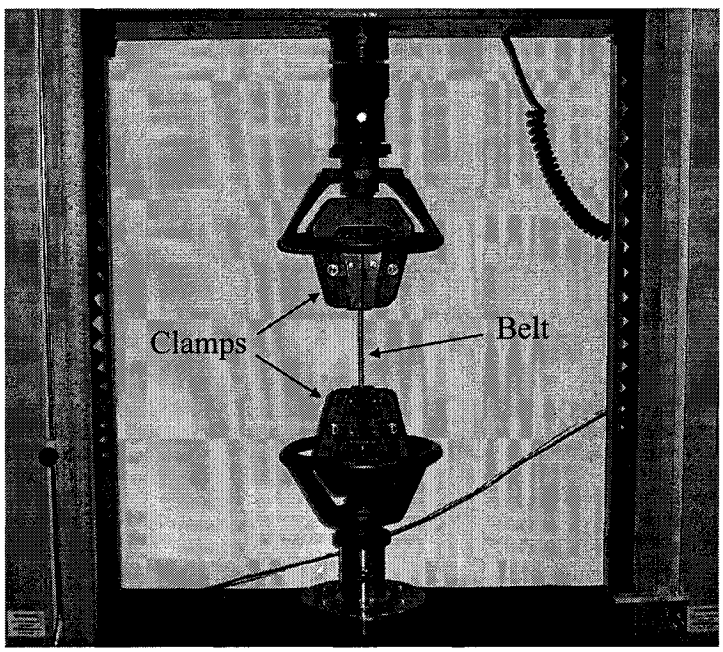

Figure 4.1 – A photograph of the belt breaking load test apparatus. Clamps at the upper and lower mounts of the Instron machine secure the belt test specimen.

4.1.1.4 Results

The results of the tensile test are tabulated in Table 4.1. Many test specimens failed at the belt-grip interface, an area prone to stress concentrations that may initiate

premature belt failure. The ASTM standard requires that test data for specimens breaking in the clamps be discarded. For some specimens, the direction of failure developed at an approximate 45° angle to the longitudinal axis of the specimen. This failure indicates that the specimen was not loaded in pure tension, likely due to misalignment of the belt in the grips. Test data from misaligned specimens were considered invalid.

Table 4.1 – Results of belt breaking load testing. The bold values are the test results that were considered valid due to the location and form of the failure on the specimen.

Specimen #	Breaking Load (N)	Failure Angle	Failure Location	Validity
NE 18 GAV10535				
1	1278	45°	At grips	Invalid
2	**1656**	90°	Middle of specimen	**Valid**
3	1423	45°	At grips	Invalid
4	1616	45°	Middle of specimen	Invalid
5	1377	45°	At grips	Invalid
6	1490	90°	At grips	Invalid
7	**1576**	90°	Middle of specimen	**Valid**
8	**1646**	90°	Middle of specimen	**Valid**
T-155 MegaFlat				
1	2032	90°	At grips	Invalid
2	1836	90°	At grips	Invalid
3	**1675**	90°	Middle of specimen	**Valid**
4	1976	90°	At grips	Invalid
5	**1960**	90°	Middle of specimen	**Valid**
6	**1812**	90°	Middle of specimen	**Valid**

Figures 4.2 and 4.3 show the applied belt tension versus specimen elongation for the valid NE18 GAV10535 and T-155 belt test trials, respectively. Figure 4.4 shows the breaking loads of the NE18 GAV10535 and T-155 belt specimens.

Eight NE18 GAV10535 specimens were tested. Five of the tests were considered invalid due to the specimen failing in the grips or failing at a 45° angle. The median breaking load of the three valid tests was 1646 N. Six T-155 MegaFlat specimens were tested. Three of the test specimens failed in the grips rendering the results invalid. The median breaking load of the three valid tests was 1812 N. Every T-155 belt that failed at the grips broke at a tension greater than the median break strength of the valid test

specimens. For this reason the invalid test results for the T-155 MegaFlat belt are not ignored in Figure 4.4.

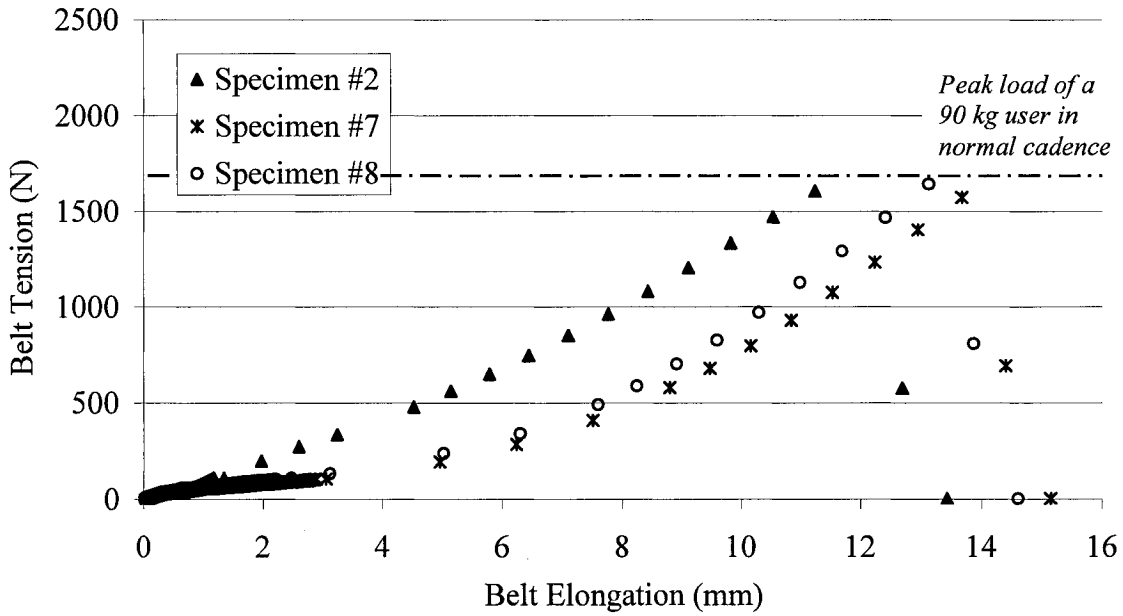

Figure 4.2 – Tension versus elongation curves for the valid NE18 GAV 535 test specimens. The dashed line indicates the 1700 N peak belt load (+1 standard deviation) predicted to occur in the DKJ with a 90 kg user in normal cadence.

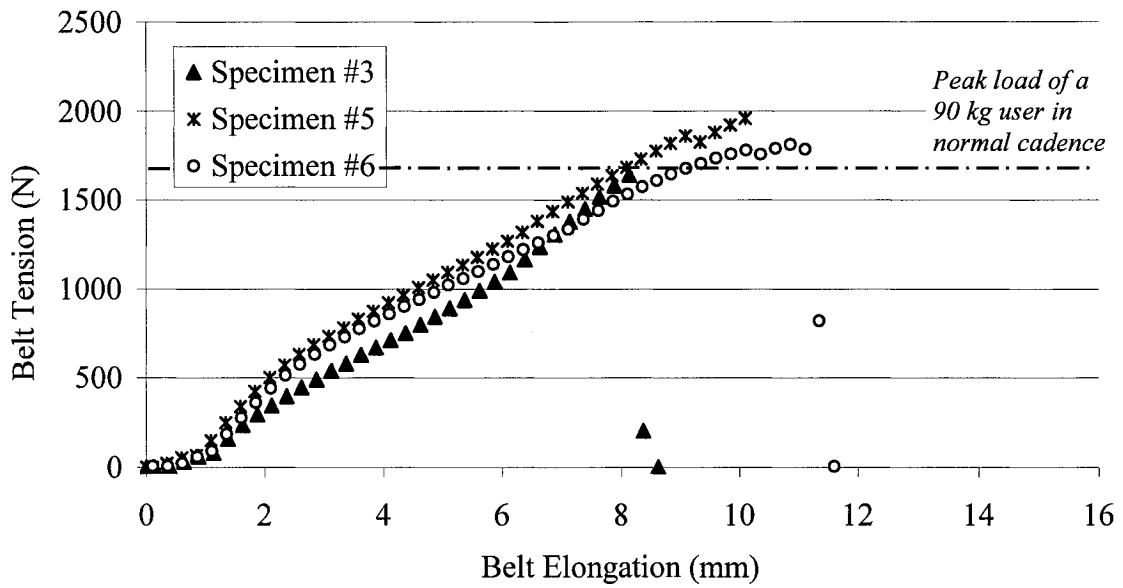

Figure 4.3 – Tension versus elongation data for the three valid T-155 MegaFlat test specimens. The dashed line indicates the 1700 N peak belt load (+1 standard deviation) predicted to occur in the DKJ with a 90 kg user in normal cadence.

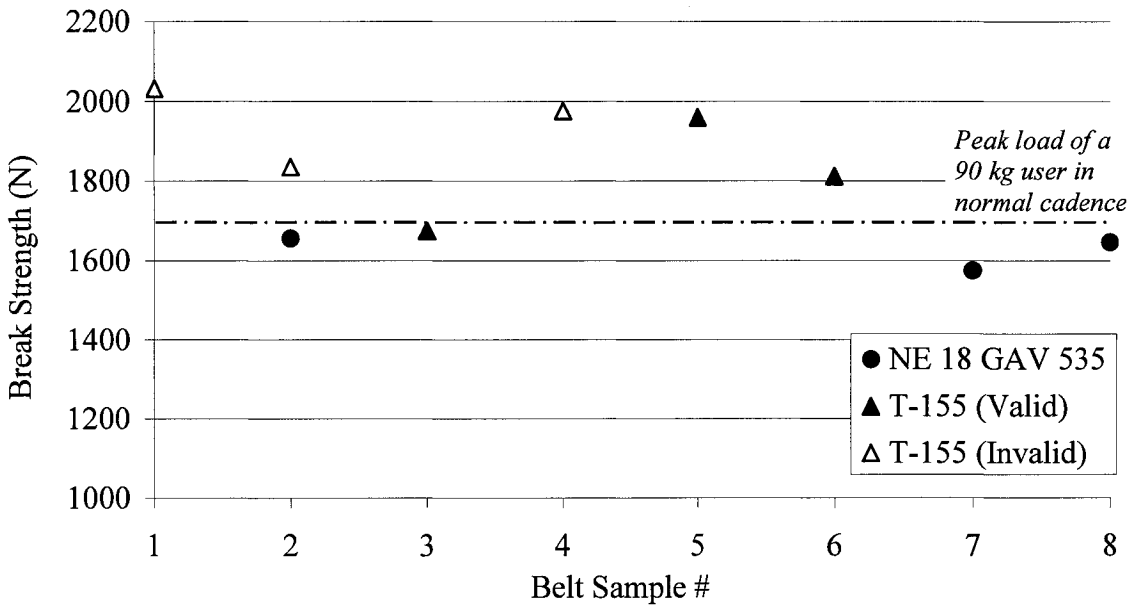

Figure 4.4 – Breaking load results for the NE 18 GAV10535 and T-155 MegaFlat belt specimens. The dashed line indicates the 1700 N peak belt load (+ 1 standard deviation) predicted to occur in the DKJ with a 90 kg user in normal cadence.

The median experimental breaking load of the NE18 GAV10535 specimens was only 69% of the rated breaking load of 2400 N. As shown in Figure 4.2 and Figure 4.4, none of the NE18 GAV10535 specimens were strong enough to endure the 1700 N peak belt tension predicted to occur for a 90 kg user in normal cadence wearing the DKAFO. Discrepancies between the published and experimental break strengths may be due to differences in the test methods used. The test method carried out as part of this research was prone to more stress concentrations than the double-shaft test method used by the manufacturers and was therefore more prone to premature failure. Inadvertent damage to the outer bundles of reinforcement fibres could have occurred while cutting the belts by hand, especially if the cuts were not made parallel to the fibres. This could greatly reduce the specimen's strength .

Five of the six T-155 MegaFlat belt specimens were within 90% of the 2000 N rated breaking load of the belt material. The breaking loads of the six T-155 MegaFlat belt specimens were 2032 N, 1836 N, 1675 N, 1976 N, 1960 N and 1812 N. All of the T-155 MegaFlat test specimens, except for Specimen #3, therefore exhibited breaking loads greater than the 1700 N peak belt tension predicted to occur in the DKJ with a

90 kg user wearing the DKAFO in normal cadence. The T-155 MegaFlat belt was chosen as the more adequate belt to use in the DKJ.

4.1.2 Belt Friction Test

4.1.2.1 Purpose

The coefficient of friction μ of the belt on the hammer has a large influence on the performance and internal stresses of the DKJ. The hammer bending stress, required hammer angle, required hammer length, and required clamping force are sensitive to the value of μ. A simple test was performed to determine the static coefficient of friction between the T-155 MegaFlat belt and a milled plate of 7075-T651 aluminium.

4.1.2.2 Apparatus and Test Procedure

The test apparatus included a strip of T-155 belt, a 0.469 kg mass, a Pesola spring scale (Pesola AG, Rebmattli, CH-6340 Baar, Switzerland; part #41000) and a 7075-T651 aluminium plate. The Pesola spring scale had a range of 1 kg with 0.01 kg graduations and an accuracy of ±0.3% of the load. The magnitude of the weight and the precision of the spring scale were chosen to measure the coefficient of friction with an accuracy of ±0.01. The aluminium plate had the same milled surface finish as the DKJ components. Figure 4.5 illustrates the test apparatus assembly. The mass was placed on the belt specimen and the belt specimen was placed on the aluminium plate. One end of the spring scale was connected to the belt specimen via a clip. The free end of the spring scale was pulled by hand. Guide blocks (not shown) positioned below and beside the spring scale maintained the alignment of the spring scale and the belt specimen. Tension on the spring scale was gradually increased until belt motion was detected. The tension force T_s, at the onset of belt motion was recorded. A landmark on the aluminium plate helped determine the instant of belt movement. The coefficient of friction between the belt specimen and the aluminium plate was determined by:

$$\mu = \frac{T_s}{mg}, \tag{4.1}$$

where μ is the coefficient of friction of the belt, T_s is the tension in the spring scale, m is the mass measured in kilograms and g is the gravitational acceleration.

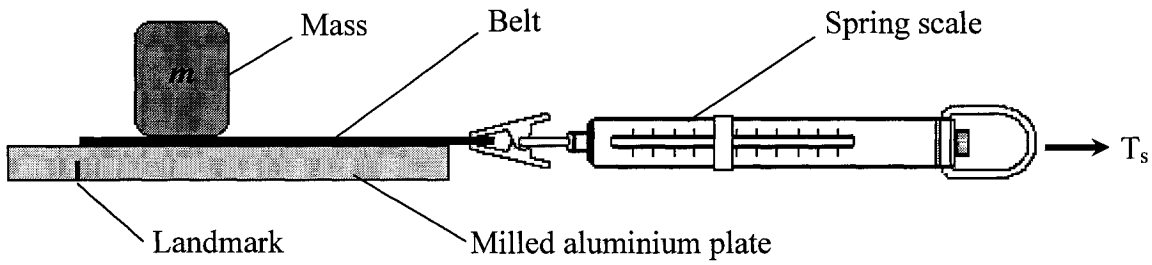

Figure 4.5 – Test setup for determining the friction coefficient of the T-155 MegaFlat belt on milled 7075-T651 aluminium.

4.1.2.3 Results

Testing was performed on both sides of the belt as one side is textured and the opposite side is smooth. The smooth side of the T-155 belt was found to have a coefficient of friction of 0.84 with the milled aluminium. The textured side of the belt was found to have a coefficient of friction of 0.20 with the milled aluminium. As discussed in Section 3.5.3.6, the belt component must have a coefficient of friction of at least 0.19 with the milled aluminium hammer and anvil components. The T-155 belt therefore possessed a sufficient coefficient of friction to be used in the DKJ.

4.2 Mechanical Testing of the Dynamic Knee Joint

Three Dynamic Knee Joints were constructed to test the mechanical and clinical performance of the DKJ. One DKJ was mechanically tested to determine the moment at failure, loading behaviour, and mechanical performance of the joint. The remaining two DKJs were used to clinically test the effectiveness of the newly designed DKJ. A custom order of factory-cut T-155 Megadyne MegaFlat belts was obtained for mechanical and clinical testing.

4.2.1 Purpose

The purpose of DKJ mechanical testing was to determine whether the DKJ was sufficiently safe for clinical testing. The goals of mechanical testing were to:

1. Validate the predicted strength of the belt installed in the DKJ.
2. Observe the overall mechanical performance of the DKJ and ensure that all of the components function appropriately.
3. Determine the highest knee moment that can be supported by the DKJ.
4. Observe the loading behaviour of the DKJ and measure the amount of knee flexion offered by the DKJ with respect to the applied DKJ flexion moment.
5. Determine if plastic deformation or other modes of failure occurred in any components of the DKJ during testing.
6. Observe any wear on the individual DKJ components following repeated loading.
7. Identify any performance issues that may exist in the DKJ design.

4.2.2 Apparatus

The solenoid and control system were not connected to the DKJ during mechanical testing. The DKJ was connected to a 4482 Instron Material Testing Machine, as shown in Figure 4.6a, so that a controlled moment could be applied to the DKJ about the knee-joint axis. The ends of the DKJ uprights were pinned to the testing machine mounts using custom machined clevises. A level metal ruler was fixed to the bottom mounting clevis. A plumb line was anchored to the center of the knee axis pin and hung in front of the ruler. The plum line indicated the horizontal distance between the knee-joint axis and the line of compressive force applied to the pinned ends of the uprights. The instantaneous moment M about the knee-joint axis was calculated by $M = WL$, where W is the vertical compressive force applied by the testing machine (Figure 4.6b), and L is the perpendicular (horizontal) distance between the applied force and the knee-joint axis. A protractor was used to measure the DKJ flexion angle during testing. The protractor was adhered to the lateral side-plate of the DKJ and centered on the knee-joint axis with the 0-180° line aligned with the longitudinal axis of the lower upright. Behind the protractor, a mark on the center of the bracket indicated the joint's instantaneous flexion angle λ (Figure 4.6b).

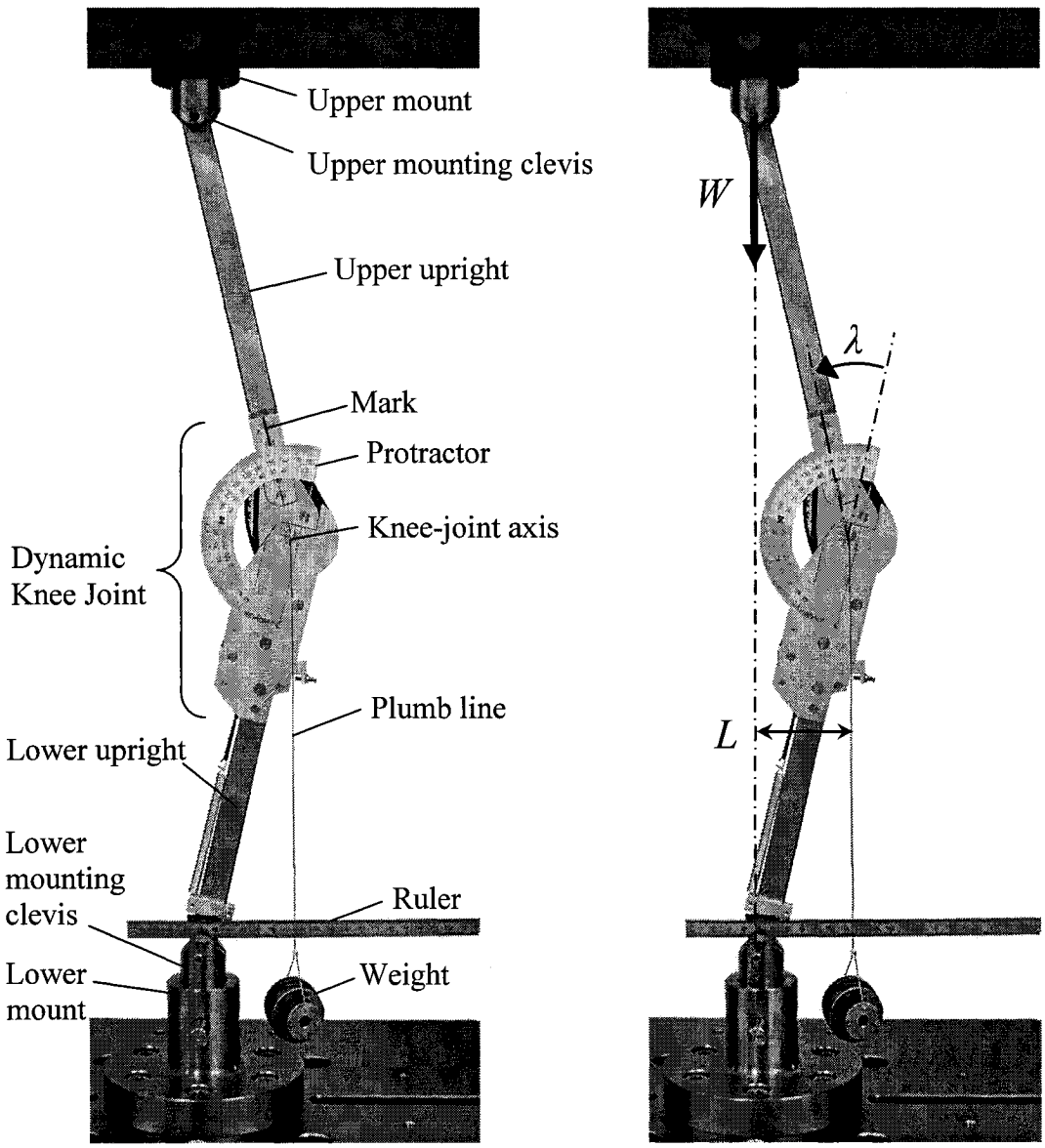

Figure 4.6 – Photographs of the test setup used to apply a knee-flexion moment to the DKJ: (a) important components of test setup, and (b) the vertical compressive force W applied by the testing machine, the perpendicular distance L, between the applied force and the knee-joint axis, indicated by the plumb line, and the DKJ flexion angle λ indicated by the mark on the protractor.

4.2.3 Test Procedure

The DKJ was set to a preload flexion angle of 10° before every vertical loading test to prevent the DKJ from buckling and to initiate flexion about the knee-joint axis pin. The initial 10° flexion angle was also necessary to horizontally offset the plumb line weight from the lower mount, as shown in Figure 4.6. The DKJ was loaded vertically, as shown in Figure 4.6b, at a rate of 508 mm/min, the maximum speed of the testing

machine. A loading speed of 6000 mm/min would accurately simulate limb loading in slow cadence. Vertical displacement of the upper testing machine mount and load values were measured at 20 Hz, the maximum sampling rate of the machine. A digital video camera recorded each load test to capture the knee-flexion angle λ, and the anterior (horizontal) displacement of the knee-joint axis, L.

Two separate tests were performed on the DKJ:

1. Failure Strength and Loading Behaviour Test

The DKJ was loaded to failure five times. For each of the five trials a new 5 mm wide, factory-cut T-155 MegaFlat belt was installed in the DKJ. The maximum holding moment of the DKJ at failure was recorded. The relationship between the applied DKJ flexion moment and the resulting DKJ flexion angle was plotted for each trial. The plot revealed the amount of negligible knee flexion that occurred before the clamping mechanism engaged the belt and the angular displacement of the DKJ for any applied DKJ flexion moment.

2. Repeated Loading and Wear Test

A new 5 mm wide, factory-cut T-155 MegaFlat belt was installed in the DKJ. Using the same belt for the entire test, the DKJ was repeatedly loaded with a compressive force of 555 N by the testing machine, to produce an average moment of 52 Nm on the DKJ, until the belt failed. A loading moment of 52 Nm was considered a safe and realistic value for repeated joint loading because this moment was 10% higher than the mean peak moment plus one standard deviation created by a 90 kg user in normal cadence. The data collected in repeated loading therefore had a safety factor of 1.1 for a 90 kg user in normal cadence. For each loading cycle, the DKJ remained at maximum load for a period of at least 10 seconds before the load was released. Following belt failure, the belt was inspected for modes of wear. At the conclusion of all mechanical testing, the remaining components of the DKJ were inspected for wear. Loading from pre-test loading, failure strength and loading behaviour testing, and repeated loading and wear testing were considered.

Prior to formal testing, the DKJ was loaded a total of 57 times in what was referred to as *pre-test loading*. Pre-test loading was carried out to fine-tune and ensure proper functioning of both the test apparatus and the DKJ. Moments applied to the DKJ in pre-test loading ranged from 30-60 Nm. No data was used from pre-test loading, however, the magnitude and number of loading cycles were considered when accounting for wear on all of the DKJ components, except for the belt. In pre-test loading the DKJ was consistently loaded to 555 N. The fixed-load produced DKJ flexion angles varying from 30° to 72°. Observation revealed that this discrepancy was caused by inconsistency in the amount of slack in the belt segment that was wrapped around the disc. More belt slack around the disc lead to more joint flexion in loading. Belt slack would form as the joint was extended following loading. The belt recoil spring was designed to remove all slack in the belt during joint extension. Further investigation revealed that the new, but tacky, T-155 MegaFlat belt material installed in the DKJ stuck to the aluminium hammer during and following loading. In joint extension, the force required to drag the tacky belt over the hammer was excessive and unsuitable for any practical strength of recoil spring. To remedy this problem, common baking powder (composed of cornstarch, monocalcium phosphate and sodium bicarbonate) was dusted onto the fresh belt material and then wiped off with a dry cloth. The powder eliminated the tacky quality of the belt, allowing the belt recoil spring to effectively perform its function. Continued mechanical testing proved that the powdered belts maintained the same holding performance under loading as the non-powdered belts. Formal testing of the DKJ was then performed.

4.2.4 Results

For the purpose of clarity in the presentation of the results, the *DKJ flexion angle* will denote the change in joint angle from the initial 10° starting position and not the absolute angle of the joint.

4.2.4.1 Results of the Failure Strength and Loading Behaviour Test

In each trial, the belt failed in tension between the disc and the hammer, labelled as points B and C, respectively in Figure 3.7. This result was expected since the belt tension is always greatest between these two points. All five belts failed in the transverse

direction, indicating that the belts failed in pure tension. Figure 4.7 shows the DKJ moment as a function of the DKJ flexion angle for the five failure test trials.

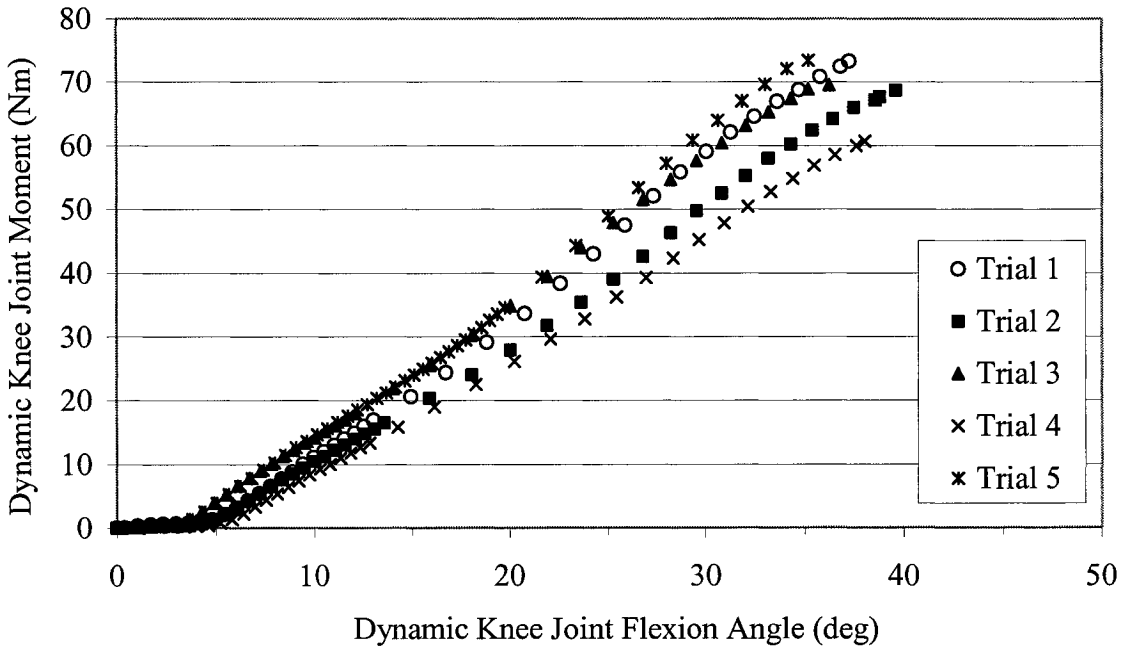

Figure 4.7 – DKJ resistance moment versus DKJ flexion angle for five separate trials loading the DKJ to failure.

Table 4.2 shows the moment at failure, DKJ flexion angle, peak horizontal distance, L, between the joint axis and the applied force, peak vertical displacement of the testing machine at the instant of failure, and the maximum belt tension at failure for all five failure tests. The greatest moment experienced by the DKJ was 73 Nm. The DKJ was designed to endure peak moments of 77 Nm for stair ascent; however, an applied moment of 77 Nm could not be realized due to the limited belt strength. The lowest failure moment was 61 Nm. Without considering a factor of safety, this was higher than the peak knee moment required for a 115 kg person in normal cadence, and 1.3 times the 47 Nm moment required for a 90 kg person in normal cadence. Changes in joint flexion angles ranged from 35° to 39° and were not proportional to the magnitude of their respective failure moments. As will be discussed further in Section 6.2.1, the factory-cut belts installed in the DKJ exhibited much higher breaking loads than the hand-cut belts tested in Section 4.1.1. Inadvertent damage incurred on the hand-cut belts by the crude belt cutting method likely compromised the breaking load of the hand-cut belts. Since the

mean moment at failure was 69 Nm, it was decided that a moment of 52 Nm would be adequate in repeated load testing. A repeated 52 Nm flexion moment would be well below the mean failure moment of the joint and the resulting data would possess a safety factor of 1.1 for a 90 kg individual in normal cadence generating peak knee moments of 47 Nm.

Table 4.2 – Results of load to failure test for the DKJ.

Trial #	Moment at Failure (Nm)	DKJ Flexion Angle (deg)	Peak Vertical Stroke (mm)	Peak Horizontal Distance (mm)	Maximum Belt Tension at Failure (N)
1	73	37	40.5	109	2655
2	69	39	44.5	113	2509
3	69	36	37.8	104	2509
4	61	38	45.0	110	2218
5	73	35	40.6	103	2655
Minimum	61	35	37.8	103	2218
Maximum	73	39	45.0	113	2655
Mean	69	37	41.7	107.8	2488
Standard Deviation	4.9	1.6	3.0	4.2	196

As shown in Figure 4.7, an inconsistency existed between the DKJ flexion angle and the DKJ resistance moment due to the friction the belt imposed on itself around the disc. Following loading, the belt would often remain very tightly wrapped around the disc, held against itself by belt friction. Throughout testing, the belt tightness on the disc fluctuated between the tightly bound state and the looser, spring-tightened state. The belt tightness on the disc directly affected the amount of DKJ flexion angle achieved under a given moment and was responsible for the discrepancy in the loading behaviour of the DKJ during failure strength testing. Figure 4.7 shows that an applied moment of 60 Nm produced different DKJ flexion angles, ranging from 29° to 38° - a difference of 24%. No immediate means of fixing the belt tightness on the disc was available during the time of testing.

As shown in Figure 4.7, initial DKJ flexion of approximately 5° resulted in negligible DKJ flexion resistance. As explained in Section 3.5.5.4, this 'free' knee flexion was the result of the disc rotating as the hammer moved from the fully open position to the fully clamped position.

Beyond the initial 5° of joint flexion, the DKJ exhibited a near-linear relationship between DKJ moment and DKJ flexion angle (Figure 4.7). In this phase, knee flexion was the sum of the belt elastic elongation, belt slip in the clamp, belt slip about the disc, and belt slip of the spacer belt (Section 3.5.11). Tensile testing of the T-155 belt revealed a mean elongation of 11.4% at tensile failure (Section 4.1.1.4). Calculation of belt elongation within the DKJ is complex since belt tension continually varies throughout the device. The only length of belt experiencing maximum constant tension lies between the disc and the hammer, labelled as points B and C in Figure 3.7. Considering that the belt length between these points is 22 mm, an elongation of 11.4% would produce 2.5 mm over this range. A 2.5 mm increase in belt length represents 5° of joint flexion. Belt elongation along the hammer and around the disc will also account for some joint flexion.

As described in Section 3.5.11, a short piece of NE 18 GAV10535 belt was inserted between the disc and the belt to act as a spacer. Under high moments, the spacer belt slipped along the disc and compressed under the pressure from the overlying belt. Belt slip and compression contributed in part to the total DKJ flexion during loading.

Mechanical testing measurements revealed that the belt's bottom end traveled 2 mm upwards from the instance the hammer first contacted the belt to complete clamping at 48 Nm. Two millimetres of belt slip resulted in 4° of extra joint flexion.

4.2.4.2 Repeated Loading and Wear Test

The belt failed following 66 load cycles. The average moment was 52 Nm with a standard deviation of 6.4 Nm. As explained in Section 4.2.4.1, changing belt tightness around the disc with each load cycle resulted in inconsistent moments on the DKJ over the course of repeated load testing. Repeated loading of the DKJ lead to considerable belt

damage at the clamping site. The belt showed no signs of wear at other locations. Several different forms of damage were observed at the clamping site. The T-155 MegaFlat belt was comprised of a polyester weave sandwiched by a thick smooth-surface coat of neoprene on one side and a thin textured-surface coat of neoprene on the other side. The primary source of belt failure was abrasive wear of the thin textured neoprene coat of the belt from the anvil. As shown in Figure 4.8, repeated clamping wore away the thin neoprene coat and exposed the low-friction polyester weave to the clamping surface of the anvil. Insufficient friction between the belt and the anvil caused the belt to slip through the clamp during loading. Upward belt travel, through the closed clamp, caused the bottom corner of the anvil to peel away the existing neoprene coating directly below the location of belt wear. This peeling enlarged the area of exposed polyester. With each subsequent loading, the belt would slip further through the clamp and peel off more neoprene. The result was an increased magnitude of joint flexion with each successive loading and rapid destruction of the belt.

Repeated clamping permanently deformed both neoprene coats at the clamping site. The deformed belt passed through the open hammer-anvil gap without resistance; however, further deformation under continued loading could have inhibited smooth movement of the belt between the open hammer and the anvil. Large cracks developed in the thick neoprene coat, where the top of the anvil met the belt. The thick neoprene coat edges curled inward, toward the center of the belt at the clamping site. Lastly, the thick neoprene coat delaminated from the polyester weave, allowing the polyester to pull through the neoprene at the clamp site when loaded in tension.

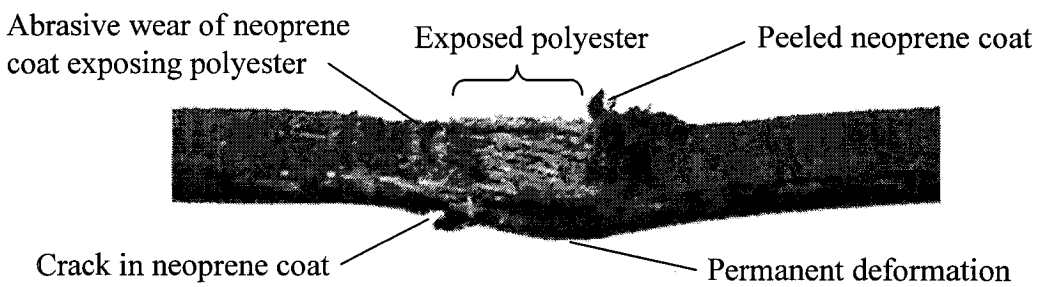

Figure 4.8 – A photograph showing four of the six modes of damage experienced by the belt at the anvil-hammer clamp site following repeated loadings in the DKJ.

Over the course of pre-test loading, failure strength and loading behaviour testing, and repeated loading and wear testing, the DKJ was mechanically loaded a total of 128 times to moments ranging from 30-73 Nm and averaging 50 Nm. Clamping mechanism performance remained consistent throughout testing. Any degradation in clamping performance was solely due to belt wear. Following mechanical testing, visual inspections of the entire DKJ assembly, including the bushings but excluding the belt component, revealed only minor abrasive wear between the disc and the side-plates.

Chapter 5. Clinical Testing

A pair of DKJs were manufactured solely for the purpose of clinical testing. The DKJs were integrated into dynamic knee-ankle-foot orthoses (DKAFO) for testing. This study was approved by the research ethics bodies at the University of Ottawa, the Rehabilitation Centre in Ottawa, and the University of Waterloo. Ethics approval documentation is found in Appendix G.

5.1 Purpose

The goals of clinically testing the DKAFO were to:

1. Determine the effect the DKAFO has on able-bodied gait.
2. Determine the clinical effectiveness of the DKAFO by determining whether the DKAFO encourages a more natural gait than conventional fixed-knee KAFOs.
3. Determine whether the DKAFO functions correctly in clinical application and determine if there are any design issues associated with the DKAFO in clinical use.

5.2 Methods

5.2.1 Test Procedure

The DKAFO was evaluated at the Rehabilitation Centre's Gait and Motion Analysis (GAMA) laboratory by means of video-based quantitative kinematic gait analysis. Two separate tests were run using two groups of test subjects.

1. The first test investigated the DKAFO's influence on able-bodied gait. For this test, three able-bodied subjects were filmed while walking naturally without a brace and walking while wearing the DKAFO. An investigation of the gait patterns for both conditions revealed modifications introduced to the subjects' gait while wearing the DKAFO.
2. The second test examined the clinical performance of the DKAFO, using three subjects with isolated quadriceps weakness. These subjects were first recorded walking with their prescribed conventional KAFO and then again wearing a custom fabricated DKAFO. A comparison of the gait patterns of the two trials

revealed whether the abnormal gait patterns associated with conventional KAFOs were reduced by the DKAFO.

5.2.2 Subjects

A convenience sample of three able-bodied male subjects and three KAFO users was recruited for clinical testing. The able-bodied subjects were selected based on their ability to wear the KAFO with minimal modifications (i.e., similar leg length and girth). Table 5.1 summarizes the relevant characteristics of each individual subject.

Table 5.1 – Relevant subject data.

Subject	Gender	Age	Weight (kg)	Braced Limb	Condition	Walking Aids
A1	Male	25	78	Right	Able-bodied	None
A2	Male	23	77	Right	Able-bodied	None
A3	Male	58	80	Right	Able-bodied	None
B1	Male	57	85	Left	Polio, Parkinson's Disease	Cane
B2	Male	60	78	Right	Polio	None
B3	Male	52	102	Left	Post-Polio	Cane

Subject B1 was previously prescribed a conventional KAFO that allowed up to 18° of stiff knee flexion in limb loading, but he found the inability to flex his knee awkward and prone to make him trip, even on level ground. Subject B1 rarely wore his KAFO and instead preferred to walk with a walker or cane. Subject B2 had walked with a KAFO for the past 12 years. His current KAFO allows 18° of free knee movement. Subject B2 almost always wore his KAFO when walking. Subject B3 was prescribed a KAFO only 5 months prior to the gait test. Subject B3 was fitted with the Horton SCKAFO but found the triggering mechanism problematic and only used the brace when walking in busy environments or outdoors. For the purposes of this research, subject B3 switched his SCKAFO to the fully extended, locked position for the walking trials.

Muscle strength for subjects with disabilities were graded by a certified orthotist using the Ashworth Scale. The Ashworth Scale is a universal system used to rate the strength of muscle groups [89]. The Ashworth Scale grades muscle strength as: 0 = no muscle contraction; 1 = flicker or trace of muscle contraction; 2 = active movement with

gravity eliminated; 3 = active movement against gravity; 4 = active movement against gravity and manually applied resistance; 5 = normal muscle strength. Modifiers + and – are used to denote intermediate levels of muscle strength.

Table 5.2 – Lower limb muscle strengths of the KAFO users graded using the Ashworth Scale.

	Subject B1		Subject B2		Subject B3	
	Right	Left	Right	Left	Right	Left
Hip Flexion	4	4-	4-	5	5	4
Hip Extension	5	4+	3	5	5	4
Knee Flexion	5	3	4-	5	5	5
Knee Extension	5	3-	3	5	5	3
Ankle Dorsiflexion	5	4	4	5	5	4
Ankle Plantar flexion	5	3	4-	5	5	5

5.2.3 Custom Dynamic Knee-Ankle-Foot Orthoses

A series of custom DKAFOs that housed the pair of prototype DKJs, were manufactured by a certified orthotist and orthotic technician over the course of clinical testing. Figure 5.1 shows photographs of the DKAFO used by subjects A1, A2 and A3. The first DKAFO was custom fit to accommodate subject A1. Subjects A2 and A3 were selected as test candidates because they shared approximately the same lower body dimensions as subject A1 and were physically compatible with the existing DKAFO. Subjects A2 and A3 used the original DKAFO custom made for subject A1. Subjects B1, B2 and B3 were each fitted with a custom DKAFO and made an extra clinical orthotic visit to the Rehabilitation Centre. The same set of DKJs, electronics and foot switches were used in all four DKAFOs.

Different types of ankle joints and footplates were used on the thermoplastic AFO sections of the various DKAFOs. Tamarack articulating ankle joints were used on some of the DKAFOs to allow the foot to dorisflex and plantar flex while providing some resistance to ankle rotation to constrain the ankle to a single plane of motion. Subject B1 had a ¾ footplate added to his DKAFO to help him create the knee extension moment needed to switch the DKAFO to swing mode at the end of stance. Due to the limited

range of motion for subject B3's affected ankle, the orthotist felt that an articulating ankle joint was inappropriate and included a fixed-ankle in his DKAFO.

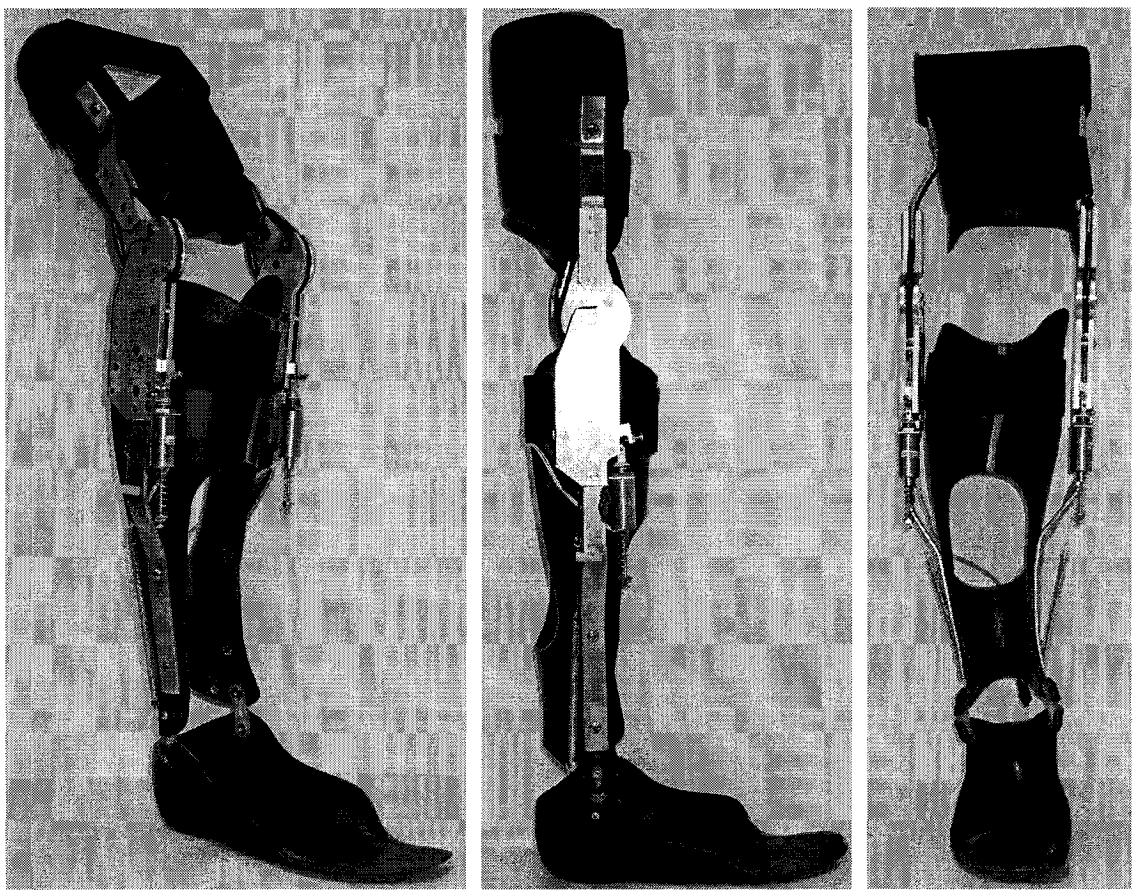

(a) (b) (c)

Figure 5.1 – Photographs of the DKJ installed in a functioning DKAFO showing: (a) three-quarters view, (b) side-view, (c) front view.

Table 5.3 – Summary of the footplates and ankle joints integrated into the DKAFOs of the KAFO users.

	Subject A1, A2, A3	Subject B1	Subject B2	Subject B3
Prescribed KAFO	N/A	No footplate, fixed ankle	Full footplate, articulating ankle	Full footplate, articulating ankle
DKAFO	¾ footplate, articulating ankle	¾ footplate, fixed ankle	Full footplate, articulating ankle	Full footplate, fixed ankle

Three presure sensors were adhered to the top surface of the AFO's footplate. The sensors were located at the heel, lateral forefoot and medial forefoot. A light emitting diode (LED) was connected in parallel to the solenoids, to provide a visual signal of whether the solenoids were active or inactive. This data was noted later in image processing and applied in data analysis.

5.2.4 Data Collection

5.2.4.1 Test Equipment

Passive reflective markers were placed on the test subject using a modified National Institutes of Health (NIH) six degree of freedom marker set. The original NIH marker set was intended for bilateral observation of the subject, positioning markers on both lateral sides of the pelvis. Due to the space constraints of the GAMA laboratory, only unilateral observation of the subjects was possible. The obscured pelvis markers were moved to the posterior side of the pelvis to ensure their visibility. A total of 16 tracking markers and 8 calibration markers were placed on the subject. Table 5.4 lists the anatomical locations of the 24 markers. Both calibration and tracking markers were physically identical, differing only in their placement and purpose. The reflective markers were whole and half white spheres of 23 mm and 35 mm diameter, respectively. The calibration markers were placed at the hip, knee and ankle joint centers to locate the endpoints of each lower body segment. These markers were worn only when videotaping the standing calibration trials. Tracking markers were used to define the position and orientation of each lower body segment. Sets of four tracking markers were placed on the foot, the shank, the thigh and the pelvis. All 16 tracking markers were worn during the standing calibration and throughout the gait trials. Test subjects wore dark clothing to contrast with the markers and facilitate image processing. The shiny, metallic areas of the brace were covered in matte black tape and paper to eliminate reflections that would possibly interfere with identification of markers in image processing. Figure 5.2 illustrates the positions of all 24 calibration and tracking markers.

Table 5.4 – Names and locations of markers used in recording limb motion of subjects.

Code	Description	Location	Marker Type
FT1	Foot	Ball of foot, lateral side	Tracking
FT2	Foot	Lateral heel	Tracking
FT3	Foot	Top of foot (metatarsals)	Tracking
LA	Lateral ankle	Lateral malleolus	Tracking
SK1	Shank	Posterior-lateral shank	Tracking
SK2	Shank	Posterior-lateral shank	Tracking
SK3	Shank	Posterior-lateral shank	Tracking
SK4	Shank	Posterior-lateral shank	Tracking
TH1	Thigh	Posterior-lateral thigh	Tracking
TH2	Thigh	Posterior-lateral thigh	Tracking
TH3	Thigh	Posterior-lateral thigh	Tracking
TH4	Thigh	Posterior-lateral thigh	Tracking
SCR1	Sacrum	Elevated on right side of sacrum	Tracking
SCR2	Sacrum	Lower on left side of sacrum	Tracking
RPS	Pelvis	Right side of posterior pelvis	Tracking
LPS	Pelvis	Left side of posterior pelvis	Tracking
TOE	Medial toe	Head of first metatarsal	Calibration
MA	Medial ankle	Medial malleolus	Calibration
LK	Lateral knee	Lateral epicondyle	Calibration
MK	Medial knee	Medial epicondyle	Calibration
RHIP	Right hip	Right greater trochanter	Calibration
LHIP	Left hip	Left greater trochanter	Calibration
RPP	Right iliac crest	Right iliac crest	Calibration
LPP	Left iliac crest	Left iliac crest	Calibration

A 8 m level walkway was used for the gait trials. Four digital video cameras (JVC, model #GR-DVL9800u) with a shutter speed of 0.004 seconds were used to capture images of the test subjects at a rate of 60 frames/s. The cameras were positioned to ensure that each marker was visible by at least two cameras throughout the trials. A spotlight was attached to each camera and focused on the walkway. Figure 5.3 shows photographs taken from the locations of all four cameras. The DKAFO foot switches and solenoids were remotely connected to the stationary control system via a 10 m cable. Figure 5.4 illustrates the layout of the 3-dimensional motion capture environment.

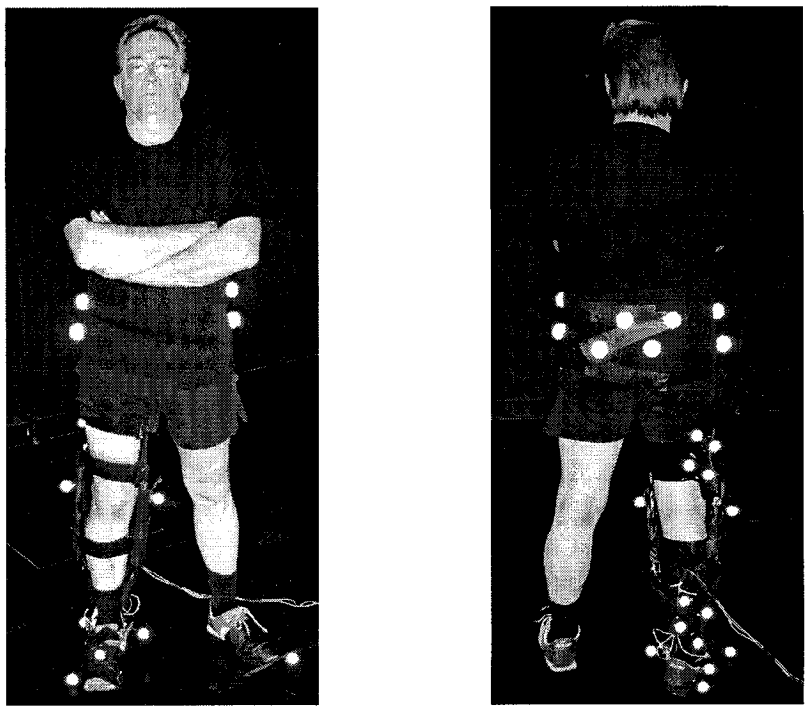

(a) (b)

Figure 5.2 – Two photographs showing the modified National Institutes of Health marker set, which positioned the markers along one leg and the pelvis. (a) A front view of the subject and (b) a rear view of the subject wearing the markers.

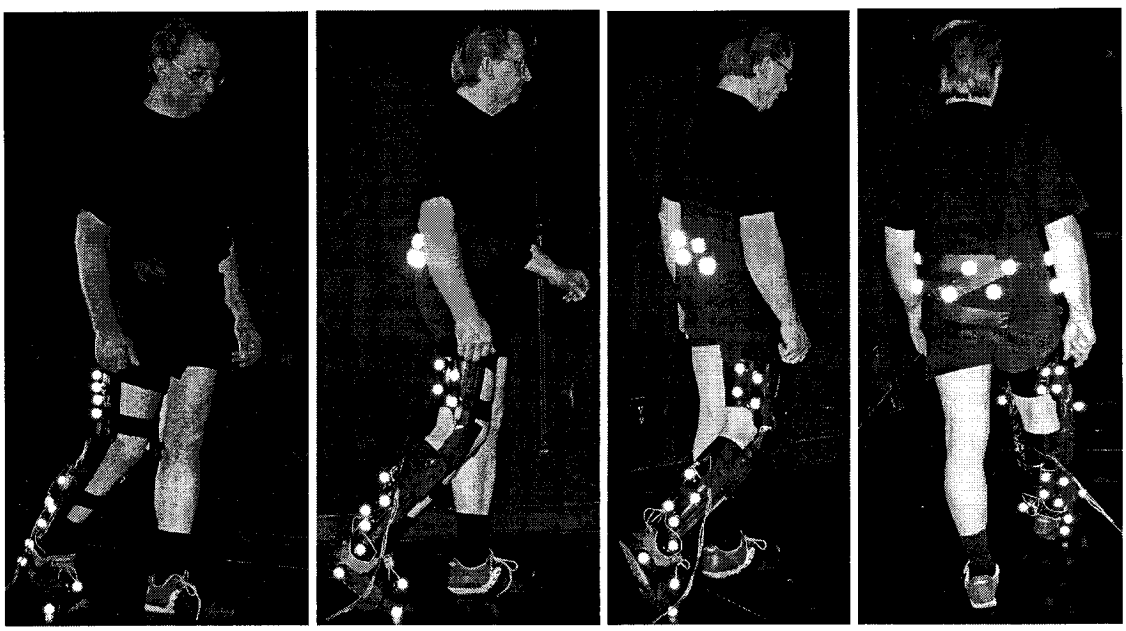

(a) (b) (c) (d)

Figure 5.3 – Photographs of the subject walking with the DKAFO, wearing tracking markers as seen by: (a) camera 1, (b) camera 2, (c) camera 3, and (d) camera 4.

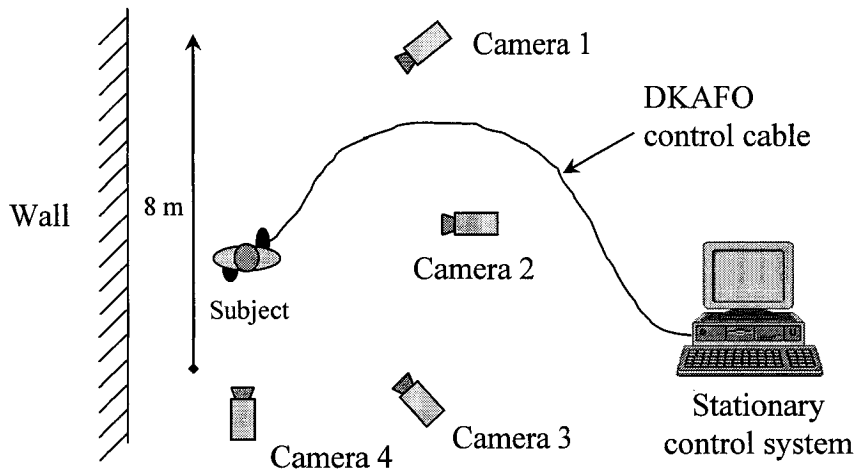

Figure 5.4 – Topographical drawing of the 3-dimensional motion capture system.

5.2.4.2 Control-System Tuning

Subjects were given a period of approximately 20 minutes to become accustomed to the DKAFO before testing. Threshold pressure levels of the three FSRs were adjusted at the beginning of the training period to accommodate the individual's gait pattern and account for the constant residual pressures applied to the FSRs due to the tightness of the shoe over the DKAFO footplate. To adjust the FSR threshold levels, the subject was asked to walk slowly and pause in terminal stance at the instant they wished the DKAFO to switch to swing mode. A lab assistant then adjusted the individual FSR threshold pressure levels accordingly to achieve solenoid activation with this pressure profile. The same process was used to identify limb loading with the FSRs. This method was effective in achieving a high level of control system reliability in walking. The FSR positions on the footplate were adjusted once the subject had spent several minutes walking with the DKAFO. If the FSRs positioned on the forefoot still experienced a substantial amount of foot pressure at the end of stance, the subject would have a difficult time switching the DKAFO to swing mode. In this case, the forefoot FSRs were moved toward the middle of the foot until an optimal position was found.

5.2.4.3 Data Capture

The four video cameras were calibrated before each set of gait trials. Calibrating the cameras involved recording a short motion capture of a precision 1 m^3 calibration cube temporarily placed at the centre of the walkway. This video data was later used to determine the exact locations of the cameras.

A short motion capture was taken of the subject standing up straight and square at the centre of the walkway, wearing all 24 tracking and calibration markers. The video data was used to create a standing calibration of the subject, defining the orientation and endpoints of the subject's foot, shank, thigh and pelvis. This information was then employed to create a dimensionally attuned model of the subject.

Following calibration, the subjects were asked to walk along the walkway at a natural cadence, wearing no brace (able-bodied subjects) or wearing their conventional KAFO (KAFO users). The process was repeated until five successful walking trials were recorded. Subjects were then given approximately 20 minutes to practice walking with the DKAFO. Following the practice session, subjects were again asked to walk along the walkway at a natural cadence while wearing the DKAFO. This process was repeated until five successful walking trials, where a full stride was captured by all four cameras, were recorded. This test procedure was performed in the same order for all six subjects.

5.2.5 Data Processing

The video data from the four cameras was uploaded onto a Windows™ based personal computer using an IEEE 1394 cable interface. The video data was processed using the Ariel Performance Analysis System (APAS) to obtain the synchronized 3-dimensional (3-D) coordinates of the tracking markers. The synchronized 3-D marker coordinates were exported as a C3D file to Visual3D. Visual3D was used to processed the maker data for visual, graphical, and quantitative analysis.

5.2.6 Data Analysis

Of the five successful walking trials recorded for each subject in each condition, the three most representative gait trials were processed. For each trial, the single stride located closest to the calibrated center of the walkway was isolated for analysis. The mean stride time, stride distance, walking speed and stance/swing duration ratio, and associated standard deviations were determined over the three trials.

The ankle angle, knee angle, sagittal (side) hip angle, frontal hip angle, pelvic obliquity (frontal pelvic angle), ankle angle velocity, knee angle velocity, and sagittal hip angle velocity were plotted over the duration of the gait cycle for each subject (Figure 5.6). Stride time was normalized to 100% of the gait cycle. Ensemble averaged data from the DKAFO condition were plotted for each subject. For comparison purposes, mean and standard deviations from the ensembled non-DKAFO condition were included on each graph.

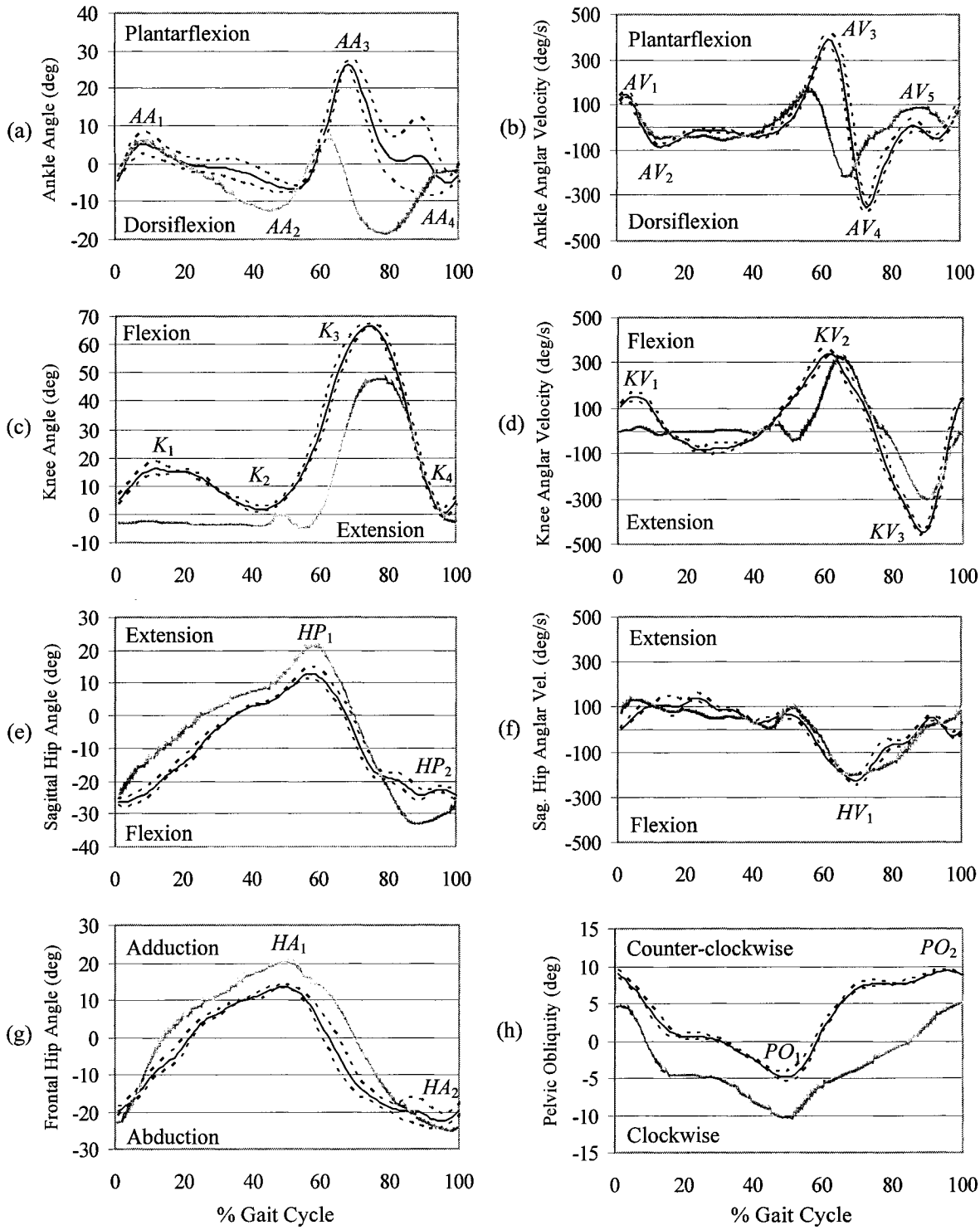

Figure 5.5 – Lower body segment angles and velocities for subject A1 while walking with no brace (solid black line), walking with the DKAFO (solid gray line). The dashed line represents one standard deviation either side of the mean for the no brace condition.

The relevant peaks of each curve were labelled and the absolute values of each peak were averaged over the three trials for each subject in each test condition and tabulated along with the standard deviation. Figure 5.7 illustrates the lower body angles that were measured for the gait analysis.

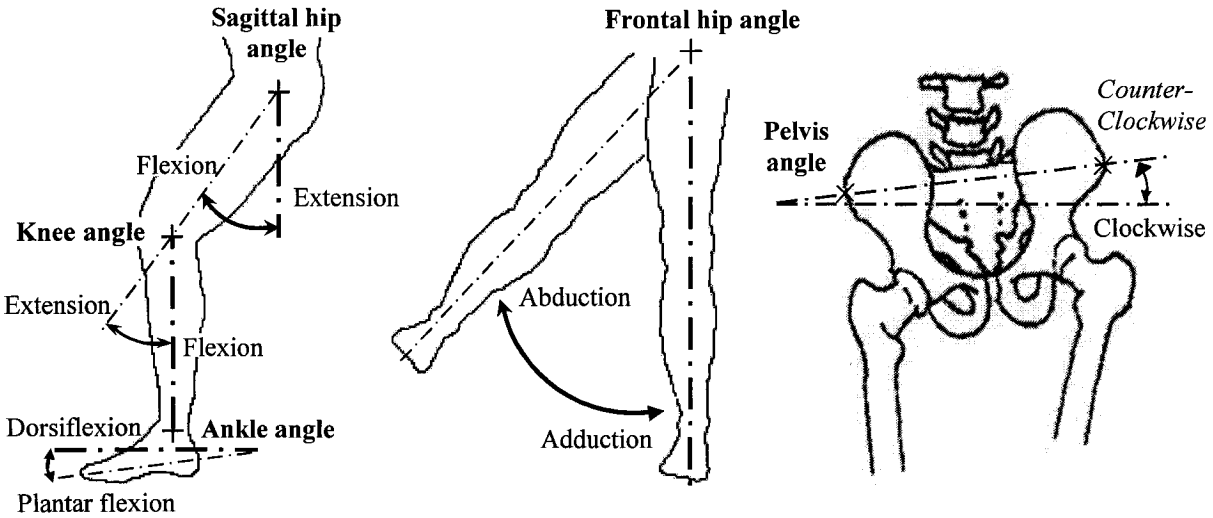

Figure 5.6 – Joint angles measured in gait analysis. The bold vertical or horizontal axis for each illustrated angle is the axis of zero angle; (a) ankle, knee and sagittal hip angle, (b) frontal hip angle as viewed from the front of the leg, and (c) pelvic obliquity as viewed from the front of the pelvis (modified from [90]). As viewed from the front, counter-clockwise rotation of the pelvis leads to a positive angle of rotation.

5.3 Results

Clinical results are presented concisely in this section in tabular form for the most important parameters. Graphs of the kinematic gait data for all six subjects can be found in Appendix F.

5.3.1 Test Results of Able-bodied Subjects

Table 5.5 summarizes the mean spatial-temporal stride parameters for the individual able-bodied subjects walking with the DKAFO and walking with no leg brace. Walking with the DKAFO required more concentration than walking without the brace and reduced the stride velocity (walking speed) of the all three subjects and the stride length of subject A1 and subject A2. Compared to walking with no brace, walking with the DKAFO resulted in slower walking speeds (A1=21.5%,, A2=25.2%, A3= 24.5%;

average of 23.7% slower) and longer stride duration (A1=26.7%, A2=34.5%, A3=17.5; average of 26.2% longer),. Walking with the DKAFO, the strides of subjects A1 and A3 were 1.3% and 11.6% shorter in length, or an average 4.3% shorter in length, while the stride of subject A2 was 0.6% longer in length, all compared to walking with no brace. There was a negligible change in stance (% of gait) between the walking with the DKAFO and walking with no brace for all three able-bodied subjects.

Table 5.5 - Mean spatial and temporal stride values for able-bodied subjects. The standard deviation is presented in brackets.

Subject	Trial	Stride Time (s)	Stride Length (m)	Stride Velocity (m/s)	Stance/Swing Ratio (% / %)
Subject A1	No brace	1.16 (0.01)	1.57 (0.01)	1.35 (0.01)	62.2 / 37.8 = 1.66 (0.23)
	DKAFO	1.47(0.05)	1.55 (0.11)	1.06 (0.96)	62.6 / 37.4 = 1.68 (0.09)
Subject A2	No brace	1.10 (0.02)	1.61 (0.02)	1.47 (0.04)	59.6 / 40.4 = 1.48 (0.11)
	DKAFO	1.48 (0.03)	1.62 (0.03)	1.10 (0.04)	59.0 / 41.0 = 1.44 (0.10)
Subject A3	No brace	1.26 (0.02)	1.38 (0.16)	1.10 (0.15)	63.7 / 36.3 = 1.76 (0.05)
	DKAFO	1.48 (0.10)	1.22 (0.02)	0.83 (0.04)	65.6 / 34.4 = 1.91 (0.11)

Table 5.6 tabulates the minimum and maximum mean joint angles and velocities for the three able-bodied subjects over the three trials. The angles and velocities are represented by numbered symbols and can be referenced to the joint angle and angular velocity curves in Figure 5.5. Symbols AA_i represent the maximum and minimum ankle angles in stance and swing, symbols AV_i represent the maximum and minimum ankle angular velocities in stance and swing, symbols K_i represent the maximum and minimum knee angles in stance and swing, symbols KV_i represent the maximum and minimum knee angular velocities in stance and swing, symbols HP_i represent the maximum and minimum hip angles, symbol HV_1 represents the minimum knee angular velocity, symbols HA_i represent the maximum and minimum frontal hip angles and symbols PO_i represent the maximum and minimum pelvic obliquity angles. Table 5.7 summarizes the lower joint ranges of motion for the three able-bodied subjects walking without a brace and walking with the DKAFO. Due to the resistance of the semi-rigid Tamarack ankle joints installed in the DKAFO, the able-bodied subjects experienced a 24.5% reduction in ankle range of motion with the DKAFO as compared to unbraced gait. The subject's peak plantar flexion velocity (AV_3) at toe-off was reduced by an average 47.8% when walking with the DKAFO (Table 5.6). The range of motion of the knee only decreased by an

average 3.6% when using the DKAFO (Table 5.7). Knee flexion during limb loading was negligible for subjects A1 and A2 when walking with the DKAFO; however, subject A3 achieved a mean 12.2° range of knee flexion motion in stance (Figure 5.7). The able-bodied subjects experienced an average 21.1% decrease in knee extension velocity (KV_3) in swing when wearing the DKAFO.

Table 5.6 – Mean peak values of lower body segment angles (deg) and angular velocities (deg/s) of able-bodied subjects walking without a brace and with the DKAFO; the standard deviation is presented in brackets. The identity of each peak is referenced in Figure 5.6. A positive percent difference in the *No Brace* and *DKAFO* values indicates an increased value in wearing the DKAFO.

	Subject A1		Subject A2		Subject A3		Average % Difference
	No Brace	DKAFO	No Brace	DKAFO	No Brace	DKAFO	
AA_1	5.2 (2.9)	5.9 (0.6)	13.2 (0.4)	4.3 (0.2)	8.7 (1.7)	12.7 (2.6)	-2.6
AA_2	-6.9 (0.8)	-12.3 (0.6)	-2.3 (0.5)	-3.2 (0.4)	-7.2 (1.1)	-1.1 (4.7)	12.2
AA_3	26.9 (0.9)	7.3 (2.7)	30.1 (2.1)	9.4 (1.9)	17.6 (0.8)	17.5 (8.2)	-47.5
AA_4	-6.2 (1.6)	-18.3 (2)	1.1 (0.9)	-10.1 (0.4)	-5.6 (0.9)	-4.1 (3.4)	-283.0
K_1	16.6 (1.6)	-2.1 (0.2)	30.1 (0.8)	-0.8 (1.9)	1.3 (0.9)	7.3 (5.8)	84.4
K_2	1.7 (1)	-5 (1.1)	7.6 (1.2)	-5.1 (0.6)	-7.4 (0.5)	-4.9 (5)	-201.9
K_3	66.9 (0.8)	48.1 (8.5)	78.8 (1)	65.1 (3.2)	45.6 (2.7)	54.6 (6.6)	-8.6
K_4	0.4 (1.6)	-2.8 (0.7)	9.4 (0.8)	-3.4 (0.7)	-6.5 (4.1)	-2.6 (5.1)	-340.8
HP_1	12.9 (1.8)	21.5 (2.2)	3.7 (1.5)	9.7 (1.5)	10.1 (1.4)	15 (4)	92.7
HP_2	-24.6 (1.5)	-33.3 (1.2)	-34.1 (0.2)	-27.9 (0.9)	-12.8 (3.4)	-25.3 (4.5)	38.0
AV_1	147.6 (16)	137.7 (12.2)	155.8 (1.8)	177.1 (14.2)	153.3 (10.1)	147.2 (21)	1.0
AV_2	-85.9 (6)	-54.4 (7.8)	-115 (6.5)	-20 (10.7)	-75.4 (3.4)	-71.3 (10.8)	-41.6
AV_3	395.1 (28.7)	170.4 (23.2)	349 (34.2)	192.1 (18.1)	359.9 (41.5)	210.7 (56)	-47.8
AV_4	-360.9 (18.2)	-221.7 (9.3)	-229.5 (32.1)	-128.7 (16.2)	-200 (25.7)	-210.7 (39.2)	-25.7
AV_5	103.3 (22.7)	105.4 (12.8)	112 (9.1)	143.3 (19.6)	65.1 (29.8)	103.5 (28)	29.7
KV_1	150.1 (19)	20.6 (13.8)	199.3 (19.3)	50.4 (25.8)	81.3 (26.5)	69.1 (46.1)	-58.7
KV_2	347.3 (17)	330.5 (38.8)	391.8 (10.8)	365 (3)	265.9 (8.7)	275.5 (10)	-2.7
KV_3	-451.4 (13.1)	-304.6 (24.3)	-467.4 (9.4)	-380.6 (39)	-279.4 (18.1)	-245.5 (12.5)	-21.1
HV_1	-228.7 (23.7)	-207.2 (28)	-246.5 (40.5)	-147.4 (8.2)	-184 (8.1)	-170.9 (25.6)	-18.9
HA_1	13.6 (0.4)	20.7 (1.2)	14 (0.5)	15.2 (1.4)	10.9 (0.4)	11.6 (0.3)	22.6
HA_2	-23.2 (1.5)	-25.5 (2.9)	-15.1 (0.6)	-16.9 (0.6)	-22.3 (5.8)	-18.8 (7.8)	1.9
PO_1	9.4 (0.2)	5.4 (1.3)	4.9 (0.7)	7.4 (0.7)	5.8 (0.4)	5.1 (0.7)	-0.6
PO_2	-4.9 (0.7)	-10.5 (0.6)	-7.7 (0.6)	-3.9 (1.1)	-3.8 (0.3)	-1.5 (0.7)	1.5

Table 5.7 – Summary of the ranges of motion (deg) of the relevant lower body joints of the three able-bodied subjects walking with no brace and walking with the DKAFO.

	A1			A2			A3			Average
	No brace	DKAFO	% Diff.	No brace	DKAFO	% Diff.	No brace	DKAFO	% Diff.	% Difference
Ankle	34.1	26.3	-22.9	32.3	19.5	-39.8	24.8	22.2	-10.8	-24.5
Knee	66.8	53.2	-20.4	71.2	70.7	-0.6	54.0	59.6	10.4	-3.6
Sagittal Hip	39.4	54.8	39.0	37.9	37.7	-0.8	23.4	41.0	75.0	37.8
Frontal Hip	36.8	46.2	25.6	29.1	32.1	10.1	33.2	30.5	-8.3	9.1
Pelvic Obl.	14.3	15.8	11.2	12.6	11.3	-10.1	9.6	6.6	-31.5	-10.1

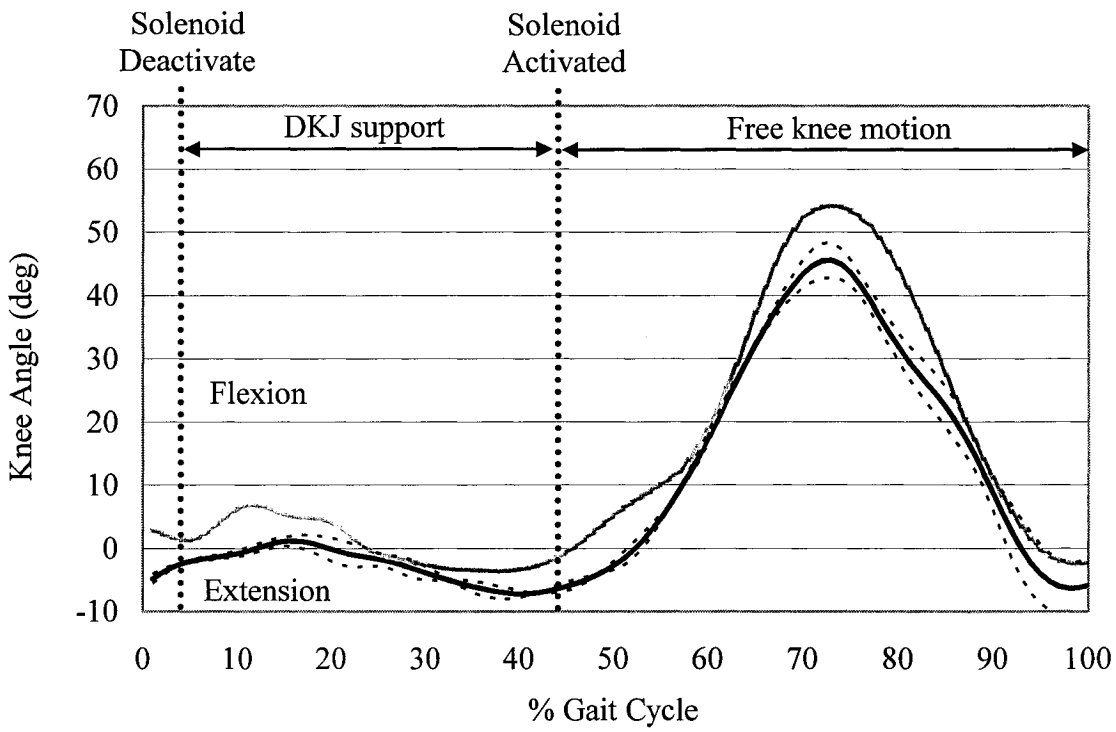

Figure 5.7 – Graph of the mean knee angle over three walking trials, over the course of one stride for subject A3 while walking with no brace (solid black line) and walking with the DKAFO (solid gray line). The dashed line represents one standard deviation either side of the mean for the no brace condition. The vertical dotted lines indicate the average instants of solenoid deactivation and activation in the stride cycle.

Wearing the DKAFO, subjects A1 and A3 displayed an increase of 39% and 75% respectively, in range of sagittal hip motion, with little change for subject A2. All three subjects experienced a mean 18.9% decrease in sagittal hip flexion velocity in early swing (HV_1). Subject A1 experienced a 52.5% increase in peak hip adduction (HA_1), from 13.6° to 20.7°, while subjects A2 and A3 experienced no notable difference in frontal hip angle when walking with the DKAFO. The DKAFO had no consistent effect

on the pelvic obliquity patterns of the able-bodied subjects; however, subjects A2 and A3 experienced smoother pelvic rotation in stance when walking with the DKAFO as seen in the pelvic obliquity curves of subject A2 and A3 in Appendix F. The solenoid activated and deactivated at appropriate instants in the gait cycle. Figure 5.7 illustrates the mean instant of solenoid activation and deactivation in the gait cycle for subject A3, as an example. Note that the solenoid timing does not coincide precisely with the approximate 65%/35%, stance/swing ratio exhibited by subject A3. Since the knee naturally begins to flex well before toe-off, the control system was set (Section 5.2.4.2) to activate the solenoid and allow free DKJ flexion at a specified foot pressure profile, before toe-off.

5.3.2 Test Results of KAFO Users

Table 5.8 summarizes the mean spatial-temporal stride parameters for the individual KAFO users. All three subjects found that they had to dedicate a substantial amount of mental effort or take smaller steps to disengage the DKJ for free knee motion at the onset of swing. The result was an appreciable decrease in stride distance and stride velocity for all three subjects.

Table 5.8 - Mean spatial and temporal stride values for KAFO users. The standard deviation is presented in brackets.

Subject	Trial	Stride Time (s)	Stride Length (m)	Stride Velocity (m/s)	Stance/Swing Ratio (% / %)
Subject B1	Orig. KAFO	1.73 (0.04)	1.27 (0.02)	0.73 (0.03)	58.3 / 41.7 = 1.40 (0.03)
	DKAFO	2.55 (0.07)	0.91 (0.03)	0.36 (0.00)	74.7 / 25.3 = 2.96 (0.22)
Subject B2	Orig. KAFO	1.40 (0.04)	1.31 (0.05)	0.93 (0.06)	60.7 / 39.3 = 1.55 (0.06)
	DKAFO	1.75 (0.03)	1.10 (0.05)	0.63 (0.02)	63.9 / 36.1 = 1.78 (0.14)
Subject B3	Orig. KAFO	1.98 (0.22)	0.82 (0.07)	0.42 (0.08)	59.4 / 40.6 = 1.47 (0.10)
	DKAFO	2.07 (0.18)	0.77 (0.11)	0.37 (0.09)	69.8 / 30.2 = 2.46 (0.08)

Walking with the DKAFO, the strides of subjects B1, B2 and B3 were 50.7%, 32.3%, and 11.9% slower, respectively, or an average of 31.6% slower; 28.3%, 16.0%, and 6.1% shorter in distance, respectively, or an average of 16.8% shorter in distance; and 47.4%, 25.0% and 4.5% longer in duration, respectively, or an average of 25.6% longer in duration, all compared to walking with their prescribed KAFO. The KAFO users also experienced an increase in stance (% of gait) walking with the DKAFO over

walking with their conventional KAFO of 28.1%, 5.3%, and 17.5% for subjects B1, B2, and B3, respectively or an average of 17.0% increase for all three subjects.

Table 5.9 tabulates the mean joint angle and velocity peaks of the KAFO users as labelled in Figure 5.6 over the three trials, walking with their original KAFO and walking with the DKAFO. The angles and velocities are represented by numbered symbols, which are described in Section 5.3.1 and can be referenced to the joint angle and angular velocity curves in Figure 5.5. Table 5.10 summarizes the KAFO users' lower body joint ranges of motion walking with their original KAFO and the DKAFO. As shown in Table 5.3, the ankle joint and footplate combinations built into the custom DKAFOs differed between DKAFOs and differed from the existing prescribed KAFOs of the KAFO users. The footplates and fixed-ankle joints included on the DKAFO of subject B1 and B3 inhibited ankle movement reducing the range of ankle motion by an average 21.4% between the two subjects. Subject B2 was the only individual that had the same combination of footplate and ankle joint on both his prescribed KAFO and his DKAFO. Walking with the DKAFO, subject B2 experienced 65.3% less dorsiflexion in stance (AA_2), from 7.5° dorsiflexion to 2.6° dorsiflexion (Table 5.9), a 34.2% decrease in ankle range of motion throughout the stride (Table 5.10) and a 50.5% reduction in peak ankle plantar flexion velocity (AV_3) in terminal stance, from 141.6 deg/s to 70.1 deg/s, all compared to walking with his prescribed KAFO. Wearing their original KAFOs, subjects B1 and B3 exhibited a negligible range of knee rotation in walking (Table 5.10). Subject B2 experienced an average peak of 19.6° of knee flexion in swing (K_3) as his KAFO allowed a limited amount of free knee flexion. Walking with the DKAFO, subjects B1 and B3 achieved average peak knee flexion angles of 14.5° (Table 5.9) and 28.3° (Figure 5.8a) in swing (K_3), respectively, while subject B2 achieved an average peak knee flexion angle of 44.3° in swing (Figure 5.8b). All three subjects thus had an increase in peak knee flexion (K_3) with the newly designed DKAFO. For subject B2, the increase in peak knee flexion was 126.1% from 19.6° to 44.3° (Table 5.9).

Together, the KAFO users experienced an average 488.1% increase in knee range of motion (Table 5.10). Subject B3 experienced an average 6.6° range of knee flexion

motion in limb loading (K_1-K_2) during stance while walking with the DKAFO (Figure 5.8a); a 560.0% increase in stance knee flexion range of motion (K_1-K_2), from 1.0° to 6.6° (Table 5.9), over walking with a fixed knee KAFO. Subjects B1 and B2 experienced negligible knee flexion in stance with both their prescribed KAFO and the DKAFO.

Table 5.9 – Mean peak values of lower body segment angles (deg) and angular velocities (deg/s) of KAFO users walking with their original KAFO and the new DKAFO; the standard deviation is presented in brackets. The identity of each peak is referenced in Figure 5.6. A positive percent difference indicates an increased parameter value when wearing the DKAFO.

	Subject B1		Subject B2		Subject B3		Average % Difference
	Orig. KAFO	DKAFO	Orig. KAFO	DKAFO	Orig. KAFO	DKAFO	
AA_1	9.1 (1)	11.7 (1.5)	8 (0.3)	7.9 (0.1)	5.5 (0.3)	7.0 (0.4)	18.5
AA_2	-7.8 (1.3)	-2.9 (1)	-7.5 (2.2)	-2.6 (0.9)	-6.7 (1.8)	-1.1 (0.7)	-70.9
AA_3	3.6 (1)	1.2 (1)	3.2 (2.6)	6.3 (0.3)	2.2 (2.1)	3.9 (1)	37.1
AA_4	-0.7 (0.8)	-1.2 (1)	-5.2 (3.1)	-2.8 (0)	0.2 (0.4)	1.8 (1.1)	296.7
K_1	3.7 (0.1)	0.0 (1.4)	1.9 (1.3)	3.8 (2.1)	0.8 (0.4)	4.4 (0.4)	143.8
K_2	1.1 (1)	-2.7 (1.5)	-0.8 (0.1)	-2.8 (0.2)	-0.2 (0.4)	-2.2 (1.6)	371.2
K_3	2.8 (0.8)	14.5 (1.4)	19.6 (0.5)	44.3 (0.8)	1.4 (0.8)	28.3 (0.7)	831.7
K_4	0 (0.2)	-2.3 (0.8)	0.3 (0.2)	1.6 (4.1)	-1.1 (0.3)	-1.7 (0.6)	-2246.2
HP_1	26.4 (1)	13.9 (1.1)	17.9 (1.3)	10.9 (0.5)	-1.9 (3.8)	8.1 (0.5)	-200.2
HP_2	-22.1 (1.6)	-22.5 (0.7)	-20.1 (0.6)	-26.8 (2.1)	-21.2 (1)	-15.7 (1.1)	2.9
AV_1	109.5 (14.1)	82.6 (20.4)	137.8 (20.7)	78.9 (20.6)	37.5 (12.6)	18.8 (7.5)	-39.0
AV_2	-52.4 (4.8)	-17.3 (7.5)	-58.0 (7.7)	-37.4 (2.7)	-32.7 (12.1)	-20.2 (13.6)	-46.9
AV_3	133.6 (5.1)	27.9 (8.6)	141.6 (16.2)	70.1 (17.2)	54.6 (15.7)	29.3 (16.8)	-58.7
AV_4	-37.8 (9)	-21.5 (5)	-90 (38.5)	-110.2 (8.5)	-11.4 (6.9)	-24.9 (18.2)	32.3
AV_5	58.9 (15.6)	45 (17.2)	132.2 (35.7)	55.7 (12.7)	25.3 (10.9)	42.2 (36.2)	-4.9
KV_1	33 (11.2)	16.7 (2.7)	13.9 (14.5)	4.3 (5)	13.6 (5.7)	36.0 (6.3)	15.2
KV_2	39.9 (3.6)	84.7 (34)	183.3 (13)	259.3 (19.4)	20.7 (6)	175.9 (12.1)	301.2
KV_3	-30.6 (17.4)	-113.1 (13.1)	-136 (22.8)	-220.3 (19)	-21.1 (7)	-153.4 (46.5)	319.3
HV_1	-135.5 (7.6)	-34.9 (12.5)	-160.9 (16.7)	-113.9 (4.7)	-57.7 (21.4)	-82.6 (14.8)	-20.1
HA_1	16.8 (1.9)	17 (0.7)	18.8 (0.6)	9.5 (0.7)	12.6 (2.1)	15.3 (1.1)	-9.3
HA_2	-10.4 (1.2)	-4.1 (2.6)	-10.8 (0.9)	-16.9 (0.3)	-7.1 (1.8)	-8.8 (1.2)	6.6
PO_1	4.1 (1)	4.0 (0.5)	3.1 (0.2)	0.9 (0.6)	0.8 (0.1)	2.2 (0.3)	29.5
PO_2	-5.3 (0.2)	-4.6 (1.2)	-5.1 (0.3)	-3.3 (2)	-7.8 (1.2)	-7.3 (0.2)	-18.4

Table 5.10 – Ranges of motion (deg) of the measured lower body joints averaged over three trials for all three KAFO users walking with their original KAFO and the DKAFO. A positive percent difference between the compared ranges of motion indicates an increased range of motion when wearing the DKAFO.

	B1			B2			B3			Average % Difference
	Orig. KAFO	DKAFO	% Diff.	Orig. KAFO	DKAFO	% Diff.	Orig. KAFO	DKAFO	% Diff.	
Ankle	17.0	14.6	-13.9	16.8	11.0	-34.2	12.1	8.6	-28.8	-25.7
Knee	4.3	17.5	303.0	20.3	47.0	131.3	2.9	32.6	1030.0	488.1
Sagittal Hip	48.5	36.3	-25.1	39.3	37.7	-4.1	19.4	23.8	22.8	-2.1
Frontal Hip	27.2	21.0	-22.6	29.7	26.4	-11.0	19.8	24.1	22.0	-3.9
Pelvis Obl.	9.4	8.5	-9.5	8.2	4.2	-49.0	8.6	9.6	11.2	-15.7

All three subjects achieved a more normal knee angle velocity pattern (Appendix F) in walking with the DKAFO due to the free knee movement in swing. Walking with the DKAFO, subject B2 achieved a 41.5% increase in peak knee flexion velocity (KV_2), from 183.3 deg/s to 259.3 deg/s (Table 5.9), and a 62.0% increase in peak knee extension velocity (KV_3), from 136.0 deg/s to 220.3 deg/s over walking with his original KAFO that allowed a limited 20.3° of free knee flexion (Table 5.10). Walking with the DKAFO, the KAFO users experienced an average 301.2% increase (Table 5.9) in knee flexion velocity in swing (KV_2) and an average 319.3% increase (Table 5.9) in knee extension velocity in swing (KV_3) compared to walking with their prescribed KAFO. These velocities (KV_2, KV_3) were greater because the KAFO users achieved a much greater range of knee motion in a relatively similar amount of time, walking with the DKAFO compared to walking with their prescribed KAFO. The DKAFO had no consistent or substantial effect on the sagittal hip angle (HP_1, HP_2) or sagittal hip angle velocity (HV_1) of the KAFO users. The only notable change was a 47.5% reduction in the average peak hip extension angle (HP_1) (Table 5.9) of subject B1 from 26.4° to 13.9°. Subject B1 experienced 60.6% less hip abduction (HA_2) from 10.4° to 4.1° (Table 5.9) walking with the DKAFO over walking with his original KAFO (Figure 5.9a). The reduction in hip abduction was accompanied by a more conventional pelvic obliquity pattern with the pelvis returning to the neutral position in pre-swing (60%-80% of the gait cycle) while walking with the DKAFO (Figure 5.9b). Walking with his original KAFO, subject B1's pelvis remained abnormally tilted downward, on the side of the braced leg in pre-swing.

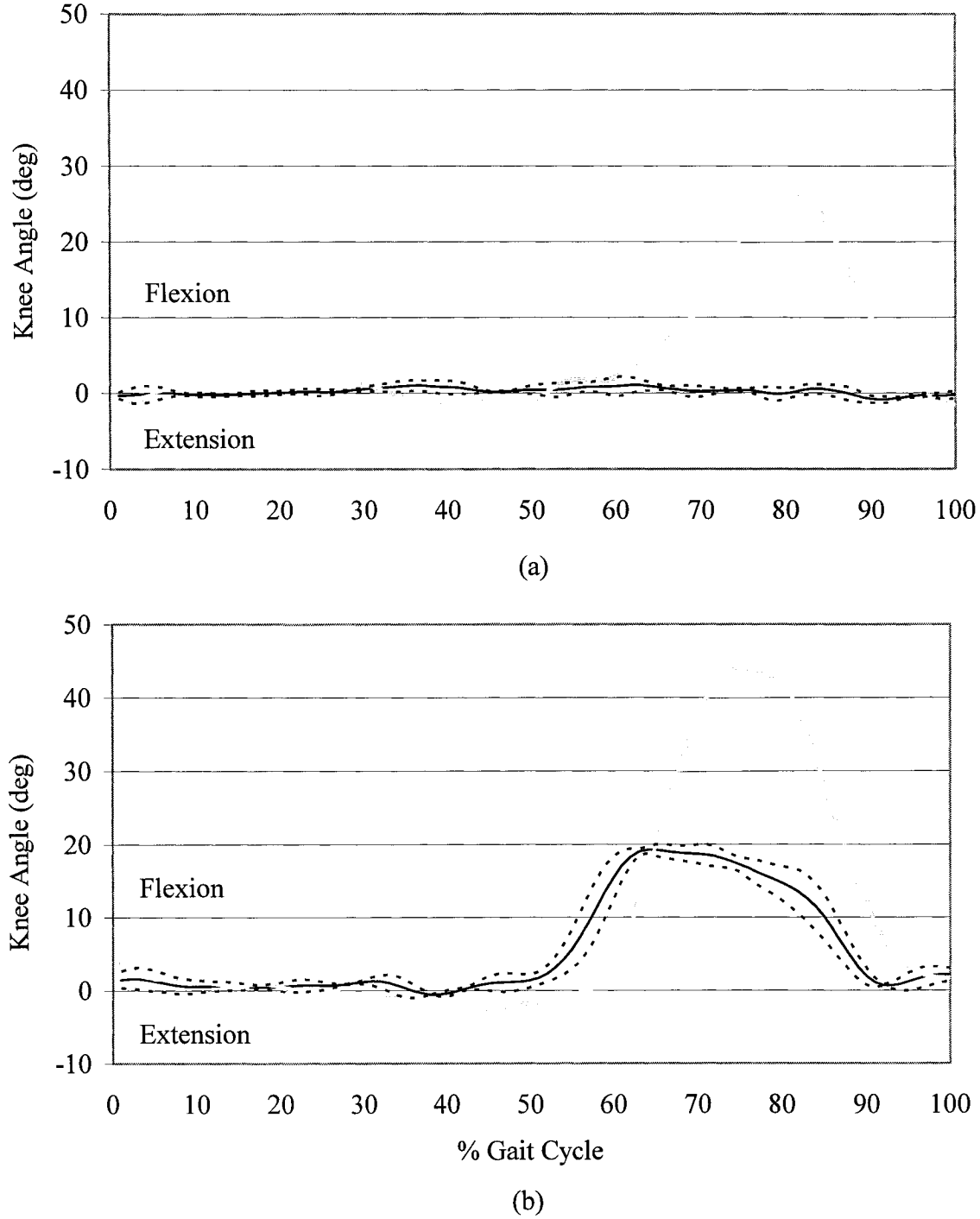

Figure 5.8 – Graph of the mean knee angle over three walking trials, over the course of one stride for (a) subject B3 and (b) subject B2, while walking with a fixed-knee KAFO (solid black line) and walking with the DKAFO (solid gray line). The dashed lines represent one standard deviation either side of the ean for the fixed-knee KAFO condition. In Figure (a), note the average 6.6° range of knee flexion achieved in limb loading (0-20% of stride cycle) when walking with the DKAFO.

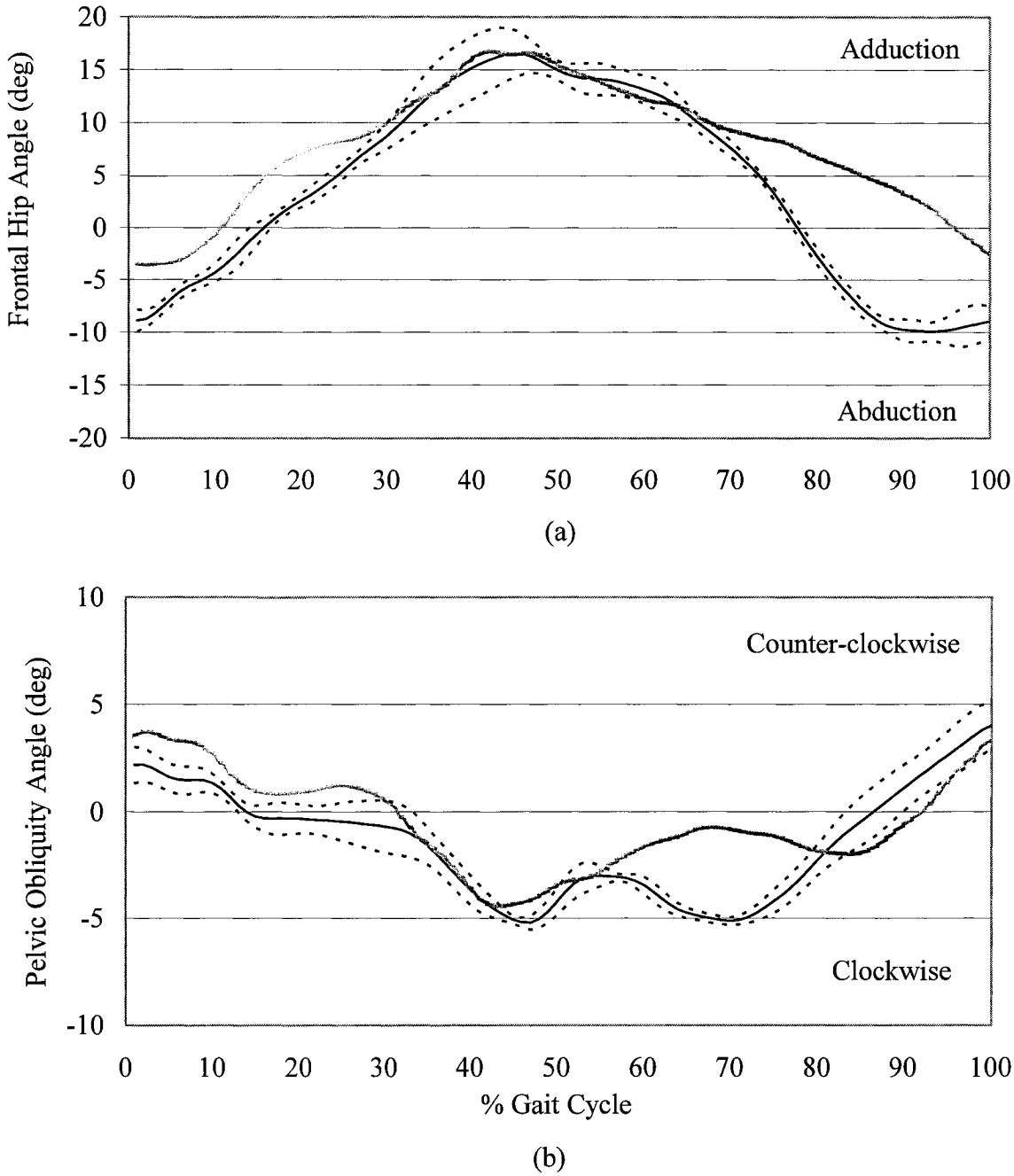

Figure 5.9 – (a) Frontal hip angle and (b) pelvic obliquity for subject B1, walking with his original KAFO (solid black line) and the DKAFO (solid gray line). The dashed lines represent one standard deviation from the KAFO condition.

Subject B2 exhibited an average of 11.0% decreased range of frontal hip motion and an average 49.0% decreased range of pelvis motion (Table 5.10) when walking with the DKAFO over walking with his original KAFO. When walking with the DKAFO, the

frontal hip rotation pattern of subject B3 remained within one standard deviation of the mean frontal hip rotation angle achieved in walking with the prescribed KAFO. There was no appreciable change in pelvic obliquity range of motion for subject B3 between test cases; however, his pelvic obliquity pattern was more conventional when walking with the DKAFO since his pelvis returned closer to the neutral position at the end of stance (60% gait cycle). Walking with his original KAFO, subject B3's pelvis abnormally dropped on the side of the braced leg in terminal stance (Appendix F).

5.3.3 DKAFO Performance

The test subjects had varying levels of success triggering the DKAFO to disengage when entering the swing phase of gait. Success in handling the DKAFO was most often dependent on the subject's ability to provide a knee extension moment to disengage the DKJ lock mechanism prior to swing. All subjects initially found the knee extension requirement difficult to satisfy consistently; however, their experience walking with the DKAFO increased over the course of the gait test and lead to an increased ability to control the DKAFO. All test subjects were able to achieve unimpeded knee flexion in swing, especially subjects B2 and B3 who experienced a considerable increase in swing phase knee flexion compared to walking with their prescribed KAFO.

The solenoid reaction time was adequate throughout clinical testing. Once the threshold pressures for the FSRs were custom set to accommodate the walking pattern of the individual test subject, the FSRs and control system were very reliable in activating and deactivating the solenoid at the onset of terminal stance and limb loading. Figure 5.7 includes the mean instant of solenoid activation and deactivation on a graph plotting the average knee angle of subject A3 over the course of a stride while wearing the DKAFO.

5.3.4 Participant Feedback

Following the gait test, a questionnaire was given to each participant that focused on the performance and structure of the DKAFO. Participants also provided informal feedback of their thoughts on the DKAFO and how it compared to their existing brace.

Subjects A1, A2 and A3 could not compare the DKAFO performance to an existing KAFO, but did comment on the feeling of security and control issues of the DKAFO.

All six subjects found that an increased amount of mental effort was required to walk with the DKAFO, specifically, disengaging the DKJ for free knee motion at the onset of swing. Subjects B1 and B3 preferred the DKAFO over their prescribed KAFOs since the new orthosis required less effort to walk and fostered improved gait. Subject B2 preferred his prescribed KAFO to the DKAFO because he required an excessive amount of concentration to disengage the DKAFO in walking. Subject B1 expressed a desire for some form of audio feedback when walking with the DKAFO to assure him that the DKAFO was switched to stance support mode. Subject B3 found the DKAFO lighter, less bulky and easier to control than his prescribed Horton SCKAFO. All six subjects felt a sufficient amount of knee security in stance with the DKAFO.

Chapter 6. Discussion

6.1 Comparison of the DKAFO with Existing SCKAFOs

The DKJ is thinner, lighter, more functional and projected to be less expensive than any commercial SCKAFO offering comparable performance. Orthotic knee joints that present a large frontal profile are obstructive and cosmetically unappealing. The Horton Stance Control Orthosis and 9001 E-Knee both measure approximately 24 mm in thickness. The DKJ is approximately 33% thinner, measuring only 16 mm thick. Overly heavy orthotic knee joints can negatively affect the energy expenditure and gait patterns of the user in walking. The DKJ is lighter than existing orthotic knee joints offering similar performance. Excluding the solenoid, the DKJ weighs 339 grams. This is 7% lighter than the Horton Stance Control Orthotic Knee Joint, which weighs 365 grams, and appreciably lighter than the 9001 E-Knee by Becker Orthopedic, which weighs 780 grams. Including the solenoid, the DKJ weighs 424 grams.

A major disadvantage of all commercial SCKAFOs is their cost. Conventional KAFO joints cost between $150-$300 CDN. The sale price of a pair of commercial SCKAFO joints begins at $2200 CDN minimum. The Becker 9001 E-Knee joint and control system costs nearly $4200 CDN. When the cost of material and labour to integrate the joints into a KAFO are added, the total price of a SCKAFO is often too expensive for many potential clients to afford. The simple design of the DKJ requires relatively inexpensive manufacturing methods. A projected cost estimate to manufacture a pair of DKJs including the cost of solenoids was $570 CDN, based on a manufacturing run of 100 DKJ units. This cost estimate suggests that a pair of DKJs will have a much lower sale price than current commercial SCKAFOs.

All commercial SCKAFOs rigidly lock the knee from flexing in stance. The result is an abrupt deceleration of the body's center of gravity during limb loading, translating into a jerky gait pattern for brace wearers and a high load transfer to their anatomical joints. Non-functional commercial orthotic knee joints do exist that offer controlled spring-resisted knee flexion. For instance, the LR-9002 Load Response Knee Joint by

Becker Orthopedic, employs a spiral spring to allow 18° of controlled knee flexion in stance. Controlled knee flexion is not available in any commercial SCKAFOs. The DKJ does, however, offer controlled knee flexion in loading, as shown in Figure 5.7 and 5.8. The result is a functional orthotic knee joint that encourages a smoother, more natural gait pattern than commercial SCKAFO designs. The DKJ will also support the knee at any knee angle in stance. This performance feature surpasses OttoBock's FreeWalk SCKAFO and Fillauer's Swing Phase Lock SCKAFO, which can only support a fully extended knee and Becker Orthopedic's 9001 E-Knee, which will only support the knee in a finite number of locking positions.

6.2 Mechanical Testing

6.2.1 Implications of the Mechanical Testing Results

The results of mechanical strength testing of the DKJ revealed that the factory-cut T-155 MegaFlat belts installed in the DKJ possessed a median break strength of 2509 N (Table 4.2). The hand-cut T-155 MegaFlat belts used in breaking load testing (Section 4.1.1), possessed a median break strength of 1812 N; 38% lower than the break strength of the factory-cut belts. This result was expected as the crude method of hand cutting the belts occasionally damaged the polyester cables lining the edge of the belt. The 5 mm wide belts housed only six polyester cables across the belt's width, running the length of the belt. Minor damage to the two peripheral cables would have been sufficient to appreciably reduce the breaking load of the belt. In fact, the hand-cut belts possessed a breaking load just over four-sixths the breaking load of the factory cut belts.

A key goal of mechanical testing was to validate the static strength of the DKJ. The DKJ was designed to endure peak loads of 77 Nm with a static-load safety factor of 3. The maximum DKJ flexion moment achieved in mechanical testing prior to tensile failure of the belt was 73 Nm or 95% of the designed limit load. Due to the limited strength of the belt, an applied moment of 77 Nm could not be realized and it was not possible to validate the safety factor of the other DKJ components. Following mechanical testing of the DKJ, the remaining components of the DKJ were inspected. Excluding the belt, no other component showed any visual signs of wear or strain from loading. The

belt failed after 66 loading cycles at a mean applied moment of 52 Nm due to wear of the belt's neoprene coat at the clamp site. The mode of belt failure after repeated loading was not catastrophic and therefore still considered safe for proceeding with clinical testing.

The results from mechanical testing indicated that the DKJ was sufficiently safe for laboratory controlled clinical testing. The DKJ and all of the individual components functioned as intended. The lowest joint failure moment observed in mechanical testing was 61 Nm and was considered the limit failure moment for clinical testing. A maximum subject weight of 100 kg was included in the search criteria in the recruitment of clinical test subjects. As indicated in Table 3.7, test subjects that weigh 100 kg were expected to generate a peak DKJ moment of 52 Nm in normal cadence. The DKAFO therefore offered a safety factor of 1.2 for 100 kg subjects in normal cadence.

6.2.2 Limitations of Mechanical Testing

Due to the narrow width of the T-155 test specimen in friction testing (Section 4.1.2) only a limited sized mass could be used for the test since the mass had to balance on the narrow belt specimen. Ideally, a much heavier mass should have been used to more accurately simulate the clamping force experienced in the DKJ. However, even if an appropriate mass were used to simulate the peak clamping force in the DKJ, the pulling force required to move the belt would have been beyond the capabilities of a human hand.

Mechanical testing was limited by the capabilities of the testing apparatus and the performance capabilities of the material testing machine. The test apparatus could only apply a moment on the DKJ in the sagittal plane. As mentioned in Section 2.1.1.3, the anatomical knee also rotates in the transverse and frontal planes; however, these movements are relatively low in magnitude and would most likely have no effect on the DKJ.

The 4482 Instron material testing machine was capable of loading the DKJ at a maximum speed of 508 mm/min, only 8% of the equivalent 6000 mm/min loading rate

estimated to be experienced by the knee in slow cadence [7]. The effect of loading rate on the DKJ is unclear since neither the neoprene nor the polyester materials comprising the T-155 MegaFlat belt are viscoelastic.

6.2.3 Sources of Error in Mechanical Testing

The 4482 Series Instron material testing machine loaded the DKJ at a maximum rate of 508 mm/min and measured the load at maximum sampling rate of 20 Hz. The material testing machine therefore measured the load data with every 0.42 mm of vertical displacement. The accuracy of the measured moment of failure was limited by the resolution of the sampling rate of the material testing machine since the peak DKJ holding moment at failure could have potentially occurred between sampling points.

The Pesola spring scale used in measuring the coefficient of friction of the T-155 MegaFlat belt had an accuracy of ±0.3% of the load. Therefore, the measured coefficient of friction μ=0.84 had a calculated spring scale accuracy of ±0.003.

The average load applied to the DKJ in mechanical testing was approximately 0.5% of the load cell's capacity. The load accuracy for the 4482 Series Instron material testing machine at this level of loading was approximately ±1% of the load. The 73 Nm moment achieved in mechanical testing therefore had an accuracy of ±0.7 Nm. The ruler measuring the perpendicular distance L, between the applied force of the testing machine and the knee-joint axis had a precision of ±0.5 mm. The precision of the ruler created an uncertainty of ±0.3 Nm for a 73 Nm moment. The protractor fixed to the DKJ had a precision of ±0.5°.

6.3 Clinical Testing

6.3.1 Implications of Clinical Testing

The main objective of designing a new DKAFO was to provide free knee rotation in swing while resisting knee flexion in stance at any knee or ankle angle when the limb is loaded. All three KAFO users achieved a substantial increase in knee flexion in swing when walking with the DKAFO compared to their prescribed KAFO. The KAFO users

experienced a 488.1% increase in knee joint range of motion walking with the DKAFO compared to walking with their prescribed KAFOs. The knee angle pattern achieved by all three KAFO users, while walking with the DKAFO, more closely resembled a normal knee angle pattern (Figure 5.5c) than walking with a fixed-knee KAFO. Due to the elastic-resistance of the DKJ, subjects A3 and B3 achieved smooth knee flexion in limb loading during stance when walking with the DKAFO as shown in Figure 5.7 and Figure 5.8a, respectively. This result demonstrates that the DKAFO does offer a more natural loading response of the knee than fixed-knee KAFOs.

Due to time constraints, all of the test subjects had only 20 minutes of practice walking with the DKAFO before starting the gait trials. Ideally, potential users should have at least two weeks of practice with the DKAFO to control the brace consistently, effectively, and comfortably. Limited by the short accommodation period, all six test subjects were challenged by the requirement to create a knee extension moment in terminal stance to disengage the DKJ mechanism to achieve the free knee motion for swing. The test subjects found that the knee extension requirement demanded substantial mental concentration and alterations to their gait pattern. For instance, subject A1 found knee extension easiest when he maintained a constant extension moment about the knee throughout stance. Subject B1 took smaller steps with his non-braced leg to create the knee extension moment in terminal stance. The mental and physical demands of controlling the DKAFO lead to a considerable decrease in both stride velocity and stride distance for all six subjects compared to the stride values achieved while walking with no brace or an original prescribed KAFO. All six subjects were unable to consistently disengage the DKJ in terminal stance for free knee motion in swing. The mental and physical effort required to control the DKAFO is expected to decrease substantially with sufficient practice walking with the brace and with formal gait training.

The DKAFO did not adversely affect gait in any considerable manner. The able-bodied subjects exhibited only minor deviations from normal gait patterns when walking with the DKAFO. The semi-rigid Tamarack ankle joints and restrictive footplate largely inhibited ankle motion. Ankle motion resistance created by the Tamarack joints and a

reduced stride velocity experienced when walking with the DKAFO probably caused the reduced plantar flexion velocity exhibited by all three subjects at toe-off. The diminished knee flexion angle achieved by Subjects A1 and A2 in limb loading was likely caused by a combination of knee flexion resistance applied by the DKAFO in stance plus a conscious effort by the subjects to create a constant knee extension moment in stance to disengage the DKJs before swing. The decreased knee extension velocity in swing experienced by all three subjects was likely influenced by friction of the DKJs and the addition of DKAFO weight to the subject's lower leg. The increased range of sagittal hip motion experienced by subjects A1 and A3 could possibly be attributed to abnormal sagittal pelvis rotation created by conscious effort to create a knee extension moment in terminal stance to disengage the DKJs. The reduced stride velocity and the addition of DKAFO weight to the entire leg could have caused the decreased peak hip flexion velocity in swing experienced by all three subjects.

Pelvic obliquity was smoothed out over the course of the stride when walking with the DKAFO. The smoother pelvic obliquity motion exhibited by subjects A2 and A3 was likely influenced by the shorter strides and slower walking speed of the subject when wearing the DKAFO. Future clinical testing that involves bilateral gait analysis could monitor the motion and position of the non-braced leg in chorus with the braced leg and could be used to analyze the cause of smoother frontal pelvis rotation when walking with the DKAFO.

Subject A2 experienced a decreased range of ankle motion when walking with the DKAFO, which was likely influenced by his reduced stride length and motion resistance from the stiff, semi-rigid Tamarack ankle joints installed in the DKAFO. A reduction in stride velocity, when walking with the DKAFO, probably lead to the reduction in peak ankle plantar flexion velocity for subject A2. The lower peak hip extension angle experienced by subject B1 with the DKAFO was likely caused by the accompanied reduction in stride length. While walking with the DKAFO, subject B1 exhibited a substantial decrease in hip abduction, indicating that subject B1 experienced less circumduction of his braced leg while bringing his braced leg forward in swing. The

reduced circumduction of the braced leg was accompanied by a more conventional pelvic obliquity pattern. Walking with the DKAFO, subject B1's pelvis returned to the neutral position, near 0°, in late stance compared to walking with his prescribed KAFO, where his pelvis remained pitched downwards through late stance and into initial swing (Figure 5.9b). The improved pelvic obliquity pattern of subject B1, walking with the DKAFO, as shown in Figure 5.9b, can be compared to the conventional pelvic obliquity pattern in Figure 5.5h exhibited by subject A1 in walking with no brace. The more conventional, neutral pelvis position adopted by subject B1 when walking with the DKAFO may lead to less stress on his hip and lower back, which may be caused by the abnormal dropping of the pelvis when walking with the prescribed KAFO.

Walking with the DKAFO, subjects A2 and A3 experienced no considerable change in their frontal hip angle pattern or pelvic obliquity pattern to suggest any reduction in leg circumduction or hip hiking in swing. Subject B2 experienced a regular amount of pelvic obliquity when walking with his original KAFO. While the pelvic obliquity of subject A2 was reduced when walking with the DKAFO, it was most probably caused by the accompanied reduction in stride velocity and stride length. Walking with the DKAFO, subject B3 did experience a more normal pelvic obliquity pattern since he slightly lifted his pelvis to a near 0° angle in late stance; however this pattern was not accompanied by a marked reduction in hip abduction as experienced by subject B1.

6.3.2 Limitations of Clinical Testing

A notable limitation of the clinical test was the relatively short period of time each subject was given to practice walking with the DKAFO before the gait test. Due to the stationary nature of the DKAFO's control system, subjects were constrained to the GAMA laboratory when walking with the DKAFO. Subjects were given approximately 20 minutes of DKAFO walking practice before commencing the gait test. Ideally, test subjects should have at least two weeks of DKAFO practice before gait testing.

The gait tests were performed in the same order (i.e. walking with no brace or a KAFO before walking with the DKAFO) for all subjects. Subject performance may have

been influenced by the sequence in which the tests were carried out. Future gait trials should be performed in random order to eliminate potential bias in the data.

When walking with the DKAFO, the subject's gait pattern was affected by the DKAFO as well as their efforts to provide an extension moment at the end of stance to disengage the DKJ for free knee motion in swing. Kinematic gait analysis data was not able to identify which gait pattern changes were caused by the mechanical constraints of the DKAFO and which gait pattern changes were caused by the subject's conscious effort or inablilty to extend the knee at the end of stance.

Ideally, the passive marker set would be adhered to the subject's skin to obtain the most accurate position of the anatomical body segment. Unfortunately, errors would exist even in this situation since skin moves over bone, creating an inaccurate reading of the body segment's position. Many of the markers were adhered to the test subject's clothing, introducing further error as the clothing could have moved relative to the subject's skin. Clothing could not be removed to accommodate these markers as the markers were located on the subject's pelvis. The leg braces used in clinical testing covered the majority of the user's leg. The marker set was therefore adhered to the outer surface of the KAFOs and DKAFOs. The results of the test data therefore indicate the knee angle and knee velocity of the user's brace and not their actual knee. Some relative movement exists between the user's leg and the brace. While the data does not indicate the true knee angle and true knee velocity, the difference between the knee angle of the brace and the user's true knee angle is a few degrees.

6.3.3 Sources of Error in Clinical Testing

Poor subject posture, such as standing with slightly bent knees or a wide stance during the standing calibration stage, could have lead to an offset in the values of some joint angles. This offset only affected the researcher's ability to define the zero point for extension angle of the joints. Data involving relative joint angles such as joint range of motion and joint angular velocity were not affected. In the video processing stage, distortion or occlusion of the reflective marker may have created some error in the ability

of the computer to determine the true 3-D marker position (i.e., pelvis marker being blocked by the hand, etc.). The majority of this error was eliminated when the marker position data was filtered before modeling.

6.4 Future Work

6.4.1 Recommended Improvements to the Dynamic Knee Joint

Several improvements must be made to the current DKJ design if a safe, reliable, commercially competitive DKAFO is to be realized.

6.4.1.1 Reduction of Joint Flexion Under Loading

Mechanical testing measured an appreciable amount of DKJ flexion in loading. As explained in Section 6.1, a limited amount of controlled knee flexion can be beneficial; however, the DKJ presented excessive flexion angles in mechanical loading. DKJ flexion angles of 20° to 25° were experienced in mechanical testing under an applied flexion moment of 47 Nm, the average peak moment plus one standard deviation generated by a 90 kg user in normal cadence. Ideally, the DKJ should offer no more than 15° of flexion under a 47 Nm flexion moment. The amount of DKJ flexion in loading must be reduced.

Under loading, controlled DKJ flexion is a sum of elastic elongation of the belt, belt slip in the clamp, belt slip about the disc, and belt slip of the spacer belt. Eliminating or decreasing the DKJ flexion allowed by one of these components can reduce the total amount of DKJ flexion offered in loading. Belt slip of the spacer belt can be eliminated by manufacturing the disc with a larger lower radius to properly distance the belt from the knee axis and remove the need for a spacer belt and the component of knee flexion associated with it. Adding a discreet clip or clamp to hold the wrapped belt tightly around the disc and prevent slack from forming in the wrapped belt and may reduce belt slip about the disc. A reduction in belt slack on the disc will also reduce variations in the DKJ flexion angle experienced under constant knee flexion moments (Section 4.2.4.1). A belt with a higher tensile elastic modulus than the T-155 MegaFlat belt would stretch less under loading and allow less knee-joint flexion.

The DKJ will always allow a limited degree of knee flexion during loading. Some potential clients may not tolerate any knee flexion in stance and may opt for a brace that provides immediate rigid knee support in stance. The DKAFO is however targeted at the more functional sector of the population inflicted with isolated quadriceps weakness. These potential clients may benefit more from an orthosis that allows controlled flexion in stance.

6.4.1.2 Development of a New Belt

The results of mechanical testing in Section 4.2 concluded that the T-155 MegaFlat belt material had insufficient tensile strength and wear resistance to be included in a commercially safe DKAFO. An exhaustive search for an adequate belt material could not uncover a more suitable off-the-shelf material. A custom belt material must be developed with sufficient flexibility, tensile strength, wear resistance, and coefficient of friction to produce an adequately safe DKJ. Many of the investigated belt manufacturers, listed in Appendix D, offer engineering services and manufacturing facilities dedicated to designing and fabricating custom belts for customers.

A relatively flexible 5 mm wide belt with a tensile breaking load of 8400 N should be possible to develop. A belt with a tensile breaking load of 8400 N would provide a safety factor of 3 for a 90 kg user in stair ascent. The T-155 MegaFlat belt used in the prototype was mainly composed of neoprene with only a single ply of polyester weave reinforcing the belt. Increasing the polyester content in the belt would greatly increase the belt strength. Stronger reinforcement fibres such as Kevlar® or Zylon®, which are 3.5 and 6.6 times stronger than polyester, respectively, could also be used to increase the belt's strength. Polyurethane and polyvinyl chloride may be investigated as alternative belt coating materials that may offer improved wear resistance.

As highlighted in the failure mode analysis (Section 3.5.10), brittle tensile belt failure under extreme loading is one of the greatest safety issues facing the DKJ design. Instant tensile failure of the belt could cause the user to stumble or fall, possibly causing serious injury. A more gradual or less consequential failure of the belt must precede any

tensile failure. The future belt component could be designed to fail in shear before reaching tensile failure loads. The belt coating could be designed to shear or delaminate from the fibre carcass at the clamp site under a predetermined belt tension. The shear-failure belt tension would be designed lower than the breaking tension of the belt. Loading the DKJ to belt shear failure would lead to delamination of the belt coats at the clamp site, resulting in an increased amount of knee flexion in loading - a warning that the belts had failed in shear and will require immediate changing.

In designing an improved belt, the coefficient of friction between the belt and the hammer material must be considered. As calculated in Equation 3.16, the belt must possess a coefficient of friction of at least 0.19 with the aluminium hammer for the DKJ to achieve adequate performance. If the improved belt material offers an insufficient coefficient of friction with aluminium, the hammer and anvil may be hard-anodized to increase friction. Consideration must be given to the effects anodizing will have on the fatigue strength of the treated components.

The wear resistance and compressive yield strength of the belt coat material will have to be considered in designing a suitable belt. Ideally, the DKJ should require servicing and potential belt replacement no more than every six months. If the belt requires replacement only twice per year, it will have to endure an approximate 500,000 loading cycles.

6.4.1.3 Modifications to the Hammer and Anvil

Belt destruction at the clamping site must be eliminated or greatly reduced. The sharp stress gradients experienced by the belt at both ends of the clamp site, as illustrated by points *U* and *S* in Figure 3.7, encouraged cracking and plastic deformation of the belt coats. The leading edge corners of the anvil and lower hammer should be redesigned with significantly larger radii. Larger radii on the corners of the hammer and anvil, would decrease the stress gradients on the belt at the edges of the clamp site, thereby reducing the associated belt damage. A larger radius on the lower leading edge corner of the anvil would also eliminate the anvil's ability to peel off the belt's neoprene coat. A

modification to the design to distribute the clamping load on the belt over a larger surface area would reduce wear of the belt. This could be done, for example, by having the hammer clamping force act on the belt via an intermediate clamping element with a large surface area.

6.4.1.4 Preventing Abrasive Wear of the Aluminium Components

The DKJ experienced abrasive wear between the disc and the side-plates and, to a lesser amount, between the side-plates and the hammer. The DKJs used in clinical testing suffered more abrasive wear than the DKJ used in mechanical testing due to a greater level of use. Future embodiments of the DKJ should integrate thin washers composed of a material such as Mylar® or nylon between the side-plates, the pivoting hammer, and disc. The aluminium solenoid plunger collar endured considerable abrasive wear from rubbing against the solenoid trim screw and the goose-head trim screw. Future solenoid collars should be made from a harder material such as stainless steel.

6.4.1.5 Weight Reduction

The heaviest prototype DKAFO weighed 2.26 kg (4.99 lbs), slightly less than the target weight of 2.30 kg (5.0 lbs) set early in the design process. The DKJ weighed 0.339 kg (0.756 lbs), excluding the weight of the 0.086 kg solenoid. Though the weight of the DKJ was comparable to the weight of commercial SCKAFO joints, future efforts should be made to further reduce the weight of the DKJ to increase its clinical effectiveness, commercial appeal and compensate for eventual integration of the circuitry, battery and solenoids. The use of more advanced stress analysis methods, such as finite element analysis, to analyze stresses on the side-plate component may reveal areas of potential weight reduction. To reduce the weight of the disc, holes may be drilled around the knee-joint axis hole at the midpoint of the disc's lower radius. This method could remove an appreciable amount of material from the disc without compromising strength.

6.4.1.6 Optimization of the Dynamic Knee Joint Dimensions

Due to time constraints, DKJ prototype manufacturing commenced before a commercially viable belt material was found. Final optimization of the DKJ dimensions was not performed during the design stage due to the uncertainty of the coefficient of friction of the belt to be used in the DKJ. The coefficient of friction between the belt and the hammer affects the stresses experienced throughout the DKJ. Once an adequate belt material has been developed, the belt coefficient of friction may be considered in calculating the optimal dimensions of the individual DKJ components.

The substantial length of the 207.7 mm long DKJ, largely influenced the bulky frontal profile of the brace. As shown in Figure 5.1c, the uprights on the DKAFO are formed to position the DKJs a comfortable distance from the knee. This feature is standard to all KAFOs and creates a bulge in the front profile of the brace that cannot be avoided. The relatively long DKJ created a longer than necessary bulge in the front profile of the brace that decreased its cosmetic appeal and increased its obstructive potential. The total length of the DKJ also subtracts from the length of the uprights. Sufficient upright length is required to reduce the shearing forces on the bolts connecting the upright to the thermoplastic shells. Sufficient upright length may therefore become an issue for smaller clients. Future efforts should be made to decrease the length of the entire DKJ. Unfortunately, the length of most components and their relative spacing with each other serve a functional purpose and were minimized in the design stage. Possible areas of optimization include the vertical distance between the top of the lower upright and the bottom of the hammer and the length of the brackets.

To make the DKJ design more discreet, the belt and belt recoil spring should remain fully housed between the side-plates of the device. Section 3.5.5.7 offers two possible design modifications for housing the belt and belt recoil spring between the side-plates.

6.4.1.7 Titanium Parts

Theoretical dynamic strength analysis of the hammer and brackets indicate infinite-life safety factors of 2.3 and 2.8, respectively. An ideal infinite-life safety factor of three is desired for all DKJ components. Future models may have the hammer and brackets machined from Ti-6Al-4V titanium alloy, which is approximately 67% heavier but nearly twice as strong as 7075-T651 aluminium.

Several manufacturing issues are associated with titanium alloys. Depending on metal market prices, Ti-6Al-4V titanium alloy can cost nine times more than 7075-T651 aluminium and is approximately three times more expensive to machine than aluminium. Due to the relatively poor machinability of titanium, tool bits can become worn relatively quickly and potentially lead to a decrease in machining tolerance in moderate-size production runs.

6.4.1.8 Upright Material

Conventional off-the-shelf uprights are manufactured for conventional fixed knee KAFOs and are intended to support the relatively small knee moments experienced by a constantly extended knee in gait. Unfortunately, the strongest off-the-shelf uprights do not provide a sufficient factor of safety for a 90 kg subject, loading the DKAFO with a flexed knee for a high number of cycles. Dynamic stress analysis of the 304-2B stainless steel- ¼ temper uprights installed on the DKJ indicated an infinite life safety factor of 1.6 (Section 3.5.4.2). Future models of the DKAFO may include uprights made of hardened stainless steel or Ti-6V-4Al titanium alloy. While the uprights must be sufficiently strong, they must also be ductile enough for orthotists to bend and form.

Stainless steel uprights constitute 26% of the DKAFO's weight (Section 3.4.7). Titanium is only 60% as dense as stainless steel, therefore, incorporating titanium uprights into future models of the DKAFO would reduce the total weight of the orthosis by approximately 0.355 kg or 16%. Unfortunately, titanium uprights will increase the total cost of the orthosis. Becker Orthopedic sells their 9001 E-Knee with a choice of custom aluminium, stainless steel, or titanium uprights.

6.4.1.9 Integrating Double-Stepped Pins

The single ended shoulder pins, which included the disc pin, hammer spring shoulder pin, and lower shoulder pin (Figure 3.2), were inadequate in maintaining a precise distance between the two side-plates. The non-stepped, press fit pin ends traveled out of position over the course of DKJ use and required excessive attention during DKJ assembly. Future embodiments of the DKJ should incorporate steps on both ends of all of the pins. Double-stepped pins will maintain a consistent distance between the side-plates.

6.4.1.10 Reduction of Power Consumption

The two solenoids currently installed in the DKAFO draw a combined current of 1.64 Amps at 8.6 volts. The solenoids are active throughout the swing phase of gait and therefore experience a duty cycle of approximately 40% during normal walking. The DKAFO must provide at least 16 hours of use between charges to be a truly practical device. A rechargeable 9 volt battery offering 10.5 Amp hours would therefore be required to power the DKAFO for an entire day. Batteries offering these specifications are too large and heavy to be incorporated into a practical DKAFO system. A more efficient electronic actuator is required.

A direct current micro-motor may be substituted into the DKJ design. The micro-motor could position a blocking element in the path of the hammer to selectively prevent hammer rotation. Direct current micro-motors draw approximately 10% of the power of conventional solenoids that offer equivalent mechanical force. A suitable micro-motor may also be smaller and lighter than the current solenoid.

6.4.1.11 Integrate Conventional Upright Fastening Methods

The uprights are currently press fit onto two pins on the DKJ. Future embodiments of the DKJ must incorporate a more conventional method of fastening if the device is to be sold as a commercial product. Many orthotists do not have the equipment to press the uprights onto the DKJ. In the orthotics field, uprights are most commonly riveted or bolted to the orthotic joint. An epoxy or thread-lock is typically used to fix the bolt in place.

6.4.1.12 Future Control System

The future control system will replace the current personal computer with a compact dedicated circuit and variable power source with a rechargeable battery pack, both of which may be attached to the upper DKAFO or clipped to the user's clothing. Sensor pressure thresholds will require periodic adjustment since the constant residual pressure applied to the FSRs by the user's footwear may change with varying shoe tightness. A button may be added to the control system to calibrate the threshold pressure levels of the FSRs. The button would only require the user to lift their braced foot off the ground when the button is activated in order to reset the zero levels of the FSRs. The control system logic may be developed to discern whether the user is standing or walking and deactivate the solenoid when the user is standing to avoid intermittent solenoid activation that may consume excessive power and generate unwanted noise.

6.4.2 Cyclic Load Testing of the DKJ

Once an adequate belt material has been developed, cyclic load testing of the DKJ must be performed to validate the cycle life of the device. A test set up similar to the one used in strength testing the DKJ (Section 4.2) could be employed to deliver a repeated DKJ flexion moment of 47 Nm, the equivalent peak moment plus one standard deviation applied by a 90 kg user in normal cadence. To satisfy a target life of three years the DKAFO would have to endure approximately three million cycles.

6.4.3 Future Clinical Testing

Following a reiteration of the DKJ design and miniaturization of the control system, a broader clinical study should be performed with a greater number of test subjects to allow for statistical analysis of DKAFO effectiveness. Participants should have DKAFO gait training and several weeks of practice before performing future gait analysis, to ensure that the subjects are comfortable working the DKAFO consistently and effectively. Kinetic and bilateral gait analysis may be performed to help distinguish which gait pattern changes are caused by the DKAFO and which gait pattern changes are related to the need for the user to create an extension moment of the knee in pre-swing.

Chapter 7. Conclusions

A new electro-mechanical dynamic orthotic knee joint was designed and developed and successfully provided knee flexion resistance in stance and allowed free knee motion in swing. The dynamic orthotic knee joint was thinner, lighter in weight, and projected to be less expensive than any orthotic knee joint offering similar function on the market. A further improvement over existing SCKAFO knee joint designs was that the new DKJ provided resistance to knee flexion in stance without rigidly locking the knee from flexion, thereby offering controlled shock-absorbing knee flexion during limb loading.

Mechanical testing revealed that the orthotic joint offered a sufficient holding moment to be safely tested clinically, in a controlled environment. The DKJ provided a sufficient holding moment to support a 90 kg DKAFO user in normal cadence with a safety factor of 1.3. However, to support a heavier user, provide knee support in stair ascent or obtain a greater DKJ safety factor, a greater maximum DKJ holding moment is required. The belt component exhibited excessive wear at the clamp site following a relatively low number of loading cycles in mechanical testing. The DKJ also experienced an excessive amount of flexion under loading in mechanical testing, indicating that the current DKJ would not offer enough knee flexion support during stance for all potential users. A superior belt material must be developed that is stronger, less elastic, and more wear resistant. Such a belt will increase the DKJ's holding moment, reduce flexion in loading, and increase the cycle life.

The DKJ flexion angle achieved under a given flexion moment changed with variations in the belt wrap tightness around the disc. A clip or mechanism must be added to maintain consistent belt tightness around the disc to in turn create a more consistent DKJ load response. Cyclic load testing must be performed on the DKJ to validate the cycle life of the device and the fatigue strength of the individual DKJ components once a stronger, more wear resistant, belt has been developed.

As desired, the DKAFO had minimal effect on the gait patterns of the able-bodied subjects in clinical testing. All three KAFO users achieved greater knee flexion when walking with the DKAFO compared to walking with their original KAFOs, especially during swing. As providing knee flexion during swing while supporting the limb during stance was the main objective of the new DKAFO, this is a very positive result. Two subjects achieved controlled knee flexion in stance when walking with the DKAFO, similar to the knee response seen in normal gait. One KAFO user showed considerably less circumduction of the braced leg in swing when walking with the DKAFO compared to walking with his original KAFO. Two KAFO users achieved more conventional pelvic obliquity patterns when walking with the DKAFO compared to walking with their original KAFOs. These results suggest that even with the limited amount of practice time subjects had walking with the DKAFO, the DKAFO encouraged a more normal gait pattern in some KAFO users compared to their prescribed KAFO. The DKAFO also successfully allowed knee extension in stance and prevented knee flexion at any knee angle. These functions were important design goals and will give the user the ability to walk uneven ground, climb steps and recover from a stumble.

Most test subjects had an insufficient amount of time to practice walking with the DKAFO and had difficulty disengaging the knee joint mechanism at the end of stance. All six test subjects found that the requirement to provide a knee extension moment in terminal stance demanded considerable mental concentration and alterations to their gait pattern. The efforts to control the DKAFO in walking lead to a substantial decrease in stride velocity and stride length for all six subjects. A greater amount of training time with the DKAFO would increase the user's ability to control the DKAFO and improve gait performance when walking with the DKAFO. All of the test participants found that the DKAFO structure was light and attractive and provided sufficient knee flexion support in stance. Two of the three KAFO users participating in the clinical study preferred the DKAFO to their original KAFO.

Future clinical studies on the DKAFO should include kinetic gait analysis to help distinguish which gait pattern changes are caused by the DKAFO and which gait pattern

changes are related to the need to create a knee extension moment in terminal stance. Future clinical studies should also allow participants considerably more time to practice with the DKAFO and involve a larger number of test participants so that statistical analysis may be used to analyze the effectiveness of the DKAFO.

Several improvements must be made to the DKJ design if a safe, reliable, commercially competitive DKAFO is to be realized. Notable design improvements include: weight reduction of the DKJ and optimization of the DKJ dimensions, improved power-consumption of the control system, miniaturization and further development of the control system, integration of conventional upright fastening methods and housing the belt, and belt recoil mechanism within the confines of the side-plates. Effectively addressing these design issues will produce a dynamic knee-ankle-foot orthosis that has the potential to give clients inflicted with lower limb weakness an improved level of mobility, security, confidence and health.

References

[1] United States Department of Health and Human Services, "Current estimates from the national health interview survey, 1992" Centers for Disease Control and Prevention, National Center for Health Statistics, Series 10, no. 189, Jan. 1996.

[2] "What is a KAFO?" Jan 30, 2005. Available: http://www.aodmobility.com/body_kafos.htm.

[3] A.G. McMillan, K.K. Kendrick, J.W. Michael, J. Aronson and G.W. Horton, "Preliminary evidence for effectiveness of a stance control orthosis," *Journal of Prosthetics and Orthotics*, vol. 16, no. 1, pp. 6-13, January 2004.

[4] R. Waters, J. Campbell, L. Thomas, L. Hugos and P. Davis, "Energy cost of walking in lower extremity plaster casts," *Journal of Bone Joint Surgery*, vol. 64, pp. 896-899, 1982.

[5] J. Perry, *Gait Analysis – Normal and Pathological Function*. New York: McGraw-Hill, 1992.

[6] J. Rose and J. Gamble, *Human Walking*. Baltimore: Williams & Wilkins, 1994.

[7] D. Winter, *The Biomechanics and Motor Control of Human Gait: Normal, Elderly and Pathological*. Waterloo: University of Waterloo Press, 1991.

[8] P. Bowker, D.N. Condie, D.L. Bader and D.J. Pratt, *Biomechanical Basis of Orthotic Management.* Oxford: Butterwoth Heinemann, 1993.

[9] R. Riener, M. Rabuffetti and C. Frigo, "Stair ascent and descent at different inclinations," *Gait and Posture*, vol.15, pp. 32-44, 2002.

[10] T.P. Andriacchi, G.B. Anderson, R.W. Fermier, D. Stern and J.O. Galante, "A study of lower limb mechanics during stair-climbing," *Journal of Bone Joint Surgery*, vol. 62A, pp. 749-757, 1980.

[11] G.D. Marovich, P.O. Riley, D.E. Krebs, R.W. Mann and W.A. Hodge, "Biomechanical analysis of knee motion upon stair ascent and descent," *ABS 13th Vermont*, pp. 116-117, August 1989.

[12] P.A. Costigan, K.J. Deluzio and U.P. Wyss, "Knee and hip kinetics during normal stair climbing" *Gait and Posture*, vol.16, pp. 31-37, 2002.

[13] T.J. Supan and C.F. Hovorka, "A review of thermoplastic ankle foot orthoses adjustments/replacements in young cerebral palsy and spina bifida patients," *Journal of Prosthetics and Orthotics*, vol. 7, no. 1, pp.15-22, 1995.

[14] "Hodgson Orthotics, Prosthetics & Sports Medicine," February 2, 2005. Available: http://www.hodgsonorthotics.com/foot.htm.

[15] P.L. Allard, M. Duhaime, P.S. Thiry and G. Drown, "Use of gait stimulation in the evaluation of a spring-loaded knee joint orthosis for Duchene muscular dystrophy patients," *Medical & Biological Engineering & Computing*, vol.19, pp. 165-170, 1981.

[16] K.R. Kaufman, S.E. Irby, J. Mathewson, R.W. Wirta and D.H. Sutherland, "Energy-efficient knee-ankle foot orthosis: A case study," *Journal of Prosthetics and Orthotics*, vol.8, no.3, pp. 79, 1996.

[17] J.W. Michael, "Prosthetic primer: prosthetic knees," *inMotion Magazine*, vol.9, no.6, November/December 1999.

[18] J. F. Lehmann and J. B. Stonebridge, "Knee lock device for knee ankle orthoses for spinal cord injured patients: an evaluation," *Archives of Physical Medicine and Rehabilitation*, vol. 59, pp. 207-211, 1978.

[19] M.L. Jerrell, "Stance control orthoses: revolutionizing patient care," *O&P Business News*, vol. 12, no. 19, pp. 24-32, October 2003.

[20] A. Harris. "Automatically releasing knee brace," U.S. Patent 4632096, 1986.

[21] S.E. Irby, K.R. Kaufman and D.H. Sutherland, "Electronically controlled long leg brace," *Southern Biomedical Engineering Conference,* 1996, pp.427-430.

[22] R. Harrison, E. Lemaire, Y. Jeffreys and L. Goudreau, "Design and pilot testing of an orthotic stance-phase control knee joint," *Orthopadie-Technik, English edition III*, 2001.

[23] D.D. Raftopoulos, C.W. Armstrong, L. Poulos and T. Spyropoulos, "A novel design of a knee-ankle-foot orthosis and its evaluation," *Advances in Bioengineering Conference*, 1986, pp.128-129.

[24] B.C. Weddendorf, "Automatic locking orthotic knee device," U.S. Patent 5267950, 1993.

[25] Y. Tokuhara, O. Kameyama, T. Kubota, M. Matsuura and R. Ogawa, "Biomechanical study of gait using an intelligent brace," *Journal of Orthopaedic Science*, vol. 5, pp. 342-348, 2000.

[26] W.N. Myers, M.D. Shadoan, J.C. Forbes, K.J. Baker and D.C. Rice, "Selectively lockable knee brace," U.S. Patent 5490831, 1996.

[27] "Releasable conical roller-clutch for knee brace," MFS-31258, NASA Tech Briefs, pp. 56, December 2002.

[28] W.N. Myers, "Releasable roller clutch," U.S. Patent 6135255, 2000.

[29] J. Kofman, P. Allard, M. Duhaime, H. Labelle and M. Vanasse, "A functional knee-ankle orthosis for Duchenne Muscular Dystrophy patients using a spring-loaded knee joint mechanism," *Orthopadie-Technik*, vol.36, pp. 403-407, 1985.

[30] N.G.A. Van Leerdam, "The swinging UTX orthosis, biomedical fundamentals and conceptual design," Ph.D. thesis, University of Twente, Enschede, The Netherlands, 1993.

[31] E.D. Lemaire, The Rehabilitation Centre, Ottawa, ON, Canada, private communication, June 2003.

[32] B.J. Hatton, D.L. Hatton and Z.G. Wallace, "Articulating knee supports," U.S. Patent Application Publication #US 2002/0169402 A1, 2002.

[33] J. Michael. "Horton's Stance Control Orthosis: self-locking joint," John Michael's Corner, November 15, 2000. Available: http://www.oandp.com/news/jmcorner/2000-11/6.asp.

[34] J. Michael, "Short report from AOPA Meeting in Chicago," John Michael's Corner, November 9, 2002. Available: http://www.oandp.com/news/jmcorner/2002-11/3.asp.

[35] "Fillaur Swing Phase Lock Manual," Fillauer Website, August 27, 2004. Available: http://www.fillauer.com/products/SPL/.

[36] N. Sclater, *Mechanisms and Mechanical Devices Sourcebook.* New York: McGraw-Hill, 2001.

[37] D. McCormack, "Prosthetic knee designs: biomechanics and functional classification," *Irish Journal of Orthopaedic Surgery and Trauma*, vol. 2, no. 1, 1997.

[38] J. Otto, "Prosthetic knees: what's on the way?" *The O&P Edge*, October 2003.

[39] H. Wagner and M. Krukenberg, "Brake-action knee joint," U.S. Patent 5704945, 1998.

[40] S. Blumentritt, H.W. Scherer, J.W. Michael and T. Schmaiz, "Transfemoral amputees walking on a rotary hydraulic prosthetic knee mechanism: a preliminary report," *Journal of Prosthetics and Orthotics*, vol.10, no.3, pp. 61-70, 1998.

[41] G. Totten, *Handbook of Hydraulic Fluid Technology*. New York: Marcel Dekker Inc., 1999.

[42] W.C. Orthwein, *Clutches and Brakes – Design and Selection*. New York: Marcel Dekker Inc., 1986.

[43] B. Hamrock, B. Jacobson and S. Schmid, *Fundamentals of Machine Elements*. New York: McGraw-Hill, 1999.

[44] U. Hindhede, *Machine Design Fundamentals – A Practical Approach*. New York: John Wiley and Sons, 1983.

[45] D. Edwards, "Controlled coupling hydra-matic fundamentals," April 4, 2003. Available: http://www.autotran.us/jhmCpg89.htm.

[46] J. M. Vranish, "Three-dimensional roller locking sprags," U.S. Patent 5482144, 1996.

[47] J.B. Pittman, "Anti-reverse actuator mechanism," U.S. Patent 4408728, 1983.

[48] K.Kampf and H.Geisthoff, "Pawl freewheel clutch," U.S. Patent 5054594, 1991.

[49] Y. Hitomi, "Anti-reverse structure for a spinning reel," U.S. Patent 5350132, 1994.

[50] S. J. McCormick, "Hoist load brake," U.S. Patent 5141085, 1992.

[51] K.H. Hirano, E. Shinohara and T. Higashimoto, "Reversal Preventative Device," U.S. Patent 5494232, 1996.

[52] H.L. Neufeld, "Selective anti-reverse mechanism," U.S. Patent 4323203, 1982.

[53] L.G. Hlava, "Easily assembled anti-reverse actuator," U.S. Patent 4735376, 1988.

[54] R.B. Klamer, "Roller skate having three control modes," U.S. Patent 4932676, 1990.

[55] C.A. Cederblad, "Clutched winch," U.S. Patent 4234166, 1980.

[56] O.E. Lohman, "Brake device for a cycle," U.S. Patent 4638890, 1987.

[57] H.O. Henze, "Anti reverse mechanism for fishing reels," U.S. Patent 3974978, 1976.

[58] W.O. Nelson, "Automatic variable speed bicycle transmission," U.S. Patent 3388617, 1962.

[59] J.M. Vranish, "Electromagnetic brake/clutch device," U.S. Patent 5275261, 1994.

[60] J.S. Baer, "Helical spring clutch," U.S. Patent 3966024, 1976.

[61] F.E. Lederman, "Shiftable roller clutch," U.S. Patent 5152726, 1992.

[62] J.E. Cilley, "Reverse motion brake mechanism," U.S. Patent 2709506, 1955.

[63] T.N. Brammall, "Conical cable lock," U.S. Patent 4681356, 1987.

[64] P.L. Allard and J.R. Sibille, "Knee joint orthosis," U.S. Patent 4456003, 1984.

[65] J. Glancy, "Elastic materials as a source of external power in orthotics – a preliminary report," *Orthotics and Prosthetics*, vol. 30, no. 1, pp. 13-21, 1976.

[66] T. Harris, "How seat belts work", HowStuffWorks.com, April 24, 2003. Available: http://auto.howstuffworks.com/seatbelt.htm.

[67] D.J. Cunningham, "Clamping means for a strap," U.S. Patent 4838388, 1989.

[68] D.A. McKernon and D.J. Cunningham, "Clamping means for a strap," U.S. Patent 4718148, 1988.

[69] H-H. Ernst, "Deflection clamping device," U.S. Patent 4854644, 1989.

[70] G.F. Lewis, "Belt locking device with electrical energizing means," U.S. Patent 353001, 1967.

[71] C.C. Irwin, D.F. Manz and J.T. Auman, "Linear locking seat belt retractor," U.S. Patent 4838388, 1989.

[72] A.G. Smithson, "Retractor locking mechanism," U.S. Patent 6155513, 2000.

[73] J. Takada, "Device for preventing a belt from being pulled from a retractor," U.S. Patent 4185791, 1980.

[74] J. Takada, "Seatbelt clamp," U.S. Patent 4552407, 1985.

[75] G. R. Kutti, "Belt clamping guide loop," U.S. Patent 4549770, 1985.

[76] C.A. Collins, "Seat belt system with locking guide loop assembly," U.S. Patent 5411292, 1995.

[77] P.O. Weman, "Vehicle occupant restraint system," U.S. Patent 3847434, 1974.

[78] D.A. Pickett, "Belt clamping apparatus with self-aligning feature," U.S. Patent 4310175, 1982.

[79] H.D. Adomeit, "Safety belt clamping device," U.S. Patent RE30707, 1981.

[80] S.E. Irby, K.R. Kaufman, R.W. Wirta and D.H. Sutherland, "Optimization and application of a wrap-spring clutch to a dynamic knee-ankle-foot orthosis," *IEEE Transactions on Rehabilitation Engineering*, vol.7, no.2, pp. 130-134, 1999.

[81] D.G. Ullman, *The Mechanical Design Process*. 2nd Edition, New York: McGraw-Hill, 1997.

[82] D. Popovic and L. Schwirtlich, "Design and evaluation of the self-fitting modular orthosis (SFMO)", *IEEE Transactions on Rehabilitation Engineering*, vol.1, no.3, pp. 165-173, 1993.

[83] K. Cerny, J. Perry and J.M. Walker, "Effect of an unrestricted knee-ankle-foot orthosis on the stance phase of gait in healthy persons," *Orthopedics*, vol. 13, no. 10, pp. 1121-1127, 1990.

[84] R.L. Norton, *Machine Design – An Integrated Approach*. 2nd Edition, New Jersey: Prentice-Hall, 2000.

[85] J.E. Shigley and C.R. Mischke, *Mechanical Engineering Design*. 6th Edition, New York: McGraw Hill, 2001.

[86] R.E. Peterson, *Stress Concentration Factors*. New York: John Wiley & Sons, 1974.

[87] E. Oberg, F.D. Jones, H.L. Horton and H.H. Ryffel, *Machinery's Handbook*. 27th Edition, New York: Industria Press Inc, 2004.

[88] ASTM *Standard Test Methods for Rubber (Elastomeric) Belting, Flat Type*, ASTM Standard D378-00, 2000.

[89] Medical Research Council of the UK, "Aids to the investigation of peripheral nerve injuries," Memorandum No. 45: London: Pendragon House, pp. 6-7, 1976.

[90] S.B. Michaud, S.A. Gard and D.S. Childress, "A preliminary investigation of pelvic obliquity patterns during gait in persons with transtibial and transfemoral amputation," *Journal of Rehabilitation Research*, vol. 37, no. 1, pp 1–10, January/February 2000.

Appendix A – Early Design Concepts

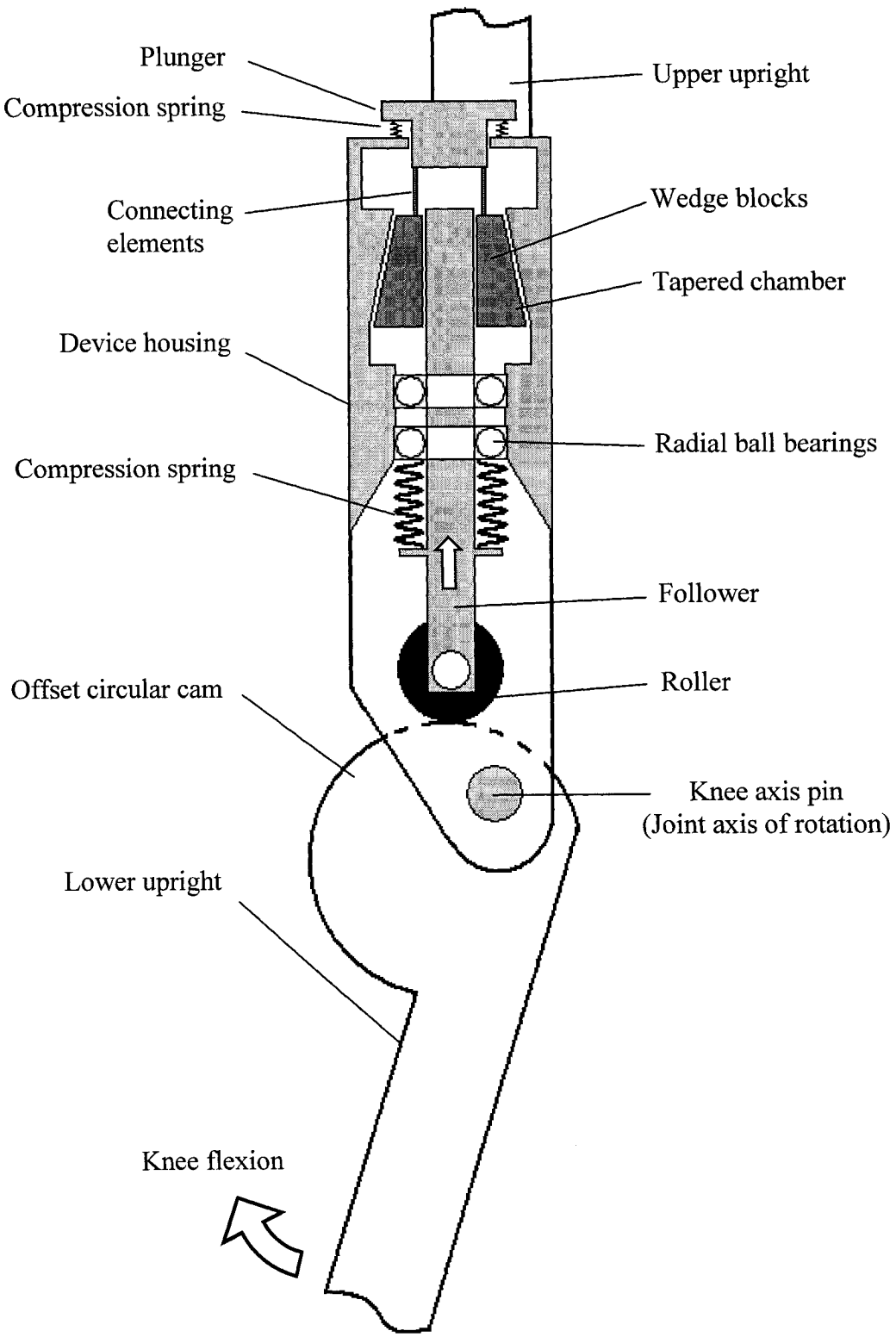

Figure A.1 – The Cam and Follower joint design.

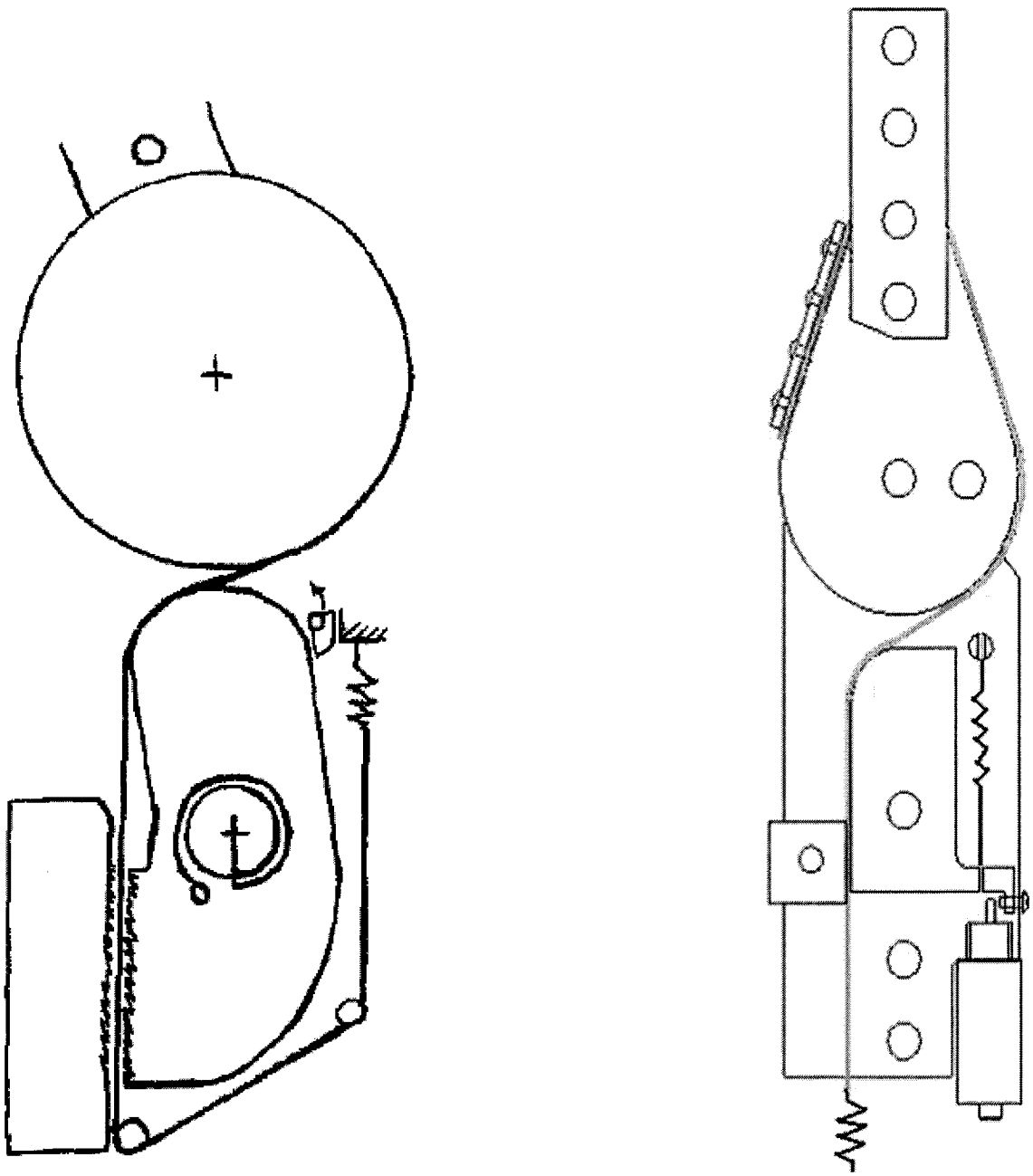

(a) (b)

Figure A.2 – (a) Original conceptual sketch of the Dynamic Knee Joint; (b) a drawing of an intermediate embodiment of the Dynamic Knee Joint.

Appendix B - Bill of Materials

Table B.1 – Bill of Materials.

Item	Part #	Qty	Material	Source	Details
Disc	G1	1	7075 Aluminium	Custom machined	¼" plate
Bracket	G2	1	7075 Aluminium	Custom machined	¼" plate
Hammer	G3	1	7075 Aluminium	Custom machined	¼" plate
Anvil	G4	1	7075 Aluminium	Custom machined	¼" plate
Left side-plate	G5	1	7075 Aluminium	Custom machined	¼" plate
Right side-plate	G6	1	7075 Aluminium	Custom machined	¼" plate
Recoil spring bracket	G7	2	7075 Aluminium	Custom machined	¼" plate
Belt	K1	1	Neoprene, Polyester	Megadyne	Part# T-155
Solenoid	C1	1	---	Saia Burgess	Push-type Ledex tubular solenoid Part # 195203-231
Solenoid plunger	C2	1	Nickel plated 12L14 steel	Saia Burgess	Included with solenoid
Solenoid bracket	C3	1	Steel	Custom machined	1/16" plate or thinner
Solenoid nut	C4	1	Brass	Saia Burgess	0.3750-32 UNEF 2.3mm thick
Solenoid collar	C5	1	Aluminum	Custom machined	Accommodates UNC 4-40 set screw
Disc pin	P1	1	17-4PH Stainless	Custom machined	5/16" bar; accommodates UNC 4-40 screw
Hammer pin	P2	1	17-4PH Stainless	Custom machined	5/16" bar
Anvil pin	P3	1	17-4PH Stainless	Custom machined	1/4" bar
Anvil stop pin	P4	1	17-4PH Stainless	Custom machined	3/16" bar; hole at midpoint
Bumper pin	P5	1	17-4PH Stainless	Custom machined	3/16" bar; hole at midpoint
Solenoid trim pin	P6	1	17-4PH Stainless	Custom machined	3/16" bar; hole at midpoint
Lower peg	P7	1	17-4PH Stainless	Custom machined	1/4" bar
Hammer spring shoulder pin	P8	1	17-4PH Stainless	Custom machined	5/16" bar; accommodates UNC 4-40 screw; UNC 4-40 screw hole through midpoint
Upper peg	P9	4	17-4PH Stainless	Custom machined	1/4" bar
Shoulder pin	P10	1	17-4PH Stainless	Custom machined	5/16" bar; accommodates UNC 4-40 screw
Extension stop pin	P11	1	17-4PH Stainless	Custom machined	1/4" bar
Face screw	S1	3	Steel	Off the shelf	UNC 4-40, ¼" long, pan head
Clamping screws	S2	3	Steel	Off the shelf	UNC 4-40, 3/8" long, pan head
Solenoid trim screw	S3	1	Steel	Off the shelf	UNC 4-40, 3/8" long, set screw
Goose-head trim screw	S4	1	Steel	Off the shelf	UNC 4-40, 1/2" long, pan head
Hammer stop screw	S5	1	Steel	Off the shelf	UNC 4-40, 1/16" long, set screw

Table B.1 – Continued.

Item	Part #	Qty	Material	Source	Details
Anvil-stop trim screw	S6	1	Steel	Off the shelf	UNC 4-40, 3/8" long, set screw
Bumper trim screw	S7	1	Steel	Off the shelf	UNC 4-40, 3/8" long, set screw
Upper hammer spring screw	S8	1	Steel	Off the shelf	UNC 4-40, 1/2" long, pan head
Lower hammer spring screw	S9	1	Steel	Off the shelf	UNC 4-40, 1/4" long, pan head
Solenoid Plunger screw	S10	1	Steel	Off the shelf	UNC 6-32, 1 ¼", pan head
Spring bracket screw	S11	2	Steel	Off the shelf	UNC 4-40, 3/8" long, pan head
Clamping bar	W1	1	Steel	Custom machined	1/16" plate with UNC 4-40 clearance holes
Face washer	W2	1	Steel	Off the shelf	UNC 6-32 washer
Solenoid washer	W3	1	Steel	Off the shelf	UNC 6-32 washer
Hammer spring	T1	1	Steel	Century Spring Corp.	Part # C-13, utility extension spring
Solenoid recoil spring	T2	1	Steel	Century Spring Corp.	Part # C-668, utility extension spring; 9.525mm x 38.1mm x 50.8mm
Belt recoil spring	T3	1	Steel	Century Spring Corp.	Part # C-13, utility extension spring; 6.35mm x 63.5mm x 0.508mm
Bumper	T4	1	Rubber	Off the shelf	5mm rubber grommet
Disc bushing	B1	1	Composite	GGB North America	Part # 0806DU
Hammer bushing	B2	1	Composite	GGB North America	Part # 0806DU
Upper upright	U1	1	304-2B Stainless, ¼ Temper	Becker Orthopaedic	3/4" x 3/16", Part #1001-A6S #7
Lower upright	U2	1	304-2B Stainless, ¼ Temper	Becker Orthopaedic	3/4" x 3/16", Part #1001-A6S #8

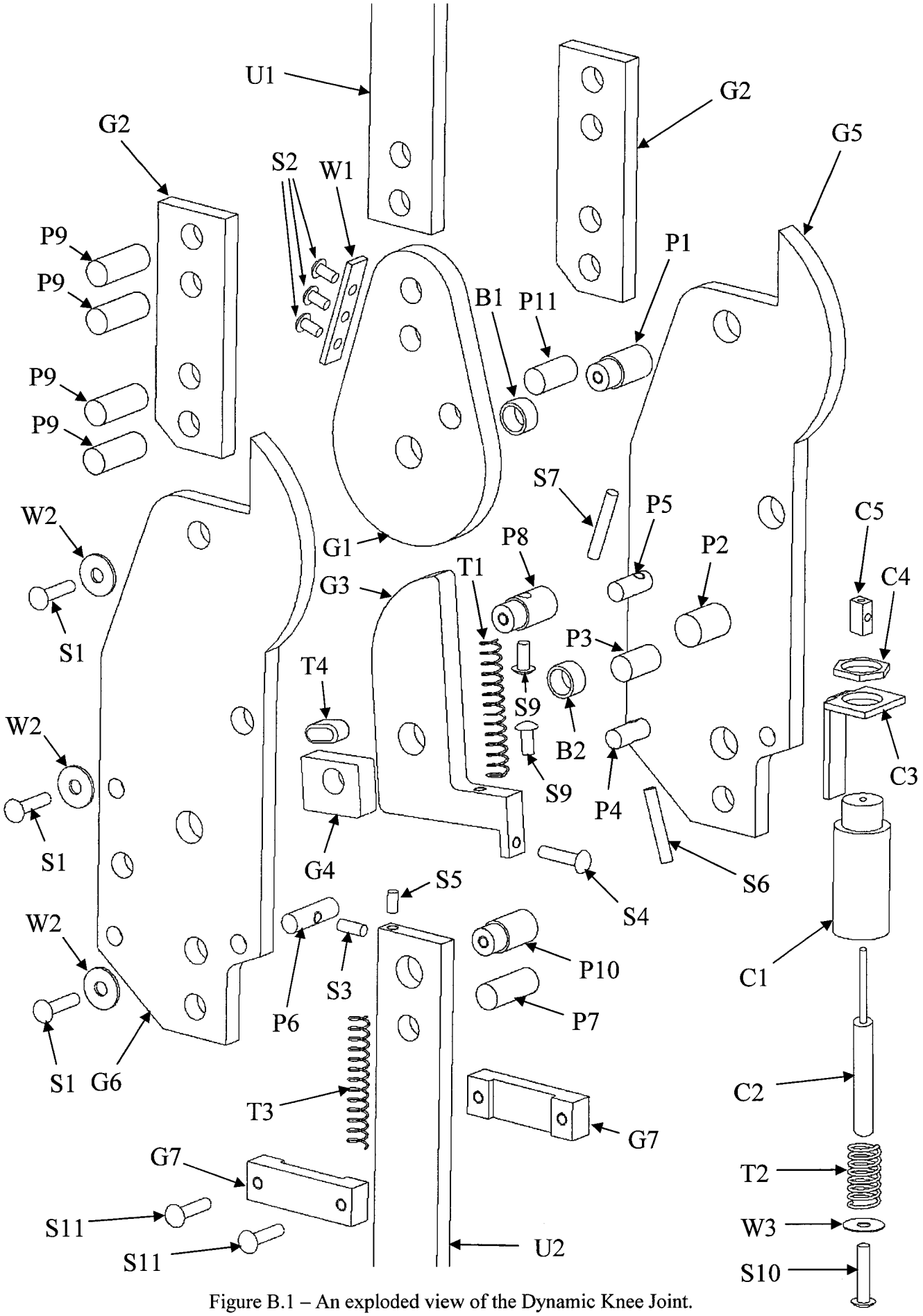

Figure B.1 – An exploded view of the Dynamic Knee Joint.

Appendix C – Dimensions and Stress Analysis Results

Table C.1 – Important DKJ dimensions.

Symbol	Description	Value
H_1	y-distance between point D and the hammer axis of rotation	31.3 mm
H_2	y-distance from force Fc and the hammer axis of rotation	12.4 mm
H_3	x-distance from point D and the hammer axis of rotation	6.5 mm
H_4	Half hammer width	11 mm
H_5	Hammer width	22 mm
H_6	Distance from the top of the anvil to the hammer axis of rotation	41.6 mm
H_7	Distance from bottom of the anvil to the hammer axis of rotation	19.4 mm
R_1	Distance between disc axis of rotation and the midline of the outer belt	27.5 mm
R_2	Radius of curvature of the upper hammer	25 mm
Ω	Angle of the clamped hammer with the y-axis	4°
θ	Angle of belt contact with hammer radius R_2	70°
μ	Coefficient of friction of T-155 belt (smooth side) with milled aluminium	0.84
ϕ	Angle between y-axis and the tangent of the belt at point C on the hammer	70°
γ	Angle between y-axis and the tangent of the belt at point D on the hammer	35°

Table C.2 – Peak forces and moments (90 kg user in stair ascent).

Symbol	Description	Value
M_{Kmax}	Maximum flexion moment applied to a single DKJ for a 90 kg user in stair ascent	77 Nm
T_{BC}	Belt tension in belt section *BC*	2800 N
T_{BCx}	Belt tension in belt section *BC* (*x*-component)	2630 N
T_{BCy}	Belt tension in belt section *BC* (*y*-component)	958 N
T_{EF}	Belt tension in belt section *EF*	1000 N
T_{EFx}	Belt tension in belt section *EF* (*x*-component)	0 N
T_{EFy}	Belt tension in belt section *EF* (*y*-component)	1000 N
F_{fx}	Belt friction force on hammer (*x*-component)	1030 N
F_{fy}	Belt friction force on hammer (*y*-component)	1470 N
F_{Dx}	Total force applied by belt on hammer (*x*-component)	1600 N
F_{Dy}	Total force applied by belt on hammer (*y*-component)	1520 N
F_{D}	Total force applied by belt on hammer	2210 N
F_{G}	Friction force between belt and hammer/anvil at clamping site	500 N
F_{C}	Clamping force at point *G*	3250 N
μ_{req}	Required coefficient of friction	0.19

Table C.3 – Peak pin stresses (90 kg user in stair ascent).

Symbol	Description	Stress (MPa)	Safety Factor
Hammer pin			
τ_s	Hammer pin shear stress	54.5	4.7
σ_b	Hammer pin bearing stress	111.5	4.5
σ_d	Hammer pin bending stress	56.3	9.1
τ_t	Tearout stress in hammer	62.9	4.0
Anvil pin			
τ_s	Anvil pin shear stress	58.4	4.4
σ_b	Anvil pin bearing stress	95.5	5.3
σ_d	Anvil pin bending stress	75.3	6.8
τ_{t1}	Tearout stress in anvil	51.2	4.9
τ_{t2}	Tearout stress in side-plate from anvil pin	46.7	5.4
Disc pin			
τ_s	Disc pin shear stress	56.8	4.5
σ_b	Disc pin bearing stress	45.3	8.5
σ_d	Disc pin bending stress	58.6	8.8
Upper bracket pins			
τ_s	Bracket pin shear stress	71.7	3.6
σ_b	Bracket pin bearing stress with upright	158.9	3.3
σ_d	Bracket pin bending stress	92.5	5.6
τ_{t1}	Tearout stress in upright from bracket pin	79.5	3.25
τ_{t2}	Tearout stress in bracket from upper bracket pin	35.8	7.0
Lower bracket pins			
τ_s	Bracket pin shear stress	86.7	3.0
σ_b	Bracket pin bearing stress with disc	141.9	3.5
σ_d	Bracket pin bending stress	111.9	4.6
τ_{t1}	Tearout stress in disc from bracket pin	81.1	3.1
τ_{t2}	Tearout stress in disc from lower bracket pin	43.2	5.8

Table C.4 – Peak bending stresses (90 kg user in stair ascent).

Symbol	Description	Stress (MPa)	Safety Factor
σ_{dh1}	Hammer compressive stress	162.6	3.1
σ_{dh2}	Hammer tensile stress	109.7	4.4
σ_{ds}	Side-plate tensile stress in bending	102.3	4.9
σ_{db}	Bracket tensile stress in bending	99.4	5.1
σ_{du}	Upright tensile stress in bending	203.2	2.5

Table C.5 – Peak bearing stresses (90 kg user in stair ascent).

Symbol	Description	Stress (MPa)	Safety Factor
$\sigma_{a/h}$	Anvil-hammer bearing stress	60.7	8.3
$\sigma_{b/h}$	Belt-hammer clamping stress	11.8	42.5

Table C.6 - Infinite Life Safety Factors (90 kg user in normal cadence).

Description	Infinite Life Safety Factor, n_∞
Hammer tensile stress in bending	2.3
Side-plate bending	2.6
Bracket bending	2.8
Upright bending	1.6
Lower bracket pin bending stress (highest pin stress)	3.9

Table C.7 – Cycle life of highest stressed components (90 kg user in normal cadence).

Description	Cycle Life, N (cycles)
Hammer tensile stress in bending	4.8×10^{8}
Side-plate bending	1.6×10^{9}
Bracket bending	8.7×10^{7}
Upright bending	7.7×10^{12}
Lower bracket pin bending stress (highest pin stress)	7.6×10^{12}

Appendix D - Investigated Belt Material

Table D.1 – Investigated belt manufacturers and distributors.

Manufacturer/Supplier	Contact	Product
Bally Ribbon	www.ballyribbon.com	12,000 webbing materials
Majestic Webbing Industry Company Limited	www.majestic-webbing.com.tw	Various webbing
Narricot Industries	www.narricot.com	Woven narrow fabrics
Polycam India	www.indiamart.com/diplast/	Manufacturer and supplier of narrow fabrics & polypropylene yarns
National Webbing Products Company	www.nationalwebbing.com	Manufacturer of commercial and military specification web belts
Brecoflex	www.brecoflex.com	Heavy duty timing and drive belts
Chiorino	www.chiorino.co.uk	High performance flat belting
Mectrol Corporation	www.mectrol.com	Reinforced urethane belts
Belt Technologies	www.belttechnologies.com	Stainless steel belts
Tandem Products	www.tandemproducts.com	Polyurethane belts
Otis Canada Steel	www.otis.com	Steel reinforced polyurethane belts
Twaron	www.twaron.com	Twaron Aramid fibre
VIS US	www.visusa.com	High strength nylon belts
Roulunds	www.roulunds.com	Power transmission belts
KKRubber	www.kkrubber.com	Rubber belting
YKK Tapecraft	www.tapecraft.com	Webbing
Habasit	www.habasitusa.com	Power transmission/conveyor belts
Biscor	www.biscor.com	PTFE & silicone rubber belts
Megadyne America	www.megadyne.it	Power transmission/conveyor belts
Durabelt	www.durabelt.com	Power transmission/conveyor belts
Jason Industrial	www.jasonindustrial.com	Power transmission belts
Conitech	www.conitech-usa.com	Drive belts and components
SPD/SI	www.sdp-si.com	Timing belts
NSW Plastics	www.nswplastics.com	Kevlar® and steel reinforced
Scandura Conveyor Belting	www.scandura.net	Conveyer belting
Ammeraal Beltech	www.ammeraal-beltechusa.com	Conveyer belting
TSE Industries Inc.	www.tse-industries.com	Conveyer belting and components
Belting Industries Inc.	www.beltingindustries.com	Woven endless belts
Belt Corporation of America	www.beltcorp.com	Timing belts, endless belts
Bekaert	www.bekaert.com	Steel reinforcing threads
Paragear	www.paragear.com	Parachute webbing thread
Anatech	(703)-941-8860	Belt coating services
Avanti	www.avanti-conveyors.co.uk	Conveyer belting
Tension Technology International	www.tensiontech.com	Consulting, design and engineering services in ropes, cables and textiles
Dupont	www.dupont.com	Kevlar® aramid fibre
Zylon Corporation	www.zylon.com	Zylon®
Honeywell	www.performancefibers.com	Securus fiber webbing
Mulco	www.mulco.de	Power transmission belts
Webbing and Tapes	www.webbing.co.nz	Polypropylene Webbing
Toyobo	toyobo.co.jp/e/seihin/kc/pbo/menu/fra_menu_en.htm	Zylon® Developer

Appendix E - Failure Mode Analysis

Table E.1 – Failure mode analysis.

Event	Result	Consequence
Belt breaks	DKJ will not resist flexion	User may collapse
Belt-disc connection fails	DKJ will not resist flexion	User may collapse
Belt-recoil spring connection fails	Belt will slacken above clamp site and DKJ may not resist flexion	Possibility of an excessive amount of free-fall knee flexion before the DKJ engages
Belt permanently deforms from clamping	Belt recoil spring may not be able to pull warped portion of belt through hammer-anvil gap. Belt slack may develop above clamp site	Possibility of an excessive amount of free-fall knee flexion before the DKJ engages
Belt wears significantly from clamping/rubbing	Reduction of the coefficient of friction of the belt leading to belt slip in the clamp	Increased knee flexion under loading
Hammer yields plastically	Clamping force is reduced allowing the belt to slip at the clamp site	May lead to insufficient knee flexion resistance
Solenoid fails to engage hammer	Knee unable to flex in swing	User may stumble
Solenoid fails to disengage hammer	Hammer cannot clamp onto belt; no flexion resistance	User may collapse
Solenoid engages hammer at wrong time	Hammer cannot clamp onto belt; no flexion resistance	User may collapse
Belt recoil spring fails to collect belt	Slack develops in belt	Possibility of an excessive amount of free fall knee flexion before the DKJ engages
Hammer spring fails	Hammer-anvil gap may not open sufficiently to allow belt travel; belt may slacken above clamp site	Possibility of an excessive amount of free-fall knee flexion before the DKJ engages
Debris enters device between hammer-belt-anvil components	Hammer may not effectively clamp onto belt leading to some belt slip in the clamp	Depending on the degree of belt slip, consequences could range from excessive knee flexion in stance to no knee flexion support in stance

Appendix F – Kinematic Gait Analysis Data

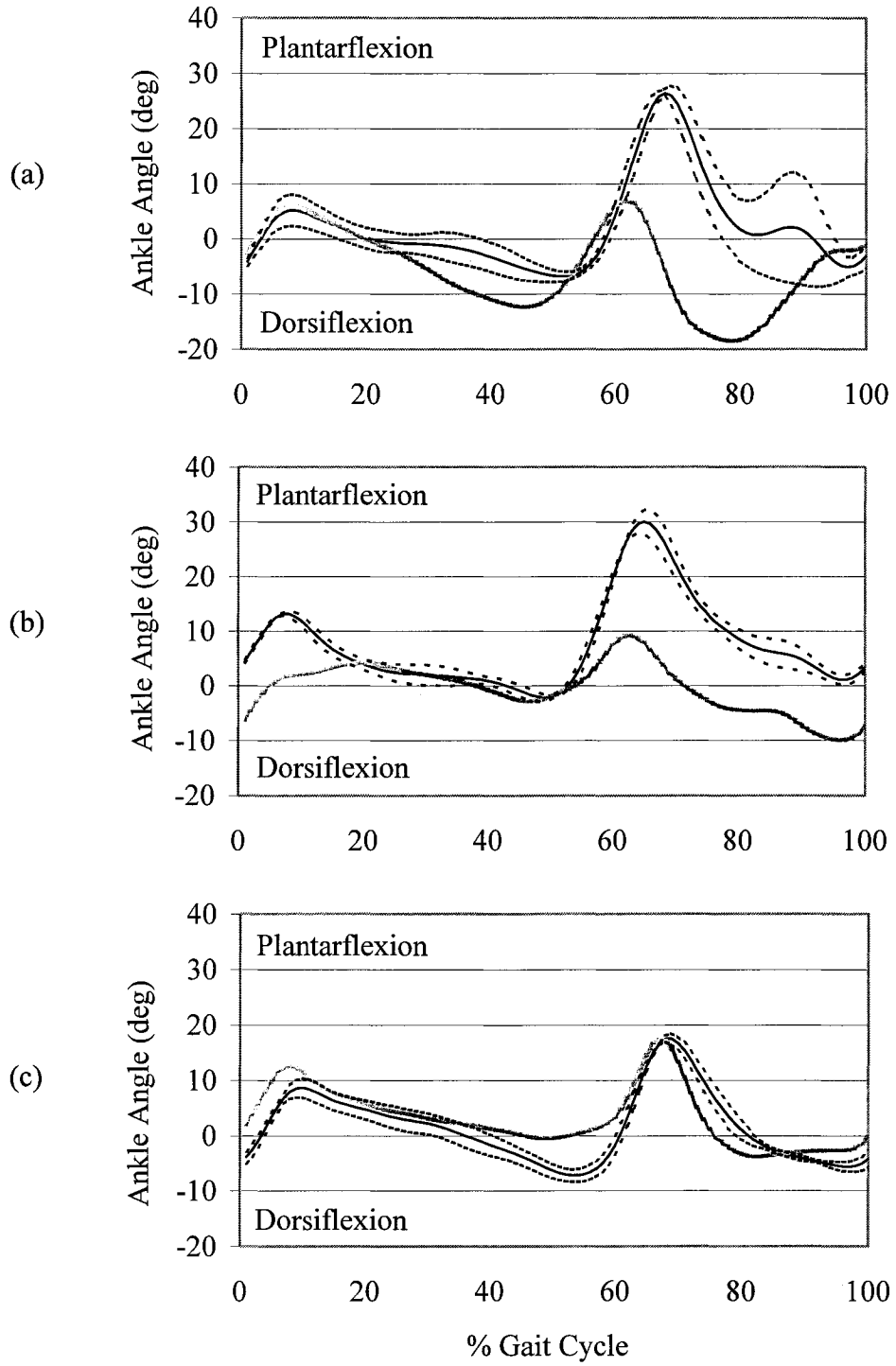

Figure F.1 - Graphs of the ankle angle over three walking trials, over the course of one stride for (a) subject A1, (b) subject A2, and (c) subject A3 while walking with no brace (solid black line) and walking with the DKAFO (solid gray line). The dashed lines represent one standard deviation either side of the mean for the no-brace condition.

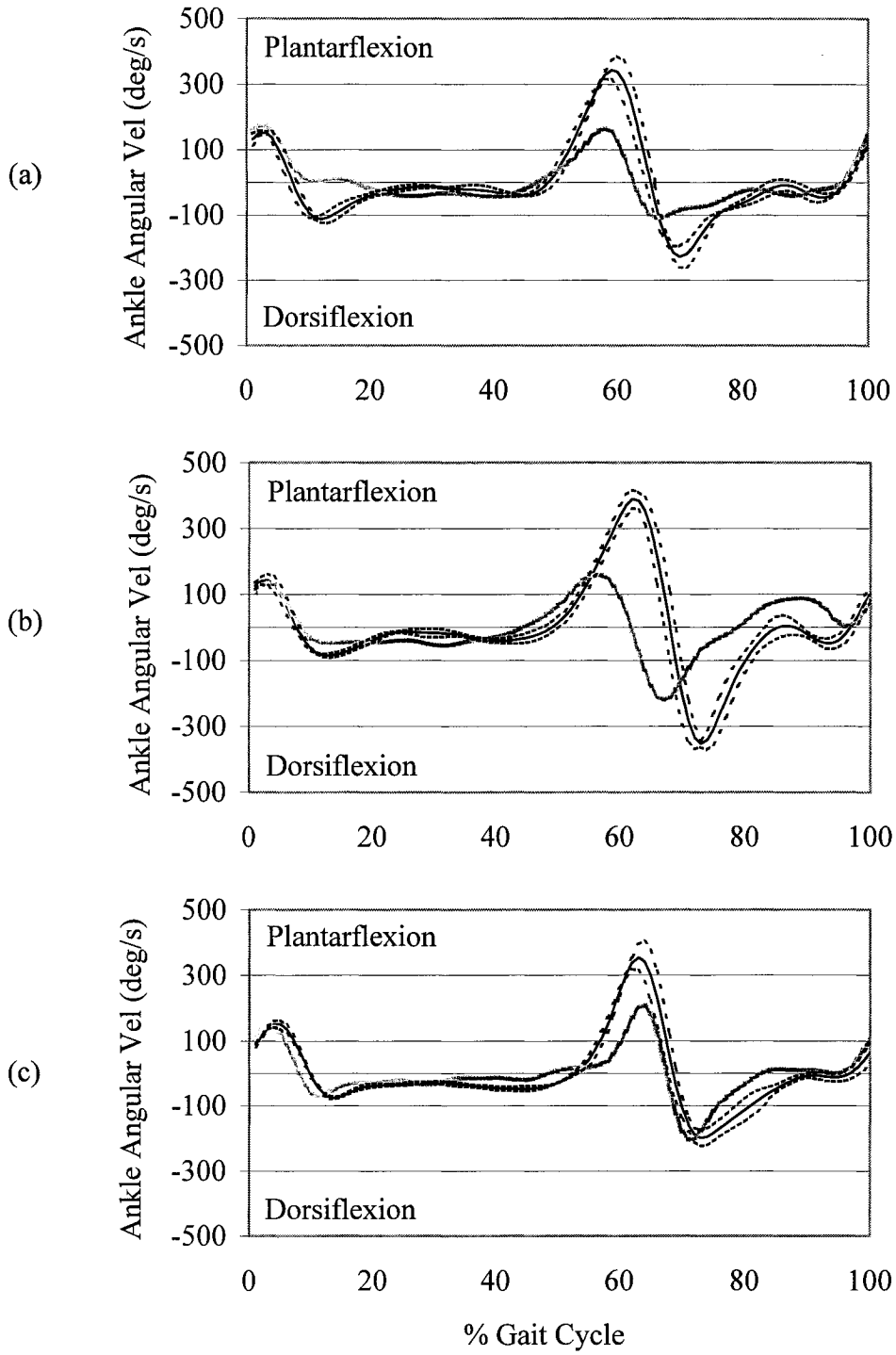

Figure F.2 - Graphs of the ankle angle velocity over three walking trials, over the course of one stride for (a) subject A1, (b) subject A2, and (c) subject A3 while walking with no brace (solid black line) and walking with the DKAFO (solid gray line). The dashed lines represent one standard deviation either side of the mean for the no-brace condition.

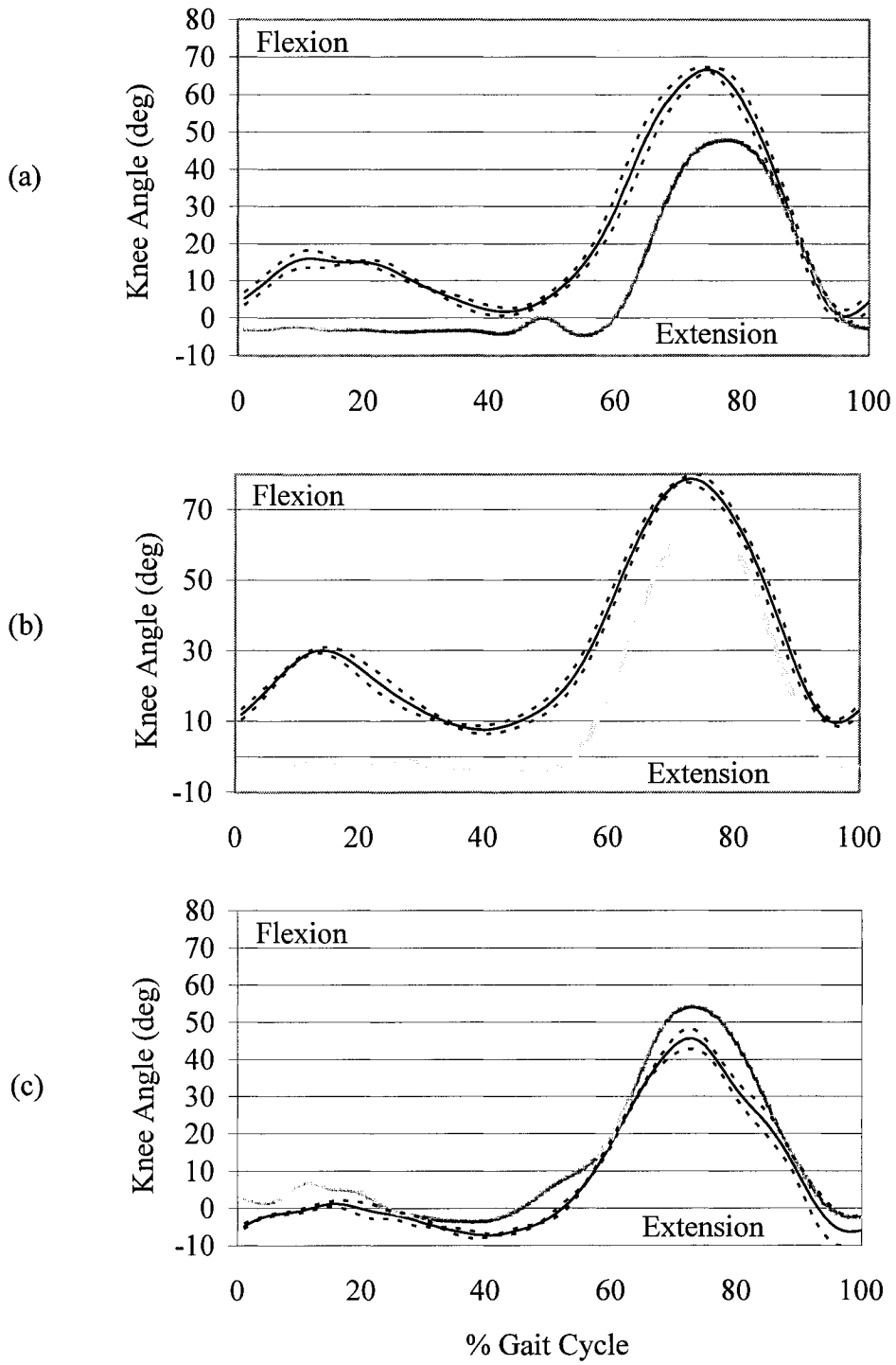

Figure F.3 - Graphs of the knee angle over three walking trials, over the course of one stride for (a) subject A1, (b) subject A2, and (c) subject A3 while walking with no brace (solid black line) and walking with the DKAFO (solid gray line). The dashed lines represent one standard deviation either side of the mean for the no-brace condition.

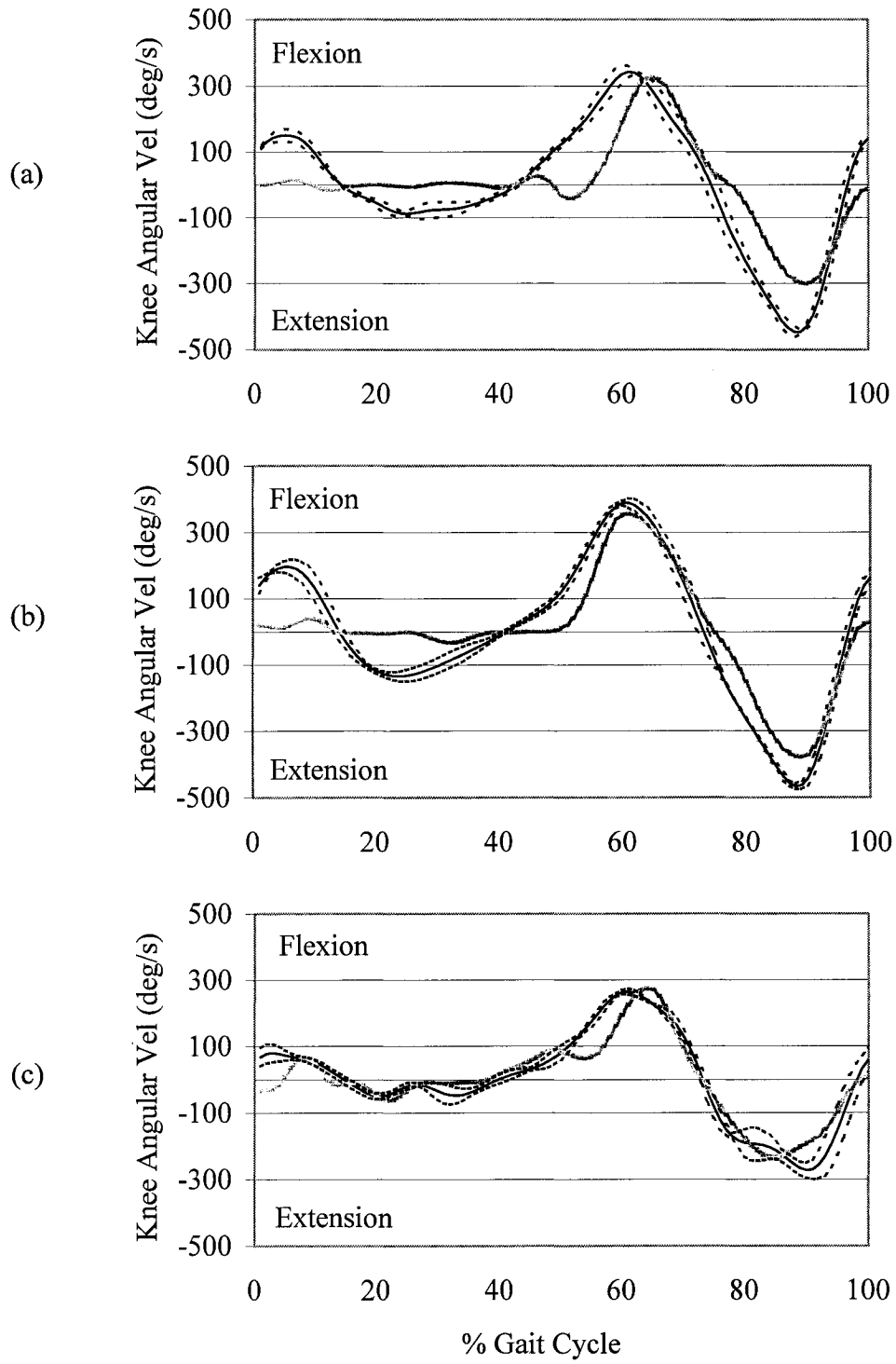

Figure F.4 - Graphs of the knee angle velocity over three walking trials, over the course of one stride for (a) subject A1, (b) subject A2, and (c) subject A3 while walking with no brace (solid black line) and walking with the DKAFO (solid gray line). The dashed lines represent one standard deviation either side of the mean for the no-brace condition.

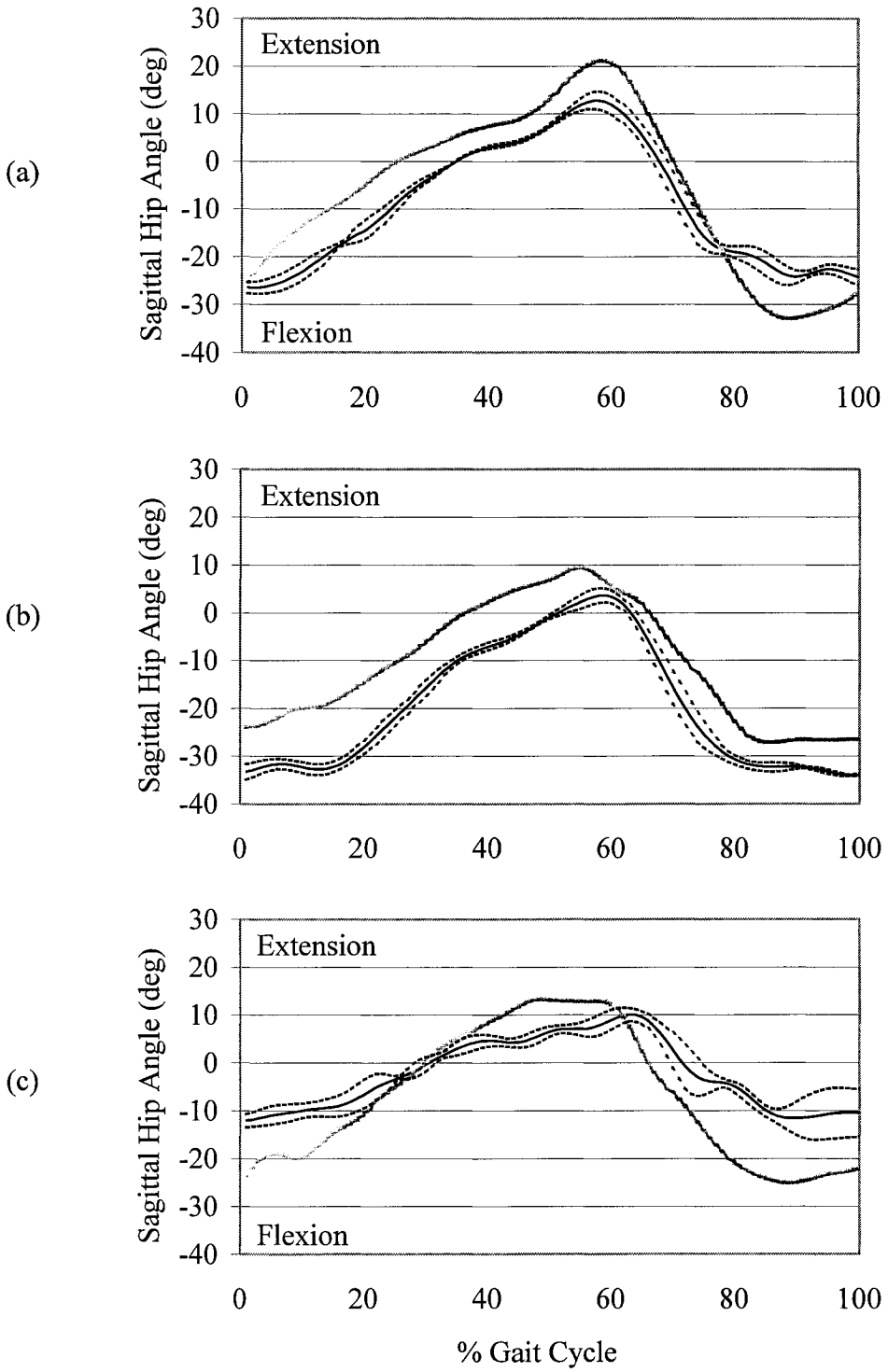

Figure F.5 - Graphs of the sagittal hip angle over three walking trials, over the course of one stride for (a) subject A1, (b) subject A2, and (c) subject A3 while walking with no brace (solid black line) and walking with the DKAFO (solid gray line). The dashed lines represent one standard deviation either side of the mean for the no-brace condition.

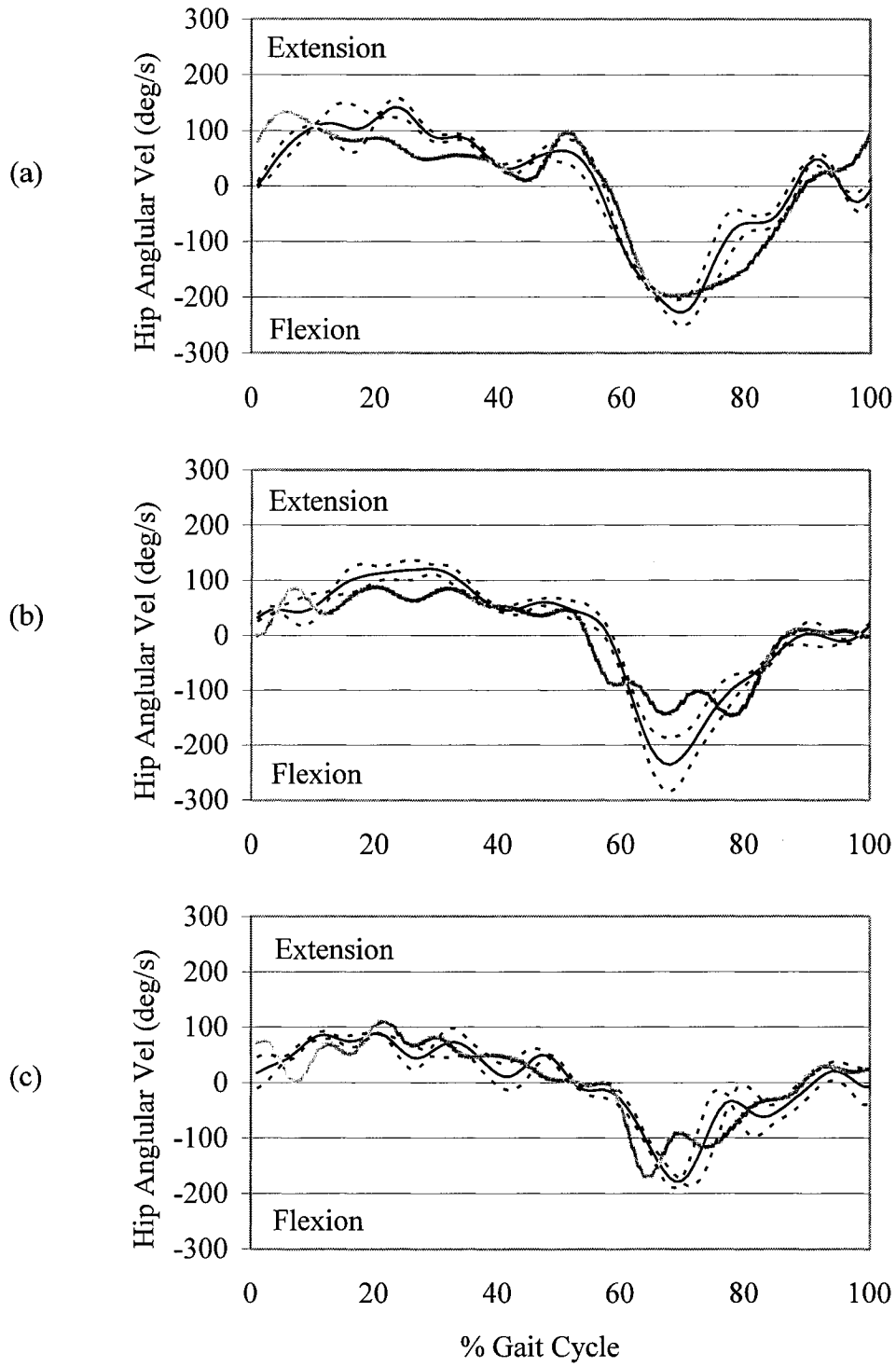

Figure F.6 - Graphs of the sagittal hip angular velocity over three walking trials, over the course of one stride for (a) subject A1, (b) subject A2, and (c) subject A3 while walking with no brace (solid black line) and walking with the DKAFO (solid gray line). The dashed lines represent one standard deviation either side of the mean for the no-brace condition.

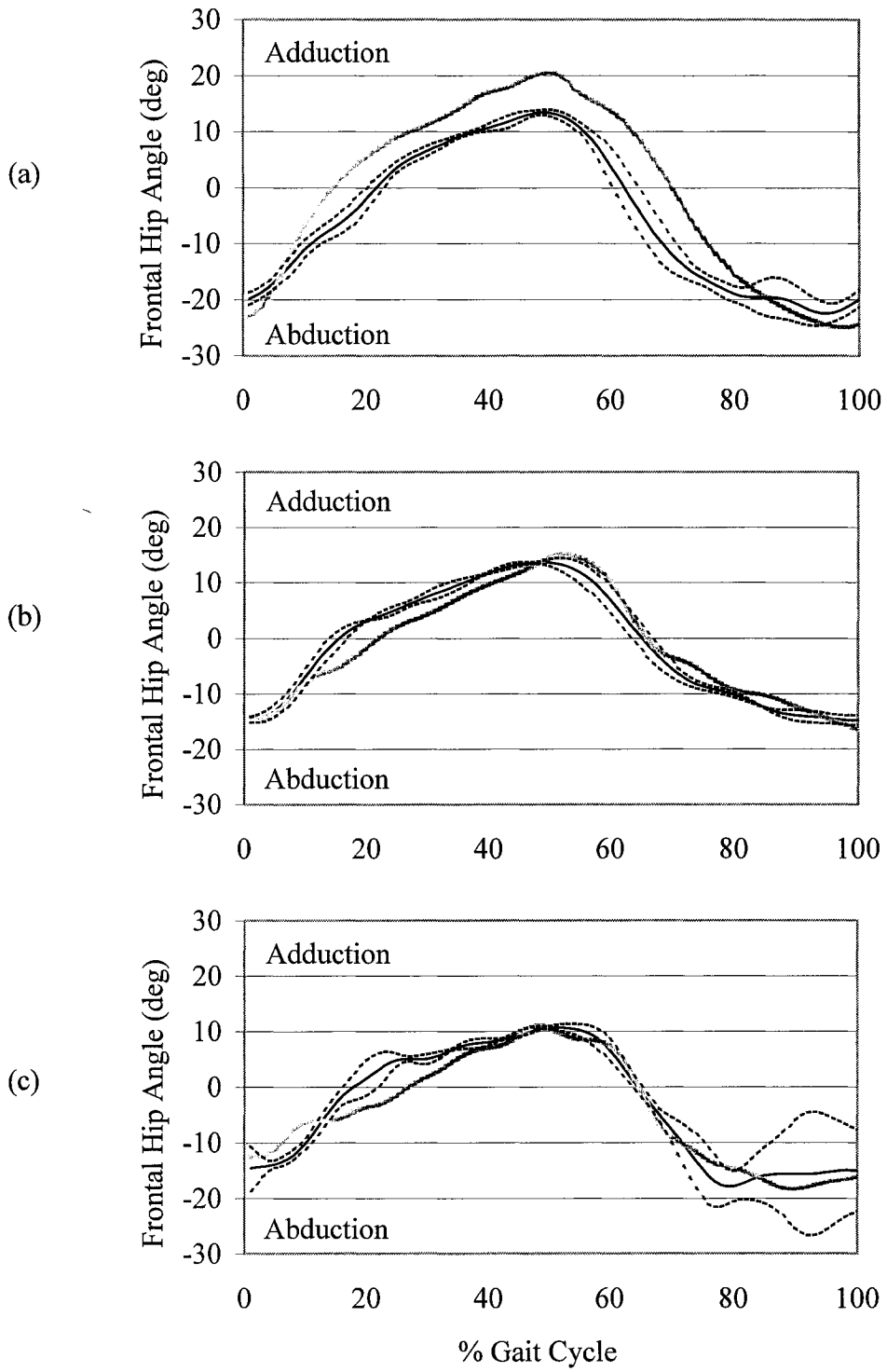

Figure F.7 - Graphs of the frontal hip angle over three walking trials, over the course of one stride for (a) subject A1, (b) subject A2, and (c) subject A3 while walking with no brace (solid black line) and walking with the DKAFO (solid gray line). The dashed lines represent one standard deviation either side of the mean for the no-brace condition.

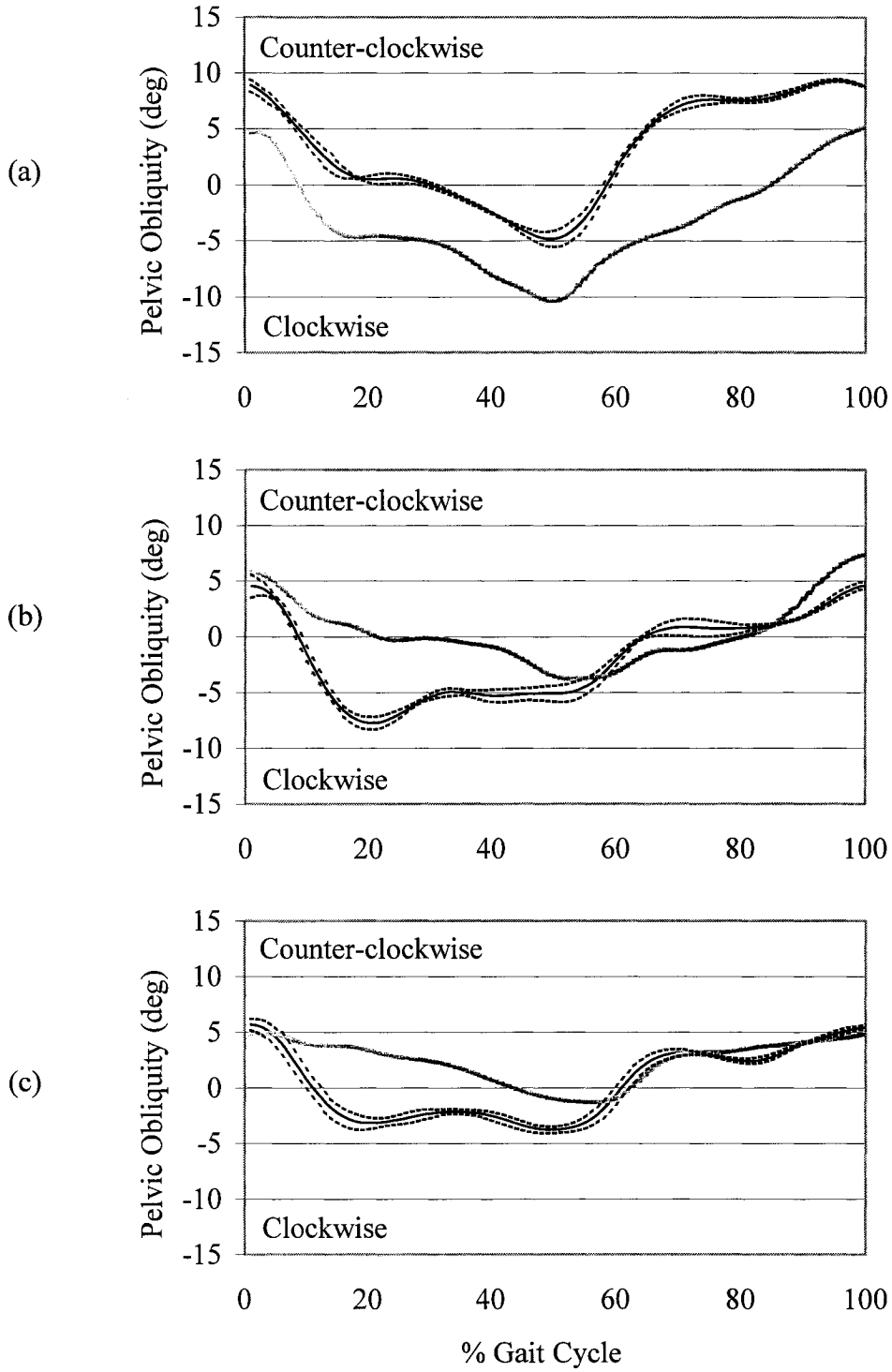

Figure F.8 - Graphs of the pelvic obliquity angle over three walking trials, over the course of one stride for (a) subject A1, (b) subject A2, and (c) subject A3 while walking with no brace (solid black line) and walking with the DKAFO (solid gray line). The dashed lines represent one standard deviation either side of the mean for the no-brace condition.

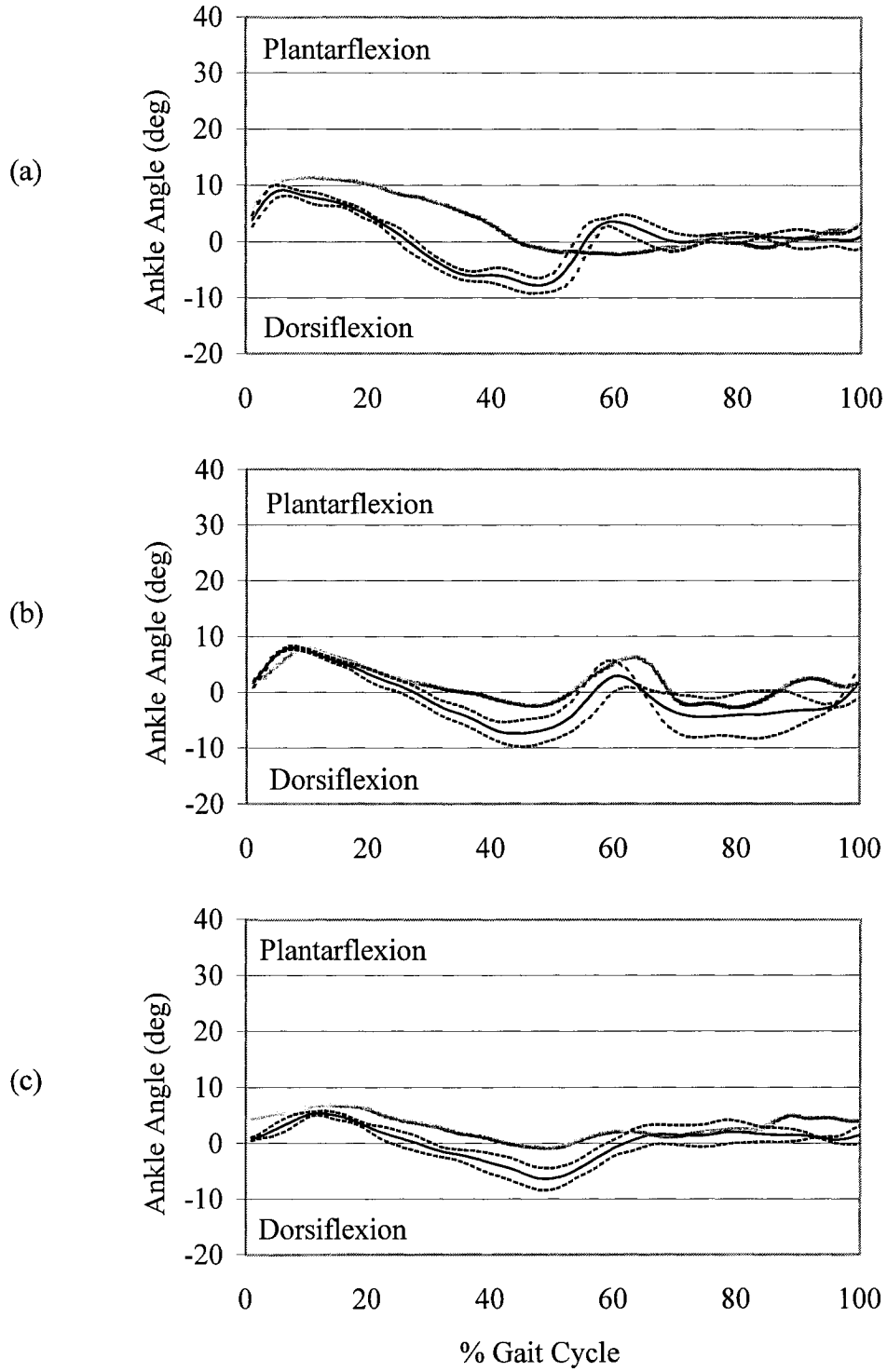

Figure F.9 - Graphs of the ankle angle over three walking trials, over the course of one stride for (a) subject B1, (b) subject B2, and (c) subject B3 while walking with a locked-knee KAFO (solid black line) and walking with the DKAFO (solid gray line). The dashed lines represent one standard deviation either side of the mean for the locked-knee condition.

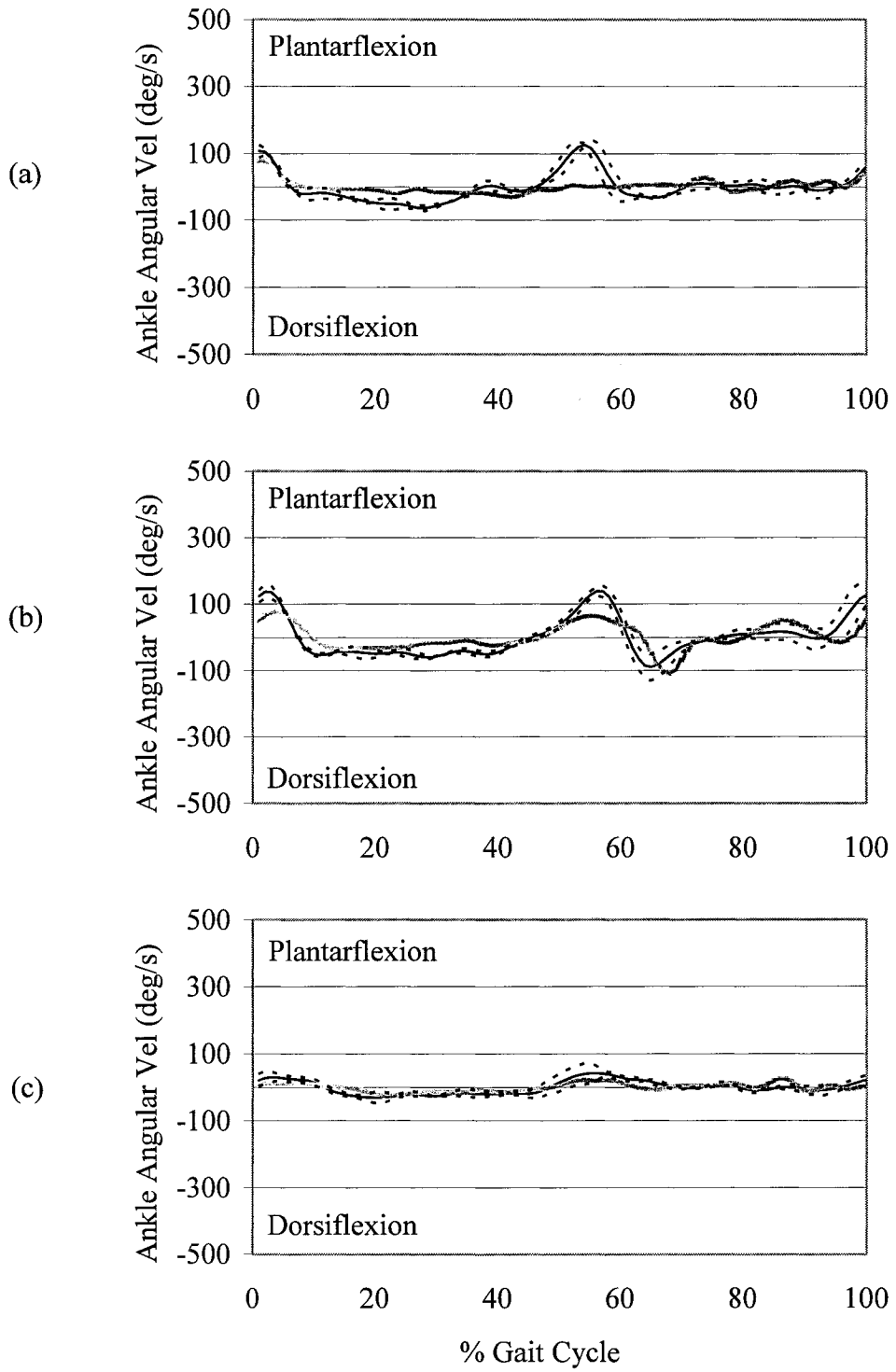

Figure F.10 - Graphs of the ankle angular velocity over three walking trials, over the course of one stride for (a) subject B1, (b) subject B2, and (c) subject B3 while walking with a locked-knee KAFO (solid black line) and walking with the DKAFO (solid gray line). The dashed lines represent one standard deviation either side of the mean for the locked-knee condition.

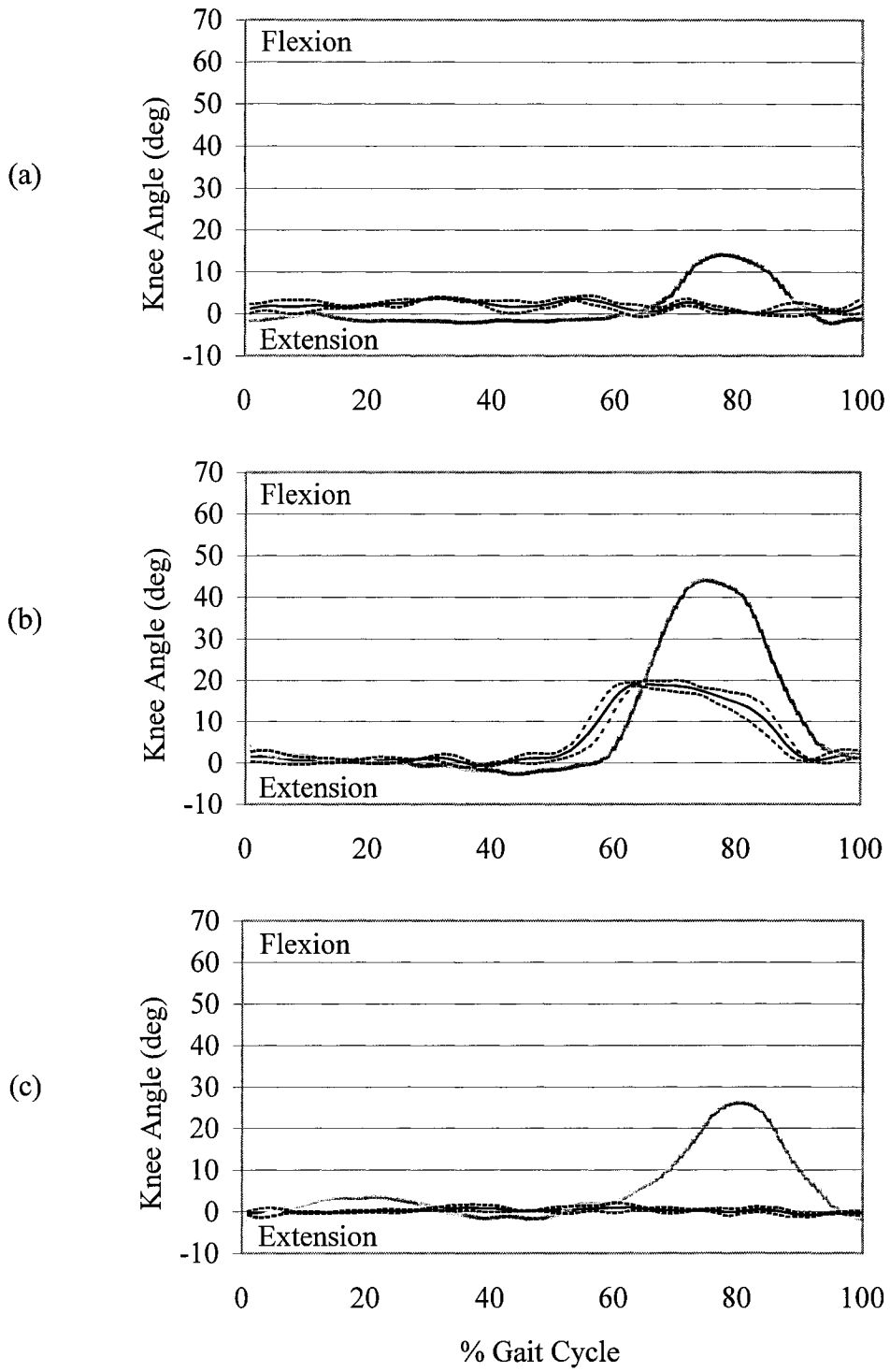

Figure F.11 - Graphs of the knee angle over three walking trials, over the course of one stride for (a) subject B1, (b) subject B2, and (c) subject B3 while walking with a locked-knee KAFO (solid black line) and walking with the DKAFO (solid gray line). The dashed lines represent one standard deviation either side of the mean for the locked-knee condition.

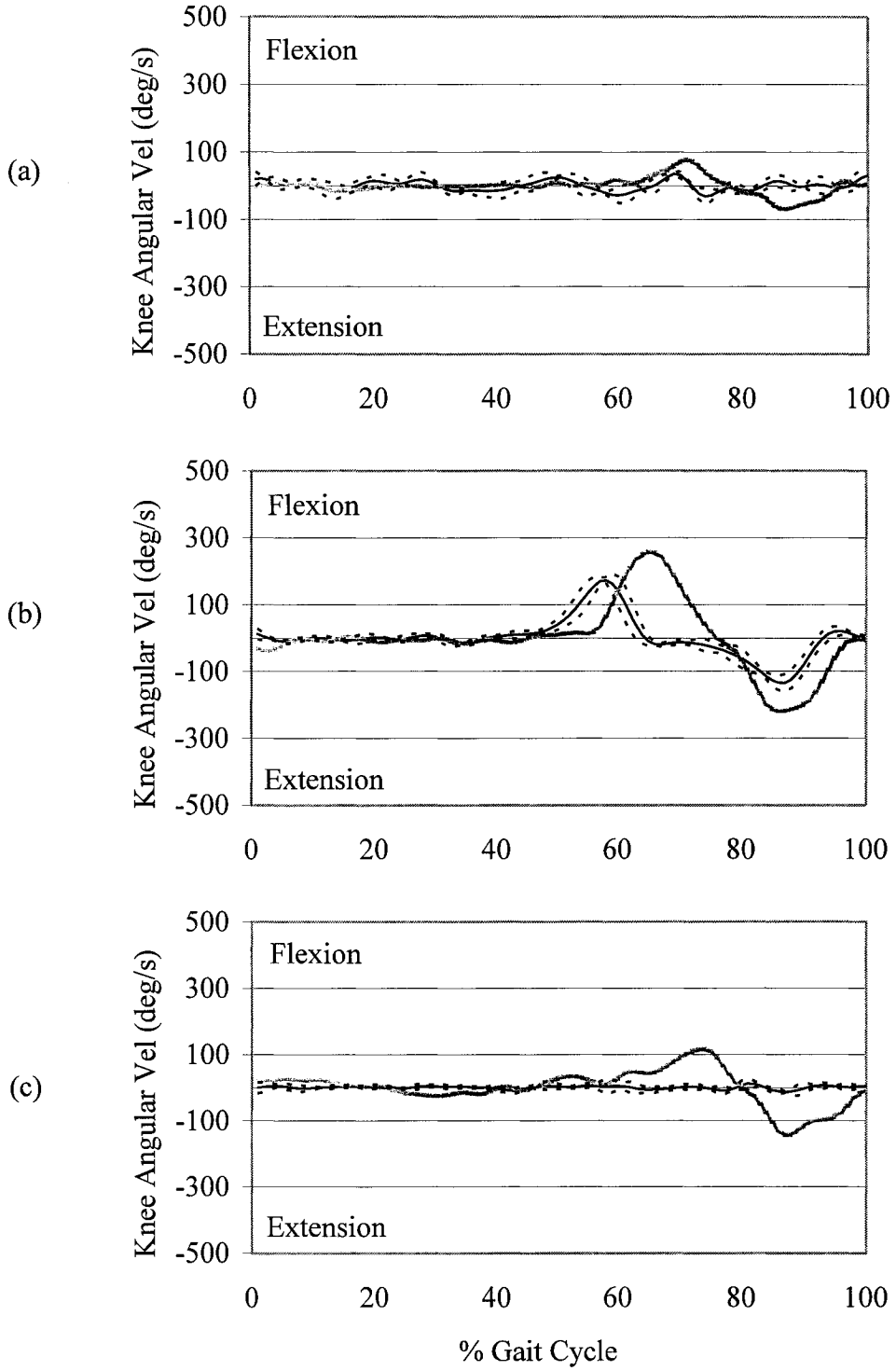

Figure F.12 - Graphs of the knee angular velocity over three walking trials, over the course of one stride for (a) subject B1, (b) subject B2, and (c) subject B3 while walking with a locked-knee KAFO (solid black line) and walking with the DKAFO (solid gray line). The dashed lines represent one standard deviation either side of the mean for the locked-knee condition.

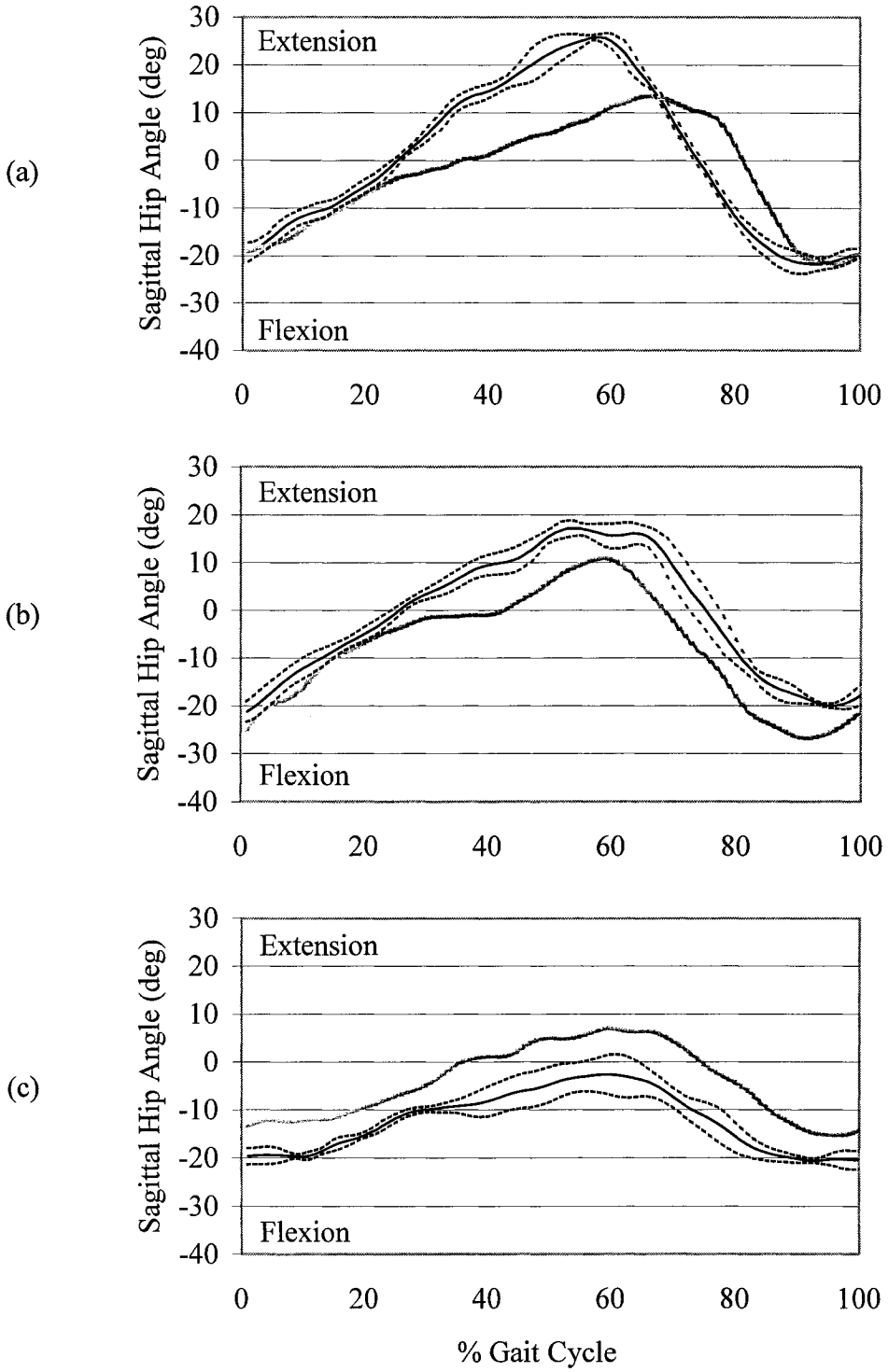

Figure F.13 - Graphs of the sagittal hip angle over three walking trials, over the course of one stride for (a) subject B1, (b) subject B2, and (c) subject B3 while walking with a locked-knee KAFO (solid black line) and walking with the DKAFO (solid gray line). The dashed lines represent one standard deviation either side of the mean for the locked-knee condition.

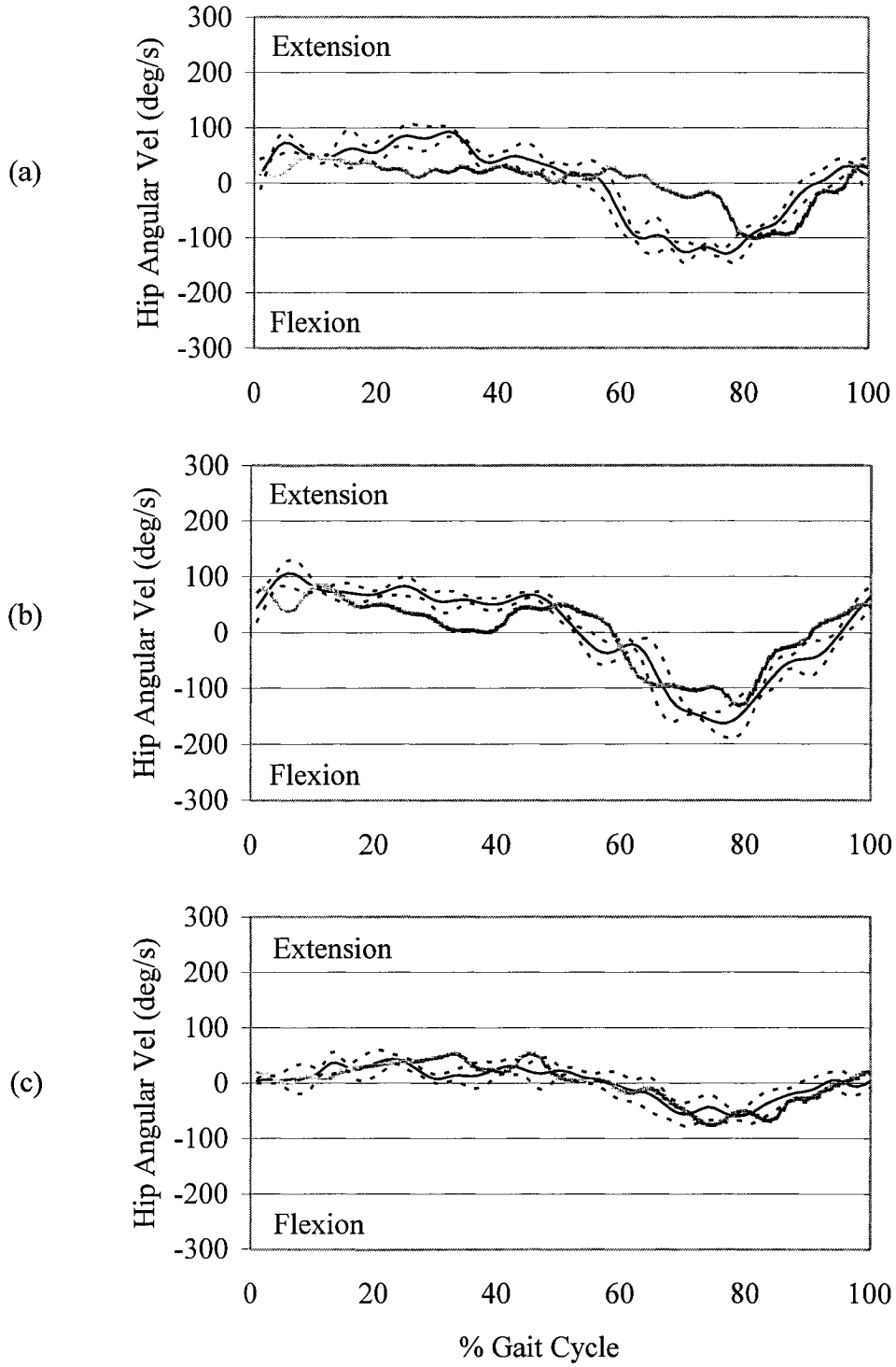

Figure F.14 - Graphs of the sagittal hip angular velocity over three walking trials, over the course of one stride for (a) subject B1, (b) subject B2, and (c) subject B3 while walking with a locked-knee KAFO (solid black line) and walking with the DKAFO (solid gray line). The dashed lines represent one standard deviation either side of the mean for the locked-knee condition.

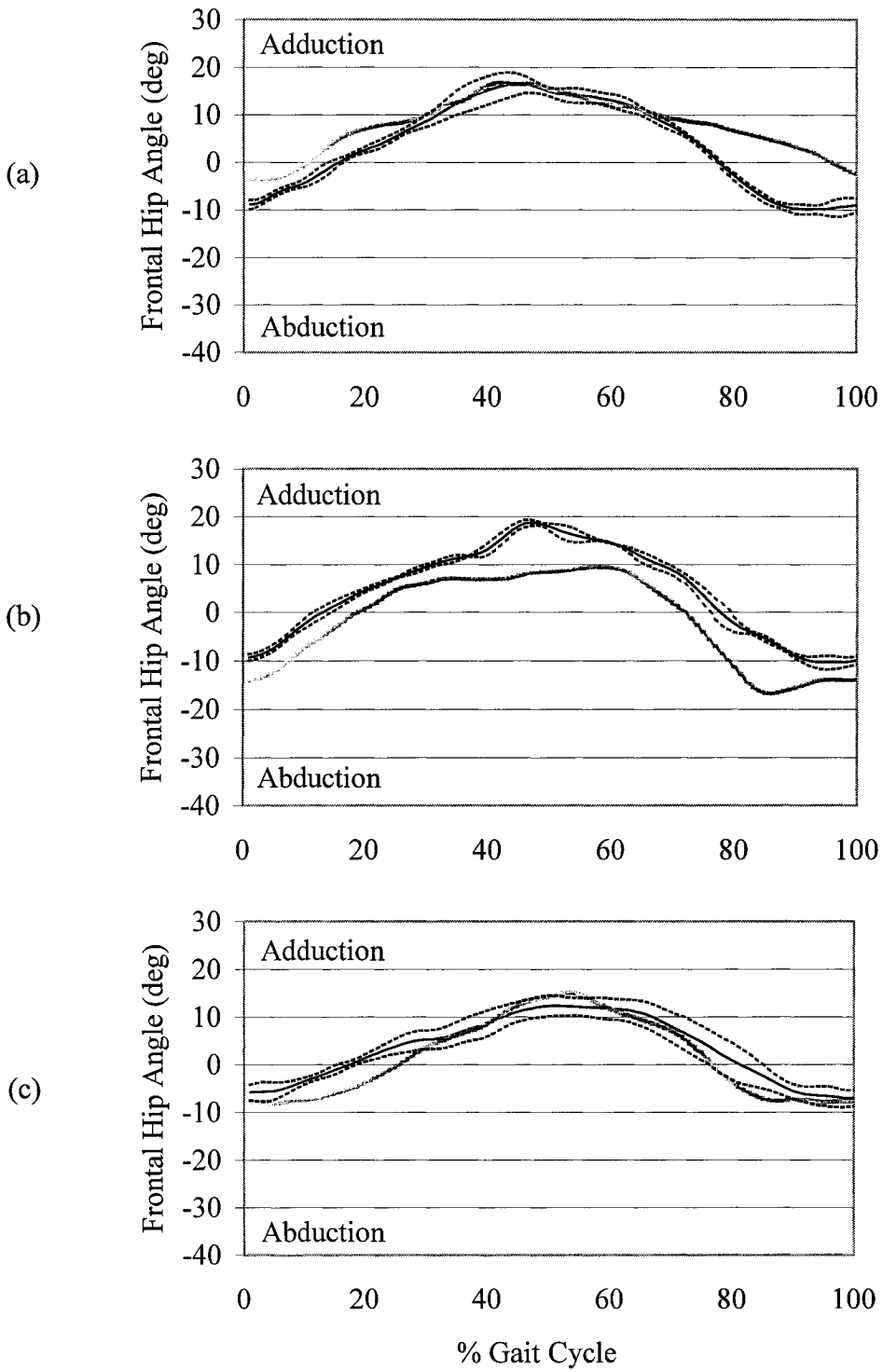

Figure F.15 - Graphs of the frontal hip angle over three walking trials, over the course of one stride for (a) subject B1, (b) subject B2, and (c) subject B3 while walking with a locked-knee KAFO (solid black line) and walking with the DKAFO (solid gray line). The dashed lines represent one standard deviation either side of the mean for the locked-knee condition.

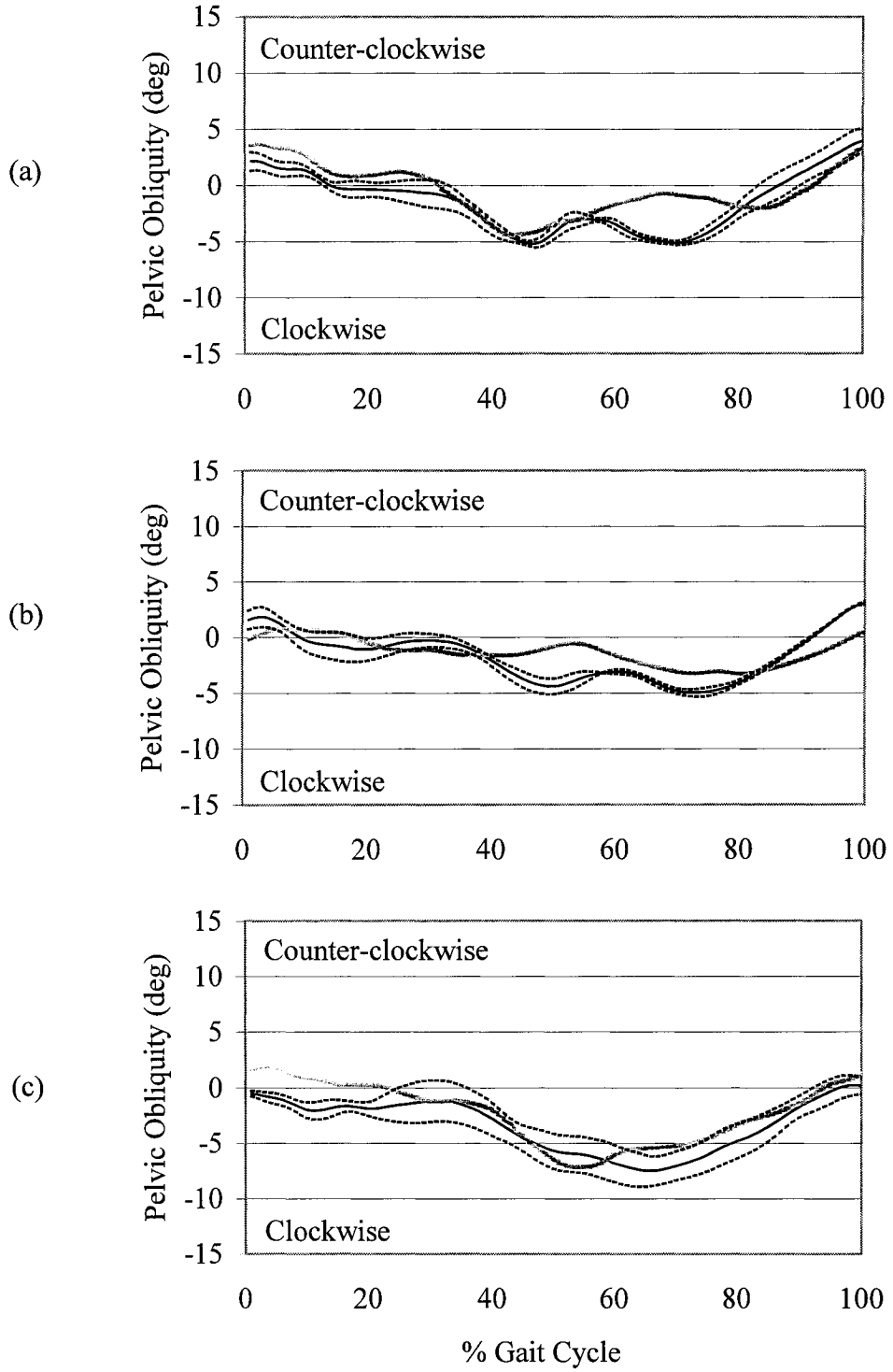

Figure F.16 - Graphs of the pelvic obliquity angle over three walking trials, over the course of one stride for (a) subject B1, (b) subject B2, and (c) subject B3 while walking with a locked-knee KAFO (solid black line) and walking with the DKAFO (solid gray line). The dashed lines represent one standard deviation either side of the mean for the locked-knee condition.